RADAR SIGNAL ANALYSIS AND PROCESSING USING MATLAB®

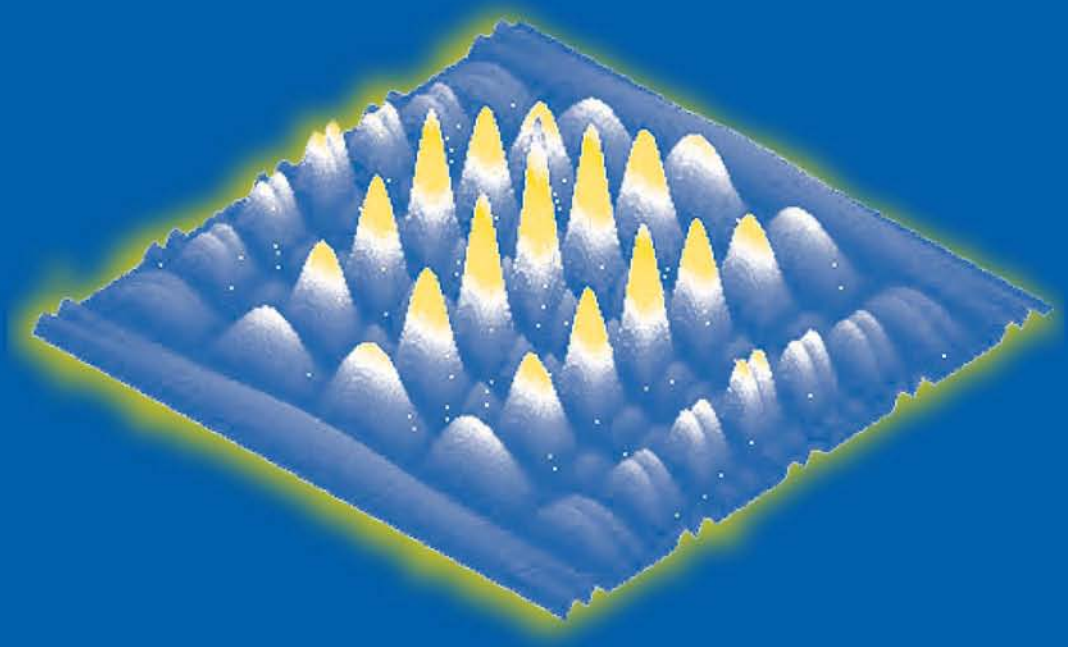

Bassem R. Mahafza

MATLAB® examples

CRC Press
Taylor & Francis Group
A CHAPMAN & HALL BOOK

RADAR SIGNAL ANALYSIS AND PROCESSING USING MATLAB®

RADAR SIGNAL ANALYSIS AND PROCESSING USING MATLAB®

Bassem R. Mahafza
deciBel Research Inc.
Huntsville, Alabama, U.S.A.

CRC Press
Taylor & Francis Group
Boca Raton London New York

CRC Press is an imprint of the
Taylor & Francis Group, an **informa** business
A CHAPMAN & HALL BOOK

Chapman & Hall/CRC
Taylor & Francis Group
6000 Broken Sound Parkway NW, Suite 300
Boca Raton, FL 33487-2742

Printed in the United States of America on acid-free paper
10 9 8 7 6 5 4 3 2 1

International Standard Book Number-13: 978-1-4200-6643-2 (Hardcover)

Library of Congress Cataloging-in-Publication Data

Mahafza, Bassem R.
Radar signal analysis and processing using MATLAB / Bassem R. Mahafza.
p. cm.
"A CRC title."
Includes bibliographical references and index.
ISBN 978-1-4200-6643-2 (hardback : alk. paper)
1. Radar cross sections. 2. Signal processing. 3. Radar targets. 4. MATLAB. I. Title.

TK6575.M267 2008
621.3848--dc22 2008014584

Visit the Taylor & Francis Web site at
http://www.taylorandfrancis.com

and the CRC Press Web site at
http://www.crcpress.com

To my four sons:

Zachary,

Joseph,

Jacob, and

Jordan

Table of Contents

Preface

In the year 2000 my book *Radar Systems Analysis and Design Using MATLAB*[1]® was published. This book very quickly turned into a bestseller which prompted the publication of its second edition in the year 2005. At the time of its publication, it was based on my years of teaching graduate level courses on radar systems analysis and design including advanced topics in radar signal processing. The motivation behind it was to introduce a college-suitable comprehensive textbook that provides hands-on experience with MATLAB® companion software. Over the years, I have also taught numerous industry courses on the subject of radar systems. Based on my combined teaching experience and real-world work at deciBel Research, Inc., the following conclusion has become very evident to me: There is big appetite and demand for textbooks and reference books that are primarily focused on aspects of radar signals and signal processing. Having arrived at this conclusion, I decided to write this textbook, *Radar Signal Analysis and Processing Using MATLAB*®, which is focused on radar signal analysis and processing.

Unlike other books on the subject, the emphasis is not on signal processing per se, but on signals and signal processing in the context of radar applications. Many good textbooks are already available on signal processing but not on signal processing as it applies to radar applications. This new textbook has many desirable features that include clear and concise presentation of the theory and companion user-friendly MATLAB code. This code is reconfigurable to demonstrate the theory and perform the associated analysis/design trades as well as allow users to vary the inputs in order to better analyze their relevant and unique requirements. This new book should serve as a reference book or as a textbook for a graduate level courses on the subject. It concentrates on the fundamentals and adopts a rigorous mathematical approach of the subject. Many examples and end of chapter problems are included. Finally, a companion Instructor's Manual is also available through the publisher for professors who adopt this book as a text. The Instructor's Manual includes many other problems not listed in the text and their solutions.

---

1. All MATLAB® functions and programs provided in this book were developed using MATLAB R2007b with the Signal Processing Toolbox, on a PC with Windows XP Professional operating system.

® MATLAB® is a registered trademark of the The MathWorks, Inc. For product information, please contact: The MathWorks, Inc., 3 Apple Hill Drive, Natick, MA 01760-2098 USA. Web: *www.mathworks.com*.

Radar Signal Analysis and Processing Using MATLAB® is written so that it can be used as a reference book or as a textbook for two graduate level courses with emphasis on signals and signal processing. Instructors using this book as a text may choose the following chapter breakdown for their curriculum. Chapters 1 through Chapter 7 can be used for the first course, while Chapters 8 through 11 may be used for the second course. Chapter 11 (Target Tracking), Chapter 12 (Synthetic Aperture Radar), and Chapter 13 (Radar Cross Section) from my other book *Radar Systems Analysis and Design Using MATLAB®* may also be used to supplement both courses.

Radar Signal Analysis and Processing Using MATLAB® introduces numerous programs and functions of MATLAB using version R2007a. All MATLAB programs and functions provided in this book can be downloaded from the CRC Press Website. For this purpose and using your favorite Internet browser type in *www.crcpress.com* and hit return. Once you reach the main CRC Press home page, scroll down to the link called *"Electronic Products"* and double click on *"Downloads & Updates,"* then follow the instructions on the screen.

Chapter 1 of this book presents an overview of radar systems operation and design. The approach is to derive the radar range equation and analyze the different radar parameters in the context of this radar equation. The surveillance radar equation is derived. Special topics that affect radar signal processing are presented and analyzed in the context of the radar equation. This includes the effects of system noise, wave propagation, jamming, and target Radar Cross Section (RCS). Chapter 2 introduces a top level review of elements of signal theory that are relevant to radar detection and radar signal processing. It is assumed that the reader has sufficient and adequate background in signals and systems as well as in the Fourier transform and its associated properties.

In Chapter 3 a review of random variables and processes is presented. Instructors using this text may assume that students have already acquired the necessary background as a prerequisite to this course and, thus, may elect to omit this chapter from their syllabus, except for Section 3.6. Chapter 4 is focused on the matched filter. It presents the unique characteristic of the matched filter and develops a general formula for the output of the matched filter that is valid for any waveform. Chapters 5 and 6 analyze the output of the matched filter in the context of the ambiguity function. In Chapter 5 several analog waveforms are analyzed; this includes the single unmodulated pulse, the Linear Frequency Modulation (LFM) pulse, unmodulated pulse train, LFM pulse train, stepped frequency waveforms, and nonlinear FM waveforms. Chapter 6 is concerned with discrete coded waveforms. In this chapter, unmodulated pulse-train codes are analyzed as well as binary codes, polyphase codes, and frequency codes.

Chapter 7 introduces the subject of radar target detection and pulse integration. Swerling models are analyzed in the context of noncoherent integration and the square law detector. The topic of Constant False Alarm Rate (CFAR) is also presented in detail. Chapter 8 introduces the most common techniques in radar signal processing. The matched filter receiver as well as the stretch processor receiver are analyzed. Chapter 9 is concerned with radar clutter. Comprehensive analysis of the subject of clutter is introduced, including the Moving Target Indicator (MTI). Chapter 10 is primarily concerned with radar Doppler processing. Both continuous wave and pulsed radars are considered. Pulse Doppler radars are introduced and analyzed. Chapter 11 is focused on adaptive array processing. For this purpose, a top level overview of phased array antennas is first introduced followed by beamforming and the most common techniques in adaptive array processing.

Bassem R. Mahafza
bmahafza@dbresearch.net
Huntsville, AL
February 2008

Chapter 1 Radar Systems - An Overview

This chapter presents an overview of radar systems operation and design. The approach is to introduce few definitions first, followed by detailed derivation of the radar range equation. Different radar parameters are analyzed in the context of the radar equation. The search or surveillance radar equation will also be derived. Where appropriate, a few examples are introduced. Special topics that affect radar signal processing are also presented and analyzed in the context of the radar equation. This includes the effects of system noise, wave propagation, jamming, and target Radar Cross Section (RCS).

1.1. Range Measurements

Consider a radar systems that transmits a periodic sequence, with period T, of square pulses, each of width τ, shown in Fig. 1.1. The period is referred to as the Pulse Repetition Interval (PRI) and the inverse of the PRI is called the Pulse Repetition Frequency (PRF), denoted by f_r. If the peak transmitted power for each pulse is referred to as P_t, then the average transmitted power over one full period is

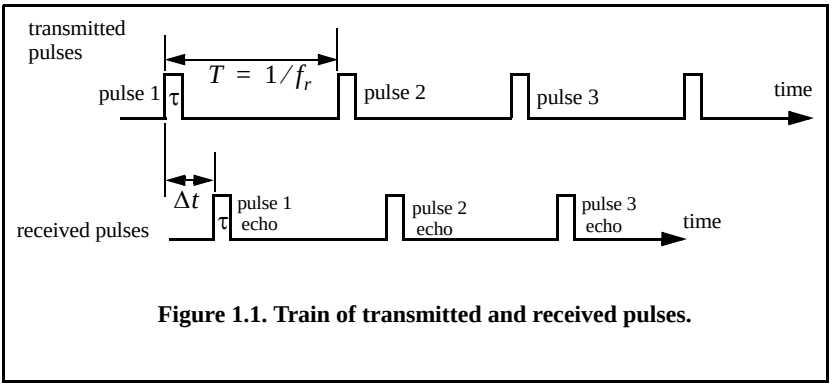

Figure 1.1. Train of transmitted and received pulses.

$$P_{av} = P_t \times \frac{\tau}{T} \tag{1.1}$$

The ratio of the pulse width to the PRI is called transmit duty cycle, denoted by dt. The pulse energy is $E_x = P_t\tau = P_{av}T = P_{av}/f_r$.

The top portion of Fig. 1.1 represents the transmitted sequence of pulses, while the lower portion represents the received radar echoes reflected from a target at some range R. By measuring the two-way time delay, Δt, the radar receiver can determine the range as follows:

$$R = \frac{c\Delta t}{2} \tag{1.2}$$

where: $c = 3 \times 10^8 m/s$ is the speed of light, and the factor 2 is used to account for the round trip (two-way) delay.

The range corresponding to the two-way time delay $\Delta t = T$, where T is the pulse repetition interval is referred to as the radar unambiguous range, R_u. Consider the case shown in Fig. 1.2. Echo 1 represents the radar return from a target at range $R_1 = c\Delta t/2$ due to pulse 1. Echo 2 could be interpreted as the return from the same target due to pulse 2, or it may be the return from a far-away target at range R_2 due to pulse 1 again. That is,

$$R_{2a} = \frac{c\Delta t}{2} \qquad or \qquad R_{2b} = \frac{c(T + \Delta t)}{2} \tag{1.3}$$

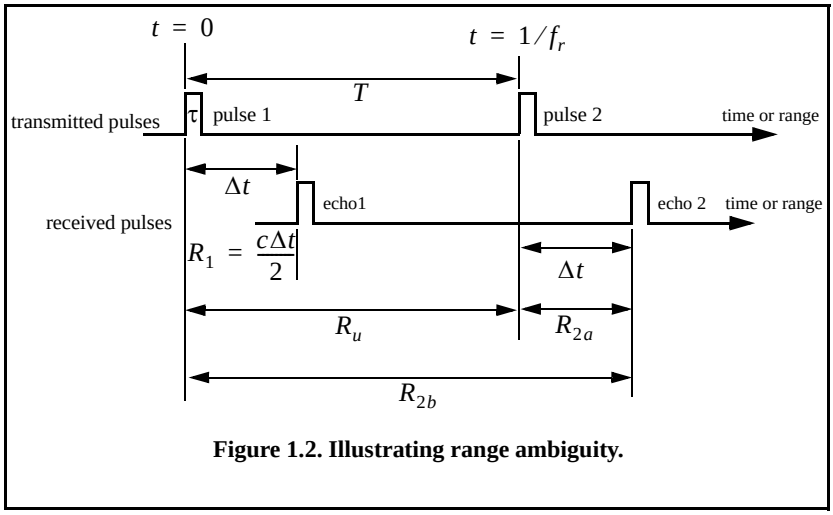

Figure 1.2. Illustrating range ambiguity.

Clearly, range ambiguity is associated with echo 2. Once a pulse is transmitted, the radar must wait a sufficient length of time so that returns from targets at maximum range are back before the next pulse is emitted. It follows that the maximum unambiguous range must correspond to half of the PRI:

$$R_u = c\frac{T}{2} = \frac{c}{2f_r} \tag{1.4}$$

Example:

A certain airborne pulsed radar has peak power $P_t = 10KW$ *and uses two PRFs,* $f_{r1} = 10KHz$ *and* $f_{r2} = 30KHz$. *What are the required pulse widths for each PRF so that the average transmitted power is constant and is equal to* $1500Watts$ *? Compute the pulse energy in each case.*

Solution:

Since P_{av} *is constant, both PRFs have the same duty cycle,*

$$d_t = \frac{1500}{10 \times 10^3} = 0.15$$

The pulse repetition intervals are

$$T_1 = \frac{1}{10 \times 10^3} = 0.1ms$$

$$T_2 = \frac{1}{30 \times 10^3} = 0.0333ms$$

It follows that

$$\tau_1 = 0.15 \times T_1 = 15\mu s$$

$$\tau_2 = 0.15 \times T_2 = 5\mu s$$

$$E_{x1} = P_t\tau_1 = 10 \times 10^3 \times 15 \times 10^{-6} = 0.15 \ Joules$$

$$E_{x2} = P_2\tau_2 = 10 \times 10^3 \times 5 \times 10^{-6} = 0.05 \ Joules$$

1.2. Range Resolution

Range resolution, denoted as ΔR, is a radar metric that describes its ability to detect targets in close proximity to each other as distinct objects. Radar sys-

tems are normally designed to operate between a minimum range R_{min} and maximum range R_{max}. The distance between R_{min} and R_{max} along the radar line of sight is divided into M range bins (gates), each of width ΔR,

$$M = \frac{R_{max} - R_{min}}{\Delta R} \tag{1.5}$$

Targets separated by at least ΔR will be completely resolved in range.

In order to derive an exact expression for ΔR, consider two targets located at ranges R_1 and R_2, corresponding to time delays t_1 and t_2, respectively. This is illustrated in Fig. 1.3. Denote the difference between those two ranges as ΔR:

$$\Delta R = R_2 - R_1 = c\frac{(t_2 - t_1)}{2} = c\frac{\delta t}{2} \tag{1.6}$$

The question that needs to be answered is: What is the minimum time, δt, such that target 1 at R_1 and target 2 at R_2 will appear completely resolved in range (different range bins)? In other words, what is the minimum ΔR?

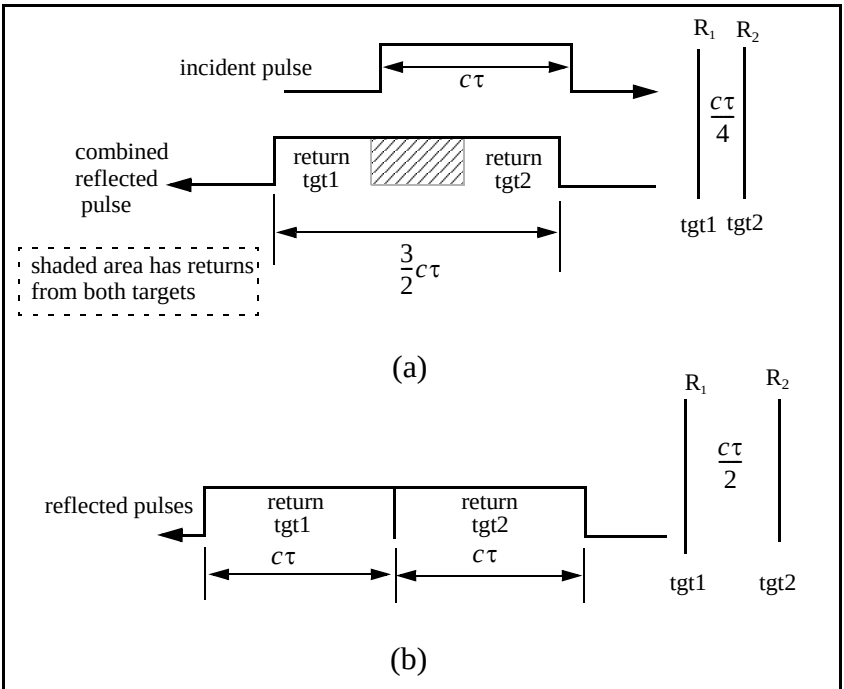

Figure 1.3. (a) Two unresolved targets. (b) Two resolved targets.

First, assume that the two targets are separated by $c\tau/4$, τ is the pulse width. In this case, when the pulse trailing edge strikes target 2, the leading edge would have traveled backward a distance $c\tau$, and the returned pulse would be composed of returns from both targets (i.e., unresolved return), as shown in Fig. 1.3a. If the two targets are at least $c\tau/2$ apart, then as the pulse trailing edge strikes the first target, the leading edge will start to return from target 2, and two distinct returned pulses will be produced, as illustrated by Fig. 1.3b. This means ΔR should be greater or equal to $c\tau/2$. Since the radar bandwidth B is equal to $1/\tau$, then

$$\Delta R = \frac{c\tau}{2} = \frac{c}{2B} \tag{1.7}$$

In general, radar users and designers alike seek to minimize ΔR in order to enhance the radar performance. As suggested by Eq. (1.7), in order to achieve fine range resolution one must minimize the pulse width. This will reduce the average transmitted power and increase the operating bandwidth. Achieving fine range resolution while maintaining adequate average transmitted power can be accomplished by using pulse compression techniques.

Example:

A radar system has an unambiguous range of 100 Km and a bandwidth 0.5 MHz. Compute the required PRF, PRI, ΔR, and τ.

Solution:

$$PRF = \frac{c}{2R_u} = \frac{3\times10^8}{2\times10^5} = 1500 \ \ Hz$$

$$PRI = \frac{1}{PRF} = \frac{1}{1500} = 0.6667 \ \ ms$$

It follows,

$$\Delta R = \frac{c}{2B} = \frac{3\times10^8}{2\times0.5\times10^6} = 300 \ \ m$$

$$\tau = \frac{2\Delta R}{c} = \frac{2\times300}{3\times10^8} = 2 \ \ \mu s$$

1.3. Doppler Frequency

Radars use Doppler frequency to extract target radial velocity (range rate), as well as to distinguish between moving and stationary targets or objects, such as clutter. The Doppler phenomenon describes the shift in the center frequency of

an incident waveform due to the target motion with respect to the source of radiation. Depending on the direction of the target's motion, this frequency shift may be positive or negative. A waveform incident on a target has equiphase wavefronts separated by λ, the wavelength. A closing target will cause the reflected equiphase wavefronts to get closer to each other (smaller wavelength). Alternatively, an opening or receding target (moving away from the radar) will cause the reflected equiphase wavefronts to expand (larger wavelength), as illustrated in Fig. 1.4.

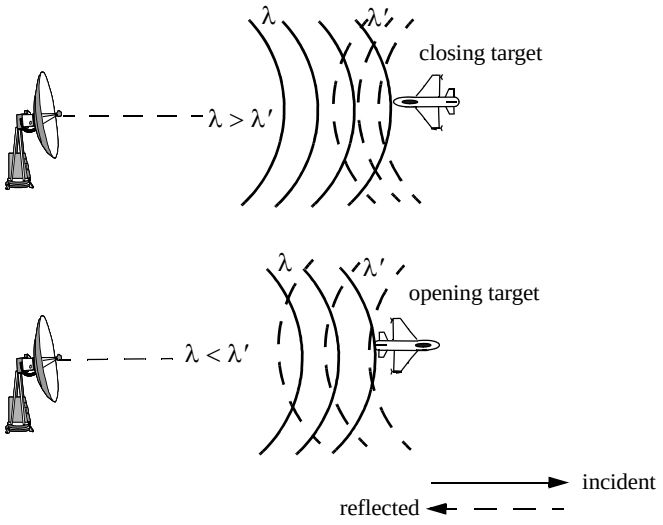

Figure 1.4. Effect of target motion on the reflected equiphase waveforms.

The result formula for the Doppler frequency can be derived with the help of Fig. 1.5. Assume a target closing on the radar with radial velocity (target velocity component along the radar line of sight) v. Let R_0 refer to the range at time t_0 (time reference); then the range to the target at any time t is

$$R(t) = R_0 - vt \tag{1.8}$$

Assume a radar transmitted signal given by

$$x(t) = A\cos(2\pi f_0 t) \tag{1.9}$$

where f_0 is the radar operating center frequency. It follows that the signal received by the radar is

$$x_r(t) = x(t - \phi(t)) \tag{1.10}$$

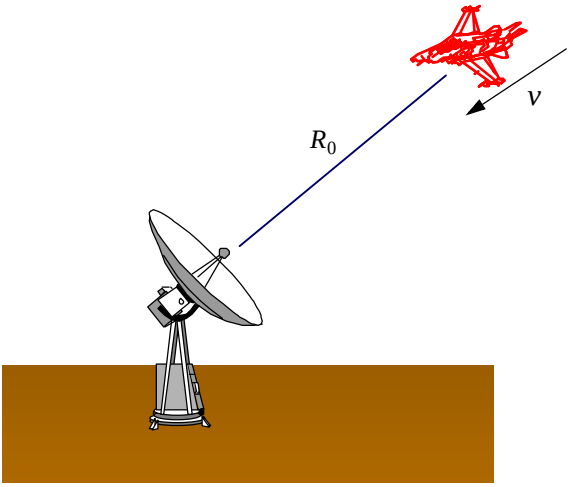

Figure 1.5. Closing target with velocity *v*.

where

$$\phi(t) = \frac{2}{c}(R_0 - vt) \tag{1.11}$$

Substituting Eq. (1.9) and Eq. (1.11) into Eq. (1.10) and collecting terms yields

$$x_r(t) = A_r \cos\left[2\pi\left(f_0 t - f_0\frac{2R_0}{c} + \frac{2f_0 vt}{c}\right)\right] \tag{1.12}$$

where A_r is a constant. The phase term

$$\psi_0 = 2\pi f_0 \frac{2R_0}{c} \tag{1.13}$$

is used to measure initial target detection range, and the term $2f_0 v/c$ represents a frequency shift due to target velocity (i.e., Doppler frequency shift). The Doppler frequency is given by

$$f_d = \frac{2f_0 v}{c} = \frac{2v}{\lambda} \tag{1.14}$$

where λ is the wavelength given by

$$\lambda = \frac{c}{f_0} \tag{1.15}$$

Note that if the target were going away from the radar (opening or receding target), then

$$f_d = -\frac{2f_0 v}{c} = -\frac{2v}{\lambda} \tag{1.16}$$

as illustrated in Fig. 1.6.

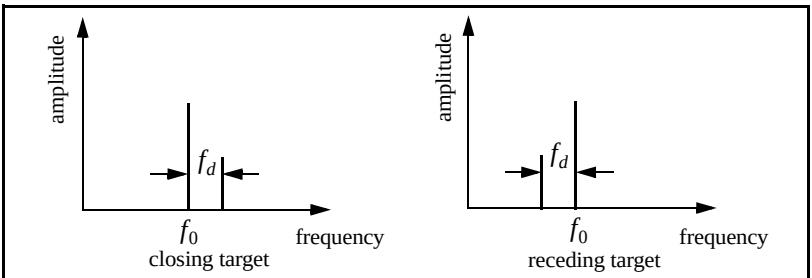

Figure 1.6. Spectra of received signal showing Doppler shift.

In general the target Doppler frequency depends on the target velocity component in the direction of the radar (radial velocity). Figure 1.7 shows three targets all having velocity v. Target 1 has zero Doppler shift; target 2 has maximum Doppler frequency as defined in Eq. (1.15). The amount of Doppler frequency of target 3 is $f_d = 2v\cos\theta/\lambda$, where $v\cos\theta$ is the radial velocity; and θ is the total angle between the radar line of sight and the target.

A more general expression for f_d that accounts for the total angle between the radar and the target is

$$f_d = \frac{2v}{\lambda}\cos\theta \tag{1.17}$$

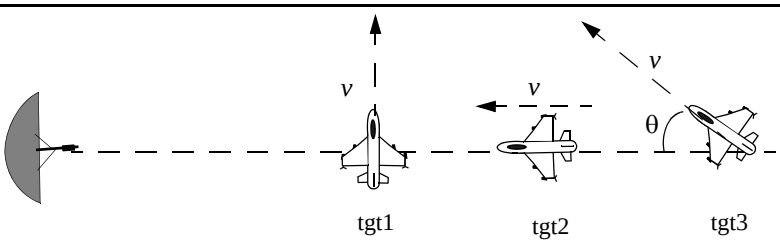

Figure 1.7. Target 1 generates zero Doppler. Target 2 generates maximum Doppler. Target 3 is in between.

and for an opening target is

$$f_d = \frac{-2v}{\lambda}\cos\theta \qquad \textbf{(1.18)}$$

where $\cos\theta = \cos\theta_e \cos\theta_a$. The angles θ_e and θ_a are, respectively, the elevation and azimuth angles; see Fig. 1.8.

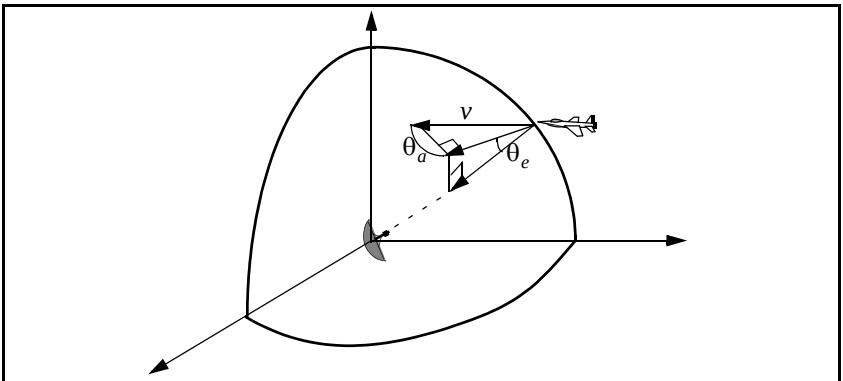

Figure 1.8. Radial velocity is proportional to the azimuth and elevation angles.

***Example**:*

Compute the Doppler frequency measured by the radar shown in the figure below.

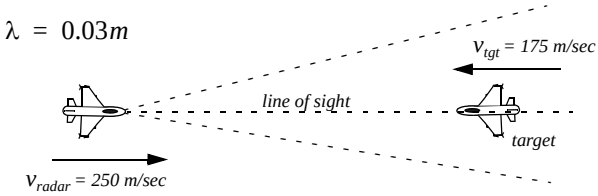

Solution:

The relative radial velocity between the radar and the target is $v_{radar} + v_{tgt}$. *Using Eq. (1.15) yields*

$$f_d = 2\frac{(250 + 175)}{0.03} = 28.3KHz$$

Similarly, if the target were opening, the Doppler frequency is

$$f_d = 2\frac{250 - 175}{0.03} = 5KHz$$

1.4. Coherence

A radar is said to be coherent if the phase of any two transmitted pulses is consistent; i.e., there is a continuity in the signal phase from one pulse to the next. One can view coherence as the radar's ability to maintain an integer multiple of wavelengths between the equiphase wavefront from the end of one pulse to the equiphase wavefront at the beginning of the next pulse. Coherency can be achieved by using a STAble Local Oscillator (STALO). A radar is said to be coherent-on-receive or quasi-coherent if it stores in its memory a record of the phases of all transmitted pulses. In this case, the receiver phase reference is normally the phase of the most recently transmitted pulse.

Coherence also refers to the radar's ability to accurately measure (extract) the received signal phase. Since Doppler represents a frequency shift in the received signal, only coherent or coherent-on-receive radars can extract Doppler information. This is because the instantaneous frequency of a signal is proportional to the time derivative of the signal phase.

1.5. The Radar Equation

Consider a radar with an isotropic antenna (one that radiates energy equally in all directions). Since these kinds of antennas have a spherical radiation pattern, we can define the peak power density (power per unit area) at any point in space as

$$P_D = \frac{Peak\ \ transmitted\ \ power}{area\ \ of\ \ a\ \ sphere} \qquad \frac{watts}{m^2} \tag{1.19}$$

The power density at range R away from the radar (assuming a lossless propagation medium) is

$$P_D = P_t/(4\pi R^2) \tag{1.20}$$

where P_t is the peak transmitted power and $4\pi R^2$ is the surface area of a sphere of radius R. Radar systems utilize directional antennas in order to increase the power density in a certain direction. Directional antennas are usually characterized by the antenna gain G and the antenna effective aperture A_e. They are related by

$$G = (4\pi A_e)/\lambda^2 \tag{1.21}$$

where λ is the wavelength. The relationship between the antenna's effective aperture A_e and the physical aperture A is

$$A_e = \rho A \qquad 0 \le \rho \le 1 \tag{1.22}$$

ρ is referred to as the aperture efficiency, and good antennas require $\rho \to 1$. In this book we will assume, unless otherwise noted, that A and A_e are the same. We will also assume that antennas have the same gain in the transmitting and receiving modes. In practice, $\rho \approx 0.7$ is widely accepted.

The gain is also related to the antenna's azimuth and elevation beam widths by

$$G = K\frac{4\pi}{\theta_e \theta_a} \tag{1.23}$$

where $K \le 1$ and depends on the physical aperture shape; the angles θ_e and θ_a are the antenna's elevation and azimuth beam widths, respectively, in radians. When the antenna has a continuous aperture, an excellent approximation of Eq. (1.23) can be written as

$$G \approx \frac{26000}{\theta_e \theta_a} \tag{1.24}$$

where in this case the azimuth and elevation beam widths are given in degrees.

The power density at a distance R away from a radar using a directive antenna of gain G is then given by

$$P_D = \frac{P_t G}{4\pi R^2} \tag{1.25}$$

When the radar radiated energy impinges on a target, the induced surface currents on that target radiate electromagnetic energy in all directions. The amount of the radiated energy is proportional to the target size, orientation, physical shape, and material, which are all lumped together in one target-specific parameter called the Radar Cross Section (RCS) denoted by σ.

The radar cross section is defined as the ratio of the power reflected back to the radar to the power density incident on the target,

$$\sigma = \frac{P_r}{P_D} \ m^2 \tag{1.26}$$

where P_r is the power reflected from the target. The total power delivered to the radar receiver at the back-end of the antenna is

$$P_r = \frac{P_t G \sigma}{(4\pi R^2)^2} A_e \tag{1.27}$$

Substituting the value of A_e from Eq. (1.21) into Eq. (1.27) yields

$$P_r = \frac{P_t G^2 \lambda^2 \sigma}{(4\pi)^3 R^4} \tag{1.28}$$

Let S_{min} denote the minimum detectable signal power. It follows that the maximum radar range R_{max} is

$$R_{max} = \left(\frac{P_t G^2 \lambda^2 \sigma}{(4\pi)^3 S_{min}} \right)^{1/4} \tag{1.29}$$

Equation (1.29) suggests that in order to double the radar maximum range one must increase the peak transmitted power P_t sixteen times; or equivalently, one must increase the effective aperture four times.

In practical situations the returned signals received by the radar will be corrupted with noise, which introduces unwanted voltages at all radar frequencies. Noise is random in nature and can be described by its Power Spectral Density (PSD) function. The noise power N is a function of the radar operating bandwidth, B. More precisely

$$N = Noise\ \ PSD \times B \tag{1.30}$$

The receiver input noise power is

$$N_i = kT_0B \tag{1.31}$$

where $k = 1.38 \times 10^{-23}\ Joule/degree\ Kelvin$ is Boltzmann's constant, and $T_0 = 290$ is the receiver input noise temperature in degrees Kelvin. It is always desirable that the minimum detectable signal (S_{min}) be greater than the noise power. The sensitivity of a radar receiver is normally described by a figure of merit called the noise figure F (see Section 1.9 for details). The noise figure is defined as

$$F = \frac{(SNR)_i}{(SNR)_o} = \frac{S_i/N_i}{S_o/N_o} \tag{1.32}$$

$(SNR)_i$ and $(SNR)_o$ are, respectively, the Signal to Noise Ratios (SNR) at the input and output of the receiver. The input signal power is S_i; and the input noise power immediately at the antenna terminal is N_i. The values S_o and N_o are, respectively, the output signal and noise power.

The receiver effective noise temperature excluding the antenna is (see Section 1.9)

$$T_e = T_0(F-1) \tag{1.33}$$

where F is the receiver noise figure. It follows that the total effective system noise temperature T_s is given by

$$T_s = T_e + T_a = T_0(F-1) + T_a = T_0F - T_0 + T_a \tag{1.34}$$

where T_a is the antenna temperature.

In many radar applications it is desirable to set the antenna temperature T_a to T_0 and thus, Eq. (1.34) is reduced to

$$T_s = T_0F \tag{1.35}$$

Using Eq. (1.35) and Eq. (1.31) in Eq. (1.32) yields

$$S_i = kT_0BF(SNR)_o \tag{1.36}$$

The minimum detectable signal power can be written as

$$S_{min} = kT_0BF(SNR)_{o_{min}} \tag{1.37}$$

The radar detection threshold is set equal to the minimum output SNR, $(SNR)_{o_{min}}$. Substituting Eq. (1.37) in Eq. (1.29) gives

$$R_{max} = \left(\frac{P_tG^2\lambda^2\sigma}{(4\pi)^3kT_0BF(SNR)_{o_{min}}} \right)^{1/4} \tag{1.38}$$

or equivalently,

$$(SNR)_{o_{min}} = \frac{P_tG^2\lambda^2\sigma}{(4\pi)^3kT_0BFR_{max}^4} \tag{1.39}$$

In general, radar losses denoted as L reduce the overall SNR, and hence

$$(SNR)_o = \frac{P_tG^2\lambda^2\sigma}{(4\pi)^3kT_0BFLR^4} \tag{1.40}$$

Equivalently, Eq. (1.40) can be rewritten using Eq. (1.35) as

$$(SNR)_o = \frac{P_tG^2\lambda^2\sigma}{(4\pi)^3kT_sBLR^4} \tag{1.41}$$

In this book, the antenna temperature is assumed to be negligible; therefore, Eq. (1.40) will be dominantly used as the Radar Equation.

Example:

Given a certain C-band radar with the following parameters: Peak power $P_t = 1.5MW$, *operating frequency* $f_0 = 5.6GHz$, *antenna gain* $G = 45dB$, *effective temperature* $T_0 = 290K$, *noise figure* $F = 3dB$, *pulse width* $\tau = 0.2\mu\text{sec}$. *The radar threshold is* $(SNR)_{min} = 20dB$. *Assume target cross section* $\sigma = 0.1m^2$. *Compute the maximum range.*

Solution:

The radar bandwidth is

$$B = \frac{1}{\tau} = \frac{1}{0.2 \times 10^{-6}} = 5MHz$$

The wavelength is

$$\lambda = \frac{c}{f_0} = \frac{3 \times 10^8}{5.6 \times 10^9} = 0.054m$$

From Eq. (1.40) we have

$$(R^4)_{dB} = (P_t + G^2 + \lambda^2 + \sigma - (4\pi)^3 - kT_0B - F - (SNR)_{o_{min}})_{dB}$$

where, before summing, the dB calculations are carried out for each of the individual parameters on the right-hand side. We can now construct the following table with all parameters computed in dB:

P_t	λ^2	G^2	kT_0B	$(4\pi)^3$	F	$(SNR)_{o_{min}}$	σ
61.761	–25.421	$90dB$	–136.987	32.976	$3dB$	$20dB$	–10

It follows that

$$R^4 = 61.761 + 90 - 25.352 - 10 - 32.976 + 136.987 - 3 - 20 = 197.420dB$$

$$R^4 = 10^{(197.420/10)} = 55.208 \times 10^{18}m^4$$

$$R = \sqrt[4]{55.208 \times 10^{18}} = 86.199Km$$

Thus, the maximum detection range is $86.2Km$.

Figure 1.9 shows plots of the SNR versus detection range for the following parameters: Peak power $P_t = 1.5MW$, operating frequency $f_0 = 5.6GHz$, antenna gain $G = 45dB$, radar losses $L = 6dB$, and noise figure $F = 3dB$. The radar bandwidth is $B = 5MHz$. The radar minimum and maximum detection ranges are $R_{min} = 25Km$ and $R_{max} = 165Km$. This figure can be reproduced using the following MATLAB code which utilizes MATLAB function *"radar_eq.m."*

```
close all;
clear all
pt = 1.5e+6; % peak power in Watts
freq = 5.6e+9; % radar operating frequency in Hz
g = 45.0; % antenna gain in dB
sigma = 0.1; % radar cross section in m squared
b = 5.0e+6; % radar operating bandwidth in Hz
nf = 3.0; %  noise figure in dB
loss = 6.0; % radar losses in dB
range = linspace(25e3,165e3,1000);
snr = radar_eq(pt, freq, g, sigma, b, nf, loss, range);
rangekm  = range ./ 1000;
plot(rangekm,snr,'linewidth',1.5)
grid;
xlabel ('Detection range in Km');
ylabel ('SNR in dB');
```

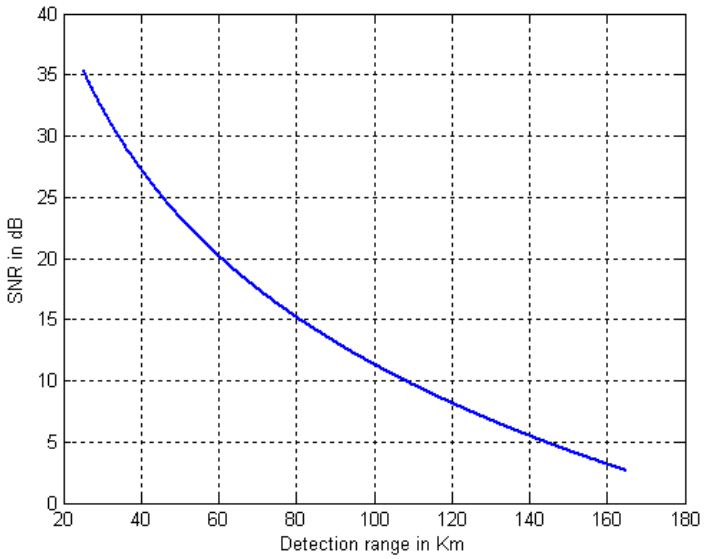

Figure 1.9. SNR versus detection range.

1.6. Surveillance Radar Equation

The first task a certain radar system has to accomplish is to continuously scan a specified volume in space searching for targets of interest. Once detection is established, target information such as range, angular position, and possibly target velocity are extracted by the radar signal and data processors. Depending on the radar design and antenna, different search patterns can be adopted.

Search volumes are normally specified by a search solid angle Ω in steradians, as illustrated in Fig. 1.10. Define the radar search volume extent for both azimuth and elevation as Θ_A and Θ_E. Consequently, the search volume is computed as

$$\Omega = (\Theta_A \Theta_E)/(57.296)^2 \quad steradians \tag{1.42}$$

where both Θ_A and Θ_E are given in degrees. The radar antenna $3dB$ beamwidth can be expressed in terms of its azimuth and elevation beam widths θ_a and θ_e, respectively. It follows that the antenna solid angle coverage is $\theta_a \theta_e$ and, thus, the number of antenna beam positions n_B required to cover a solid angle Ω is

$$n_B = \frac{\Omega}{\theta_a \theta_e} \tag{1.43}$$

In order to develop the search radar equation, start with Eq. (140). Using the relations $\tau = 1/B$ and $P_t = P_{av}T/\tau$, where T is the PRI and τ is the pulse width, yields

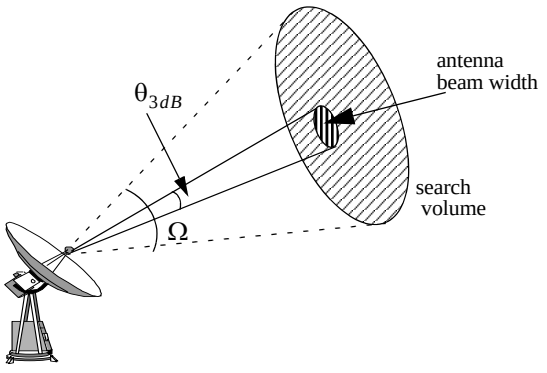

Figure 1.10. A cut in space showing the antenna beam width and the search volume.

$$SNR = \frac{T}{\tau} \frac{P_{av} G^2 \lambda^2 \sigma \tau}{(4\pi)^3 k T_0 F L R^4} \tag{1.44}$$

Define the time it takes the radar to scan a volume defined by the solid angle Ω as the scan time T_{sc}. The time on target can then be expressed in terms of T_{sc} as

$$T_i = \frac{T_{sc}}{n_B} = \frac{T_{sc}}{\Omega} \theta_a \theta_e \tag{1.45}$$

Assume that during a single scan only one pulse per beam per PRI illuminates the target. It follows that $T_i = T$ and, thus, Eq. (1.44) can be written as

$$SNR = \frac{P_{av} G^2 \lambda^2 \sigma}{(4\pi)^3 k T_0 F L R^4} \frac{T_{sc}}{\Omega} \theta_a \theta_e \tag{1.46}$$

Substituting Eq. (1.21) and Eq. (1.45) into Eq. (1.46) and collecting terms yield the search radar equation (based on a single pulse per beam per PRI) as

$$SNR = \frac{P_{av} A_e \sigma}{4\pi k T_0 F L R^4} \frac{T_{sc}}{\Omega} \tag{1.47}$$

The quantity $P_{av}A$ in Eq. (1.47) is known as the power aperture product. In practice, the power aperture product (PAP) is widely used to categorize the radar's ability to fulfill its search mission. Normally, a power aperture product is computed to meet a predetermined SNR and radar cross section for a given search volume defined by Ω.

Figure 1.11 shows a plot of the PAP versus detection range. using the following parameters:

σ	T_{sc}	$\theta_e = \theta_a$	R	$F + L$	SNR
$0.1\ m^2$	$2.5\,\text{sec}$	$2°$	$250Km$	$13dB$	$15dB$

This figure can be reproduced using the following MATLAB code which utilizes the MATLAB function *"power_aperture.m."*

```
close all;
clear all;
tsc = 2.5; % scan time is 2.5 seconds
sigma = 0.1; % radar cross section in m squared
te = 900.0; % effective noise temperature in Kelvin
snr = 15; % desired SNR in dB
nf = 6.0; % noise figure in dB
```

```
loss = 7.0; % radar losses in dB
az_angle = 2; % search volume azimuth extent in degrees
el_angle = 2; % search volume elevation extent in degrees
range = linspace(20e3,250e3,1000);
pap = power_aperture(snr,tsc,sigma/10,range,nf,loss,az_angle,el_angle);
rangekm  = range ./ 1000;
plot(rangekm,pap,'linewidth',1.5)
grid
xlabel ('Detection range in Km');
ylabel ('Power aperture product in dB');
```

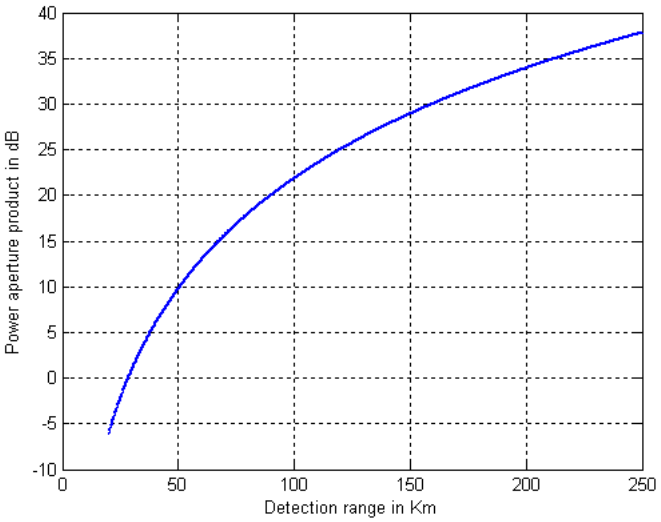

Figure 1.11. Power aperture product versus detection range.

Example:

Compute the power aperture product corresponding to the radar that has the following parameters: Scan time $T_{sc} = 2s$, *noise figure* $F = 8dB$, *losses* $L = 6dB$, *search volume* $\Omega = 7.4\ steradians$, *range of interest* $R = 75Km$, *and required SNR* $20dB$. *Assume that* $\sigma = 3.162m^2$.

Solution:

Note that $\Omega = 7.4\ steradians$ *corresponds to a search sector that is three fourths of a hemisphere. Thus, we conclude that* $\Theta_a = 180°$ *and* $\Theta_e = 135°$. *Using the MATLAB function "power_aperture.m" with the following syntax:*

PAP = power_aperture(20, 2, 3.162, 75e3, 8, 6, 180, 135)

one computes the power aperture product as 36.2 dB.

Example:

Compute the power aperture product for an X-band radar with the following parameters: Signal-to-noise ratio $SNR = 15dB$*; losses* $L = 8dB$*; search volume* $\Omega = 2°$*; scan time* $T_{sc} = 2.5s$*; noise figure* $F = 5dB$*. Assume a* $-10dBsm$ *target cross section, and range* $R = 250Km$*. Also, compute the peak transmitted power corresponding to 30% duty factor if the antenna gain is 45 dB. Assume a circular aperture.*

Solution:

The angular coverage is $2°$ *in both azimuth and elevation. It follows that the solid angle coverage is*

$$\Omega = \frac{2 \times 2}{(57.23)^2} = -29.132dB$$

Note that the factor $360/2\pi = 57.23$ *converts degrees into steradians. When the aperture is circular Eq. (1.47) is reduced to (details are left as an exercise)*

$$(SNR)_{dB} = (P_{av} + A + \sigma + T_{sc} - 16 - R^4 - kT_0 - L - F - \Omega)_{dB}$$

σ	T_{sc}	16	R^4	kT_0
–10	3.979	12.041	215.918	–203.977

It follows that

$$15 = P_{av} + A - 10 + 3.979 - 12.041 - 215.918 + 203.977 - 5 - 8 + 29.133$$

Then the power aperture product is

$$P_{av} + A = 38.716dB$$

Now, assume the radar wavelength to be $\lambda = 0.03m$*, then*

$$A = \frac{G\lambda^2}{4\pi} = 3.550dB$$

$$P_{av} = -A + 38.716 = 35.166dB$$

$$P_{av} = 10^{3.5166} = 3285.489W$$

$$P_t = \frac{P_{av}}{d_t} = \frac{3285.489}{0.3} = 10.9512KW$$

1.7. Radar Cross Section

Electromagnetic waves are normally diffracted or scattered in all directions when incident on a target. These scattered waves are broken down into two parts. The first part is made of waves that have the same polarization as the receiving antenna. The other portion of the scattered waves will have a different polarization to which the receiving antenna does not respond. The two polarizations are orthogonal and are referred to as the Principal Polarization (PP) and Orthogonal Polarization (OP), respectively. The intensity of the *backscattered* energy that has the same polarization as the radar's receiving antenna is used to define the target RCS. When a target is illuminated by RF energy, it acts like a virtual antenna and will have near and far scattered fields. Waves reflected and measured in the near field are, in general, spherical. Alternatively, in the far field the wavefronts are decomposed into a linear combination of plane waves. Assume the power density of a wave incident on a target located at range R away from the radar is P_{Di}, as illustrated in Fig. 1.12. The amount of reflected power from the target is

$$P_r = \sigma P_{Di} \tag{1.48}$$

where σ denotes the target cross section. Define P_{Dr} as the power density of the scattered waves at the receiving antenna. It follows that

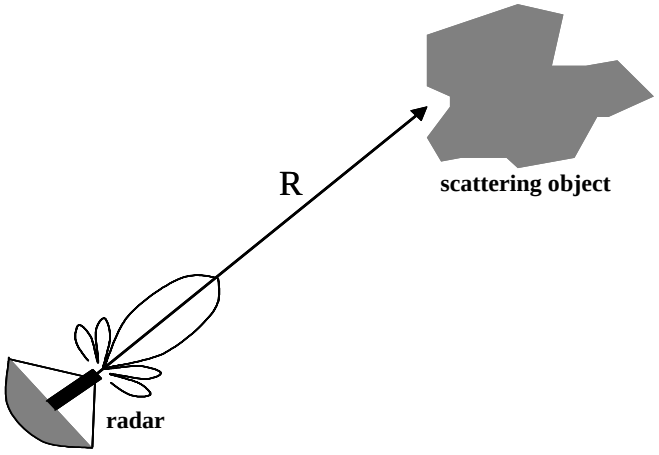

Figure 1.12. Scattering object located at range R.

$$P_{Dr} = P_r/(4\pi R^2) \tag{1.49}$$

Equating Eqs. (1.48) and (1.49) yields

$$\sigma = 4\pi R^2\left(\frac{P_{Dr}}{P_{Di}}\right) \tag{1.50}$$

and in order to ensure that the radar receiving antenna is in the far field (i.e., scattered waves received by the antenna are planar), Eq. (1.50) is modified to

$$\sigma = 4\pi R^2 \lim_{R\to\infty}\left(\frac{P_{Dr}}{P_{Di}}\right) \tag{1.51}$$

The RCS defined by Eq. (1.51) is often referred to as either the monostatic RCS, the backscattered RCS, or simply target RCS.

The backscattered RCS is measured from all waves scattered in the direction of the radar and has the same polarization as the receiving antenna. It represents a portion of the total scattered target RCS σ_t, where $\sigma_t > \sigma$. Assuming a spherical coordinate system defined by (ρ, θ, φ), then at range ρ the target scattered cross section is a function of (θ, φ). Let the angles (θ_i, φ_i) define the direction of propagation of the incident waves. Also, let the angles (θ_s, φ_s) define the direction of propagation of the scattered waves. The special case, when $\theta_s = \theta_i$ and $\varphi_s = \varphi_i$, defines the monostatic RCS. The RCS measured by the radar at angles $\theta_s \neq \theta_i$ and $\varphi_s \neq \varphi_i$ is called the bistatic RCS.

The total target scattered RCS is given by

$$\sigma_t = \frac{1}{4\pi}\int_{\varphi_s=0}^{2\pi}\int_{\theta_s=0}^{\pi}\sigma(\theta_s, \varphi_s)\sin\theta_s \; d\theta \; d\varphi_s \tag{1.52}$$

The amount of backscattered waves from a target is proportional to the ratio of the target extent (size) to the wavelength, λ, of the incident waves. In fact, a radar will not be able to detect targets much smaller than its operating wavelength. The frequency region, where the target extent and the wavelength are comparable, is referred to as the Rayleigh region. Alternatively, the frequency region where the target extent is much larger than the radar operating wavelength is referred to as the optical region.

1.7.1. RCS Dependency on Aspect Angle and Frequency

Radar cross section fluctuates as a function of radar aspect angle and frequency. For the purpose of illustration, isotropic point scatterers are considered. Consider the geometry shown in Fig. 1.13. In this case, two unity $(1m^2)$

isotropic scatterers are aligned and placed along the radar line of sight (zero aspect angle) at a far field range R. The spacing between the two scatterers is 1 meter. The radar aspect angle is then changed from zero to 180 degrees, and the composite RCS of the two scatterers measured by the radar is computed.

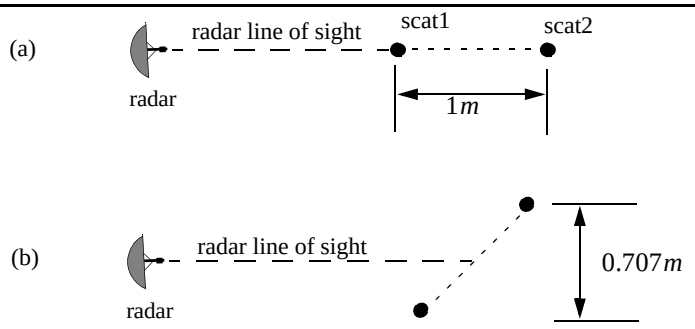

Figure 1.13. RCS dependency on aspect angle. (a) Zero aspect angle, zero electrical spacing. (b) $45°$ **aspect angle,** 1.414λ **electrical spacing.**

This composite RCS consists of the superposition of the two individual radar cross sections. At zero aspect angle, the composite RCS is $2m^2$. Taking scatterer-1 as a phase reference, when the aspect angle is varied, the composite RCS is modified by the phase that corresponds to the electrical spacing between the two scatterers. For example, at aspect angle $10°$, the electrical spacing between the two scatterers is

$$elec\text{–}spacing = \frac{2 \times (1.0 \times \cos(10°))}{\lambda} \quad \textbf{(1.53)}$$

λ is the radar operating wavelength.

Figure 1.14 shows the composite RCS corresponding to this experiment. This plot can be reproduced using the MATLAB code listed below. As clearly indicated by Fig. 1.14, RCS is dependent on the radar aspect angle; thus, knowledge of this constructive and destructive interference between the individual scatterers can be very critical when a radar tries to extract the RCS of complex or maneuvering targets. This is true for two reasons. First, the aspect angle may be continuously changing. Second, complex target RCS can be viewed to be made up from contributions of many individual scattering points distributed on the target surface. These scattering points are often called scattering centers. Many approximate RCS prediction methods generate a set of scattering centers that define the backscattering characteristics of such complex targets. The figures can be reproduced using the following MATLAB program.

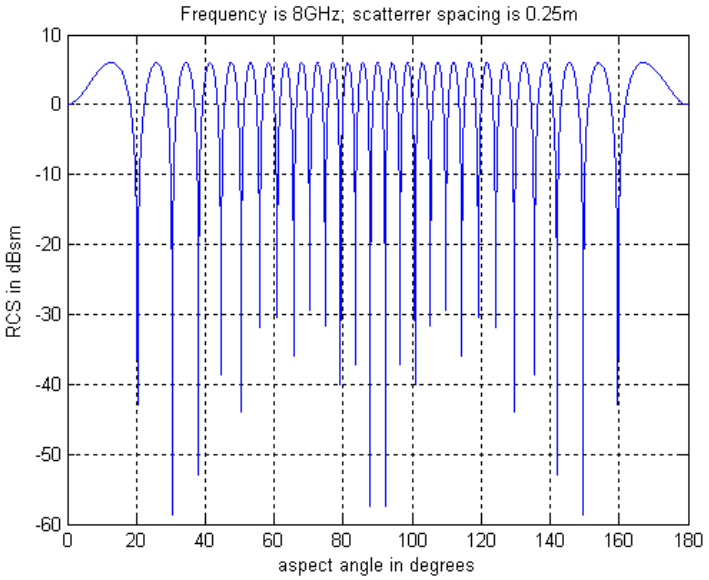

Figure 1.14. Illustration of RCS dependency on aspect angle.

```
clear all; close all;
% This program produces Fig. 1.14. This code demonstrates the effect of aspect angle
% on RCS. The radar is observing two unity point scatterers separated by scat_spacing.
% Initially the two scatterers are aligned with radar line of sight. The aspect angle is
% changed from 0 degrees to 180 degrees and the equivalent RCS is computed.
% The RCS as measured by the radar versus aspect angle is then plotted.
scat_spacing = 0.25; % 0.25 meter scatterers spacing
freq = 8e9; % operating frequency
eps = 0.00001;
wavelength = 3.0e+8 / freq;
% Compute aspect angle vector
aspect_degrees = linspace(0, 180, 500);
aspect_radians = (pi/180) .* aspect_degrees;
% Compute electrical scatterer spacing vector in wavelength units
elec_spacing = (2.0 * scat_spacing / wavelength) .* cos(aspect_radians);
% Compute RCS (rcs = RCS_scat1 + RCS_scat2)
% Scat1 is taken as phase reference point
rcs = abs(1.0 + cos((2.0 * pi) .* elec_spacing) + i * sin((2.0 * pi) .* elec_spacing));
rcs = rcs + eps;
rcs = 20.0*log10(rcs); % RCS in dBsm
% Plot RCS versus aspect angle
figure (1);
plot(aspect_degrees,rcs);
```

```
grid; xlabel('aspect angle in degrees'); ylabel('RCS in dBsm');
title(' Frequency is 8GHz; scatterer spacing is 0.25m');
```

Next, to demonstrate RCS dependency on frequency, consider the experiment shown in Fig. 1.15. In this case, two far field unity isotropic scatterers are aligned with radar line of sight, and the composite RCS is measured by the radar as the frequency is varied from 8 GHz to 12.5 GHz (X-band). Figs. 1.16 and 1.17 show the composite RCS versus frequency for scatterer spacing of 0.25 and 0.75 meters. The figures can be reproduced using the following MATLAB function.

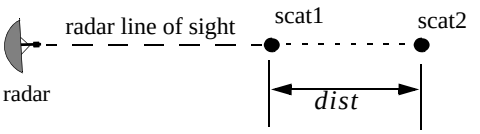

Figure 1.15. Experiment setup which demonstrates RCS dependency on frequency; dist = 0.25, or 0.75 m.

```
clear all; close all;
% This program demonstrates the dependency of RCS on wavelength
% The radar line of sight is aligned with the two scatterers
% A plot of RCS variation versus frequency if produced
eps = 0.0001;
scat_spacing = 0.25;
freql = 8e9;
frequ = 12.5e9;
freq = linspace(freql,frequ,500);
wavelength = 3.0e+8 ./ freq;
% Compute electrical scatterer spacing vector in wavelength units
elec_spacing = 2.0 * scat_spacing ./ wavelength;
% Compute RCS (RCS = RCS_scat1 + RCS_scat2)
rcs = abs (  1 + cos((2.0 * pi) .* elec_spacing) ...
          + i * sin((2.0 * pi) .* elec_spacing));
rcs = rcs + eps;
rcs = 20.0*log10(rcs); % RCS ins dBsm
% Plot RCS versus frequency
figure (1);
plot(freq./1e9,rcs);
grid;
xlabel('Frequency in GHz');
ylabel('RCS in dBsm');
% title(' X=Band; scatterer spacing is 0.25 m'); % Fig. 1.16
% title(' X=Band; scatterer spacing is 0.75 m'); % Fig. 1.17
```

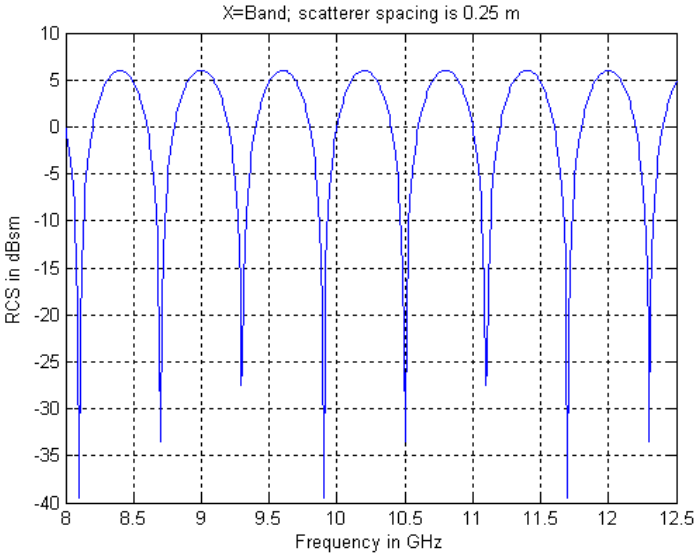

Figure 1.16. Illustration of RCS dependency on frequency.

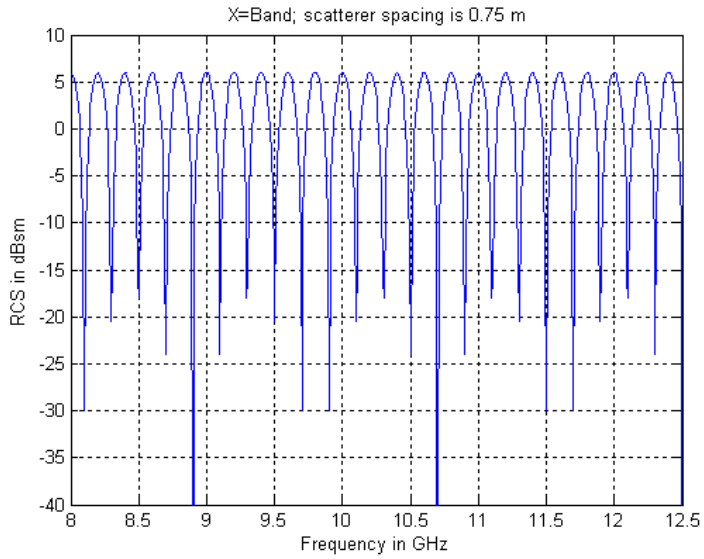

Figure 1.17. Illustration of RCS dependency on frequency.

1.7.2. RCS Dependency on Polarization

Normalized Electric Field

In most radar simulations, it is desirable to obtain the complex-valued electric field scattered by the target at the radar. In such cases, it is useful to use a quantity called the normalized electric field. It is assumed that the incident electric field has a magnitude of unity and is phase centered at a point at the target (usually the center of gravity). More precisely,

$$E_i = e^{jk(\vec{r}_i \cdot \vec{r})} \tag{1.54}$$

where $\vec{r}_i$ is the direction of incidence and $\vec{r}$ a location at the target, each with respect to the phase center. The normalized scattered field is then given by

$$E_s = \sigma E_i \tag{1.55}$$

The quantity E_s is independent of radar and target location. It may be combined with an incident magnitude and phase.

Polarization

The x and y electric field components for a wave traveling along the positive z direction are given by

$$E_x = E_1 \sin(\omega t - kz) \tag{1.56}$$

$$E_y = E_2 \sin(\omega t - kz + \delta) \tag{1.57}$$

where $k = 2\pi/\lambda$, ω is the wave frequency, the angle δ is the time phase angle at which E_y leads E_x, and finally, E_1 and E_2 are, respectively, the wave amplitudes along the x and y directions. When two or more electromagnetic waves combine, their electric fields are integrated vectorially at each point in space for any specified time. In general, the combined vector traces an ellipse when observed in the x-y plane. This is illustrated in Fig. 1.18.

The ratio of the major to the minor axes of the polarization ellipse is called the Axial Ratio (AR). When AR is unity, the polarization ellipse becomes a circle, and the resultant wave is then called circularly polarized. Alternatively, when $E_1 = 0$ and $AR = \infty$, the wave becomes linearly polarized.

Equations (1.56) and (1.57) can be combined to give the instantaneous total electric field,

$$\vec{E} = \hat{a}_x E_1 \sin(\omega t - kz) + \hat{a}_y E_2 \sin(\omega t - kz + \delta) \tag{1.58}$$

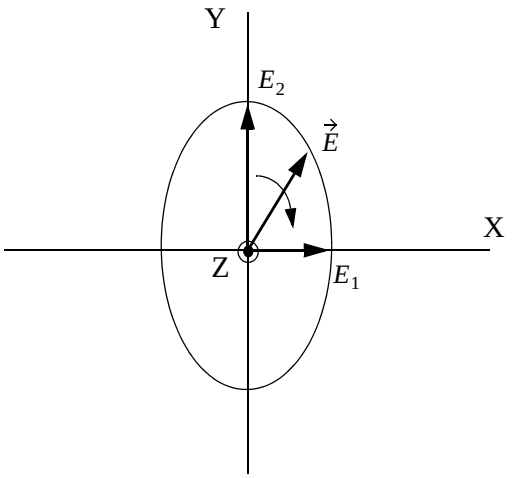

Figure 1.18. Electric field components along the x and y directions. The positive z direction is out of the page.

where $\hat{a}_x$ and $\hat{a}_y$ are unit vectors along the x and y directions, respectively. At $z = 0$, $E_x = E_1 \sin(\omega t)$ and $E_y = E_2 \sin(\omega t + \delta)$, then by replacing $\sin(\omega t)$ by the ratio E_x / E_1 and by using trigonometry properties Eq. (1.58) can be rewritten as

$$\frac{E_x^2}{E_1^2} - \frac{2E_x E_y \cos\delta}{E_1 E_2} + \frac{E_y^2}{E_2^2} = (\sin\delta)^2 \qquad \textbf{(1.59)}$$

which has no dependency on ωt.

In the most general case, the polarization ellipse may have any orientation, as illustrated in Fig. 1.19. The angle ξ is called the tilt angle of the ellipse. In this case, AR is given by

$$AR = \frac{OA}{OB} \qquad (1 \le AR \le \infty) \qquad \textbf{(1.60)}$$

When $E_1 = 0$, the wave is said to be linearly polarized in the y direction, while if $E_2 = 0$, the wave is said to be linearly polarized in the x direction. Polarization can also be linear at an angle of $45°$ when $E_1 = E_2$ and $\xi = 45°$. When $E_1 = E_2$ and $\delta = 90°$, the wave is said to be Left Circularly Polarized (LCP), while if $\delta = -90°$ the wave is said to Right Circularly Polarized (RCP). It is a common notation to call the linear polarizations along the x and y directions by the names horizontal and vertical polarizations, respectively.

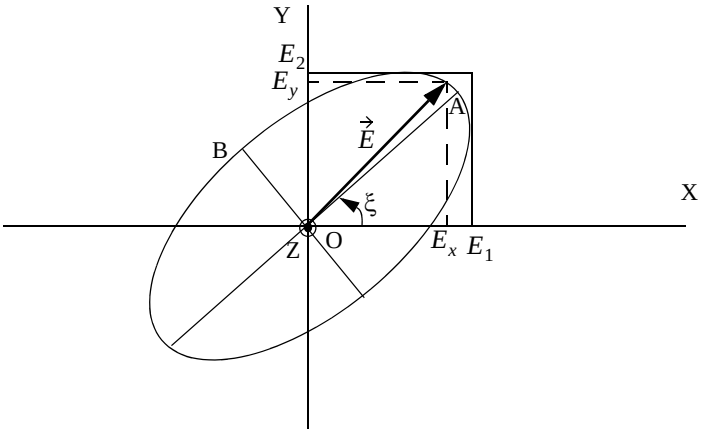

Figure 1.19. Polarization ellipse in the general case.

In general, an arbitrarily polarized electric field may be written as the sum of two circularly polarized fields. More precisely,

$$\vec{E} = \overrightarrow{E_R} + \overrightarrow{E_L} \tag{1.61}$$

where $\overrightarrow{E_R}$ and $\overrightarrow{E_L}$ are the RCP and LCP fields, respectively. Similarly, the RCP and LCP waves can be written as

$$\overrightarrow{E_R} = \overrightarrow{E_V} + j\overrightarrow{E_H} \tag{1.62}$$

$$\overrightarrow{E_L} = \overrightarrow{E_V} - j\overrightarrow{E_H} \tag{1.63}$$

where $\overrightarrow{E_V}$ and $\overrightarrow{E_H}$ are the fields with vertical and horizontal polarizations, respectively. Combining Eqs. (1.62) and (1.63) yields

$$E_R = \frac{E_H - jE_V}{\sqrt{2}} \tag{1.64}$$

$$E_L = \frac{E_H + jE_V}{\sqrt{2}} \tag{1.65}$$

Using matrix notation, Eqs. (1.64) and (1.65) can be rewritten as

$$\begin{bmatrix} E_R \\ E_L \end{bmatrix} = \frac{1}{\sqrt{2}} \begin{bmatrix} 1 & -j \\ 1 & j \end{bmatrix} \begin{bmatrix} E_H \\ E_V \end{bmatrix} = [T] \begin{bmatrix} E_H \\ E_V \end{bmatrix} \tag{1.66}$$

$$\begin{bmatrix} E_H \\ E_V \end{bmatrix} = \frac{1}{\sqrt{2}} \begin{bmatrix} 1 & 1 \\ j & -j \end{bmatrix} \begin{bmatrix} E_R \\ E_L \end{bmatrix} = [T]^{-1} \begin{bmatrix} E_H \\ E_V \end{bmatrix} \tag{1.67}$$

For many targets the scattered waves will have different polarization than the incident waves. This phenomenon is known as depolarization or cross-polarization. However, perfect reflectors reflect waves in such a fashion that an incident wave with horizontal polarization remains horizontal, and an incident wave with vertical polarization remains vertical but is phase shifted $180°$. Additionally, an incident wave that is RCP becomes LCP when reflected, and a wave that is LCP becomes RCP after reflection from a perfect reflector. Therefore, when a radar uses LCP waves for transmission, the receiving antenna needs to be RCP polarized in order to capture the PP RCS, and LCP to measure the OP RCS.

Target Scattering Matrix

Target backscattered RCS is commonly described by a matrix known as the scattering matrix and is denoted by $[S]$. When an arbitrarily linearly polarized wave is incident on a target, the backscattered field is then given by

$$\begin{bmatrix} E_1^s \\ E_2^s \end{bmatrix} = [S] \begin{bmatrix} E_1^i \\ E_2^i \end{bmatrix} = \begin{bmatrix} s_{11} & s_{12} \\ s_{21} & s_{22} \end{bmatrix} \begin{bmatrix} E_1^i \\ E_2^i \end{bmatrix} \tag{1.68}$$

The superscripts i and s denote incident and scattered fields. The quantities s_{ij} are in general complex and the subscripts 1 and 2 represent any combination of orthogonal polarizations. More precisely, $1 = H, R$, and $2 = V, L$. From Eq. (1.50), the backscattered RCS is related to the scattering matrix components by the following relation:

$$\begin{bmatrix} \sigma_{11} & \sigma_{12} \\ \sigma_{21} & \sigma_{22} \end{bmatrix} = 4\pi R^2 \begin{bmatrix} |s_{11}|^2 & |s_{12}|^2 \\ |s_{21}|^2 & |s_{22}|^2 \end{bmatrix} \tag{1.69}$$

It follows that once a scattering matrix is specified, the target backscattered RCS can be computed for any combination of transmitting and receiving polarizations. The reader is advised to see Ruck et al. (1970) for ways to calculate the scattering matrix $[S]$. Rewriting Eq. (1.69) in terms of the different possible orthogonal polarizations yields

$$\begin{bmatrix} E_H^s \\ E_V^s \end{bmatrix} = \begin{bmatrix} s_{HH} & s_{HV} \\ s_{VH} & s_{VV} \end{bmatrix} \begin{bmatrix} E_H^i \\ E_V^i \end{bmatrix} \tag{1.70}$$

$$\begin{bmatrix} E_R^s \\ E_L^s \end{bmatrix} = \begin{bmatrix} s_{RR} & s_{RL} \\ s_{LR} & s_{LL} \end{bmatrix} \begin{bmatrix} E_R^i \\ E_L^i \end{bmatrix} \tag{1.71}$$

By using the transformation matrix $[T]$ in Eq. (1.66), the circular scattering elements can be computed from the linear scattering elements

$$\begin{bmatrix} s_{RR} & s_{RL} \\ s_{LR} & s_{LL} \end{bmatrix} = [T] \begin{bmatrix} s_{HH} & s_{HV} \\ s_{VH} & s_{VV} \end{bmatrix} \begin{bmatrix} 1 & 0 \\ 0 & -1 \end{bmatrix} [T]^{-1} \tag{1.72}$$

and the individual components are

$$s_{RR} = \frac{-s_{VV} + s_{HH} - j(s_{HV} + s_{VH})}{2} \tag{1.73}$$

$$s_{RL} = \frac{s_{VV} + s_{HH} + j(s_{HV} - s_{VH})}{2} \tag{1.74}$$

$$s_{LR} = \frac{s_{VV} + s_{HH} - j(s_{HV} - s_{VH})}{2} \tag{1.75}$$

$$s_{LL} = \frac{-s_{VV} + s_{HH} + j(s_{HV} + s_{VH})}{2} \tag{1.76}$$

Similarly, the linear scattering elements are given by

$$\begin{bmatrix} s_{HH} & s_{HV} \\ s_{VH} & s_{VV} \end{bmatrix} = [T]^{-1} \begin{bmatrix} s_{RR} & s_{RL} \\ s_{LR} & s_{LL} \end{bmatrix} \begin{bmatrix} 1 & 0 \\ 0 & -1 \end{bmatrix} [T] \tag{1.77}$$

and the individual components are

$$s_{HH} = \frac{-s_{RR} + s_{RL} + s_{LR} - s_{LL}}{2} \tag{1.78}$$

$$s_{VH} = \frac{j(s_{RR} - s_{LR} + s_{RL} - s_{LL})}{2} \tag{1.79}$$

$$s_{HV} = \frac{-j(s_{RR} + s_{LR} - s_{RL} - s_{LL})}{2} \tag{1.80}$$

$$s_{VV} = \frac{s_{RR} + s_{LL} + js_{RL} + s_{LR}}{2} \tag{1.81}$$

1.8. Radar Equation with Jamming

Any deliberate electronic effort intended to disturb normal radar operation is usually referred to as an Electronic Countermeasure (ECM). This may also include chaff, radar decoys, radar RCS alterations (e.g., radio frequency absorbing materials), and of course, radar jamming.

Jammers can be categorized into two general types: (1) barrage jammers and (2) deceptive jammers (repeaters). When strong jamming is present, detection capability is determined by receiver signal-to-noise plus interference ratio rather than SNR. In fact, in most cases, detection is established based on the signal-to-interference ratio alone.

Barrage jammers attempt to increase the noise level across the entire radar operating bandwidth. Consequently, this lowers the receiver SNR and, in turn, makes it difficult to detect the desired targets. This is the reason barrage jammers are often called maskers (since they mask the target returns). Barrage jammers can be deployed in the main beam or in the sidelobes of the radar antenna. If a barrage jammer is located in the radar main beam, it can take advantage of the antenna maximum gain to amplify the broadcasted noise signal. Alternatively, sidelobe barrage jammers must either use more power or operate at a much shorter range than main-beam jammers. Main-beam barrage jammers can either be deployed on-board the attacking vehicle or act as an escort to the target. Sidelobe jammers are often deployed to interfere with a specific radar, and since they do not stay close to the target, they have a wide variety of stand-off deployment options.

Repeater jammers carry receiving devices on board in order to analyze the radar's transmission and then send back false target-like signals in order to confuse the radar. There are two common types of repeater jammers: spot noise repeaters and deceptive repeaters. The spot noise repeater measures the transmitted radar signal bandwidth and then jams only a specific range of frequencies. The deceptive repeater sends back altered signals that make the target appear in some false position (ghosts). These ghosts may appear at different ranges or angles than the actual target. Furthermore, there may be several ghosts created by a single jammer. By not having to jam the entire radar bandwidth, repeater jammers are able to make more efficient use of their jamming power. Radar frequency agility may be the only way possible to defeat spot noise repeaters.

In general a jammer can be identified by its effective operating bandwidth B_J and by its Effective Radiated Power (ERP), which is proportional to the jammer transmitter power P_J. More precisely,

$$ERP = P_J G_J / L_J \tag{1.82}$$

where G_J is the jammer antenna gain and L_J is the total jammer loss. The effect of a jammer on a radar is measured by the Signal-to-Jammer ratio (S/J).

Consider a radar system whose detection range R in the absence of jamming is governed by

$$SNR = \frac{P_t G^2 \lambda^2 \sigma}{(4\pi)^3 k T_s B_r L R^4} \tag{1.83}$$

The term Range Reduction Factor (RRF) refers to the reduction in the radar detection range due to jamming. More precisely, in the presence of jamming the effective radar detection range is

$$R_{dj} = R \times RRF \tag{1.84}$$

In order to compute RRF, consider a radar characterized by Eq. (1.83) and a barrage jammer whose output power spectral density is J_o (i.e., Gaussian-like). Then the amount of jammer power in the radar receiver is

$$J = kT_J B_r \tag{1.85}$$

where T_J is the jammer effective temperature. It follows that the total jammer plus noise power in the radar receiver is given by

$$N_i + J = kT_s B_r + kT_J B_r \tag{1.86}$$

In this case, the radar detection range is now limited by the receiver signal-to-noise plus interference ratio rather than SNR. More precisely,

$$\left(\frac{S}{J+N}\right) = \frac{P_t G^2 \lambda^2 \sigma}{(4\pi)^3 k (T_s + T_J) B_r L R^4} \tag{1.87}$$

The amount of reduction in the signal-to-noise plus interference ratio because of the jammer effect can be computed from the difference between Eqs. (1.83) and (1.87). It is expressed (in dB) by

$$\Upsilon = 10.0 \times \log\left(1 + \frac{T_J}{T_s}\right) \tag{1.88}$$

Consequently, the RRF is

$$RRF = 10^{\frac{-\Upsilon}{40}} \tag{1.89}$$

Figures 1.20 a and b show typical value for the RRF versus the radar wavelength and detection range using the following parameters

Symbol	Value
te	*500 kelvin*
pj	*500 KW*
gj	*3 dB*
g	*45 dB*
freq	*10 GHz*
bj	*10 MHZ*
rangej	*750 Km*
lossj	*1 dB*

This figure can be reproduced using the following MATLAB code

```
clear all;
close all;
te = 730.0; % radar effective temp in Kelvin
pj  = 15; % jammer peak power in W
gj = 3.0; % jammer antenna gain in dB
g = 40.0; % radar antenna gain
freq = 10.0e+9; % radar operating frequency in Hz
bj  = 1.0e+6; % radar operating bandwidth in Hz
rangej = 400.0; % radar to jammer range in Km
lossj = 1.0; % jammer losses in dB
c = 3.0e+8;
k = 1.38e-23;
lambda = c / freq;
gj_10 = 10^( gj/10);
g_10 = 10^( g/10);
lossj_10 = 10^(lossj/10);
index = 0;
for wavelength = .01:.001:1
  index = index +1;
  jamer_temp = (pj * gj_10 * g_10 *wavelength^2) / ...
    (4.0^2 * pi^2 * k * bj * lossj_10 * (rangej * 1000.0)^2);
  delta = 10.0 * log10(1.0 + (jamer_temp / te));
  rrf(index) = 10^(-delta /40.0);
end
w = 0.01:.001:1;
figure (1)
semilogx(w,rrf,'k')
grid
xlabel ('Wavelength in meters')
ylabel ('Range reduction factor')
index = 0;
```

```
for ran =rangej*.3:10:rangej*2
  index = index + 1;
  jamer_temp = (pj * gj_10 * g_10 *lambda^2) / ...
    (4.0^2 * pi^2 * k * bj * lossj_10 * (ran * 1000.0)^2);
  delta = 10.0 * log10(1.0 + (jamer_temp / te));
  rrf1(index) = 10^(-delta /40.0);
end
figure(2)
ranvar = rangej*.3:10:rangej*2 ;
plot(ranvar,rrf1,'k')
grid
xlabel ('Radar to jammer range in Km')
ylabel ('Range reduction factor')
index = 0;
for pjvar = pj*.01:100:pj*2
  index = index + 1;
  jamer_temp = (pjvar * gj_10 * g_10 *lambda^2) / ...
    (4.0^2 * pi^2 * k * bj * lossj_10 * (rangej * 1000.0)^2);
  delta = 10.0 * log10(1.0 + (jamer_temp / te));
  rrf2(index) = 10^(-delta /40.0);
end
```

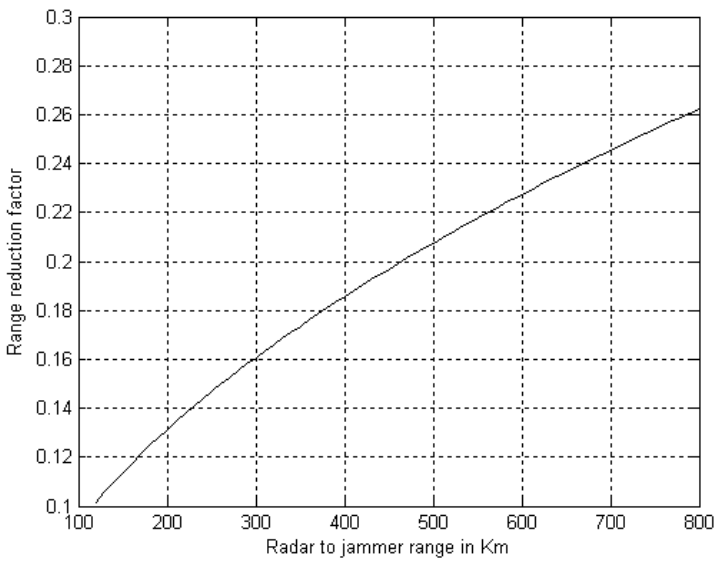

Figure 1.20a. Range reduction factor versus radar to jammer range. This plot was generated using the function *"range_red_factor.m."*

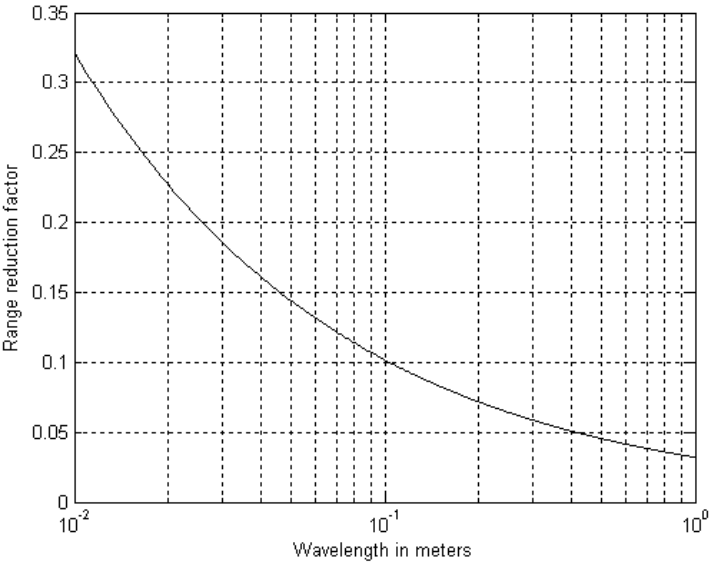

Figure 1.20b. Range reduction factor versus radar operating wavelength. This plot was generated using the function *"range_red_factor.m."*

1.9. Noise Figure

Any signal other than the target returns in the radar receiver is considered to be noise. This includes interfering signals from outside the radar and thermal noise generated within the receiver itself. Thermal noise (thermal agitation of electrons) and shot noise (variation in carrier density of a semiconductor) are the two main internal noise sources within a radar receiver.

The power spectral density of thermal noise is given by

$$S_n(\omega) = \frac{|\omega| h}{\pi\left[\exp\left(\frac{|\omega| h}{2\pi kT}\right) - 1\right]} \tag{1.90}$$

where $|\omega|$ is the absolute value of the frequency in radians per second, T is the temperature of the conducting medium in degrees Kelvin, k is Boltzman's constant, and h is Plank's constant ($h = 6.625 \times 10^{-34}$ $Joules$). When the condition $|\omega| \ll 2\pi kT/h$ is true, it can be shown that Eq. (1.90) is approximated by

$$S_n(\omega) \approx 2kT \tag{1.91}$$

This approximation is widely accepted, since, in practice, radar systems operate at frequencies less than $100GHz$; and, for example, if $T = 290K$, then $2\pi kT/h \approx 6000GHz$.

The mean-square noise voltage (noise power) generated across a $1\ ohm$ resistance is then

$$\langle n^2 \rangle = \frac{1}{2\pi} \int_{-2\pi B}^{2\pi B} 2kT \quad d\omega = 4kTB \tag{1.92}$$

where B is the system bandwidth. Any electrical system containing thermal noise and having input resistance R_{in} can be replaced by an equivalent noiseless system with a series combination of a noise equivalent voltage source and a noiseless input resistor R_{in} added at its input. This is illustrated in Fig. 1.21.

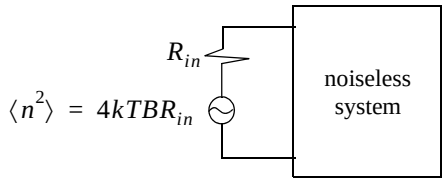

Figure 1.21. Noiseless system with an input noise voltage source.

The amount of noise power that can physically be extracted from $\langle n^2 \rangle$ is one fourth the value computed in Eq. (1.92). Consider a noisy system with power gain A_P, as shown in Fig. 1.22. The noise figure is defined by

$$F_{dB} = 10 \log \frac{total\ noise\ power\ out}{noise\ power\ out\ due\ to\ R_{in}\ alone} \tag{1.93}$$

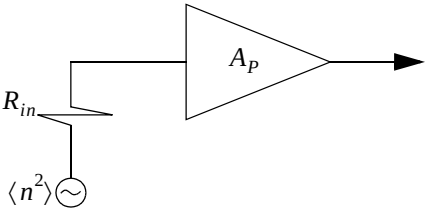

Figure 1.22. Noisy amplifier replaced by its noiseless equivalent and an input voltage source in series with a resistor.

More precisely,

$$F_{dB} = 10 \log \frac{N_o}{N_i A_p} \tag{1.94}$$

where N_o and N_i are, respectively, the noise power at the output and input of the system.

If we define the input and output signal power by S_i and S_o, respectively, then the power gain is

$$A_P = \frac{S_o}{S_i} \tag{1.95}$$

It follows that

$$F_{dB} = 10\log\left(\frac{S_i/Ni}{S_o/N_o}\right) = \left(\frac{S_i}{N_i}\right)_{dB} - \left(\frac{S_o}{N_o}\right)_{dB} \tag{1.96}$$

where

$$\left(\frac{S_i}{N_i}\right)_{dB} > \left(\frac{S_o}{N_o}\right)_{dB} \tag{1.97}$$

Thus, the noise figure is the loss in the signal-to-noise ratio due to the added thermal noise of the amplifier $((SNR)_o = (SNR)_i - F \ \ in \ \ dB)$.

One can also express the noise figure in terms of the system's effective temperature T_e. Consider the amplifier shown in Fig. 1.22, and let its effective temperature be T_e. Assume the input noise temperature is T_0. Thus, the input noise power is

$$N_i = kT_0B \tag{1.98}$$

and the output noise power is

$$N_o = kT_0B \ A_p + kT_eB \ A_p \tag{1.99}$$

where the first term on the right-hand side of Eq. (1.99) corresponds to the input noise, and the latter term is due to thermal noise generated inside the system. It follows that the noise figure can be expressed as

$$F = \frac{(SNR)_i}{(SNR)_o} = \frac{S_i}{kT_0B} \ kBA_p \ \frac{T_0 + T_e}{S_o} = 1 + \frac{T_e}{T_0} \tag{1.100}$$

Equivalently, we can write

$$T_e = (F-1)T_0 \tag{1.101}$$

Example:

An amplifier has a 4dB noise figure; the bandwidth is $B = 500\ KHz$. *Calculate the input signal power that yields a unity SNR at the output. Assume* $T_0 = 290K$ *and an input resistance of one ohm.*

Solution:

The input noise power is

$$kT_0B = 1.38 \times 10^{-23} \times 290 \times 500 \times 10^3 = 2.0 \times 10^{-15} W$$

Assuming a voltage signal, then the input noise mean squared voltage is

$$\langle n_i^2 \rangle = kT_oB = 2.0 \times 10^{-15}\ v^2$$

$$F = 10^{0.4} = 2.51$$

From the noise figure definition we get

$$\frac{S_i}{N_i} = F\left(\frac{S_o}{N_o}\right) = F$$

and

$$\langle s_i^2 \rangle = F\langle n_i^2 \rangle = 2.51 \times 2.0 \times 10^{-15} = 5.02 \times 10^{-15}\ v^2$$

Finally,

$$\sqrt{\langle s_i^2 \rangle} = 70.852nv$$

Consider a cascaded system as in Fig. 1.23. Network 1 is defined by noise figure F_1, power gain G_1, bandwidth B, and temperature T_{e1}. Similarly, network 2 is defined by F_2, G_2, B, and T_{e2}. Assume the input noise has temperature T_0.

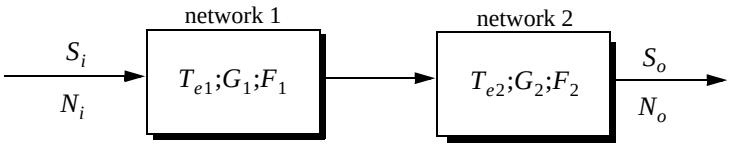

Figure 1.23. Cascaded linear system.

The output signal power is

$$S_o = S_i G_1 G_2 \tag{1.102}$$

The input and output noise powers are, respectively, given by

$$N_i = kT_0 B \tag{1.103}$$

$$N_o = kT_0 B G_1 G_2 + kT_{e1} B G_1 G_2 + kT_{e2} B G_2 \tag{1.104}$$

where the three terms on the right-hand side of Eq. (1.104), respectively, correspond to the input noise power, thermal noise generated inside network 1, and thermal noise generated inside network 2.

Now if we use the relation $T_e = (F-1)T_0$ along with Eq. (1.02), we can express the overall output noise power as

$$N_o = F_1 N_i G_1 G_2 + (F_2 - 1) N_i G_2 \tag{1.105}$$

It follows that the overall noise figure for the cascaded system is

$$F = \frac{(S_i/N_i)}{(S_o/N_o)} = F_1 + \frac{F_2 - 1}{G_1} \tag{1.106}$$

In general, for an n-stage system we get

$$F = F_1 + \frac{F_2 - 1}{G_1} + \frac{F_3 - 1}{G_1 G_2} + \ldots + \frac{F_n - 1}{G_1 G_2 G_3 \cdot \cdot \cdot G_{n-1}} \tag{1.107}$$

Also, the n-stage system effective temperatures can be computed as

$$T_e = T_{e1} + \frac{T_{e2}}{G_1} + \frac{T_{e3}}{G_1 G_2} + \ldots + \frac{T_{en}}{G_1 G_2 G_3 \cdot \cdot \cdot G_{n-1}} \tag{1.108}$$

As suggested by Eq. (1.107) and Eq. (1.108), the overall noise figure is mainly dominated by the first stage. Thus, radar receivers employ low noise power amplifiers in the first stage in order to minimize the overall receiver noise figure. However, for radar systems that are built for low RCS operations every stage should be included in the analysis.

Example:

A radar receiver consists of an antenna with cable loss $L = 1dB = F_1$, *an RF amplifier with* $F_2 = 6dB$, *and gain* $G_2 = 20dB$, *followed by a mixer whose noise figure is* $F_3 = 10dB$ *and conversion loss* $L = 8dB$, *and finally, an integrated circuit IF amplifier with* $F_4 = 6dB$ *and gain* $G_4 = 60dB$. *Find the overall noise figure.*

Solution:

From Eq. (1.107) we have

$$F = F_1 + \frac{F_2 - 1}{G_1} + \frac{F_3 - 1}{G_1 G_2} + \frac{F_4 - 1}{G_1 G_2 G_3}$$

G_1	G_2	G_3	G_4	F_1	F_2	F_3	F_4
$-1dB$	$20dB$	$-8dB$	$60dB$	$1dB$	$6dB$	$10dB$	$6dB$
0.7943	100	0.1585	10^6	1.2589	3.9811	10	3.9811

It follows that

$$F = 1.2589 + \frac{3.9811 - 1}{0.7943} + \frac{10 - 1}{100 \times 0.7943} + \frac{3.9811 - 1}{0.158 \times 100 \times 0.7943} = 5.3629$$

$$F = 10\log(5.3628) = 7.294dB$$

1.10. Effects of the Earth's Surface on the Radar Equation

So far, in developing the radar equation it was implicitly assumed that the radar electromagnetic waves travel as if they were in free space. Furthermore, all analysis presented did not account for the effects of the earth's atmosphere nor the effects of the earth's surface. Despite the fact that *"free space analysis"* may be adequate to provide a general understanding of radar systems, it is only an approximation. In order to accurately predict radar performance, we must modify free space analysis to include the effects of the earth and its atmosphere. Radar clutter is not considered to be part of this analysis. This is true because clutter is almost always assumed to be a distributed target that can be dealt with by the radar signal processor separately. Clutter is the subject of discussion in a later chapter of this book.

In this chapter, the effects of the earth's atmosphere are considered first. Then, the effect of the earth' surface on the radar equation is analyzed. The earth's surface impact on the radar equation manifests itself by introducing an additional power term in the radar equation. This term is called the *pattern propagation factor* and is denoted by symbol F. The propagation factor, can actually introduce constructive as well as distructive interference in the SNR depending on the radar frequency and the geometry under consideration. In general, the pattern propagation factor is defined by

$$F = \left| E / E_0 \right| \qquad \textbf{(1.109a)}$$

where E is the electric field in the medium and E_0 is the free space electric field. In this case the radar equation is now given by

$$(SNR)_o = \frac{P_t G^2 \lambda^2 \sigma}{(4\pi)^3 k T_0 B F L R^4} F^4 \qquad \textbf{(1.109b)}$$

1.10.1. Earth's Atmosphere

The earth's atmosphere is composed of several layers, as illustrated in Fig. 1.24. The first layer, which extends in altitude to about 20 Km, is known as the troposphere. Electromagnetic waves refract (bend downward) as they travel in the troposphere. The troposphere refractive effect is related to its dielectric constant, which is a function of pressure, temperature, water vapor, and gaseous content. Additionally, due to gases and water vapor in the atmosphere, radar energy suffers a loss. This loss is known as the atmospheric attenuation. Atmospheric attenuation increases significantly in the presence of rain, fog, dust, and clouds.

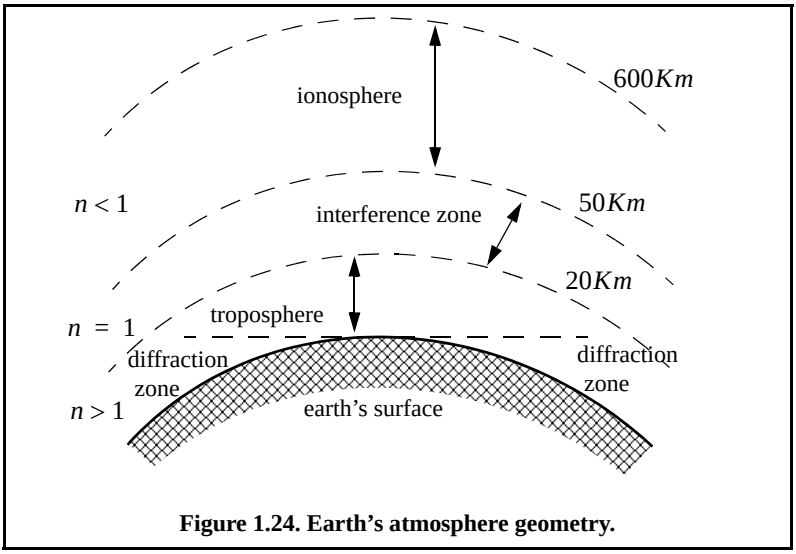

Figure 1.24. Earth's atmosphere geometry.

The region above the troposphere (altitude from 20 to 50 Km) behaves like free space, and thus little refraction occurs in this region. This region is known as the interference zone. The ionosphere extends from about 50 Km to about 600 Km. It has very low gas density compared to the troposphere. It contains a significant amount of ionized free electrons. The ionization is primarily caused by the sun's ultraviolet and X-rays. This presence of free electrons in the ionosphere affects electromagnetic wave propagation in different ways. These

effects include refraction, absorption, noise emission, and polarization rotation. The degree of degradation depends heavily on the frequency of the incident waves. For example, frequencies lower than about 4 to 6 MHz are completely reflected from the lower region of the ionosphere. Frequencies higher than 30 MHz may penetrate the ionosphere with some level of attenuation. In general, as the frequency is increased the ionosphere's effects become less prominent. The region below the horizon, close to the earth's surface, is called the diffraction region. *Diffraction* is a term used to describe the bending of radar waves around physical objects. Two types of diffraction are common. They are knife edge and cylinder edge diffraction.

In order to effectively study the effects of the atmosphere on the propagation of radar waves, it is necessary to have accurate knowledge of the height-variation of the index of refracting in the troposphere and the ionosphere. The index of refraction is a function of the geographic location on the earth, weather, time of day or night, and the season of the year. Therefore, analyzing the atmospheric propagation effects under all parametric conditions is an overwhelming task. Typically, this problem is simplified by analyzing atmospheric models that are representative of an average of atmospheric conditions.

1.10.2. Refraction

In free space, electromagnetic waves travel in straight lines. However, in the presence of the earth's atmosphere, they bend (refract), as illustrated in Fig. 1.25. *Refraction* is a term used to describe the deviation of radar wave propagation from a straight line. The deviation from straight line propagation is caused by the variation of the index of refraction. The index of refraction is defined as

$$n = c/v \tag{1.110}$$

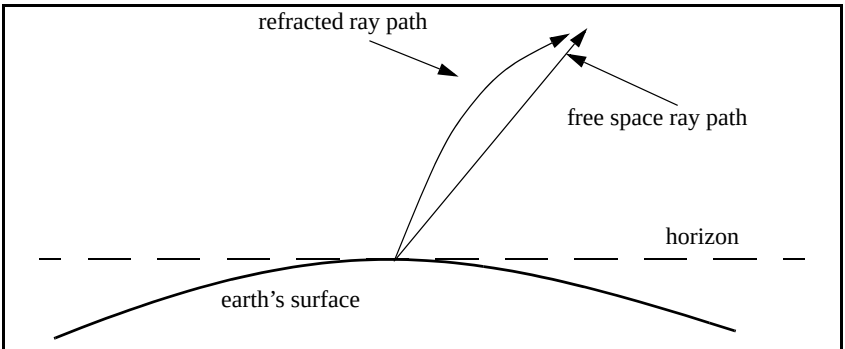

Figure 1.25. Bending of radio waves due to the variation in the atmosphere index of refraction.

where c is the velocity of electromagnetic waves in free space and v is the wave group velocity in the medium. Close to the earth's surface the index of refraction is almost unity; however, with increasing altitude the index of refraction decreases gradually.

The discussion presented in this chapter assumes a well-mixed atmosphere, where the index of refraction decreases in a smooth monotonic fashion with height. The rate of change of the earth's index of refraction n with altitude h is normally referred to as the refractivity gradient, dn/dh. As a result of the negative rate of change in dn/dh, electromagnetic waves travel at slightly higher velocities in the upper troposphere than in the lower part. As a result of this, waves traveling horizontally in the troposphere gradually bend downward. In general, since the rate of change in the refractivity index is very slight, waves do not curve downward appreciably unless they travel very long distances through the troposphere.

Refraction affects radar waves in two different ways depending on height. For targets that have altitudes typically above 100 meters, the effect of refraction is illustrated in Fig. 1.26. In this case, refraction imposes limitations on the radar's capability to measure target position. Refraction introduces an error in measuring the elevation angle. In a well mixed atmosphere, the refractivity gradient close to the earth's surface is almost constant. However, temperature changes and humidity lapses close to the earth's surface may cause serious changes in the refractivity profile. When the refractivity index becomes large enough, electromagnetic waves bend around the curve of the earth beyond the expected curvature due to earth surface. This phenomenon is called ducting and is illustrated in Fig. 1.27. Ducting can be extensive over the sea surface during a hot summer.

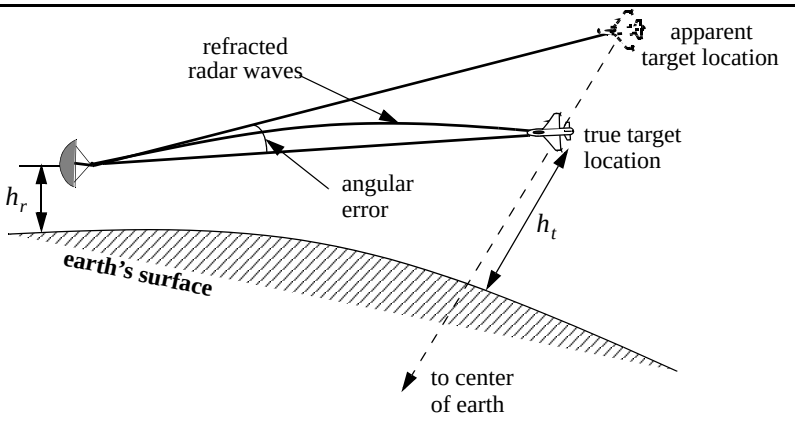

Figure 1.26. Refraction high altitude effect on electromagnetic waves.

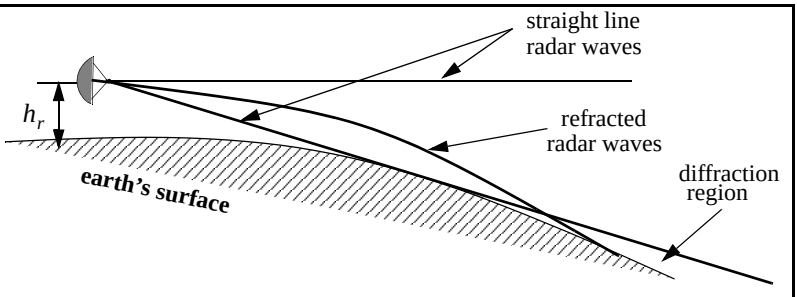

Figure 1.27. Refraction low altitude effect on electromagnetic waves.

Stratified Atmospheric Refraction Model

An approximation method for calculating the range measurement errors and the time-delay errors experienced by radar waves due to refraction is presented. This method is referred to as the "stratified atmospheric model" and is capable of producing very accurate theoretical estimates of the propagation errors. The basic assumption for this approach is that the atmosphere is stratified into M spherical layers, each of thickness $\{h_m;\ m = 0, 1, \ldots, M\}$, and a constant refractive index $\{n_m;\ m = 0, 1, \ldots, M\}$, as illustrated in Fig. 1.28. In this figure, β_0 is the apparent elevation angle and β_{0M} is the true elevation angle. The free space path is denoted by R_{0M}, while the refracted path is composed of $\{R_0, R_1, R_2, \ldots, R_M\}$. From the figure,

$$r_{(m+1)} = r_0 + \sum_{i=0}^{m} h_i \qquad ;\ m = 0, 1, \ldots, M \tag{1.111}$$

where r_0 is the actual radius of the earth and is equal to 6375 Km. Using the law of sines, the angle of incidence α_0 is given by

$$\frac{\sin\alpha_0}{r_0} = \frac{\sin(180 + \beta_0)}{r_1} \tag{1.112}$$

Using Snell's law for spherically symmetrical surfaces, the m^{th} angle, β_m, that the ray makes with the horizon in layer m is given by

$$n_{(m-1)} r_{(m-1)} \cos\beta_{(m-1)} = n_m r_m \cos\beta_m \tag{1.113}$$

Consequently,

$$\beta_m = \text{acos}\left[\frac{n_{(m-1)} r_{(m-1)}}{n_m r_m} \cos\beta_{(m-1)}\right] \tag{1.114}$$

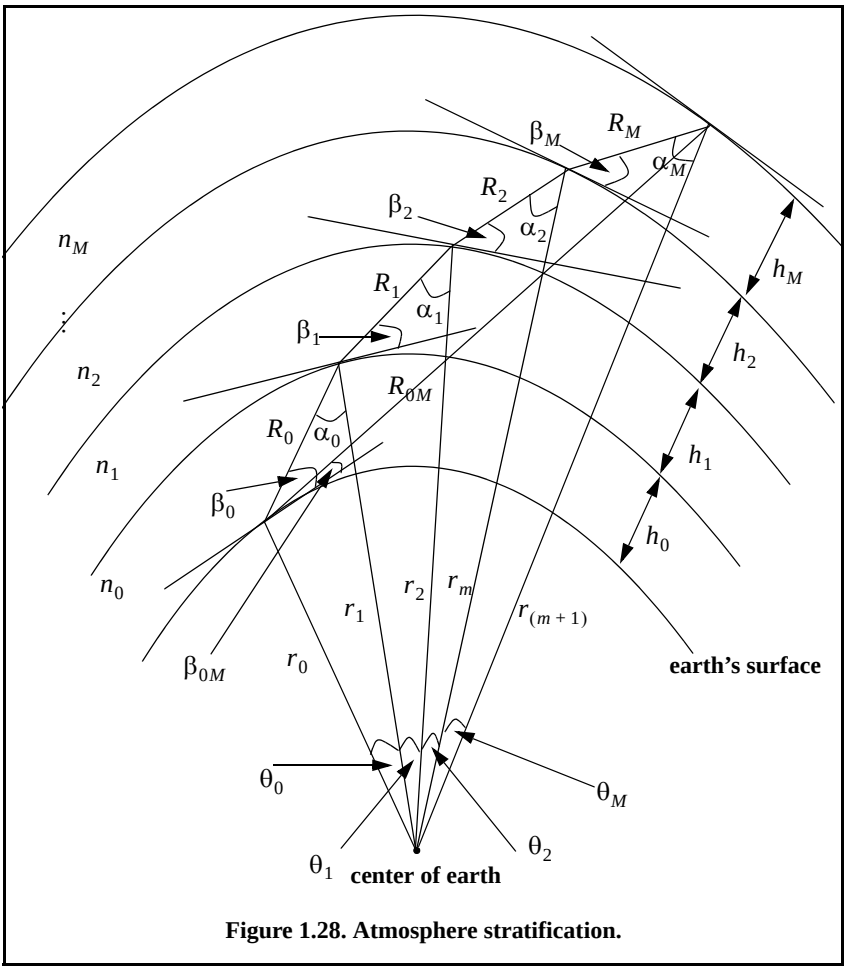

Figure 1.28. Atmosphere stratification.

From Eq. (1.112) one can write the general expression for the angle of incidence. More precisely,

$$\alpha_m = \operatorname{asin}\left[\frac{r_m}{r_{(m+1)}}\cos\beta_m\right] \tag{1.115}$$

Applying the law of sines of the direct path R_{0M} yields

$$\beta_{0M} = \operatorname{acos}\left\{\frac{r_{(M+1)}}{R_{0M}}\sin\left[\sum_{i=0}^{M}\theta_i\right]\right\} \tag{1.116}$$

where

$$R_{0M}^2 = r_0^2 + r_{(m+1)}^2 - 2r_0 r_{(m+1)} \cos\left[\sum_{i=0}^{M} \theta_i\right] \tag{1.117}$$

$$\theta_i = \frac{\pi}{2} - \beta_i - \alpha_i \tag{1.118}$$

The refraction angle error is measured as the difference between the apparent and true elevation angles. Thus, it is given by

$$\Delta\beta_M = \beta_0 - \beta_{0M} \tag{1.119}$$

Note that for $M = 0$,

$$R_{00} = R_0 \quad and \quad \Delta\beta_M = 0 \tag{1.120}$$

Furthermore, when $\beta_0 = 90°$,

$$R_{0M} = \sum_{i=0}^{M} h_i \tag{1.121}$$

Now, in order to determine the time-delay error due to refraction, refer again to Fig. 1.28. The time it takes an electromagnetic wave to travel through a given layer, $\{R_i;\ i = 0, 1, \ldots, M\}$, is defined as $\{t_i;\ i = 0, 1, \ldots, M\}$ where

$$t_i = R_i / \varphi_i \tag{1.122}$$

and where φ_i is the phase velocity in the ith layer and is defined by

$$\varphi_i = c / n_i \tag{1.123}$$

It follows that the total time of travel of the refracted wave in a stratified atmosphere is given by

$$t_T = \frac{1}{c} \sum_{i=0}^{M} n_i R_i \tag{1.124}$$

The free space travel time of an unrefracted wave is denoted by t_{0M},

$$t_{0M} = R_{0M} / c \tag{1.125}$$

Therefore, the range error ΔR that results from refraction is

$$\Delta R = \sum_{i=0}^{M} n_i R_i - R_{0M} \tag{1.126}$$

By using the law of cosines one computes R_i as

$$R_i^2 = r_i^2 + r_{(i+1)}^2 - 2r_i r_{(i+1)} \cos\theta_i \tag{1.127}$$

The results stated in Eqs. (1.125) and (1.26) are valid only in the troposphere. In the ionosphere, which is a dispersive medium, the index of refraction is also a function of frequency. In this case, the group velocity must be used when estimating the range errors of radar measurements. Thus, the total time of travel in the medium is now given by

$$t_T = \frac{1}{c} \sum_{i=0}^{M} \frac{R_i}{n_i} \tag{1.128}$$

Finally, the range error in the ionosphere is

$$\Delta R = \sum_{i=0}^{M} \frac{R_i}{n_i} - R_{0M} \tag{1.129}$$

1.10.3. Four-Third Earth Model

An effective and fairly accurate technique for dealing with refraction is to replace the actual earth with an imaginary earth whose radius is $r_e = kr_0$, where $r_0 = 6375Km$ is the actual earth radius, and k is

$$k = \frac{1}{1 + r_0(dn/dh)} \tag{1.130}$$

When the refractivity gradient is assumed to be constant with altitude and is equal to 39×10^{-9} per meter, then $k = 4/3$. Using an effective earth radius $r_e = (4/3)r_0$ produces what is known as the "*four-third earth model.*" In general, choosing

$$r_e = r_0(1 + 6.37 \times 10^{-3}(dn/dh)) \tag{1.131}$$

produces a propagation model where waves travel in straight lines. Selecting the correct value for k depends heavily on the region's meteorological conditions. At low altitudes (typically less than 10 Km) when using the 4/3 earth model, one can assume that radar waves (beams) travel in straight lines and do not refract. This is illustrated in Fig. 1.29.

1.10.4. Ground Reflection

When radar waves are reflected from the earth's surface, they suffer a loss in amplitude and a change in phase. Three factors that contribute to these changes

they are the smooth surface reflection coefficient, the divergence factor due to earth's curvature, and the surface roughness.

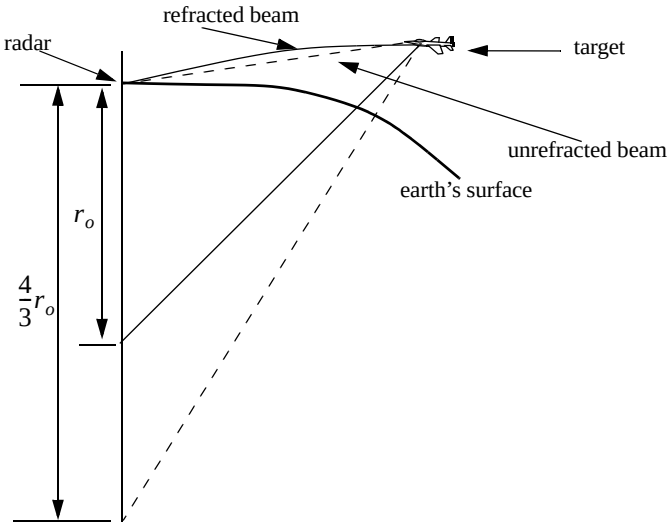

Figure 1.29. Geometry for 4/3 earth.

Smooth Surface Reflection Coefficient

The smooth surface reflection coefficient depends on the frequency, the surface dielectric coefficient, and the radar grazing angle. The vertical polarization and the horizontal polarization reflection coefficients are

$$\Gamma_v = \frac{\varepsilon \sin\psi_g - \sqrt{\varepsilon - (\cos\psi_g)^2}}{\varepsilon \sin\psi_g + \sqrt{\varepsilon - (\cos\psi_g)^2}} \tag{1.132}$$

$$\Gamma_h = \frac{\sin\psi_g - \sqrt{\varepsilon - (\cos\psi_g)^2}}{\sin\psi_g + \sqrt{\varepsilon - (\cos\psi_g)^2}} \tag{1.133}$$

where ψ_g is the grazing angle (incident angle) and ε is the complex dielectric constant of the surface, and are given by

$$\varepsilon = \varepsilon' - j\varepsilon'' = \varepsilon' - j60\lambda\sigma \tag{1.134}$$

where λ is the wavelength and σ the medium conductivity in mhos/meter. Typical values of ε' and ε'' can be found tabulated in the literature.

Note that when $\psi_g = 90°$, we get

$$\Gamma_h = \frac{1-\sqrt{\varepsilon}}{1+\sqrt{\varepsilon}} = -\frac{\varepsilon-\sqrt{\varepsilon}}{\varepsilon+\sqrt{\varepsilon}} = -\Gamma_v \qquad \textbf{(1.135)}$$

while when the grazing angle is very small ($\psi_g \approx 0$), we have

$$\Gamma_h = -1 = \Gamma_v \qquad \textbf{(1.136)}$$

Tables 1.1 and 1.2 show some typical values for the electromagnetic properties of soil and sea water. Figure 1.30 shows the corresponding magnitude plots for Γ_h and Γ_v, while Fig. 1.31 shows the phase plots for seawater at $28°C$ where ε' = 65 and ε" = 30.7 at X-band. The plots shown in these figures show the general typical behavior of the reflection coefficient.

Table 1.1. Electromagnetic properties of soil.

Frequency GHz	Moisture content by volume							
	0.3%		10%		20%		30%	
	ε'	ε''	ε'	ε''	ε'	ε''	ε'	ε''
0.3	2.9	0.071	6.0	0.45	10.5	0.75	16.7	1.2
3.0	2.9	0.027	6.0	0.40	10.5	1.1	16.7	2.0
8.0	2.8	0.032	5.8	0.87	10.3	2.5	15.3	4.1
14.0	2.8	0.350	5.6	1.14	9.4	3.7	12.6	6.3
24	2.6	0.030	4.9	1.15	7.7	4.8	9.6	8.5

Table 1.2. Electromagnetic properties of sea water.

Frequency GHz	Temperature					
	$T = 0°C$		$T = 10°C$		$T = 20°C$	
	ε'	ε''	ε'	ε''	ε'	ε''
0.1	77.8	522	75.6	684	72.5	864
1.0	77.0	59.4	75.2	73.8	72.3	90.0
2.0	74.0	41.4	74.0	45.0	71.6	50.4
3.0	71.0	38.4	72.1	38.4	70.5	40.2
4.0	66.5	39.6	69.5	36.9	69.1	36.0
6.0	56.5	42.0	63.2	39.0	65.4	36.0
8.0	47.0	42.8	56.2	40.5	60.8	36.0

Observation of Fig. 1.30 indicates the following conclusions: (1) The magnitude of the reflection coefficient with horizontal polarization is equal to unity at very small grazing angles and it decreases monotonically as the angle is increased. (2) The magnitude of the vertical polarization has a well-defined minimum. The angle that corresponds to this condition is called Brewster's

polarization angle. For this reason, airborne radars in the look-down mode utilize mainly vertical polarization to significantly reduce the terrain bounce reflections. (3) For horizontal polarization the phase is almost π; however, for vertical polarization the phase changes to zero around the Brewster's angle. (4) For very small angles (less than $2°$) both $|\Gamma_h|$ and $|\Gamma_v|$ are nearly one; $\angle\Gamma_h$ and $\angle\Gamma_v$ are nearly π. Thus, little difference in the propagation of horizontally or vertically polarized waves exists at low grazing angles. Figure 1.30 can be reproduced using the following MATLAB code.

```
close all; clear all
psi = 0.01:0.05:90;
[rh,rv] = ref_coef (psi, 65,30.7);
gamamodv = abs(rv); gamamodh = abs(rh); subplot(2,1,1)
plot(psi,gamamodv,'k',psi,gamamodh,'k -.','linewidth',1.5); grid
legend ('Vertical Polarization', 'Horizontal Polarization')
title('Reflection coefficient - magnitude')
pv = -angle(rv); ph = angle(rh); subplot(2,1,2)
plot(psi,pv,'k',psi,ph,'k -.','linewidth',1.5); grid
legend ('Vertical Polarizatio', 'Horizontal Polarization')
title('Reflection coefficient - phase'); xlabel('Grazing angle in degrees');
```

Figures 1.31 and 1.32 show the magnitudes of the horizontal and vertical reflection coefficients as a function of grazing angle for four soils at 8 GHz.

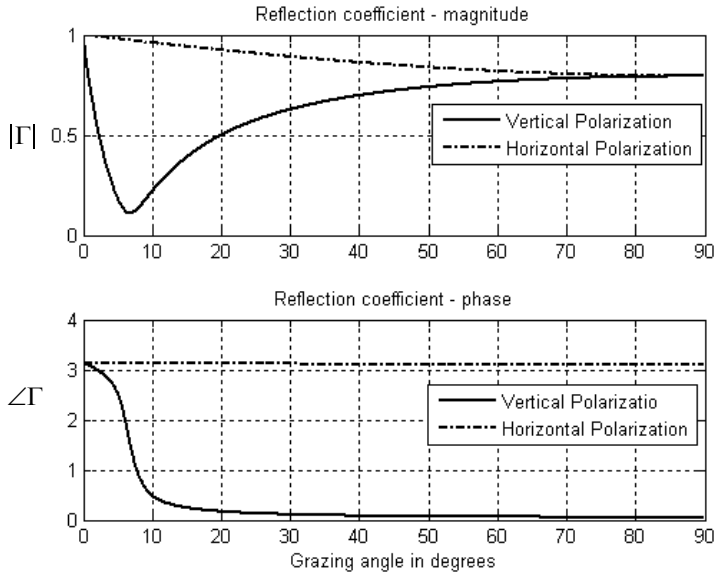

Figure 1.30. Reflection coefficient magnitude.

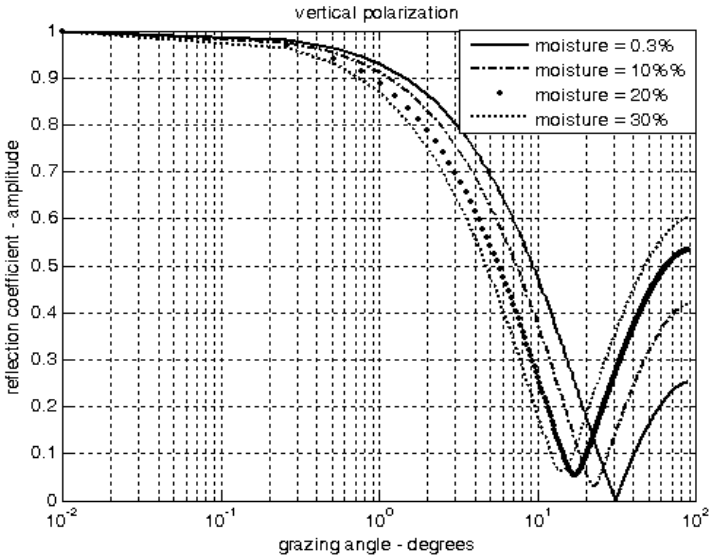

Figure 1.31. Vertical reflection coefficient for soil at 8 GHz.

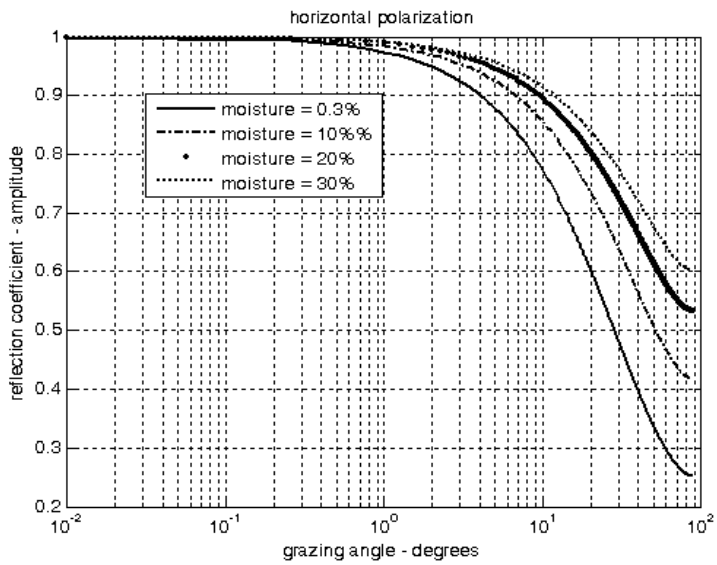

Figure 1.32. Horizontal reflection coefficient for soil at 8 GHz.

Divergence

The overall reflection coefficient is also affected by the round earth divergence factor, D. When an electromagnetic wave is incident on a round earth surface, the reflected wave diverges because of the earth's curvature. This is illustrated in Fig. 1.33. Due to divergence the reflected energy is defocused, and the radar power density is reduced. The divergence factor can be derived using geometrical considerations.

The divergence factor can be expressed as

$$D = \sqrt{\frac{r_e \; r \; \sin\psi_g}{[(2r_1 r_2 / \cos\psi_g) + r_e r \sin\psi_g](1 + h_r / r_e)(1 + h_t / r_e)}} \tag{1.137}$$

where all the parameters in Eq. (1.137) are defined in Fig. 1.34. Since the grazing ψ_g is always small when the divergence D is very large, the following approximation is adequate in most radar cases of interest:

$$D \approx \frac{1}{\sqrt{1 + \dfrac{4r_1 r_2}{r_e r \sin 2\psi_g}}} \tag{1.138}$$

Rough Surface Reflection

In addition to divergence, surface roughness also affects the reflection coefficient. Surface roughness is given by

$$S_r = e^{-2\left(\frac{2\pi h_{rms} \sin\psi_g}{\lambda}\right)^2} \tag{1.139}$$

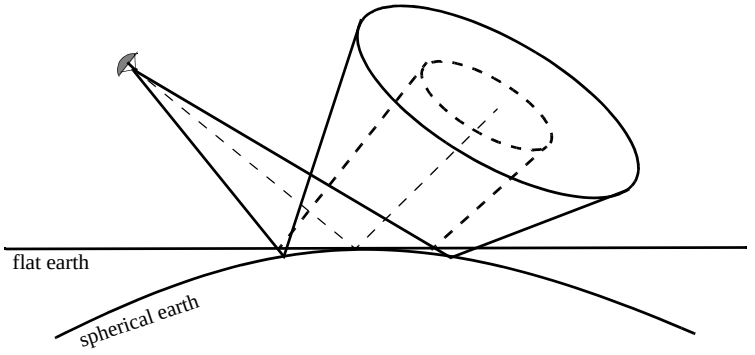

Figure 1.33. Illustration of divergence. Solid line: Ray perimeter for spherical earth. Dashed line: Ray perimeter for flat earth.

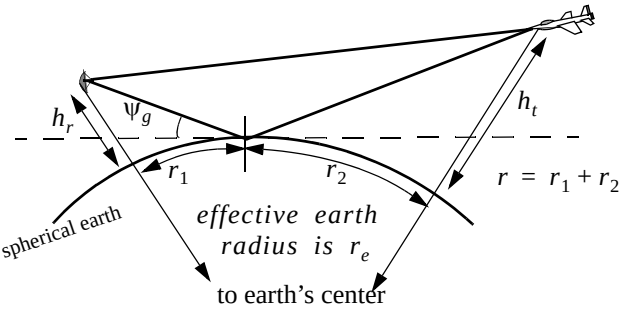

Figure 1.34. Definition of variables in Eq. (1.137).

where h_{rms} is the root mean square (rms) surface height irregularity. Another form for the rough surface reflection coefficient that is more consistent with experimental results is given by

$$S_r = e^{-z} I_0(z) \tag{1.140}$$

$$z = 2\left(\frac{2\pi h_{rms} \sin\psi_g}{\lambda}\right)^2 \tag{1.141}$$

where I_0 is the modified Bessel function of order zero.

Total Reflection Coefficient

In general, rays reflected from rough surfaces undergo changes in phase and amplitude, which results in the diffused (noncoherent) portion of the reflected signal. Combining the effects of smooth surface reflection coefficient, divergence, and the rough surface reflection coefficient, one express the total reflection coefficient Γ_t as

$$\Gamma_t = \Gamma_{(h,v)} D S_r \tag{1.142}$$

$\Gamma_{(h,v)}$ is the horizontal or vertical smooth surface reflection coefficient, D is divergence, and S_r is the rough surface reflection coefficient.

1.10.5. The Pattern Propagation Factor - Flat Earth

Consider the geometry shown in Fig. 1.35. The radar is located at height h_r. The target is at range R, and is located at a height h_t. The grazing angle is ψ_g. The radar energy emanating from its antenna will reach the target via two paths: the "direct path" AB and the "indirect path" ACB.

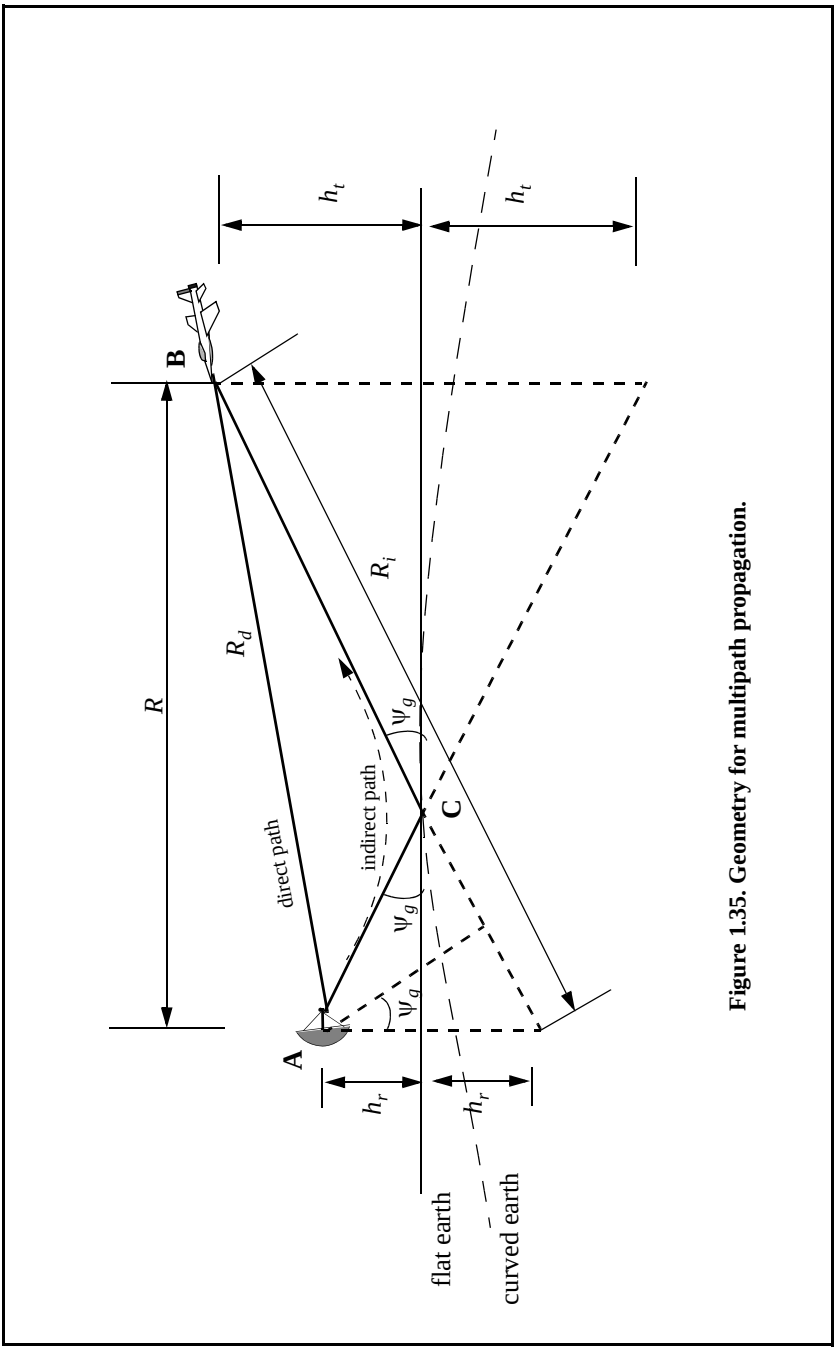

Figure 1.35. Geometry for multipath propagation.

The lengths of the paths AB and ACB are normally very close to one another and thus, the difference between the two paths is very small. Denote the direct path as R_d, the indirect path as R_i, and the difference as $\Delta R = R_i - R_d$. It follows that the phase difference between the two paths is given by

$$\Delta\Phi = \frac{2\pi\Delta R}{\lambda} \tag{1.143}$$

where λ is the radar wavelength.

The indirect signal amplitude arriving at the target is less than the signal amplitude arriving via the direct path. This is because the antenna gain in the direction of the indirect path is less than that along the direct path, and because the signal reflected from the earth's surface at point C is modified in amplitude and phase in accordance to the earth's reflection coefficient, Γ. The earth reflection coefficient is given by

$$\Gamma = \rho e^{j\varphi} \tag{1.144}$$

where ρ is less than unity and φ describes the phase shift induced on the indirect path signal due to surface roughness.

The direct signal (in volts) arriving at the target via the direct path can be written as

$$E_d = e^{j\omega_0 t} e^{j\frac{2\pi}{\lambda}R_d} \tag{1.145}$$

where the time harmonic term $\exp(j\omega_0 t)$ represents the signal's time dependency, and the exponential term $\exp(j(2\pi/\lambda)R_d)$ represents the signal spatial phase. The indirect signal at the target is

$$E_i = \rho e^{j\varphi} e^{j\omega_0 t} e^{j\frac{2\pi}{\lambda}R_i} \tag{1.146}$$

where $\rho\exp(j\varphi)$ is the surface reflection coefficient. Therefore, the overall signal arriving at the target is

$$E = E_d + E_i = e^{j\omega_0 t} e^{j\frac{2\pi}{\lambda}R_d}\left(1 + \rho e^{j\left(\varphi + \frac{2\pi}{\lambda}(R_i - R_d)\right)}\right) \tag{1.147}$$

Due to reflections from the earth's surface, the overall signal strength is then modified at the target by the ratio of the signal strength in the presence of earth to the signal strength at the target in free space. From Eq. (1.147) the modulus of this ratio is the propagation factor is

$$F = \left|\frac{E_d}{E_d + E_i}\right| = \left|1 + \rho e^{j\varphi} e^{j\Delta\Phi}\right| \quad \textbf{(1.148)}$$

which can be rewritten as

$$F = \left|1 + \rho e^{j\alpha}\right| \quad \textbf{(1.149)}$$

where $\alpha = \Delta\Phi + \varphi$. Using Euler's identity ($e^{j\alpha} = \cos\alpha + j\sin\alpha$), Eq. (1.149) can be written as

$$F = \sqrt{1 + \rho^2 + 2\rho\cos\alpha} \quad \textbf{(1.150)}$$

It follows that the signal power at the target is modified by the factor F^2. By using reciprocity, the signal power at the radar is computed by multiplying the radar equation by the factor F^4. In the following two sections we will develop exact expressions for the propagation factor for flat and curved earth.

In order to calculate the propagation factor defined in Eq. (1.150), consider the geometry of Fig. 1.35; the direct and indirect paths are computed as

$$R_d = \sqrt{R^2 + (h_t - h_r)^2} \quad \textbf{(1.151)}$$

$$R_i = \sqrt{R^2 + (h_t + h_r)^2} \quad \textbf{(1.152)}$$

which can be approximated using the truncated binomial series expansion as

$$R_d \approx R + \frac{(h_t - h_r)^2}{2R} \quad \textbf{(1.153)}$$

$$R_i \approx R + \frac{(h_t + h_r)^2}{2R} \quad \textbf{(1.154)}$$

This approximation is valid for low grazing angles, where $R \gg h_t, h_r$. It follows that

$$\Delta R = R_i - R_d \approx \frac{2h_t h_r}{R} \quad \textbf{(1.155)}$$

Substituting Eq. (1.155) into Eq. (1.143) yields the phase difference due to multipath propagation between the two signals (direct and indirect) arriving at the target. More precisely,

$$\Delta\Phi = \frac{2\pi}{\lambda}\Delta R \approx \frac{4\pi h_t h_r}{\lambda R} \quad \textbf{(1.156)}$$

As a special case, assume smooth surface with reflection coefficient $\Gamma = -1$. This assumption means that waves reflected from the surface suffer no amplitude loss, and that the induced surface phase shift is equal to $180°$. It follows that

$$F^2 = 2 - 2\cos\Delta\Phi = 4(\sin(\Delta\Phi/2))^2 \quad \textbf{(1.157)}$$

Substituting Eq. (1.156) into Eq. (1.157) yields

$$F^2 = 4\left(\sin\frac{2\pi h_t h_r}{\lambda R}\right)^2 \quad \textbf{(1.158)}$$

By using reciprocity, the expression for the propagation factor at the radar is then given by

$$F^4 = 16\left(\sin\frac{2\pi h_t h_r}{\lambda R}\right)^4 \quad \textbf{(1.159)}$$

Finally, the signal power at the radar is computed by multiplying the radar equation by the factor F^4:

$$P_r = \frac{P_t G^2 \lambda^2 \sigma}{(4\pi)^3 R^4}\ 16\left(\sin\frac{2\pi h_t h_r}{\lambda R}\right)^4 \quad \textbf{(1.160)}$$

Since the sine function varies between 0 and 1, the signal power will then vary between 0 and 16. Therefore, the fourth power relation between signal power and the target range results in varying the target range from 0 to twice the actual range in free space. In addition to that, the field strength at the radar will now have holes that correspond to the nulls of the propagation factor.

The nulls of the propagation factor occur when the sine is equal to zero. More precisely,

$$\frac{2h_r h_t}{\lambda R} = n \quad \textbf{(1.161)}$$

where $n = \{0, 1, 2, \ldots\}$. The maxima occur at

$$\frac{4h_r h_t}{\lambda R} = n + 1 \quad \textbf{(1.162)}$$

The target heights that produce nulls in the propagation factor are $\{h_t = n(\lambda R/2h_r); n = 0, 1, 2, \ldots\}$, and the peaks are produced from target heights $\{h_t = n(\lambda R/4h_r); n = 1, 2, \ldots\}$. Therefore, due to the presence of surface reflections, the antenna elevation coverage is transformed into a lobed pattern structure.

For small angles, Eq. (1.160) can be approximated by

$$P_r \approx \frac{4\pi P_t G^2 \sigma}{\lambda^2 R^8} \; (h_t h_r)^4 \tag{1.163}$$

Thus, the received signal power varies as the eighth power of the range instead of the fourth power. Also, the factor $G\lambda$ is now replaced by G/λ.

1.10.6. The Pattern Propagation Factor - Spherical Earth

In order to model the effects of multipath propagation on radar performance more accurately, we need to remove the flat earth condition and account for the earth's curvature. When considering round earth, electromagnetic waves travel in curved paths because of the atmospheric refraction. And as mentioned earlier, the most commonly used approach to mitigating the effects of atmospheric refraction is to replace the actual earth by an imaginary earth such that electromagnetic waves travel in straight lines. The fictitious effective earth radius is

$$r_e = kr_0 \tag{1.164}$$

where k is a constant and r_0 is the actual earth radius. Using the geometry in Fig. 1.36, the direct and indirect path difference is

$$\Delta R = R_1 + R_2 - R_d \tag{1.165}$$

The propagation factor is computed by using ΔR from Eq. (1.150). To compute (R_1, R_2, and R_d), the following cubic equation must first be solved for r_1:

$$2r_1^3 - 3rr_1^2 + (r^2 - 2r_e(h_r + h_t))r_1 + 2r_e h_r r = 0 \tag{1.166}$$

The solution is

$$r_1 = \frac{r}{2} - p\sin\frac{\xi}{3} \tag{1.167}$$

where

$$p = \frac{2}{\sqrt{3}}\sqrt{r_e(h_t + h_r) + \frac{r^2}{4}} \tag{1.168}$$

$$\xi = \text{asin}\left(\frac{2r_e r(h_t - h_r)}{p^3}\right) \tag{1.169}$$

Next, we solve for R_1, R_2, and R_d. From Fig. 1.36 (assume flat 4/3 earth and use small angle approximation),

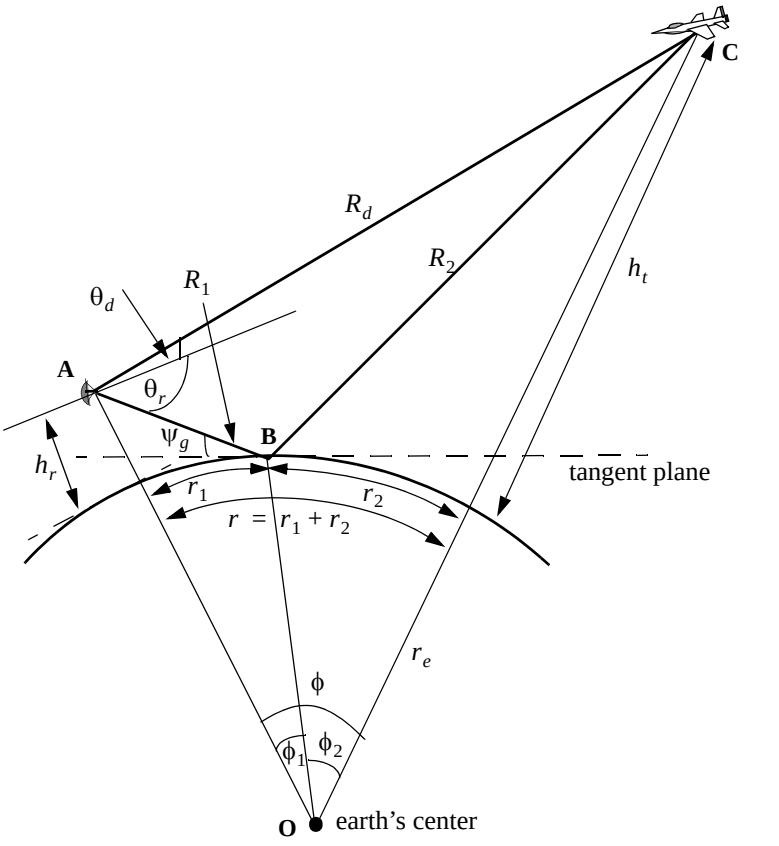

Figure 1.36. Geometry associated with multipath propagation over round earth.

$$\phi_1 = r_1/r_e;\ \ \phi_2 = r_2/r_e \tag{1.170}$$

$$\phi = r/r_e \tag{1.171}$$

Using the law of cosines to the triangles ABO and BOC yields

$$R_1 = \sqrt{r_e^2 + (r_e + h_r)^2 - 2r_e(r_e + h_r)\cos\phi_1} \tag{1.172}$$

$$R_2 = \sqrt{r_e^2 + (r_e + h_t)^2 - 2r_e(r_e + h_t)\cos\phi_2} \tag{1.173}$$

Eqs. (1.172) and (1.173) can be written in the following simpler forms:

$$R_1 = \sqrt{h_r^2 + 4r_e(r_e + h_r)(\sin(\phi_1/2))^2} \tag{1.174}$$

$$R_2 = \sqrt{h_t^2 + 4r_e(r_e + h_t)(\sin(\phi_2/2))^2} \tag{1.175}$$

Using the law of cosines on the triangle AOC yields

$$R_d = \sqrt{(h_r - h_t)^2 + 4(r_e + h_t)(r_e + h_r)\left(\sin\left(\frac{\phi_1 + \phi_2}{2}\right)\right)^2} \tag{1.176}$$

Additionally

$$r = r_e \text{acos}\left(\sqrt{\frac{(r_e + h_r)^2 + (r_e + h_t)^2 - R_d^2}{2(r_e + h_r)(r_e + h_t)}}\right) \tag{1.177}$$

Substituting Eqs. (1.174) through (1.176) directly into Eq. (1.165) may not be conducive to numerical accuracy. A more suitable form for the computation of ΔR is then derived. The detailed derivation is in Blake (1980). The results are listed below. For better numerical accuracy use the following expression to compute ΔR:

$$\Delta R = \frac{4R_1R_2(\sin\psi_g)^2}{R_1 + R_2 + R_d} \tag{1.178}$$

where

$$\psi_g = \text{asin}\left(\frac{2r_eh_r + h_r^2 - R_1^2}{2r_eR_1}\right) \approx \text{asin}\left(\frac{h_r}{R_1} - \frac{R_1}{2r_e}\right) \tag{1.179}$$

MATLAB Program *"multipath.m"*

The MATLAB program *"multipath.m"* calculates the two-way propagation factor using the 4/3 earth model for spherical earth. It assumes a known free space radar-to-target range. It can be easily modified to assume a known true spherical earth ground range between the radar and the target. Additionally, this program generates three types of plots. They are (1) the propagation factor as a function of range, (2) the free space relative signal level versus range, and (3) the relative signal level with multipath effects included. This program uses the equations presented in the previous few sections and includes the effects of the total surface reflection coefficient Γ_t. Finally, it can also be easily modified to plot the propagation factor versus target height at a fixed target range.

Using this program, Fig. 1.37 presents a plot for the propagation factor loss versus range using $f = 3GHz$, $h_r = 30.48m$, and $h_t = 60.96m$. In this

example, vertical polarization is assumed. Divergence effects are not included; neither is the reflection coefficient. More precisely in this example $D = \Gamma_t = 1$ is assumed.

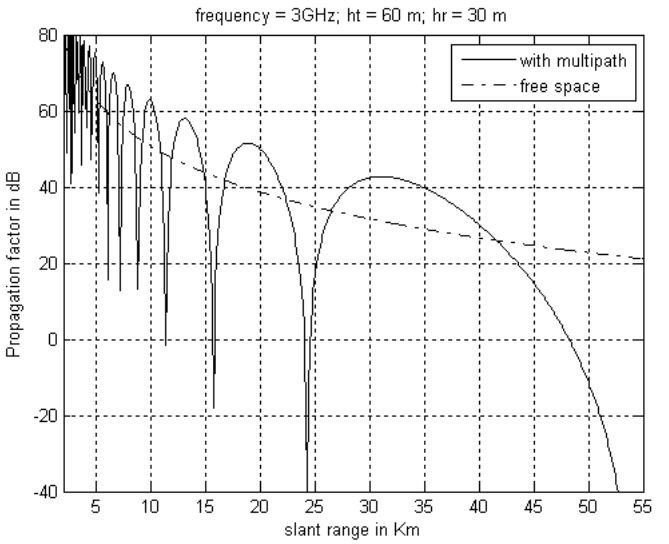

Figure 1.37. Effect of multipath on the radar sensitivity.

1.10.7. Diffraction

The analysis that led to creating the multipath model described in the previous section applies only to ground reflections from the intermediate region, as illustrated in Fig. 1.38. The effects of ground reflection below the radar horizon is governed by another physical phenomenon referred to as diffraction. The diffraction model requires calculations of the Airy function and its roots. For this purpose, the numerical approximation presented in Shatz and Polychronopoulos[1] is adopted. This numerical algorithm, described by Shatz and Polychronopoulos, is very accurate and its implementation using MATLAB is straight forward.

1. Shatz, M. P., and Polychronopoulos, G. H., *An Algorithm for Evaluation of Radar Propagation in the Spherical Earth Diffraction Region*. IEEE Transactions on Antenna and Propagation, Vol. 38, August 1990, pp. 1249-1252.

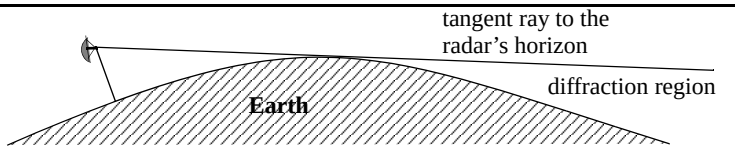

Figure 1.38. Diffraction region.

Define the following parameters,

$$x = \frac{R}{r_0} \quad , \quad y = \frac{h_r}{h_0} \quad , \quad t = \frac{h_t}{h_0} \tag{1.180}$$

where h_r is the radar altitude, h_t is target altitude, R is range to the target, h_0 and r_0 are normalizing factors given by

$$h_0 = \frac{1}{2}\left(\frac{r_e \lambda^2}{\pi^2}\right)^{1/3} \tag{1.181}$$

$$r_0 = \left(\frac{r_e^2 \lambda}{\pi}\right)^{1/3} \tag{1.182}$$

λ is the wavelength and r_e is the effective earth radius. Let $A_i(u)$ denote the Airy function defined by

$$A_i(u) = \frac{1}{\pi}\int_0^{\infty} \cos\left(\frac{q^3}{3} + uq\right)\, dq \tag{1.183}$$

The general expression for the propagation factor in the diffraction region is equal to

$$F = 2\sqrt{\pi x}\sum_{n=1}^{\infty} f_n(y) f_n(t) \exp[(e^{j\pi/6}) a_n x] \tag{1.184}$$

where (x, y, t) are defined in Eq. (1.180) and

$$f_n(u) = \frac{A_i(a_n + u e^{j\pi/3})}{e^{j\pi/3} A_i'(a_n)} \tag{1.185}$$

where a_n is the n^{th} root of the Airy function and A_i' is the first derivative of the Airy function. Shatz and Polychronopoulos showed that Eq. (1.184) can be approximated by

$$F = 2\sqrt{\pi x}\sum_{n=1}^{\infty}\frac{\widehat{A_i}(a_n + ye^{j\pi/3})}{e^{j\pi/3}A_i'(a_n)}\frac{\widehat{A_i}(a_n + te^{j\pi/3})}{e^{j\pi/3}A_i'(a_n)} \quad \textbf{(1.186)}$$

$$\exp\left[\frac{1}{2}(\sqrt{3}+j)a_n x - \frac{2}{3}(a_n + ye^{j\pi/3})^{3/2} - \frac{2}{3}(a_n + te^{j\pi/3})^{3/2}\right]$$

where

$$\widehat{A_i}(u) = A_i(u)e^{j\frac{2}{3}u^{3/2}} \quad \textbf{(1.187)}$$

Shatz and Polychronopoulos showed that sum in Eq. (1.186) represents accurate computation of the propagation factor within the diffraction region. In this book, a MATLAB program called *"diffraction.m"* was written by this author to implement Eq. (1.86) where the sum is terminated at $n \le 1500$ for accurate computation. For this purpose, another MATLAB function called *"airyzo1.m"* was used to compute the roots of Airy function and the roots of its first derivative. Figure 1.39 (after Shatz) shows a typical output generated by this program for $h_t = 1000m$, $h_r = 8000m$, and $frequency = 167MHz$.

This figure can be reproduced using the following MATLAB code.

```
% Figure 1.39 or Figure 1.40
clc
clear all
close all
freq =167e6;
hr = 8000;
ht = 1000;
R = linspace(400e3,600e3,200); % range in Km
nt =1500; % number of point used in calculating infinite series
F = diffraction(freq, hr, ht, R, nt);
figure(1)
plot(R/1000,10*log10(abs(F).^2),'k','linewidth',1)
grid
xlabel('Range in Km')
ylabel('One way propagation factor in dB')
title('frequency = 167MHz; hr = 8000 m; ht = 1000m')
```

Figure 1.40 is similar to Fig. 1.39 except in this case the following parameters are used: $h_t = 3000m$, $h_r = 200m$, and $frequency = 428MHz$. Figure 1.41 shows a plot for the propagation factor using the same parameters in Fig.

1.40; however, in this figure, both intermediate and diffraction regions are shown.

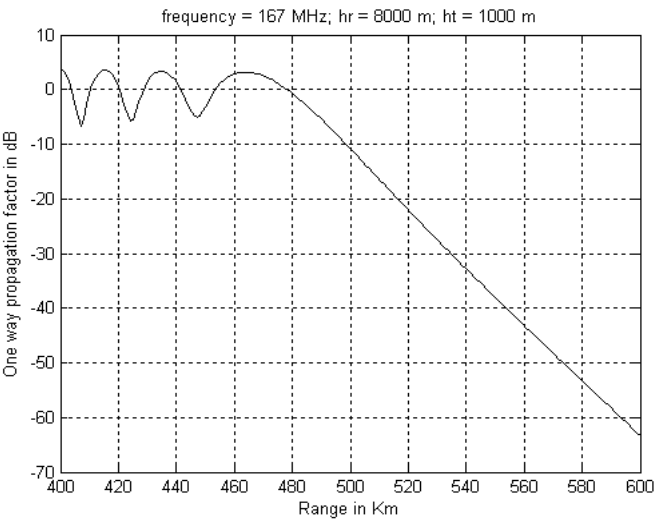

Figure 1.39. Propagation factor in the diffraction region.

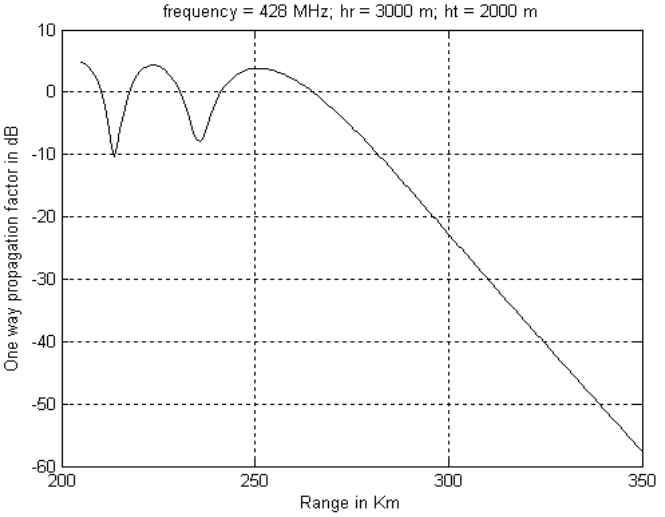

Figure 1.40. Propagation factor in the diffraction region.

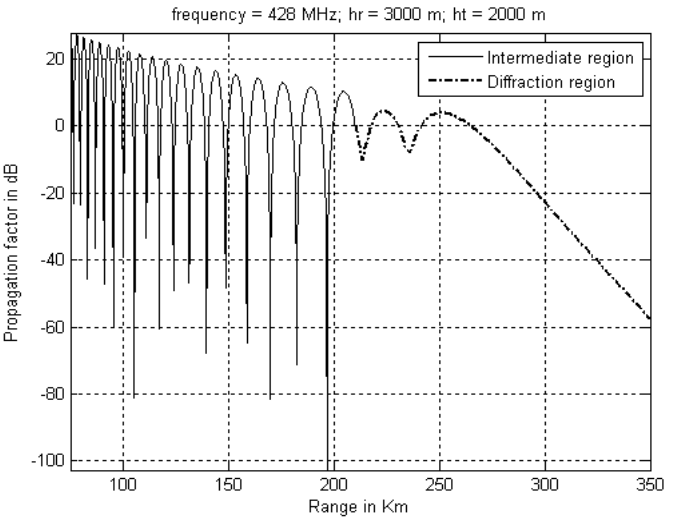

Figure 1.41. Propagation factor.

1.11. Atmospheric Attenuation

Electromagnetic waves travel in free space without suffering any energy loss. Alternatively, due to gases and water vapor in the atmosphere, radar energy suffers a loss. This loss is known as atmospheric attenuation. Atmospheric attenuation increases significantly in the presence of rain, fog, dust, and clouds. Most of the lost radar energy is normally absorbed by gases and water vapor and transformed into heat, while a small portion of this lost energy is used in molecular transformation of the atmosphere particles.

The two-way atmospheric attenuation over a range R can be expressed as

$$L_{atmosphere} = e^{-2\alpha R} \tag{1.188}$$

where α is the one-way attenuation coefficient. Water vapor attenuation peaks at about $22.3GHz$, while attenuation due to oxygen peaks at between 60 and $118GHz$. Atmospheric attenuation is severe for frequencies higher than $35GHz$. This is the reason ground-based radars rarely use frequencies higher than $35GHz$. Atmospheric attenuation is a function range, frequency, and elevation angle. Figure 1.42 shows a typical two-way atmospheric attenuation plot versus range at $3GHz$, with the elevation angle as a parameter.

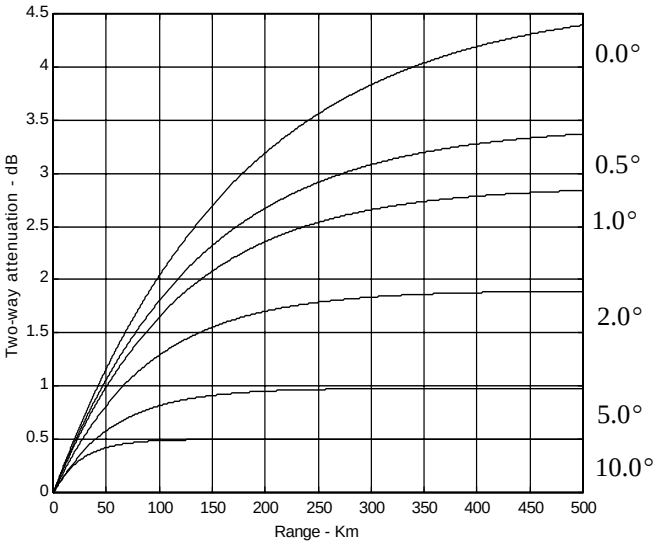

Figure 1.42. Attenuation versus range; frequency is *3 GHz.*

1.12. MATLAB Program Listings

This section presents listings for all the MATLAB programs used to produce all of the MATLAB-generated figures in this chapter. They are listed in the same order they appear in the text.

1.12.1. MATLAB Function "range_resolution.m"

The MATLAB function *"range_resolution.m"* calculates range resolution; its syntax is as follows:

[delta_R] = range_resolution(var, indicator)

where

Symbol	Description	Units	Status
var, indicator	*bandwidth, "hz"*	*Hz, none*	*inputs*
var, indicator	*pulse width, "s"*	*seconds, none*	*inputs*
delta_R	*range resolution*	*meters*	*output*

MATLAB Function** "range_resolution.m" **Listing

```
function [delta_R] = range_resolution(bandwidth, indicator)
% This function computes radar range resolution in meters
% the bandwidth must be in Hz ==> indicator = Hz.
% Bandwidth may be equal to (1/pulse width)==> indicator = seconds
c = 3.e+8; % speed of light
if(indicator == 'hz')
  delta_R = c / 2.0 / bandwidth;
else
  delta_R = c * bandwidth / 2.0;
end
return
```

1.12.2. MATLAB Function "radar_eq.m"

The function *"radar_eq.m"* implements Eq. (1.40); its syntax is as follows:

[snr] = radar_eq (pt, freq, g, sigma, b, nf, loss, range)

where

Symbol	Description	Units	Status
pt	*peak power*	*Watts*	*input*
freq	*radar center frequency*	*Hz*	*input*
g	*antenna gain*	*dB*	*input*
sigma	*target cross section*	m^2	*input*
b	*bandwidth*	*Hz*	*input*
nf	*noise figure*	*dB*	*input*
loss	*radar losses*	*dB*	*input*
range	*target range (can be either a single value or a vector)*	*meters*	*input*
snr	*SNR (single value or a vector, depending on the input range)*	*dB*	*output*

MATLAB Function** "radar_eq.m" **Listing

```
function [snr] = radar_eq(pt, freq, g, sigma, b, nf, loss, range)
% This program implements Eq. (1.40)
c = 3.0e+8; % speed of light
lambda = c / freq; % wavelength
p_peak = 10*log10(pt); % convert peak power to dB
lambda_sqdb = 10*log10(lambda^2); % compute wavelength square in dB
sigmadb = 10*log10(sigma); % convert sigma to dB
four_pi_cub = 10*log10((4.0 * pi)^3); % (4pi)^3 in dB
```

```
k_db = 10*log10(1.38e-23); % Boltzmann's constant in dB
to_db = 10*log10(290); % noise temp. in dB
b_db = 10*log10(b); % bandwidth in dB
range_pwr4_db = 10*log10(range.^4); % vector of target range^4 in dB
% Implement Equation (1.63)
num = p_peak + g + g + lambda_sqdb + sigmadb;
den = four_pi_cub + k_db + to_db + b_db + nf + loss + range_pwr4_db;
snr = num - den;
return
```

1.12.3. MATLAB Function "power_aperture.m"

The function *"power_aperture.m"* implements the search radar equation given in Eq. (1.47); its syntax is as follows:

PAP = power_aperture (snr, tsc, sigma, range, nf, loss, az_angle, el_angle)

where

Symbol	Description	Units	Status
snr	*sensitivity snr*	*dB*	*input*
tsc	*scan time*	*seconds*	*input*
sigma	*target cross section*	m^2	*input*
range	*target range*	*meters*	*input*
nf	*noise figure*	*dB*	*input*
loss	*radar losses*	*dB*	*input*
az_angle	*search volume azimuth extent*	*degrees*	*input*
el_angle	*search volume elevation extent*	*degrees*	*input*
PAP	*power aperture product*	*dB*	*output*

MATLAB Function** "power_aperture.m" **Listing

```
function PAP = power_aperture(snr,tsc,sigma,range,nf,loss,az_angle,el_angle)
% This program implements Eq. (1.47)
Tsc = 10*log10(tsc); % convert Tsc into dB
Sigma = 10*log10(sigma); % convert sigma to dB
four_pi = 10*log10(4.0 * pi); % (4pi) in dB
k_db = 10*log10(1.38e-23); % Boltzmann's constant in dB
To = 10*log10(290); % noise temp. in dB
range_pwr4_db = 10*log10(range.^4); % target range^4 in dB
omega = (az_angle/57.296) * (el_angle / 57.296);
% compute search volume in steraradians
Omega = 10*log10(omega); % search volume in dB
% implement Eq. (1.79)
PAP = snr + four_pi + k_db + To + nf + loss + range_pwr4_db + Omega ...
```

```
  - Sigma - Tsc;
return
```

1.12.4. MATLAB Function "range_red_factor.m"

The function *"range_red_factor.m"* implements Eqs. (1.88) and (1.89). This function generates plots of RRF versus (1) the radar operating frequency, (2) radar to jammer range, and (3) jammer power. Its syntax is as follows:

[RRF] = range_red_factor (te, pj, gj, g, freq, bj, rangej, lossj)

where

Symbol	Description	Units	Status
te	*radar effective temperature*	*K*	*input*
pj	*jammer peak power*	*W*	*input*
gj	*jammer antenna gain*	*dB*	*input*
g	*radar antenna gain on jammer*	*dB*	*input*
freq	*radar operating frequency*	*Hz*	*input*
bj	*jammer bandwidth*	*Hz*	*input*
rangej	*radar to jammer range*	*Km*	*input*
lossj	*jammer losses*	*dB*	*input*

MATLAB Function** "range_red_factor.m" **Listing

```
function RRF = range_red_factor (ts, pj, gj, g, freq, bj, rangej, lossj)
% This function computes the range reduction factor and produces
% plots of RRF versus wavelength, radar to jammer range, and jammer power
c = 3.0e+8;
k = 1.38e-23;
lambda = c / freq;
gj_10 = 10^( gj/10);
g_10 = 10^( g/10);
lossj_10 = 10^(lossj/10);
index = 0;
for wavelength = .01:.001:1
  index = index +1;
  jamer_temp = (pj * gj_10 * g_10 *wavelength^2) / ...
    (4.0^2 * pi^2 * k * bj * lossj_10 * (rangej * 1000.0)^2);
  delta = 10.0 * log10(1.0 + (jamer_temp / ts));
  rrf(index) = 10^(-delta /40.0);
end
w = 0.01:.001:1;
figure (1)
semilogx(w,rrf,'k')
```

```
grid
xlabel ('Wavelength in meters')
ylabel ('Range reduction factor')
index = 0;
for ran =rangej*.3:10:rangej*2
  index = index + 1;
  jamer_temp = (pj * gj_10 * g_10 *lambda^2) / ...
    (4.0^2 * pi^2 * k * bj * lossj_10 * (ran * 1000.0)^2);
  delta = 10.0 * log10(1.0 + (jamer_temp / ts));
  rrf1(index) = 10^(-delta /40.0);
end
figure(2)
ranvar = rangej*.3:10:rangej*2 ;
plot(ranvar,rrf1,'k')
grid
xlabel ('Radar to jammer range in Km')
ylabel ('Range reduction factor')
index = 0;
for pjvar = pj*.01:100:pj*2
  index = index + 1;
  jamer_temp = (pjvar * gj_10 * g_10 *lambda^2) / ...
    (4.0^2 * pi^2 * k * bj * lossj_10 * (rangej * 1000.0)^2);
  delta = 10.0 * log10(1.0 + (jamer_temp / ts));
  rrf2(index) = 10^(-delta /40.0);
end
figure(3)
pjvar = pj*.01:100:pj*2;
plot(pjvar,rrf2,'k')
grid
xlabel ('Jammer peak power in Watts')
ylabel ('Range reduction factor')
```

1.12.5. MATLAB Function "ref_coef.m"

The function *"ref_coef.m"* calculates the horizontal and vertical magnitude and phase response of the reflection coefficient. The syntax is as follows

[rh,rv] = ref_coef (psi, epsp, epspp)

where

Symbol	Description	Status
psi	*grazing angle in degrees (can be a vector or a scalar)*	*input*
epsp	ε'	*input*

Symbol	Description	Status
epspp	ε''	*input*
rh	*horizontal reflection coefficient complex vector*	*output*
rv	*vertical reflection coefficient complex vector*	*output*

MATLAB Function** "ref_coef.m" **Listing

```
function [rh,rv] = ref_coef (psi, epsp, epspp)
eps = epsp - i .* epspp;
psirad = psi.*(pi./180.);
arg1 = eps - (cos(psirad).^2);
arg2 = sqrt(arg1);
arg3 = sin(psirad);
arg4 = eps.*arg3;
rv = (arg4-arg2)./(arg4+arg2);
rh = (arg3-arg2)./(arg3+arg2);
```

1.12.6. MATLAB Function "divergence.m"

The MATLAB function *"divergence.m"* calculates the divergence. The syntax is as follows:

D = divergence (psi, r1, r2, hr, ht)

where

Symbol	Description	Status
psi	*grazing angle in degrees (can be vector or scalar)*	*input*
r1	*ground range between radar and specular point in Km*	*input*
r2	*ground range between specular point and target in Km*	*input*
hr	*radar height in meters*	*input*
ht	*target height in meters*	*input*
D	*divergence*	*output*

MATLAB Function** "divergence.m" **Listing

```
function [D] = divergence(psi, r1, r2, hr, ht)
% calculates divergence
%      inputs  %%%%%%%%%%%%%%%%%%%%%
%   r1  ground range between radar and specular point in Km
%   r2  ground range between specular point and target in Km
%   psi grazing angle in degrees
%      parameters  %%%%%%%%%%%%%%%%%%%%
%   re  4/3 earth radius 4/3 * 6375 Km
```

```
%   r = r1 + r2
psi = psi .* pi ./180; % psi in radians
re = (4/3) * 6375e3;
r = r1 + r2;
arg1 = re .*  r . *  sin(psi) ;
arg2 = ((2 .* r1 .* r2 ./ cos(psi)) + re .* r. * sin(psi)) .* (1+hr./re) .* (1+ht./re);
D = sqrt(arg1 ./ arg2);
return
```

1.12.7. MATLAB Function "surf_rough.m"

The MATLAB function "*surf_rough.m*" calculates the surface roughness reflection coefficient. The syntax is as follows:

Sr = surf_rough (hrms, freq, psi)

where

Symbol	Description	Status
hrms	*surface rms roughness value in meters*	*input*
freq	*frequency in Hz*	*input*
psi	*grazing angle in degrees*	*input*
Sr	*surface roughness coefficient*	*output*

MATLAB Function** "surf_rough.m" **Listing

```
function Sr = surf_rough(hrms, freq, psi)
clight = 3e8;
psi = psi .* pi ./ 180; % angle in radians
lambda = clight / freq; % wavelength
g = (2.* pi .* hrms .* sin(psi) ./ lambda).^2;
Sr = exp(-2 .* g);
return
```

1.12.8. MATLAB Program "multipath.m"

```
% This program calculates and plots the propagation factor versus
% target range with a fixed target height.
% The free space radar-to-target range is assumed to be known.
clear all;
close all;
eps = 0.01;
%%%%%%%%%%%% input %%%%%%%%%%%%%%%%
ro = 6375e3; % earth radius
re = ro * 4 /3; % 4/3 earth radius
freq = 3000e6; % frequency
```

```
lambda = 3.0e8 / freq; % wavelength
hr = 30.48; % radar height in meters
ht = 2 .* hr; % target height in meters
Rd1 = linspace(2e3, 55e3, 500); % slant range 3 to 55 Km 500 points
%%%%%%%%%%%%%%%%%%%%%%%%%%%%%%%%%%%%%
% determine whether the traget is beyond the radar's line of sight
range_to_horizon = sqrt(2*re) * (sqrt(ht) + sqrt(hr)); % range to horizon
index = find(Rd1 > range_to_horizon);
if isempty(index);
   Rd = Rd1;
else
   Rd = Rd1(1:index(1)-1);
   fprintf('****** WARNING ****** \n')
   fprintf('Maximum range is beyond radar line of sight. \n')
   fprintf('Target is in diffraction region \n')
   fprintf('****** WARNING ****** \n')
end
%%%%%%%%%%%%%%%%%%%%%%%%%%%%%%%%%%%%%%%%%%%%%%%%%%%%%%%%%%%%
val1 = Rd.^2 - (ht -hr).^2;
val2 = 4 .* (re + hr) .* (re + ht);
r = 2 .* re .* asin(sqrt(val1 ./ val2));
phi = r ./ re;
p = sqrt(re .* (ht + hr) + (r.^2 ./4)) .* 2 ./ sqrt(3);
exci = asin((2 .* re .* r .* (ht - hr) ./ p.^3));
r1 = (r ./ 2) - p .* sin(exci ./3);
phi1 = r1 ./ re;
r2 = r - r1;
phi2 = r2 ./ re;
R1 = sqrt( re.^2 + (re + hr).^2 - 2 .* re .* (re + hr) .* cos(phi1));
R2 = sqrt( re.^2 + (re + ht).^2 - 2 .* re .* (re + ht) .* cos(phi2));
psi = asin((2 .* re .* hr + hr^2 - R1.^2) ./ (2 .* re .* R1));
deltaR = R1 + R2 - Rd;
%%%%%%%%%%%%%% input surface roughness %%%%%%%%%%%%%%%%
hrms = 1;
psi = psi .* 180 ./ pi;
[Sr] = surf_rough(hrms, freq, psi);
%%%%%%%%%%%%%% input divergence %%%%%%%%%%%%%%%%
[D] = divergence(psi, r1, r2, hr, ht);
%%%%%%%%%%%%%% input smooth earth ref. coefficient %%%%%%%%%%%%
epsp = 50;
epspp = 15;
[rh,rv] = ref_coef (psi, epsp, epspp);
D = 1;
 Sr =1;
gamav = abs(rv);
phv = angle(rv);
gamah = abs(rh);
phh = angle (rh);
```

```
gamav =1;
phv = pi;
Gamma_mod = gamav .* D .* Sr;
Gamma_phase = phv; %
rho = Gamma_mod;
delta_phi = 2 .* pi .* deltaR  ./ lambda;
alpha = delta_phi + phv;
F = sqrt( 1 + rho.^2 + 2 .* rho .* cos( alpha));
Ro = 185.2e3; % reference range in Km
F_free = 40 .* log10(Ro ./ Rd);
F_dbr = 40 .* log10( F .* Ro ./ Rd);
F_db = 40 .* log10( eps + F );
figure(1)
plot(Rd./1000, F_db,'k','linewidth',1)
grid
xlabel('slant range in Km')
ylabel('propagation factor in dB')
axis tight
axis([2 55 -60 20])
figure(2)
plot(Rd./1000, F_dbr,'k',Rd./1000, F_free,'k-.','linewidth',1)
grid
xlabel('slant range in Km')
ylabel('Propagation factor in dB')
axis tight
axis([2 55 -40 80])
legend('with multipath','free space')
title('frequency = 3GHz; ht = 60 m; hr = 30 m')
```

1.12.9. MATLAB Program "diffraction.m"

This function utilizes Shatz's model to calculate the propagation factor in the diffraction region. It utilizes the MATLAB function *"airy.m"* which is part of the Signal Processing Toolbox. Its syntax is as follows

F = diffraction(freq, hr, ht, R, nt);

where

% Generalized spherical earth propagation factor calculations

Symbol	Description	Status
freq	*radar operating frequency*	*Hz*
hr	*radar height*	*meters*
ht	*target height*	*meters*

Symbol	Description	Status
R	*range over which to calculate the propagation factor*	*Km*
nt	*number of data point is the series given in Eq. (1.186)*	*none*
F	*propagation factor in diffraction region*	*dB*

MATLAB Program *"diffraction.m"* ***Listing***

```
function F = diffraction(freq, hr, ht,R,nt);
%   Generalized spherical earth propagation factor calculations
%   After Shatz: Michael P. Shatz, and George H. Polychronopoulos, An
%   Algorithm for Elevation of Radar Propagation in the Spherical Earth
%   Diffraction Region. IEEE Transactions on Antenna and Propagation,
%   VOL. 38, NO.8, August 1990.
format long
re = 6373e3 * (4/3); % 4/3 earth radius in Km
[an] = airyzo1(nt);% calculate the roots of the Airy function
c = 3.0e8; % speed of light
lambda = c/freq; % wavelength
r0 = (re*re*lambda / pi)^(1/3);
h0 = 0.5 * (re*lambda*lambda/pi/pi)^(1/3);
y = hr / h0;
z = ht / h0;
%%%%%%%%%%%%
par1 = exp(sqrt(-1)*pi/3);
pary1 = ((2/3).*(an + y .* par1).^(1.5));
   pary = exp(pary1);
   parz1 = ((2/3).*(an + z .* par1).^(1.5));
   parz = exp(parz1);
   f1n = airy(an + y * par1) .* airy(an + z * par1) .* pary .*parz ;
   f1d = par1 .* par1 .* airy(1,an) .* airy(1,an);
   f1 = f1n ./ f1d;
   index = find(f1<1e6);
%%%%%%%%%%%%
F = zeros(1,size(R,2));
for range = 1:size(R,2)
   x(range) = R(range)/r0;
   f2 = exp(0.5 .* (sqrt(3) +sqrt(-1)) .*an.*x(range) - pary1 -parz1);
   victor = f1(index) .* f2(index);
   fsum = sum(victor);
   F(range) = 2 .*sqrt(pi.*x(range)) .* fsum;
end
```

1.12.10. MATLAB Program "airyzo1.m"

The function "airyzo1.m" was developed to compute the roots of the Airy function. Its syntax is as follows:

$$[an] = airyzo1(nt)$$

where the input *nt* is the number of required roots, and the output *[an]* is the roots (zeros) vector.

MATLAB Program** "airyzo1.m" **Listing

```
function [an] = airyzo1(nt)
%   This program is a modified version of a function obtained from
%   free internet source www.mathworks.com/matlabcentral/fileexchange/
%   modified by B. Mahafza (bmahafza@dbresearch.net) in 2005
%      ============================
%   Purpose: This program computes the first nt zeros of Airy
%   functions Ai(x)
%   Input :  nt    --- Total number of zeros
%   Output:  an ---    first nt roots for Ai(x)
format long
an = zeros(1,nt);
xb = zeros(1,nt);
ii = linspace(1,nt,nt);
u = 3.0.*pi.*(4.0.*ii-1)./8.0;
u1 = 1./(u.*u);
rt0 = -(u.*u).^(1.0./3.0).*((((-15.5902.*u1+.929844).* ...
u1-.138889).*u1+.10416667).*u1+1.0);
rt = 1.0e100;
while(abs((rt-rt0)./rt)> 1.e-12);
x = rt0;
ai = airy(0,x);
ad = airy(1,x);
rt=rt0-ai./ad;
if(abs((rt-rt0)./rt)> 1.e-12);
rt0 = rt;
end;
end;
an(ii)= rt;
end
```

1.12.11. MATLAB Program "fig_31_32.m"

```
% This program produces Figs. 1.31 and 1.32
close all
clear all
```

```
psi = 0.01:0.25:90;
epsp = [2.8];
epspp = [0.032];% 0.87 2.5 4.1];
[rh1,rv1] = ref_coef(psi, epsp,epspp);
gamamodv1 = abs(rv1);
gamamodh1 = abs(rh1);
epsp = [5.8] ;
epspp = [0.87];
[rh2,rv2] = ref_coef(psi, epsp,epspp);
gamamodv2 = abs(rv2);
gamamodh2 = abs(rh2);
epsp = [10.3];
epspp = [2.5];
[rh3,rv3] = ref_coef(psi, epsp,epspp);
gamamodv3 = abs(rv3);
gamamodh3 = abs(rh3);
epsp = [15.3];
epspp = [4.1];
[rh4,rv4] = ref_coef(psi, epsp,epspp);
gamamodv4 = abs(rv4);
gamamodh4 = abs(rh4);
figure(1)
semilogx(psi,gamamodh1,'k',psi,gamamodh2,'k-.', ...
psi,gamamodh3,'k.',psi,gamamodh4,'k:','linewidth',1.5);
grid
xlabel('grazing angle - degrees');
ylabel('reflection coefficient - amplitude')
legend('moisture = 0.3%','moisture = 10%%','moisture = 20%','moisture = 30%')
title('horizontal polarization')
% legend ('Vertical Polarization','Horizontal Polarization')
% pv = -angle(rv);
% ph = angle(rh);
% figure(2)
% plot(psi,pv,'k',psi,ph,'k -.');
% grid
% xlabel('grazing angle - degrees');
% ylabel('reflection coefficient - pahse')
% legend ('Vertical Polarization','Horizontal Polarization')
```

Problems

1.1. (a) Calculate the maximum unambiguous range for a pulsed radar with PRF of $200Hz$ and $750Hz$. (b) What are the corresponding PRIs?

1.2. For the same radar in Problem 1.1, assume a duty cycle of 30% and peak power of $5KW$. Compute the average power and the amount of radiated energy during the first $20ms$.

1.3. A certain pulsed radar uses pulse width $\tau = 1\mu s$. Compute the corresponding range resolution.

1.4. An X-band radar uses PRF of $3KHz$. Compute the unambiguous range and the required bandwidth so that the range resolution is $30m$. What is the duty cycle?

1.5. Compute the Doppler shift associated with a closing target with velocity 100, 200, and 350 meters per second. In each case compute the time dilation factor. Assume that $\lambda = 0.3m$.

1.6. In reference to Fig. 1.8, compute the Doppler frequency for

$v = 150m/s$, $\theta_a = 30°$, and $\theta_e = 15°$. Assume that $\lambda = 0.1m$.

1.7. (a) Develop an expression for the minimum PRF of a pulsed radar; (b) compute $f_{r_{min}}$ for a closing target whose velocity is $400m/s$. (c) What is the unambiguous range? Assume that $\lambda = 0.2m$.

1.8. An L-band pulsed radar is designed to have an unambiguous range of $100Km$ and range resolution $\Delta R \leq 100m$. The maximum resolvable Doppler frequency corresponds to $v_{target} \leq 350m/\sec$. Compute the maximum required pulse width, the PRF, and the average transmitted power if $P_t = 500W$.

1.9. Compute the aperture size for an X-band antenna at $f_0 = 9GHz$. Assume antenna gain $G = 10, 20, 30\ dB$.

1.10. An L-band radar (1500 MHz) uses an antenna whose gain is $G = 30dB$. Compute the aperture size. If the radar duty cycle is $d_t = 0.2$ and the average power is $25KW$, compute the power density at range $R = 50Km$.

1.11. For the radar described in Problem 1.9, assume the minimum detectable signal is $5dBm$. Compute the radar maximum range for $\sigma = 1.0, 10.0, 20.0m^2$.

1.12. Consider an L-band radar with the following specifications: operating frequency $f_0 = 1500MHz$, bandwidth $B = 5MHz$, and antenna gain $G = 5000$. Compute the peak power, the pulse width, and the minimum detectable signal for this radar. Assume target RCS $\sigma = 10m^2$, the single pulse SNR is $15.4dB$, noise figure $F = 5dB$, temperature $T_0 = 290K$, and maximum range $R_{max} = 150Km$.

1.13. Consider a low PRF C-band radar operating at $f_0 = 5000MHz$. The antenna has a circular aperture with radius $2m$. The peak power is $P_t = 1MW$ and the pulse width is $\tau = 2\mu s$. The PRF is $f_r = 250Hz$, and the effective temperature is $T_0 = 600K$. Assume radar losses $L = 15dB$ and target RCS $\sigma = 10m^2$. (a) Calculate the radar's unambiguous range; (b) calculate the range R_0 that corresponds to $SNR = 0dB$; (c) calculate the SNR at $R = 0.75R_0$.

1.14. Repeat the second example in Section 1.6 with $\Omega = 4°$, $\sigma = 1m^2$, and $R = 400Km$.

1.15. The atmospheric attenuation can be included in the radar equation as another loss term. Consider an X-band radar whose detection range at $20Km$ includes a $0.25dB/Km$ atmospheric loss. Calculate the corresponding detection range with no atmospheric attenuation.

1.16. Let the maximum unambiguous range for a low PRF radar be R_{max}. (a) Calculate the SNR at $(1/2)R_{max}$ and $(3/4)R_{max}$. (b) If a target with $\sigma = 10m^2$ exists at $R = (1/2)R_{max}$, what should the target RCS be at $R = (3/4)R_{max}$ so that the radar has the same signal strength from both targets.

1.17. A Millie-Meter Wave (MMW) radar has the following specifications: operating frequency $f_0 = 94GHz$, PRF $f_r = 15KHz$, pulse width $\tau = 0.05ms$, peak power $P_t = 10W$, noise figure $F = 5dB$, circular antenna with diameter $D = 0.254m$, antenna gain $G = 30dB$, target RCS $\sigma = 1m^2$, system losses $L = 8dB$, radar scan time $T_{sc} = 3s$, radar angular coverage $200°$, and atmospheric attenuation $3dB/Km$. Compute the following: (a) wavelength λ, (b) range resolution ΔR, (c) bandwidth B, (d) the SNR as a function of range, (e) the range for which $SNR = 15dB$, (f) antenna beam width, (g) antenna scan rate, (h) time on target, (i) the effective maximum range when atmospheric attenuation is considered.

1.18. A radar with antenna gain G is subject to a repeater jammer whose antenna gain is G_J. The repeater illuminates the radar with three fourths of the incident power on the jammer. (a) Find an expression for the ratio between the power received by the jammer and the power received by the radar. (b) What is this ratio when $G = G_J = 200$ and $R/\lambda = 10^5$?

1.19. A radar has the following parameters: peak power $P_t = 65KW$, total losses $L = 5dB$, operating frequency $f_o = 8GHz$, PRF $f_r = 4KHz$, duty cycle $d_t = 0.3$, circular antenna with diameter $D = 1m$, effective aperture is 0.7 of physical aperture, noise figure $F = 8dB$. (a) Derive the various parameters needed in the radar equation. (b) What is the unambiguous range? (c) Plot the SNR versus range (1 Km to the radar unambiguous range) for a 5dBsm target, and (d) if the minimum SNR required for detection is 14 dB, what is the detection range for a 6 dBsm target? What is the detection range if the SNR threshold requirement is raised to 18 dB?

1.20. A radar has the following parameters: Peak power $P_t = 50KW$; total losses $L = 5dB$; operating frequency $f_o = 5.6GHz$; noise figure $F = 10dB$ pulse width $\tau = 10\mu s$; PRF $f_r = 2KHz$; antenna beamwidth $\theta_{az} = 1°$ and $\theta_{el} = 5°$. (a) What is the antenna gain? (b) What is the effective aperture if the aperture efficiency is 60%? (c) Given a 14 dB threshold detection, what is the detection range for a target whose RCS is $\sigma = 1m^2$?

1.21. A certain radar has losses of 5 dB and a receiver noise figure of 10 dB. This radar has a detection coverage requirement that extends over 3/4 of a hemisphere and must complete it in 3 second. The base line target RCS is 6 dBsm and the minimum SNR is 15 dB. The radar detection range is less than 80 Km. What is the average power aperture product for this radar so that it can satisfy its mission?

1.22. Assume a bandwidth of $150KHz$. (a) Compute the noise figure for the three cascaded amplifiers. (b) Compute the effective temperature for the three cascaded amplifiers. (c) Compute the overall system noise figure.

1.23. An exponential expression for the index of refraction is given by $n = 1 + 315 \times 10^{-6} \exp(-0.136h)$ where the altitude h is in Km. Calculate the index of refraction for a well-mixed atmosphere at 10% and 50% of the troposphere.

1.24. A source with equivalent temperature $T_0 = 290K$ is followed by three amplifiers with specifications shown in the table below.

Amplifier	F, *dB*	G, *dB*	T_e
1	You must compute	12	350
2	10	22	
3	15	35	

1.25. Reproduce Figs. 1.30 and 1.31 by using $f = 8GHz$ and (a) $\varepsilon' = 2.8$ and $\varepsilon'' = 0.032$ (dry soil); (b) $\varepsilon' = 47$ and $\varepsilon'' = 19$ (sea water at $0°C$); (c) $\varepsilon' = 50.3$ and $\varepsilon'' = 18$ (lake water at $0°C$).

1.26. In reference to Fig. 8.16, assume a radar height of $h_r = 100m$ and a target height of $h_t = 500m$. The range is $R = 20Km$. (a) Calculate the lengths of the direct and indirect paths. (b) Calculate how long it will take a pulse to reach the target via the direct and indirect paths.

1.27. A radar at altitude $h_r = 10m$ and a target at altitude $h_t = 300m$, and assuming a spherical earth, calculate r_1, r_2, and ψ_g.

1.28. In the previous problem, assuming that you may be able to use the small grazing angle approximation: (a) Calculate the ratio of the direct to the indirect signal strengths at the target. (b) If the target is closing on the radar with velocity $v = 300m/s$, calculate the Doppler shift along the direct and indirect paths. Assume $\lambda = 3cm$.

1.29. Derive an asymptotic form for Γ_h and Γ_v when the grazing angle is very small.

1.30. In reference to Fig. 1.37, assume a radar height of $h_r = 100m$ and a target height of $h_t = 500m$. The range is $R = 20Km$. (a) Calculate the lengths of the direct and indirect paths. (b) Calculate how long it will take a pulse to reach the target via the direct and indirect paths.

1.31. Using the law of cosines, derive Eq. (1.138) from (1.137).

1.32. In the previous problem, assuming that you may be able to use the small grazing angle approximation. (a) Calculate the ratio of the direct to the indirect signal strengths at the target. (b) If the target is closing on the radar with velocity $v = 300m/s$, calculate the Doppler shift along the direct and indirect paths. Assume $\lambda = 3cm$.

1.33. In the previous problem, assuming that you may be able to use the small grazing angle approximation: (a) Calculate the ratio of the direct to the indirect signal strengths at the target. (b) If the target is closing on the radar with velocity $v = 300m/s$, calculate the Doppler shift along the direct and indirect paths. Assume $\lambda = 3cm$.

1.34. Calculate the range to the horizon corresponding to a radar at $5Km$ and $10Km$ of altitude. Assume 4/3 earth.

1.35. Develop a mathematical expression that can be used to reproduce Fig. 1.42.

1.36. Modify the MATLAB program *"multipath.m"* so that it uses the true spherical ground range between the radar and the target.

1.37. Modify the MATLAB program *"multipath.m"* so that it accounts for the radar antenna.

Chapter 2 Linear Systems and Complex Signal Representation

This chapter presents a top level overview of elements of signal theory that are relevant to radar detection and radar signal processing. It is assumed that the reader has sufficient and adequate background in signals and systems as well as in Fourier transform and its associated properties.

2.1. Signal and System Classifications

In general, electrical signals can represent either current or voltage and may be classified into two main categories: energy signals and power signals. Energy signals can be deterministic or random, while power signals can be periodic or random. A signal is said to be random if it is a function of a random parameter (such as random phase or random amplitude). Additionally, signals may be divided into lowpass or bandpass signals. Signals that contain very low frequencies (close to DC) are called lowpass signals; otherwise they are referred to as bandpass signals. Through modulation, lowpass signals can be mapped into bandpass signals.

The average power P for the current or voltage signal $x(t)$ over the interval (t_1, t_2) across a 1Ω resistor is

$$P = \frac{1}{t_2 - t_1} \int_{t_1}^{t_2} |x(t)|^2 \, dt \tag{2.1}$$

The signal $x(t)$ is said to be a power signal over a very large interval $T = t_2 - t_1$, if and only if it has finite power and satisfies the relation:

$$0 < \lim_{T \to \infty} \frac{1}{T} \int_{-T/2}^{T/2} |x(t)|^2 \, dt < \infty \tag{2.2}$$

Using Parseval's theorem, the energy E dissipated by the current or voltage signal $x(t)$ across a 1Ω resistor, over the interval (t_1, t_2), is

$$E = \int_{t_1}^{t_2} |x(t)|^2 \, dt \tag{2.3}$$

The signal $x(t)$ is said to be an energy signal if and only if it has finite energy,

$$E = \int_{-\infty}^{\infty} |x(t)|^2 \, dt \quad < \infty \tag{2.4}$$

A signal $x(t)$ is said to be periodic with period T if and only if

$$x(t) = x(t + nT) \qquad for \ \ all \ \ t \tag{2.5}$$

where n is an integer.

Example:

Classify each of the following signals as an energy signal, a power signal, or neither. All signals are defined over the interval $(-\infty < t < \infty)$*:* $x_1(t) = \cos t + \cos 2t$, $x_2(t) = \exp(-\alpha^2 t^2)$.

Solution:

$$P_{x_1} = \frac{1}{T} \int_{-T/2}^{T/2} (\cos t + \cos 2t)^2 dt = 1 \Rightarrow \ \ power \ \ signal$$

Note that since the cosine function is periodic, the limit is not necessary.

$$E_{x_2} = \int_{-\infty}^{\infty} (e^{-\alpha^2 t^2})^2 dt = 2\int_{0}^{\infty} e^{-2\alpha^2 t^2} dt = 2\frac{\sqrt{\pi}}{2\sqrt{2}\alpha} = \frac{1}{\alpha}\sqrt{\frac{\pi}{2}} \ \ \Rightarrow \ \ energy \ \ signal$$

2.2. The Fourier Transform

The Fourier Transform (FT) of the signal $x(t)$ is

$$F\{x(t)\} = X(\omega) = \int_{-\infty}^{\infty} x(t) e^{-j\omega t} \, dt \tag{2.6}$$

or

$$F\{x(t)\} = X(f) = \int_{-\infty}^{\infty} x(t)e^{-j2\pi ft}\, dt \tag{2.7}$$

and the Inverse Fourier Transform (IFT) is

$$F^{-1}\{X(\omega)\} = x(t) = \frac{1}{2\pi}\int_{-\infty}^{\infty} X(\omega)e^{j\omega t}\, d\omega \tag{2.8}$$

or

$$F^{-1}\{X(f)\} = x(t) = \int_{-\infty}^{\infty} X(f)e^{j2\pi ft}\, df \tag{2.9}$$

where, in general, t represents time, while $\omega = 2\pi f$ and f represent frequency in radians per second and Hertz, respectively. In this book we will use both notations for the transform, as appropriate (i.e., $X(\omega)$ or $X(f)$).

2.3. Systems Classification

Any system can mathematically be represented as a transformation (mapping) of an input signal into an output signal. This transformation or mapping relationship between the input signal $x(t)$ and the corresponding output signal $y(t)$ can be written as

$$y(t) = f[x(t);\ (-\infty < t < \infty)] \tag{2.10}$$

The relationship described in Eq. (2.10) can be linear or nonlinear, time invariant or time varying, causal or noncausal, and stable or nonstable systems. When the input signal is unit impulse (*Dirac delta function)* $\delta(t)$, the output signal is referred to as the system's impulse response $h(t)$.

2.3.1. Linear and Nonlinear Systems

A system is said to be linear if superposition holds true. More specifically, if

$$\begin{aligned} y_1(t) &= f[x_1(t)] \\ y_2(t) &= f[x_2(t)] \end{aligned} \tag{2.11}$$

then for a linear system

$$f[ax_1(t) + bx_2(t)] = ay_1(t) + by_2(t) \tag{2.12}$$

for any constants (a, b). If the relationship in Eq. (2.12) is not true the system is said to be nonlinear.

2.3.2. Time Invariant and Time Varying Systems

A system is said to be time invariant (or shift invariant) if a time shift at its input produces the same time shift at its output. That is if

$$y(t) = f[x(t)] \tag{2.13}$$

then

$$y(t-t_0) = f[x(t-t_0)]; -\infty < t_0 < \infty \tag{2.14}$$

If the above relationship is not true the system is called time varying system.

Any Linear Time Invariant (LTI) system can be described using the convolution integral between the input signal and the system's impulse response, as

$$y(t) = \int_{-\infty}^{\infty} x(t-u)h(u)\ du = x \otimes h \tag{2.15}$$

where the operator $\otimes$ is used to symbolically describe the convolution integral. In the frequency domain convolution translates into multiplication. That is

$$Y(f) = X(f)H(f) \tag{2.16}$$

$H(f)$ is the FT for $h(t)$ and it is referred to as the system transfer function.

2.3.3. Stable and Nonstable Systems

A system is said to be stable if every bounded input signal produces a bounded output signal. From Eq. (2.15)

$$|y(t)| = \left| \int_{-\infty}^{\infty} x(t-u)h(u)\ du \right| \leq \int_{-\infty}^{\infty} |x(t-u)||h(u)|\ du \tag{2.17}$$

If the input signal is bounded, then there is some finite constant K such that

$$|x(t)| \leq K < \infty \tag{2.18}$$

Therefore,

$$y(t) \leq K \int_{-\infty}^{\infty} |h(u)|\ du \tag{2.19}$$

which can be finite if and only if

$$\int_{-\infty}^{\infty} |h(u)| \, du < \infty \tag{2.20}$$

Thus, the requirement for stability is that the impulse response must be absolutely integrable. Otherwise, the system is said to be unstable.

2.3.4. Causal and Noncausal Systems

A causal (or physically realizable) system is one whose output signal does not begin before the input signal is applied. Thus, the following relationship is true when the system is causal:

$$y(t_0) = f[x(t); t \le t_0]; -\infty < t, t_0 < \infty \tag{2.21}$$

A system that does not satisfy Eq. (2.21) is said to be noncausal which means it cannot exist in real world.

2.4. Signal Representation Using the Fourier Series

A set of functions $S = \{\varphi_n(t) \; ; \; n = 1, \ldots, N\}$ is said to be orthogonal over the interval (t_1, t_2) if and only if

$$\int_{t_1}^{t_2} \varphi_i^*(t)\varphi_j(t)dt = \int_{t_1}^{t_2} \varphi_i(t)\varphi_j^*(t)dt = \begin{Bmatrix} 0 & i \neq j \\ \lambda_i & i = j \end{Bmatrix} \tag{2.22}$$

where the asterisk indicates complex conjugation and λ_i are constants. If $\lambda_i = 1$ for all i, then the set S is said to be an orthonormal set. An electrical signal $x(t)$ can be expressed over the interval (t_1, t_2) as a weighted sum of a set of orthogonal functions as

$$x(t) \approx \sum_{n=1}^{N} X_n \varphi_n(t) \tag{2.23}$$

where X_n are, in general, complex constants and the orthogonal functions $\varphi_n(t)$ are called basis functions. If the integral-square error over the interval (t_1, t_2) is equal to zero as N approaches infinity, i.e.,

$$\lim_{N \to \infty} \int_{t_1}^{t_2} \left| x(t) - \sum_{n=1}^{N} X_n \varphi_n(t) \right|^2 dt = 0 \tag{2.24}$$

then the set $S = \{\varphi_n(t)\}$ is said to be complete, and Eq. (2.23) becomes an equality. The constants X_n are computed as

$$X_n = \frac{\int_{t_1}^{t_2} x(t)\varphi_n^*(t)dt}{\int_{t_1}^{t_2} |\varphi_n(t)|^2 dt} \tag{2.25}$$

Let the signal $x(t)$ be periodic with period T, and let the complete orthogonal set S be

$$S = \left\{ e^{\frac{j2\pi nt}{T}} \; ; \; n = -\infty, \infty \right\} \tag{2.26}$$

Then the complex exponential Fourier series of $x(t)$ is

$$x(t) = \sum_{n=-\infty}^{\infty} X_n e^{\frac{j2\pi nt}{T}} \tag{2.27}$$

Using Eq. (2.25) yields

$$X_n = \frac{1}{T} \int_{-T/2}^{T/2} x(t) e^{\frac{-j2\pi nt}{T}} dt \tag{2.28}$$

The FT of Eq. (2.27) is given by

$$X(\omega) = 2\pi \sum_{n=-\infty}^{\infty} X_n \delta\left(\omega - \frac{2\pi n}{T}\right) \tag{2.29}$$

where $\delta(\ )$ is delta function. When the signal $x(t)$ is real we can compute its trigonometric Fourier series from Eq. (2.27) as

$$x(t) = a_0 + \sum_{n=1}^{\infty} a_n \cos\left(\frac{2\pi nt}{T}\right) + \sum_{n=1}^{\infty} b_n \sin\left(\frac{2\pi nt}{T}\right) \tag{2.30}$$

$$a_0 = X_0 \tag{2.31a}$$

$$a_n = \frac{1}{T}\int_{-T/2}^{T/2} x(t)\cos\left(\frac{2\pi nt}{T}\right)dt \tag{2.31b}$$

$$b_n = \frac{1}{T}\int_{-T/2}^{T/2} x(t)\sin\left(\frac{2\pi nt}{T}\right)dt \tag{2.31c}$$

The coefficients a_n are all zeros when the signal $x(t)$ is an odd function of time. Alternatively, when the signal is an even function of time, then all b_n are equal to zero.

Consider the periodic energy signal defined in Eq. (2.30). The total energy associated with this signal is then given by

$$E = \frac{1}{T}\int_{t_0}^{t_0+T} |x(t)|^2 dt = \frac{a_0^2}{4} + \sum_{n=1}^{\infty}\left(\frac{a_n^2}{2} + \frac{b_n^2}{2}\right) \tag{2.32}$$

2.5. Convolution and Correlation Integrals

The convolution $\rho_{xh}(t)$ between the signals $x(t)$ and $h(t)$ is defined by

$$\rho_{xh}(t) = x(t) \otimes h(t) = \int_{-\infty}^{\infty} x(\tau)h(t-\tau)d\tau \tag{2.33}$$

where τ is a dummy variable. Convolution is commutative, associative, and distributive. More precisely,

$$\begin{gathered} x(t) \otimes h(t) = h(t) \otimes x(t) \\ x(t) \otimes (h(t) \otimes g(t)) = (x(t) \otimes h(t)) \otimes g(t) = x(t) \otimes (h(t) \otimes g(t)) \end{gathered} \tag{2.34}$$

For the convolution integral to be finite at least one of the two signals must be an energy signal. The convolution between two signals can be computed using the FT:

$$\rho_{xh}(t) = F^{-1}\{X(\omega)H(\omega)\} \tag{2.35}$$

Consider an LTI system with impulse response $h(t)$ and input signal $x(t)$. It follows that the output signal $y(t)$ is equal to the convolution between the input signal and the system impulse response,

$$y(t) = \int_{-\infty}^{\infty} x(\tau)h(t-\tau)d\tau = \int_{-\infty}^{\infty} h(\tau)x(t-\tau)d\tau \tag{2.36}$$

The cross-correlation function between the signals $x(t)$ and $g(t)$ is

$$R_{xg}(t) = \int_{-\infty}^{\infty} x^*(\tau)g(t+\tau)d\tau = R^*_{gx}(-t) = \int_{-\infty}^{\infty} g^*(\tau)x(t+\tau)d\tau \tag{2.37}$$

Again, at least one of the two signals should be an energy signal for the correlation integral to be finite. The cross-correlation function measures the similarity between the two signals. The peak value of $R_{xg}(t)$ and its spread around this peak are an indication of how good this similarity is. This similarity is measured by a factor called *the correlation coefficient*, denoted by C_{xg}. For example, consider the signals $x(t)$ and $g(t)$, the correlation coefficient is

$$C_{xg} = \frac{\left|\int_{-\infty}^{\infty} x(t)\ g^*(t)dt\right|^2}{\int_{-\infty}^{\infty}|x(t)|^2dt \int_{-\infty}^{\infty}|g(t)|^2dt} = C_{gx} \tag{2.38}$$

clearly the correlation coefficient is limited to $0 \le C_{xg} = C_{gx} \le 1$, with $C_{xg} = 0$ indicating no similarity while $C_{xg} = 1$ indicates 100% similarity between the signals $x(t)$ and $g(t)$.

The cross-correlation integral can be computed as

$$R_{xg}(t) = F^{-1}\{X^*(\omega)G(\omega)\} \tag{2.39}$$

When $x(t) = g(t)$, we get the autocorrelation integral,

$$R_x(t) = \int_{-\infty}^{\infty} x^*(\tau)x(t+\tau)d\tau \tag{2.40}$$

Note that the autocorrelation function is denoted by $R_x(t)$ rather than $R_{xx}(t)$. When the signals $x(t)$ and $g(t)$ are power signals, the correlation integral becomes infinite and, thus, time averaging must be included. More precisely,

$$\bar{R}_{xg}(t) = \lim_{T\to\infty} \frac{1}{T} \int_{-T/2}^{T/2} x^*(\tau) g(t+\tau) d\tau \tag{2.41}$$

2.5.1. Energy and Power Spectrum Densities

Consider an energy signal $x(t)$. From Parseval's theorem, the total energy associated with this signal is

$$E = \int_{-\infty}^{\infty} |x(t)|^2 dt = \frac{1}{2\pi} \int_{-\infty}^{\infty} |X(\omega)|^2 d\omega \tag{2.42}$$

When $x(t)$ is a voltage signal, the amount of energy dissipated by this signal when applied across a network of resistance R is

$$E = \frac{1}{R} \int_{-\infty}^{\infty} |x(t)|^2 dt = \frac{1}{2\pi R} \int_{-\infty}^{\infty} |X(\omega)|^2 d\omega \tag{2.43}$$

Alternatively, when $x(t)$ is a current signal, we get

$$E = R \int_{-\infty}^{\infty} |x(t)|^2 dt = \frac{R}{2\pi} \int_{-\infty}^{\infty} |X(\omega)|^2 d\omega \tag{2.44}$$

The quantity $\int |X(\omega)|^2 d\omega$ represents the amount of energy spread per unit frequency across a 1Ω resistor; therefore, the Energy Spectrum Density (ESD) function for the energy signal $x(t)$ is defined as

$$ESD = |X(\omega)|^2 \tag{2.45}$$

The ESD at the output of an LTI system when $x(t)$ is at its input is

$$|Y(\omega)|^2 = |X(\omega)|^2 |H(\omega)|^2 \tag{2.46}$$

where $H(\omega)$ is the FT of the system impulse response, $h(t)$. It follows that the energy present at the output of the system is

$$E_y = \frac{1}{2\pi} \int_{-\infty}^{\infty} |X(\omega)|^2 |H(\omega)|^2 d\omega \tag{2.47}$$

Example:

The voltage signal $x(t) = e^{-5t};\ t \geq 0$ *is applied to the input of a lowpass LTI system. The system bandwidth is* $5Hz$, *and its input resistance is* 5Ω. *If* $H(\omega) = 1$ *over the interval* $(-10\pi < \omega < 10\pi)$ *and zero elsewhere, compute the energy at the output.*

Solution:

From Eqs. (2.43) and (2.47) we get

$$E_y = \frac{1}{2\pi R} \int_{\omega=-10\pi}^{10\pi} |X(\omega)|^2 |H(\omega)|^2 d\omega$$

Using Fourier transform tables and substituting $R = 5$ *yields*

$$E_y = \frac{1}{5\pi} \int_{0}^{10\pi} \frac{1}{\omega^2 + 25} d\omega$$

Completing the integration yields

$$E_y = \frac{1}{25\pi}[\text{atanh}(2\pi) - \text{atanh}(0)] = 0.01799 \ \ Joules$$

Note that an infinite bandwidth would give $E_y = 0.02$, *only 11% larger.*

The total power associated with a power signal $g(t)$ is

$$P = \lim_{T \to \infty} \frac{1}{T} \int_{-T/2}^{T/2} |g(t)|^2 dt \qquad \textbf{(2.48)}$$

The Power Spectrum Density (PSD) function for the signal $g(t)$ is $S_g(\omega)$, where

$$P = \lim_{T \to \infty} \frac{1}{T} \int_{-T/2}^{T/2} |g(t)|^2 dt = \frac{1}{2\pi} \int_{-\infty}^{\infty} S_g(\omega) d\omega \qquad \textbf{(2.49)}$$

It can be shown that

$$S_g(\omega) = \lim_{T \to \infty} \frac{|G(\omega)|^2}{T} \qquad \textbf{(2.50)}$$

Let the signals $x(t)$ and $g(t)$ be two periodic signals with period T. The complex exponential Fourier series expansions for those signals are, respectively, given by

$$x(t) = \sum_{n=-\infty}^{\infty} X_n e^{j\frac{2\pi nt}{T}} \tag{2.51}$$

$$g(t) = \sum_{m=-\infty}^{\infty} G_m e^{j\frac{2\pi mt}{T}} \tag{2.52}$$

The power cross-correlation function $\bar{R}_{gx}(t)$ was given in Eq. (2.41) and is repeated here as Eq. (2.53),

$$\bar{R}_{gx}(t) = \frac{1}{T}\int_{-T/2}^{T/2} g^*(\tau)x(t+\tau)d\tau \tag{2.53}$$

Note that because both signals are periodic the limit is no longer necessary. Substituting Eqs. (2.51) and (2.52) into Eq. (2.53), collecting terms, and using the definition of orthogonality, we get

$$\bar{R}_{gx}(t) = \sum_{n=-\infty}^{\infty} G_n^* X_n e^{j\frac{2n\pi t}{T}} \tag{2.54}$$

When $x(t) = g(t)$, Eq. (2.54) becomes the power autocorrelation function,

$$\bar{R}_x(t) = \sum_{n=-\infty}^{\infty} |X_n|^2 e^{j\frac{2n\pi t}{T}} = |X_0|^2 + 2\sum_{n=1}^{\infty} |X_n|^2 e^{j\frac{2n\pi t}{T}} \tag{2.55}$$

The power spectrum and cross-power spectrum density functions are then computed as the FT of Eqs. (2.55) and (2.54), respectively. More precisely,

$$\begin{aligned} \bar{S}_x(\omega) &= 2\pi \sum_{n=-\infty}^{\infty} |X_n|^2 \delta\left(\omega - \frac{2n\pi}{T}\right) \\ \bar{S}_{gx}(\omega) &= 2\pi \sum_{n=-\infty}^{\infty} G_n^* X_n \delta\left(\omega - \frac{2n\pi}{T}\right) \end{aligned} \tag{2.56}$$

The line (or discrete) power spectrum is defined as the plot of $|X_n|^2$ versus n, where the lines are $\Delta f = 1/T$ apart. The DC power is $|X_0|^2$, and the total power is $\sum_{n=-\infty}^{\infty} |X_n|^2$.

Consider a signal $x(t)$ and its FT $X(f)$. The corresponding autocorrelation function and power spectrum density are, respectively $\bar{R}_x(t)$ and $\bar{S}_x(f)$. A few very useful relations that will be utilized often in this book include

$$x(0) = \int_{-\infty}^{\infty} X(f)df \tag{2.57}$$

$$\int_{-\infty}^{\infty} x(t)dt = X(0) \tag{2.58}$$

$$\bar{R}_x(0) = \int_{-\infty}^{\infty} |x(t)|^2 dt = \int_{-\infty}^{\infty} |X(f)|^2 df = \bar{S}_x(0) \tag{2.59}$$

$$\int_{-\infty}^{\infty} |\bar{R}_x(t)|^2 dt = \int_{-\infty}^{\infty} |X(f)|^4 df \tag{2.60}$$

Note that Eq. (2.57) or Eq. (2.58) represents the total DC power (in the case of a power signal) or voltage (in the case of an energy signal). Equation (2.59) represents the signal's total power (for power signals) or total energy (for energy signals).

2.6. Bandpass Signals

Signals that contain significant frequency composition at a low frequency band including DC are called lowpass (LP) signals. Signals that have significant frequency composition around some frequency away from the origin are called bandpass (BP) signals. A real BP signal $x(t)$ can be represented mathematically by

$$x(t) = r(t)\cos(2\pi f_0 t + \phi_x(t)) \tag{2.61}$$

where $r(t)$ is the amplitude modulation or envelope, $\phi_x(t)$ is the phase modulation, f_0 is the carrier frequency, and both $r(t)$ and $\phi_x(t)$ have frequency components significantly smaller than f_0. The frequency modulation is

$$f_m(t) = \frac{1}{2\pi}\frac{d}{dt}\phi_x(t) \tag{2.62}$$

and the instantaneous frequency is

$$f_i(t) = \frac{1}{2\pi}\frac{d}{dt}(2\pi f_0 t + \phi_x(t)) = f_0 + f_m(t) \tag{2.63}$$

If the signal bandwidth is B and f_0 is very large compared to B, then the signal $x(t)$ is referred to as a narrow bandpass signal.

Bandpass signals can also be represented by two lowpass signals known as the quadrature components; in this case Eq. (2.61) can be rewritten as

$$x(t) = x_I(t)\cos 2\pi f_0 t - x_Q(t)\sin 2\pi f_0 t \tag{2.64}$$

where $x_I(t)$ and $x_Q(t)$ are real LP signals referred to as the quadrature components and are given, respectively, by

$$\begin{aligned} x_I(t) &= r(t)\cos\phi_x(t) \\ x_Q(t) &= r(t)\sin\phi_x(t) \end{aligned} \tag{2.65}$$

2.6.1. The Analytic Signal (Pre-Envelope)

Given a real valued signal $x(t)$ its Hilbert transform is

$$H\{x(t)\} = \hat{x}(t) = \frac{1}{\pi}\int_{-\infty}^{\infty}\frac{x(u)}{t-u}\,du \tag{2.66}$$

Observation of Eq. (2.66) indicates that the Hilbert transform is computed as the convolution between the signals $x(t)$ and $h(t) = 1/(\pi t)$. More precisely,

$$\hat{x}(t) = x(t) \otimes \frac{1}{\pi t} \tag{2.67}$$

The Fourier transform of $h(t)$ is

$$FT\{h(t)\} = FT\left\{\frac{1}{\pi t}\right\} = H(\omega) = e^{-j\frac{\pi}{2}}\mathrm{sgn}(\omega) \tag{2.68}$$

where the function $\mathrm{sgn}(\omega)$ is given by

$$\text{sgn}(\omega) = \frac{\omega}{|\omega|} = \left\{ \begin{array}{l} 1 \;;\; \omega > 0 \\ 0;\; \omega = 0 \\ -1 \;;\; \omega < 0 \end{array} \right\} \tag{2.69}$$

Thus, the effect of the Hilbert transform is to introduce a phase shift of $\pi/2$ on the spectra of $x(t)$. It follows that,

$$FT\{\hat{x}(t)\} = \hat{X}(\omega) = X(\omega) - j\,\text{sgn}(\omega)X(\omega) \tag{2.70}$$

The analytic signal $\psi(t)$ corresponding to the real signal $x(t)$ is obtained by cancelling the negative frequency contents of $X(\omega)$. Then, by definition

$$\Psi(\omega) = \left\{ \begin{array}{ll} 2X(\omega) & ;\omega > 0 \\ X(\omega) & ;\omega = 0 \\ 0 & ;\omega < 0 \end{array} \right\} \tag{2.71}$$

or equivalently,

$$\Psi(\omega) = X(\omega)(1 + \text{sgn}(\omega)) \tag{2.72}$$

It follows that

$$\psi(t) = FT^{-1}\{\Psi(\omega)\} = x(t) + j\hat{x}(t) \tag{2.73}$$

The analytic signal is often referred to as the pre-envelope of $x(t)$ because the envelope of $x(t)$ can be obtained by simply taking the modulus of $\psi(t)$.

2.6.2. Pre-Envelope and Complex Envelope of Bandpass Signals

The Hilbert transform for the bandpass signal defined in Eq. (2.64) is

$$\hat{x}_{BP}(t) = x_I(t)\sin 2\pi f_0 t + x_Q(t)\cos 2\pi f_0 t \tag{2.74}$$

The subscript BP is used to indicate that $x(t)$ is a bandpass signal. The corresponding bandpass analytic signal (pre-envelope) is then given by

$$\psi_{BP}(t) = x_{BP}(t) + j\hat{x}_{BP}(t) \tag{2.75}$$

substituting Eq. (2.64) and Eq. (2.74) into Eq. (2.75) and collecting terms yield

$$\psi_{BP}(t) = [x_I(t) + jx_Q(t)]e^{j2\pi f_0 t} = \tilde{x}_{BP}(t)e^{j2\pi f_0 t} \tag{2.76}$$

The signal $\tilde{x}_{BP}(t) = x_I(t) + jx_Q(t)$ is the complex envelope of $x_{BP}(t)$. Thus, the envelope signal and associated phase deviation are given by

$$a(t) = \left|\tilde{x}_{BP}(t)\right| = \left|x_I(t) + jx_Q(t)\right| = \left|\psi_{BP}(t)\right| \tag{2.77}$$

$$\phi(t) = \arg(\tilde{x}_{BP}(t)) = \angle\tilde{x}_{BP}(t) \tag{2.78}$$

In the remainder of this text, unless it is indicated to be otherwise, all signals will be considered to be bandpass signals and consequently the subscript BP will not be used. More specifically, a bandpass signal $x(t)$ and its corresponding pre-envelope (analytic signal) and complex envelope will shown as

$$x(t) = x_I(t)\cos 2\pi f_0 t - x_Q(t)\sin 2\pi f_0 t \tag{2.79}$$

$$\psi(t) = x(t) + j\hat{x}(t) \equiv \tilde{x}(t)e^{j2\pi f_0 t} \tag{2.80}$$

$$\tilde{x}(t) = x_I(t) + jx_Q(t) \tag{2.81}$$

Obtaining the complex envelope for any bandpass signal requires extraction of the quadrature components. Figure 2.1 shows how the quadrature components can be extracted from a bandpass signal. First, the bandpass signal is split into two parts; one part is multiplied by $2\cos 2\pi f_0 t$ and the other is multiplied by $-2\sin 2\pi f_0 t$. From the figure the two signal $z_1(t)$ and $z_2(t)$ are,

$$z_1(t) = 2x_I(t)(\cos 2\pi f_0 t)^2 - 2x_Q(t)\cos(2\pi f_0 t)\sin(2\pi f_0 t) \tag{2.82}$$

$$z_2(t) = -2x_I(t)\cos(2\pi f_0 t)\sin(2\pi f_0 t) + 2x_Q(t)(\sin 2\pi f_0 t)^2 \tag{2.83}$$

Utilizing the appropriate trigonometry identities and after lowpass filtering the quadrature components are extracted.

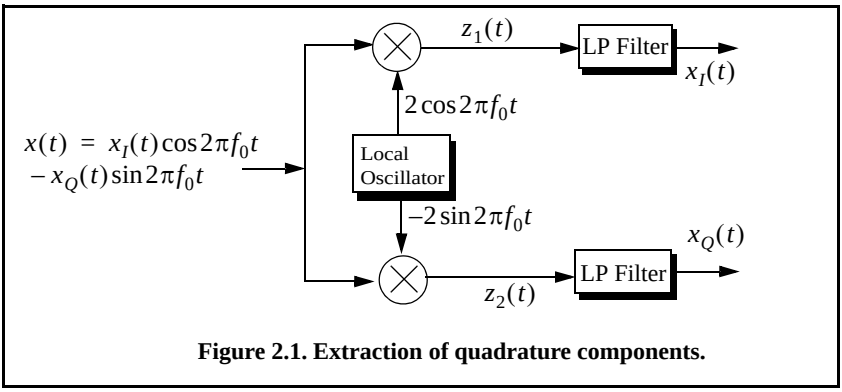

Figure 2.1. Extraction of quadrature components.

Example:

Extract the quadrature components, frequency modulation, instantaneous frequency, analytic signal, and complex envelope for the signals:

(a) $x(t) = Rect\left(\frac{t}{\tau}\right)\cos(2\pi f_0 t)$ *; (b)* $x(t) = Rect\left(\frac{t}{\tau}\right)\cos\left(2\pi f_0 t + \frac{\pi B}{\tau}t^2\right)$

Solution:

(a) *The quadrature components are extracted as described in Fig. 2.1. Define* $z_1(t) = x(t) \times 2\cos(2\pi f_0 t)$, $z_2(t) = x(t) \times (-2)\sin(2\pi f_0 t)$, *then*

$$z_1(t) = Rect\left(\frac{t}{\tau}\right)\cos(2\pi f_0 t) \times 2\cos(2\pi f_0 t) =$$

$$Rect\left(\frac{t}{\tau}\right)\cos(0) + Rect\left(\frac{t}{\tau}\right)\cos(4\pi f_0 t)$$

$$z_2(t) = Rect\left(\frac{t}{\tau}\right)\cos(2\pi f_0 t) \times (-2)\sin(2\pi f_0 t) =$$

$$Rect\left(\frac{t}{\tau}\right)\sin(0) - Rect\left(\frac{t}{\tau}\right)\sin(4\pi f_0 t)$$

Thus, the output of the LPFs are

$$x_I(t) = Rect\left(\frac{t}{\tau}\right) \quad ; \; x_Q(t) = 0$$

From Eq. (2.62) and Eq. (2.63) we get

$$f_m(t) = 0 \quad ; \; f_i(t) = f_0$$

Finally the complex envelope and the analytic signal are given by

$$\tilde{x}(t) = x_I(t) + jx_Q(t) = x_I(t) = Rect\left(\frac{t}{\tau}\right)$$

$$\psi(t) = \tilde{x}(t)e^{j2\pi f_0 t} = Rect\left(\frac{t}{\tau}\right)e^{j2\pi f_0 t}$$

(b)

$$z_1(t) = Rect\left(\frac{t}{\tau}\right)\cos\left(2\pi f_0 t + \frac{\pi B}{\tau}t^2\right) \times 2\cos(2\pi f_0 t) =$$

$$Rect\left(\frac{t}{\tau}\right)\cos\left(\frac{\pi B}{\tau}t^2\right) + Rect\left(\frac{t}{\tau}\right)\cos\left(4\pi f_0 t + \frac{\pi B}{\tau}t^2\right)$$

$$z_2(t) = Rect\left(\frac{t}{\tau}\right)\cos\left(2\pi f_0 t + \frac{\pi B}{\tau}t^2\right) \times (-2)\sin(2\pi f_0 t) =$$

$$Rect\left(\frac{t}{\tau}\right)\sin\left(\frac{\pi B}{\tau}t^2\right) - Rect\left(\frac{t}{\tau}\right)\sin\left(4\pi f_0 t + \frac{\pi B}{\tau}t^2\right)$$

Thus, the outputs of the LPFs are

$$x_I(t) = Rect\left(\frac{t}{\tau}\right)\cos\left(\frac{\pi B}{\tau}t^2\right) \quad ; \; x_Q(t) = Rect\left(\frac{t}{\tau}\right)\sin\left(\frac{\pi B}{\tau}t^2\right)$$

From Eq. (2.62) and Eq.(2.63) we get

$$f_m(t) = \frac{B}{\tau}t \quad ; \; f_i(t) = f_0 + \frac{B}{\tau}t$$

The complex envelope is

$$\tilde{x}(t) = x_I(t) + jx_Q(t) = Rect\left(\frac{t}{\tau}\right)\cos\left(\frac{\pi B}{\tau}t^2\right) + jRect\left(\frac{t}{\tau}\right)\sin\left(\frac{\pi B}{\tau}t^2\right)$$

which can be written as

$$\tilde{x}(t) = Rect\left(\frac{t}{\tau}\right)e^{j\left(\frac{\pi B}{\tau}t^2\right)}$$

Finally, the analytic signal is

$$\psi(t) = \tilde{x}(t)e^{j2\pi f_0 t} = Rect\left(\frac{t}{\tau}\right)e^{j\left(\frac{\pi B}{\tau}t^2\right)}e^{j2\pi f_0 t} = Rect\left(\frac{t}{\tau}\right)e^{j\left(2\pi f_0 t + \frac{\pi B}{\tau}t^2\right)}$$

2.7. Spectra of a Few Common Radar Signals

The spectrum of a given signal describes the spread of its energy in the frequency domain. An energy signal (finite energy) can be characterized by its Energy Spectrum Density (ESD) function, while a power signal (finite power) is characterized by the Power Spectrum Density (PSD) function. The units of the ESD are Joules/Hertz and the PSD has units Watts/Hertz.

2.7.1. Frequency Modulation Signal

The discussion presented in this section will be restricted to sinusoidal modulating signals. In this case, the general formula for an FM waveform can be expressed by

$$x(t) = A\cos\left(2\pi f_0 t + k_f\int_0^t \cos 2\pi f_m u\,du\right) \qquad \textbf{(2.84)}$$

f_0 is the radar operating frequency (carrier frequency), $\cos 2\pi f_m t$ is the modulating signal, A is a constant, and $k_f = 2\pi\Delta f_{peak}$, where Δf_{peak} is the peak frequency deviation. The phase is given by

$$\phi(t) = 2\pi f_0 t + 2\pi\Delta f_{peak}\int_0^t \cos 2\pi f_m u\,du = 2\pi f_0 t + \beta\sin 2\pi f_m t \qquad \textbf{(2.85)}$$

where β is the FM modulation index given by

$$\beta = (\Delta f_{peak})/f_m \qquad \textbf{(2.86)}$$

Let $x_r(t)$ be the received radar signal from a target at range R. It follows that

$$s_r(t) = A_r\cos(2\pi f_0(t-\Delta t) + \beta\sin 2\pi f_m(t-t_0)) \qquad \textbf{(2.87)}$$

where the delay t_0 is

$$t_0 = 2R/c \qquad \textbf{(2.88)}$$

c is the speed of light. Radar receivers utilize phase detectors in order to extract target range from the instantaneous frequency, as illustrated in Fig. 2.2. A good measurement of the phase detector output $x_o(t)$ implies a good measurement of t_0 and, hence, range. Consider the FM waveform $s(t)$ given by

$$x(t) = A\cos(2\pi f_0 t + \beta\sin 2\pi f_m t) \qquad \textbf{(2.89)}$$

which can be written as

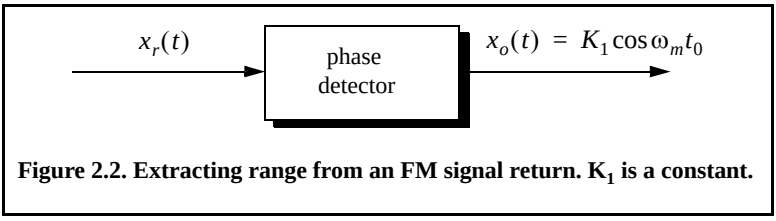

Figure 2.2. Extracting range from an FM signal return. K_1 is a constant.

$$x(t) = ARe\{e^{j2\pi f_0 t}\ e^{j\beta\sin 2\pi f_m t}\} \qquad \textbf{(2.90)}$$

where $Re\{\ \}$ denotes the real part. Since the signal $\exp(j\beta\sin 2\pi f_m t)$ is periodic with period $T = 1/f_m$, it can be expressed using the complex exponential Fourier series as

$$e^{j\beta\sin 2\pi f_m t} = \sum_{n=-\infty}^{\infty} C_n e^{jn2\pi f_m t} \qquad \textbf{(2.91)}$$

where the Fourier series coefficients C_n are given by

$$C_n = \frac{1}{2\pi}\int_{-\pi}^{\pi} e^{j\beta\sin 2\pi f_m t}\; e^{-jn2\pi f_m t}\quad dt \tag{2.92}$$

Make the change of variable $u = 2\pi f_m t$, and recognize that the Bessel function of the first kind of order n is

$$J_n(\beta) = \frac{1}{2\pi}\int_{-\pi}^{\pi} e^{j(\beta\sin u - nu)}\; du \tag{2.93}$$

Thus, the Fourier series coefficients are $C_n = J_n(\beta)$, and consequently Eq. (2.91) can now be written as

$$e^{j\beta\sin 2\pi f_m t} = \sum_{n=-\infty}^{\infty} J_n(\beta)e^{jn2\pi f_m t} \tag{2.94}$$

which is known as the Bessel-Jacobi equation. Figure 2.3 shows a plot of Bessel functions of the first kind for $n = 0, 1, 2, 3$. The total power in the signal $x(t)$ is

$$P = \frac{1}{2}A^2\sum_{n=-\infty}^{\infty}\left|J_n(\beta)\right|^2 = \frac{1}{2}A^2 \tag{2.95}$$

Substituting Eq. (2.95) into Eq. (2.90) yields

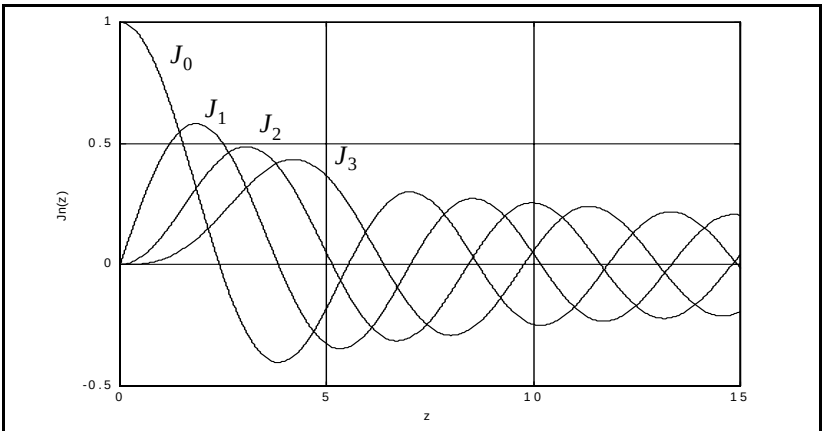

Figure 2.3. Plot of Bessel functions of order 0, 1, 2, and 3.

$$x(t) = ARe\left\{ e^{j2\pi f_0 t} \sum_{n=-\infty}^{\infty} J_n(\beta) e^{jn2\pi f_m t} \right\} \tag{2.96}$$

Expanding Eq. (2.96) yields

$$x(t) = A \sum_{n=-\infty}^{\infty} J_n(\beta) \cos(2\pi f_0 + n2\pi f_m)t \tag{2.97}$$

Finally, since $J_n(\beta) = J_{-n}(\beta)$ for n odd and $J_n(\beta) = -J_{-n}(\beta)$ for n even we can rewrite Eq. (2.97) as

$$\begin{aligned} x(t) = A\{ & J_0(\beta)\cos 2\pi f_0 t + \\ & J_1(\beta)[\cos(2\pi f_0 + 2\pi f_m)t - \cos(2\pi f_0 - 2\pi f_m)t] \\ & + J_2(\beta)[\cos(2\pi f_0 + 4\pi f_m)t + \cos(2\pi f_0 - 4\pi f_m)t] \\ & + J_3(\beta)[\cos(2\pi f_0 + 6\pi f_m)t - \cos(2\pi f_0 - 6\pi f_m)t] \\ & + J_4(\beta)[\cos((2\pi f_0 + 8\pi f_m)t + \cos(2\pi f_0 - 8\pi f_m)t)] + \ldots \} \end{aligned} \tag{2.98}$$

The spectrum of $x(t)$ is composed of pairs of spectral lines centered at f_0, as sketched in Fig. 2.4. The spacing between adjacent spectral lines is f_m. The central spectral line has an amplitude equal to $AJ_0(\beta)$, while the amplitude of the nth spectral line is $AJ_n(\beta)$. As indicated by Eq. (2.98) the bandwidth of FM signals is infinite. However, the magnitudes of spectral lines of the higher orders are small, and thus the bandwidth can be approximated (i.e., effective bandlimited) using Carson's rule,

$$B \approx 2(\beta + 1) f_m \tag{2.99}$$

When β is small, only $J_0(\beta)$ and $J_1(\beta)$ have significant values. Thus, we may approximate Eq. (2.99) by

$$\begin{aligned} x(t) \approx A\{ & J_0(\beta)\cos 2\pi f_0 t + J_1(\beta) \\ & [\cos(2\pi f_0 + 2\pi f_m)t - \cos(2\pi f_0 - 2\pi f_m)t] \} \end{aligned} \tag{2.100}$$

Finally, for small β, the Bessel functions can be approximated by

$$J_0(\beta) \approx 1 \tag{2.101}$$

$$J_1(\beta) \approx \frac{1}{2}\beta \tag{2.102}$$

Thus, Eq. (2.100) may be approximated by

$$x(t) \approx A\left\{ \cos 2\pi f_0 t + \frac{1}{2}\beta[\cos(2\pi f_0 + 2\pi f_m)t - \cos(2\pi f_0 - 2\pi f_m)t] \right\} \tag{2.103}$$

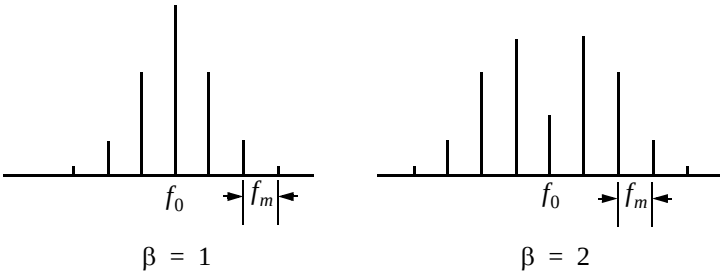

Figure 2.4. Amplitude line spectra sketch for FM signal.

Example:

If the modulation index is $\beta = 0.5$, *give an expression for the signal* $x(t)$.

Solution:

From Bessel function tables $J_0(0.5) = 0.9385$ *and* $J_1(0.5) = 0.2423$; *then using Eq. (2.100) yields*

$$x(t) \approx A\{(0.9385)\cos 2\pi f_0 t + (0.2423) \\ [\cos(2\pi f_0 + 2\pi f_m)t - \cos(2\pi f_0 - 2\pi f_m)t]\}$$

Example:

Consider an FM transmitter with output signal

$$x(t) = 100\cos(2000\pi t + \varphi(t)).$$

The frequency deviation is $4Hz$, *and the modulating waveform is* $x(t) = 10\cos 16\pi t$. *Determine the FM signal bandwidth. How many spectral lines will pass through a bandpass filter whose bandwidth is* $58Hz$ *centered at* $1000Hz$ *?*

Solution:

The peak frequency deviation is $\Delta f_{peak} = 4 \times 10 = 40Hz$. *It follows that*

$$\beta = (\Delta f_{peak})/f_m = 40/8 = 5$$
$$B \approx 2(\beta + 1)f_m = 2 \times (5 + 1) \times 8 = 96Hz$$

However, only seven spectral lines pass through the bandpass filter as illustrated in the figure shown below

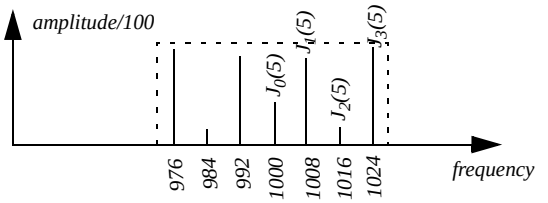

2.7.2. Continuous Wave Signal

Consider a Continuous Wave (CW) waveform given by

$$x_1(t) = \cos 2\pi f_0 t \tag{2.104}$$

The FT of $x_1(t)$ is

$$X_1(f) = \frac{1}{2}[\delta(f - f_0) + \delta(f + f_0)] \tag{2.105}$$

$\delta(\ )$ is the Dirac delta function. As indicated by the amplitude spectrum shown in Fig. 2.5, the signal $x_1(t)$ has infinitesimal bandwidth, located at $\pm f_0$.

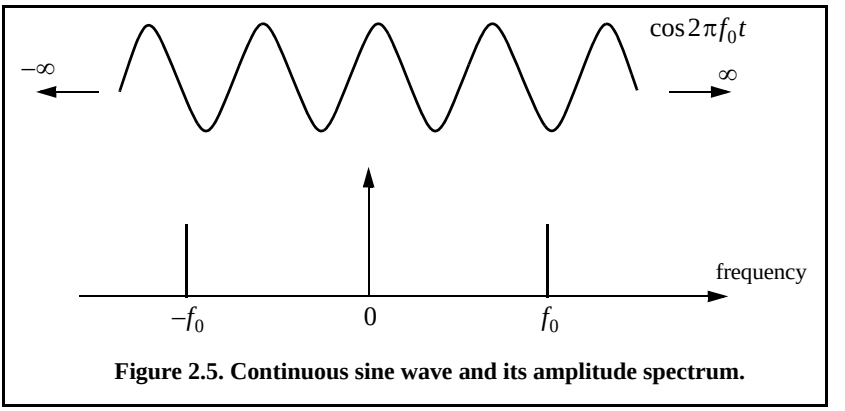

Figure 2.5. Continuous sine wave and its amplitude spectrum.

2.7.3. Finite Duration Pulse Signal

Consider the time-domain signal $x_2(t)$ given by

$$x_2(t) = x_1(t)Rect\left(\frac{t}{\tau_0}\right) = Rect\left(\frac{t}{\tau_0}\right)\cos 2\pi f_0 t \tag{2.106}$$

$$Rect\left(\frac{t}{\tau_0}\right) = \begin{cases} 1 & -\frac{\tau_0}{2} \le t \le \frac{\tau_0}{2} \\ 0 & otherwise \end{cases} \quad \textbf{(2.107)}$$

The Fourier transform of the $Rect$ function is

$$FT\left\{Rect\left(\frac{t}{\tau_0}\right)\right\} = \tau_0 Sinc(f\tau_0) \quad \textbf{(2.108)}$$

where

$$Sinc(u) = \frac{\sin(\pi u)}{\pi u} \quad \textbf{(2.109)}$$

It follows that the FT is

$$X_2(f) = X_1(f) \otimes \tau_0 Sinc(f\tau_0) = \frac{1}{2}[\delta(f-f_0) + \delta(f+f_0)] \otimes \tau_0 Sinc(f\tau_0) \quad \textbf{(2.110)}$$

which can be written as

$$X_2(f) = \frac{\tau_0}{2}\{Sinc[(f-f_0)\tau_0] + Sinc[(f+f_0)\tau_0]\} \quad \textbf{(2.111)}$$

The amplitude spectrum of $x_2(t)$ is shown in Fig. 2.6. It is made up of two $Sinc$ functions, as defined in Eq. (2.108), centered at $\pm f_0$.

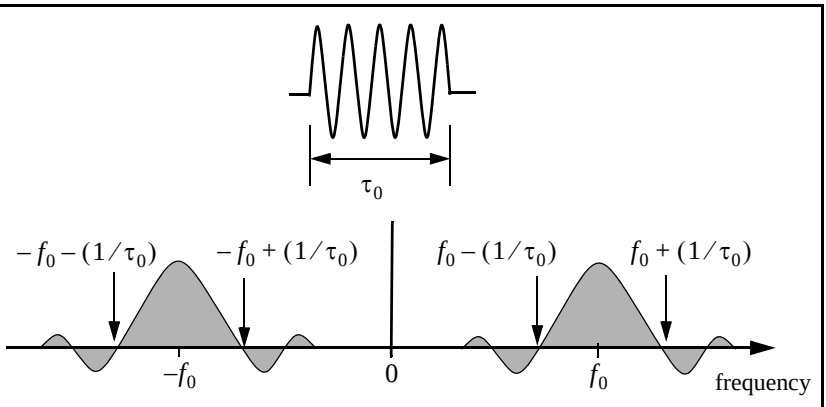

Figure 2.6. Finite duration pulse and its amplitude spectrum.

2.7.4. Periodic Pulse Signal

In this case, consider the coherent gated CW waveform $x_3(t)$ given by

$$x_3(t) = \sum_{n=-\infty}^{\infty} x_1(t)Rect\left(\frac{t-nT}{\tau_0}\right) = \cos 2\pi f_0 t \sum_{n=-\infty}^{\infty} Rect\left(\frac{t-nT}{\tau_0}\right) \quad \textbf{(2.112)}$$

The signal $x_3(t)$ is periodic, with period T (recall that $f_r = 1/T$ is the PRF), of course the condition $f_r \ll f_0$ is assumed. The FT of the signal $x_3(t)$ is

$$X_3(f) = X_1(f) \otimes FT\left\{\sum_{n=-\infty}^{\infty} Rect\left(\frac{t-nT}{\tau_0}\right)\right\} = \quad \textbf{(2.113)}$$

$$\frac{1}{2}[\delta(f-f_0)+\delta(f+f_0)] \otimes FT\left\{\sum_{n=-\infty}^{\infty} Rect\left(\frac{t-nT}{\tau_0}\right)\right\}$$

The complex exponential Fourier series of the summation inside Eq. (2.112) is

$$\sum_{n=-\infty}^{\infty} Rect\left(\frac{t-nT}{\tau_0}\right) = \sum_{n=-\infty}^{\infty} X_n e^{j\frac{nt}{T}} \quad \textbf{(2.114)}$$

where the Fourier series coefficients X_n are given by (see Eq. 2.28)

$$X_n = \frac{1}{T}FT\left\{Rect\left(\frac{t}{\tau_0}\right)\right\}\Bigg|_{f=\frac{n}{T}} = \frac{\tau_0}{T}Sinc(f\tau_0)\Big|_{f=\frac{n}{T}} = \frac{\tau_0}{T}Sinc\left(\frac{n\tau_0}{T}\right) \quad \textbf{(2.115)}$$

It follows that

$$FT\left\{\sum_{n=-\infty}^{\infty} X_n e^{j\frac{nt}{T}}\right\} = \left(\frac{\tau_0}{T}\right)\sum_{n=-\infty}^{\infty} Sinc(nf_r\tau_0)\delta(f-nf_r) \quad \textbf{(2.116)}$$

where the relation $f_r = 1/T$ was used in Eq. (2.116). Substituting Eq. (2.116) into Eq. (2.113) yields the FT of $x_3(t)$. That is

$$X_3(f) = \frac{\tau_0}{2T}[\delta(f-f_0)+\delta(f+f_0)] \otimes \sum_{n=-\infty}^{\infty} Sinc(nf_r\tau_0)\delta(f-nf_r) \qquad \textbf{(2.117)}$$

The amplitude spectrum of $x_3(t)$ has two parts centered at $\pm f_0$; each part corresponds to the spectrum of the second half of Eq. (2.117). The spectrum of the summation part is an infinite number of delta functions repeated every f_r, where the *nth* line is modulated in amplitude with the value corresponding to $Sinc(nf_r\tau_0)$. Therefore, the overall spectrum consists of an infinite number of lines separated by f_r and have $\sin u/u$ envelope that corresponds to X_n. This is illustrated in Fig. 2.7, for the positive portion of the spectrum only.

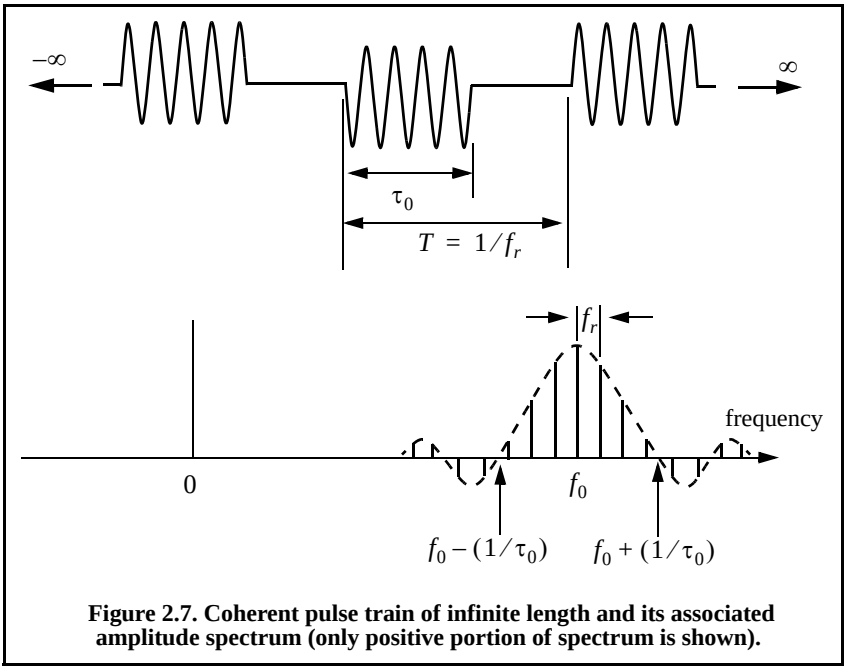

Figure 2.7. Coherent pulse train of infinite length and its associated amplitude spectrum (only positive portion of spectrum is shown).

2.7.5. Finite Duration Pulse Train Signal

Define the function $x_4(t)$ as

$$x_4(t) = \cos(2\pi f_0 t)\sum_{n=0}^{N-1} Rect\left(\frac{t-nT}{\tau_0}\right) = \cos 2\pi f_0 t \times g(t) \qquad \textbf{(2.118)}$$

where

$$g(t) = \sum_{n=0}^{N-1} Rect\left(\frac{t-nT}{\tau_0}\right) \tag{2.119}$$

The amplitude spectrum of the signal $x_4(t)$ is

$$X_4(f) = \frac{1}{2}G(f) \otimes [\delta(f-f_0) + \delta(f+f_0)] \tag{2.120}$$

where $G(f)$ is the FT of $g(t)$. This means that the amplitude spectrum of the signal $x_4(t)$ is equal to replicas of $G(f)$ centered at $\pm f_0$. Given this conclusion, we can then focus on computing $G(f)$.

The signal $g(t)$ can be written as (see top portion of Fig. 2.8)

$$g(t) = \sum_{n=-\infty}^{\infty} g_1(t) Rect\left(\frac{t-nT}{\tau_0}\right) \tag{2.121}$$

where

$$g_1(t) = Rect\left(\frac{t}{NT_t}\right) \tag{2.122}$$

It follows that the FT of Eq. (2.121) can be computed using similar analysis as that which led to Eq. (2.116). More precisely,

$$G(f) = \frac{\tau_0}{T} G_1(f) \otimes \sum_{n=-\infty}^{\infty} Sinc(nf_r\tau_0)\delta(f-nf_r) \tag{2.123}$$

and the FT of $g_1(t)$ is

$$G_1(f) = FT\left\{Rect\left(\frac{t}{T_t}\right)\right\} = T_t Sinc(fT_t) \tag{2.124}$$

Using these results the FT of $x_4(t)$ can be written as

$$X_4(f) = \frac{T_t\tau_0}{2T}\left(Sinc(fT_t) \otimes \sum_{n=-\infty}^{\infty} Sinc(nf_r\tau_0)\delta(f-nf_r)\right) \tag{2.125}$$

$$\otimes [\delta(f-f_0) + \delta(f+f_0)]$$

Therefore, the overall spectrum of $x_4(t)$ consists of a two equal positive and negative portions, centered at $\pm f_0$. Each portion is made up of $N\ Sinc(fT_t)$ functions repeated every f_r with envelope corresponding to $Sinc(nf_r\tau_0)$. This is illustrated in Fig. 2.8, only positive portion of the spectrum is shown.

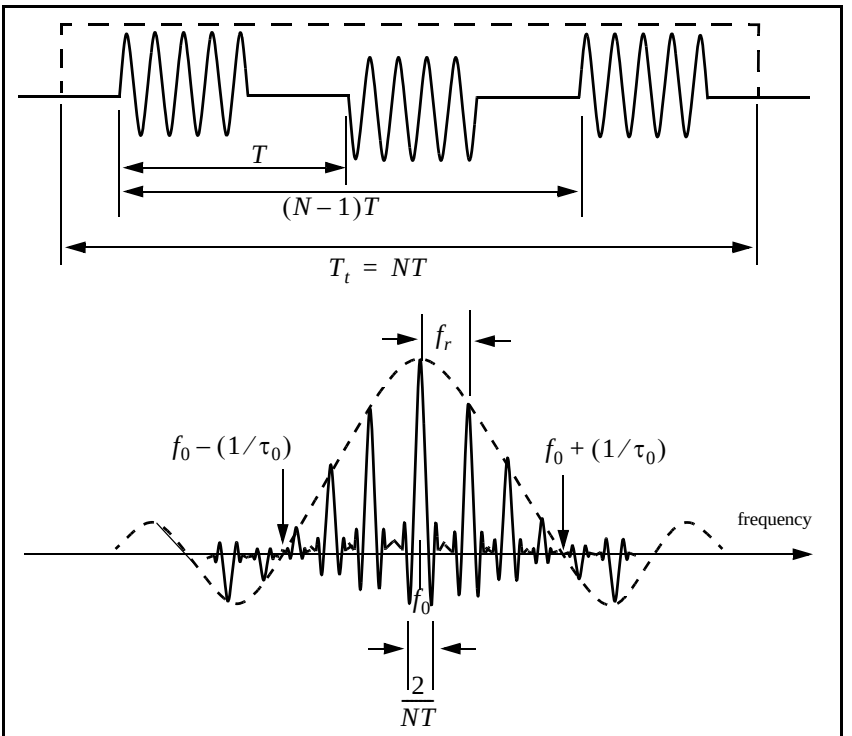

Figure 2.8. Coherent pulse train of finite length and corresponding amplitude spectrum.

2.7.6. Linear Frequency Modulation (LFM) Signal

Frequency or phase modulated signals can be used to achieve much wider operating bandwidths. Linear Frequency Modulation (LFM) is very commonly used in most modern radar systems. In this case, the frequency is swept linearly across the pulse width, either upward (up-chirp) or downward (down-chirp). Figure 2.9 shows a typical example of an LFM waveform. The pulse width is τ_0, and the bandwidth is B.

The LFM up-chirp instantaneous phase can be expressed by

$$\phi(t) = 2\pi\left(f_0 t + \frac{\mu}{2}t^2\right) \qquad -\frac{\tau_0}{2} \le t \le \frac{\tau_0}{2} \tag{2.126}$$

where f_0 is the radar center frequency, and $\mu = B/\tau_0$ is the LFM coefficient. Thus, the instantaneous frequency is

$$f(t) = \frac{1}{2\pi}\frac{d}{dt}\phi(t) = f_0 + \mu t \qquad -\frac{\tau_0}{2} \le t \le \frac{\tau_0}{2} \tag{2.127}$$

Similarly, the down-chirp instantaneous phase and frequency are given, respectively, by

$$\phi(t) = 2\pi\left(f_0 t - \frac{\mu}{2}t^2\right) \qquad -\frac{\tau_0}{2} \le t \le \frac{\tau_0}{2} \tag{2.128}$$

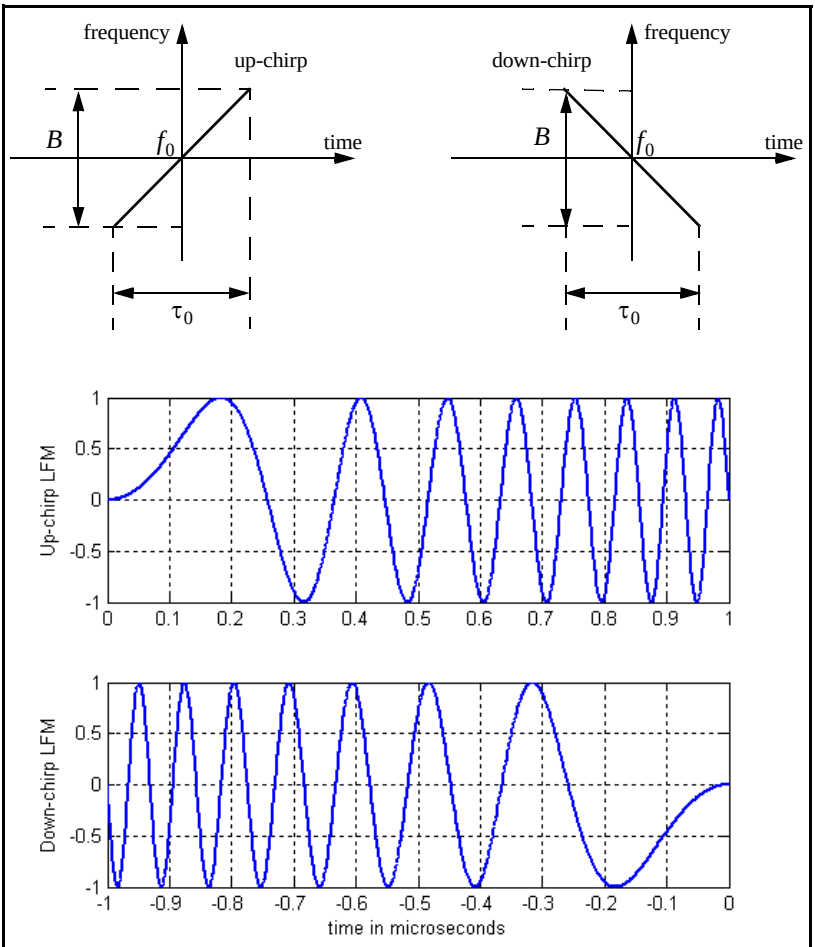

Figure 2.9. Typical LFM waveforms.

$$f(t) = \frac{1}{2\pi}\frac{d}{dt}\phi(t) = f_0 - \mu t \qquad -\frac{\tau_0}{2} \le t \le \frac{\tau_0}{2} \tag{2.129}$$

A typical LFM waveform can be expressed by

$$x_1(t) = Rect\left(\frac{t}{\tau_0}\right)e^{j2\pi\left(f_0 t + \frac{\mu}{2}t^2\right)} \tag{2.130}$$

where $Rect(t/\tau_0)$ denotes a rectangular pulse of width τ_0. Remember that the signal $x_1(t)$ is the analytic signal for the LMF waveform. It follows that

$$x_1(t) = \tilde{x}(t)e^{j2\pi f_0 t} \tag{2.131}$$

$$\tilde{x}(t) = Rect\left(\frac{t}{\tau}\right)e^{j\pi\mu t^2} \tag{2.132}$$

The spectrum of the signal $x_1(t)$ is determined from its complex envelope $\tilde{x}(t)$. The complex exponential term in Eq. (2.132) introduces a frequency shift about the center frequency f_o. Taking the FT of $\tilde{x}(t)$ yields

$$\tilde{X}(f) = \int_{-\infty}^{\infty} Rect\left(\frac{t}{\tau_0}\right)e^{j\pi\mu t^2}\ e^{-j2\pi ft}dt = \int_{-\frac{\tau_0}{2}}^{\frac{\tau_0}{2}} e^{j\pi\mu t^2}\ e^{-j2\pi ft}dt \tag{2.133}$$

Let $\mu' = \pi\mu = \pi B/\tau_0$, and perform the change of variable

$$\left(z = \sqrt{\frac{2}{\pi}}\left(\sqrt{\mu'}t - \frac{\pi f}{\sqrt{\mu'}}\right)\right) \quad ; \quad \sqrt{\frac{\pi}{2\mu'}}\ dz = dt \tag{2.134}$$

Thus, Eq. (2.133) can be written as

$$\tilde{X}(f) = \sqrt{\frac{\pi}{2\mu'}}\ e^{-j(\pi f)^2/\mu'}\int_{-z_1}^{z_2} e^{j\pi z^2/2}\ dz \tag{2.135}$$

$$\tilde{X}(f) = \sqrt{\frac{\pi}{2\mu'}}\ e^{-j(\pi f)^2/\mu'}\left\{\int_0^{z_2} e^{j\pi z^2/2}\ dz - \int_0^{-z_1} e^{j\pi z^2/2}\ dz\right\} \tag{2.136}$$

$$z_1 = -\sqrt{\frac{2\mu'}{\pi}}\left(\frac{\tau_0}{2} + \frac{\pi f}{\mu'}\right) = \sqrt{\frac{B\tau_0}{2}}\left(1 + \frac{f}{B/2}\right) \tag{2.137}$$

$$z_2 = \sqrt{\frac{\mu'}{\pi}}\left(\frac{\tau_0}{2} - \frac{\omega}{\mu'}\right) = \sqrt{\frac{B\tau_0}{2}}\left(1 - \frac{f}{B/2}\right) \tag{2.138}$$

The Fresnel integrals, denoted by $C(z)$ and $S(z)$, are defined by

$$C(z) = \int_0^z \cos\left(\frac{\pi\upsilon^2}{2}\right)d\upsilon \text{ and } S(z) = \int_0^z \sin\left(\frac{\pi\upsilon^2}{2}\right)d\upsilon \tag{2.139}$$

Fresnel integrals can be approximated by

$$C(z) \approx \frac{1}{2} + \frac{1}{\pi z}\sin\left(\frac{\pi}{2}z^2\right) \quad ; \; z \gg 1 \tag{2.140}$$

$$S(z) \approx \frac{1}{2} - \frac{1}{\pi z}\cos\left(\frac{\pi}{2}z^2\right) \quad ; \; z \gg 1 \tag{2.141}$$

Note that $C(-z) = -C(z)$ and $S(-z) = -S(z)$. Figure 2.10 shows a plot of both $C(z)$ and $S(z)$ for $0 \le z \le 4.0$. Using Eq. (2.139) into Eq. (2.136) and performing the integration yield

$$\tilde{X}(f) = \sqrt{\frac{\pi}{2\mu'}}\; e^{-j(\pi f)^2/(\mu')}\{[C(z_2) + C(z_1)] + j[S(z_2) + S(z_1)]\} \tag{2.142}$$

Figure 2.11 shows typical plots for the LFM real part, imaginary part, and amplitude spectrum. The square-like spectrum shown in Fig. 2.11c is widely known as the Fresnel spectrum.

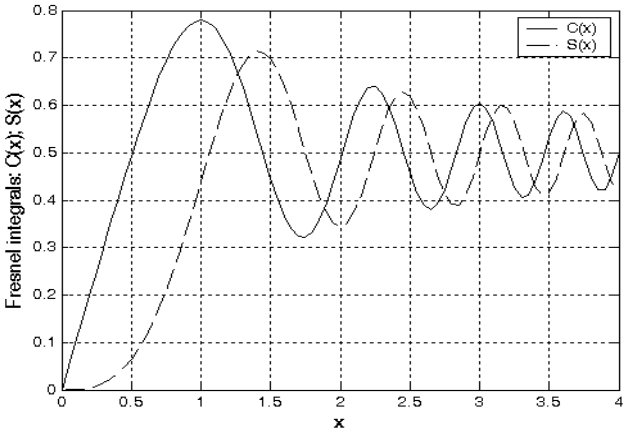

Figure 2.10. Fresnel integrals.

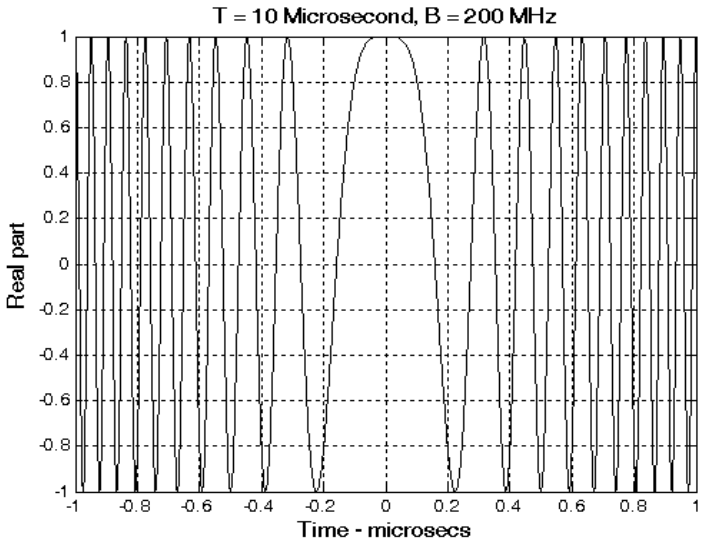

Figure 2.11a. Typical LFM waveform, real part.

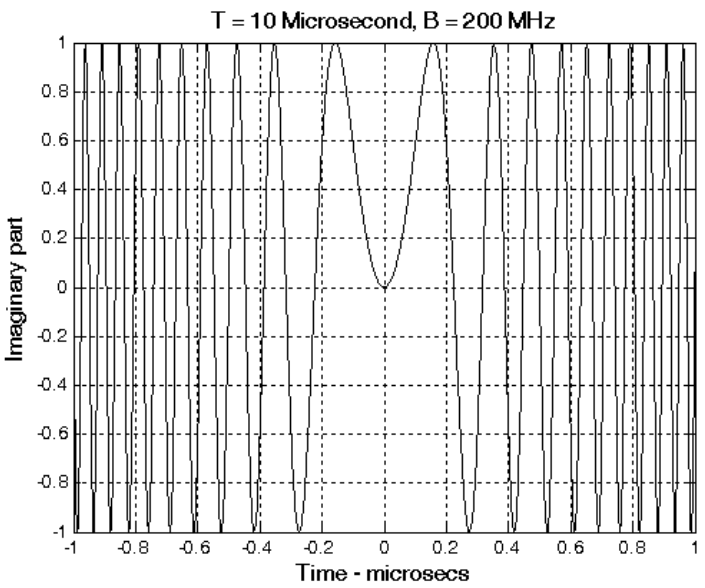

Figure 2.11b. Typical LFM waveform, imaginary part.

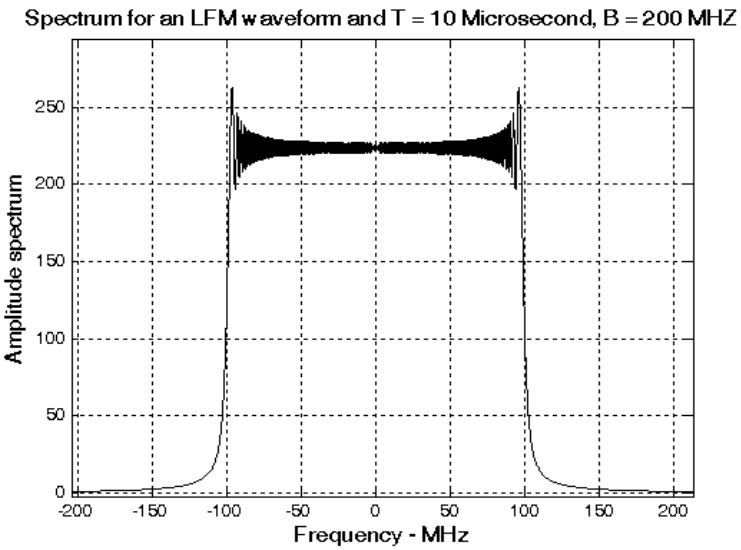

Figure 2.11c. Typical spectrum for an LFM waveform; Fresnel spectrum.

2.8. Signal Bandwidth and Duration

The signal bandwidth is the range of frequency over which the signal has a nonzero spectrum. In general, any signal can be defined using its duration (time domain) and bandwidth (frequency domain). A signal is said to be bandlimited if it has finite bandwidth. Signals that have finite durations (timelimited) will have infinite bandwidths, while bandlimited signals have infinite durations. The extreme case is a continuous sine-wave, whose bandwidth is infinitesimal.

Radar signal processing can be performed in either time domain or frequency domain. In either case, the radar signal processor assumes signals to be of finite duration (timelimited) and finite bandwidth (bandlimited). The trouble with this assumption is that timelimited and bandlimited signals cannot simultaneously exist. That is, a signal cannot have finite duration and have finite bandwidth. Because of this, it is customary to assume that radar signals are essentially limited in time and frequency.

Essentially timelimited signals are considered to be very small outside a certain finite time duration. If the FT of a signal is very small outside a certain finite frequency bandwidth, the signal is called essentially bandlimited signal.

A signal $x(t)$ over the time interval $\{T_1, T_2\}$ is said to be essentially timelimited relative to some very small signal level ε if and only if

$$\int_{T_1}^{T_2} |x(t)|^2 dt \geq (1-\varepsilon) \int_{-\infty}^{\infty} |x(t)|^2 dt \tag{2.143}$$

where the interval $\tau_e = T_2 - T_1$ is called the effective duration. The effective duration is defined as

$$\tau_e = \frac{\left(\int_{-\infty}^{\infty} |x(t)|^2 dt \right)^2}{\int_{-\infty}^{\infty} |x(t)|^4 dt} \tag{2.144}$$

Similarly, a signal $x(t)$ over the frequency interval $\{B_1, B_2\}$ is said to be essentially bandlimited relative to some small signal level η if and only if

$$\int_{B_1}^{B_2} |X(f)|^2 df \geq (1-\eta) \int_{-\infty}^{\infty} |X(f)|^2 df \tag{2.145}$$

where $X(f)$ is the FT of $x(t)$ and the band $B_e = B_2 - B_1$ is called the effective bandwidth. The effective bandwidth is defined as

$$B_e = \frac{\left(\int_{-\infty}^{\infty} |X(f)|^2 df \right)^2}{\int_{-\infty}^{\infty} |X(f)|^4 df} \tag{2.146}$$

Different, but equivalent, definitions for the effective bandwidth and effective duration can be found in the literature. In this book, the definitions cited in Burdic[1] are adopted. The quantity $B_e \tau_e$ is referred to as the time bandwidth product. In later chapters, it will be clear that large time bandwidth products are desirable in radar applications since they provide better pulse compression ratios (or compression gain).

1. Burdic, W. S., *Radar Signal Analysis*, Prentice-Hall, Englewood Cliffs, NJ, 1968.

Range resolution is defined as the reciprocal of the effective bandwidth. In Chapter 1, prior to introducing the concept of effective duration, the bandwidth was computed as the reciprocal of the pulsewidth, an approximation that is widely used and accepted, even though it is not quite 100% accurate. This is true since using one value or the other for the bandwidth does not make much difference in the overall calculation of the SNR when using the radar equation. Doppler resolution is computed as the reciprocal of the effective duration.

2.8.1. Effective Bandwidth and Duration Calculation

A few examples for computing the effective bandwidth and duration of most common radar signals are presented in this section.

Single Pulse

The single pulse was analyzed in the previous section. Consider the single pulse waveform given by

$$x(t) = Rect\left(\frac{t}{\tau_0}\right) \qquad ; \frac{-\tau_0}{2} < 0 < \frac{\tau_0}{2} \tag{2.147}$$

the effective bandwidth for this signal can be computed using Eq. (2.146). For this purpose, the denominator of Eq. (2.146) is

$$\int_{-\infty}^{\infty} |X(f)|^4 df = \int_{-\infty}^{\infty} |R_x(\tau)|^4 d\tau = \int_{-\infty}^{\infty} |\tau_0 Sinc(f\tau_0)|^4 df = \frac{2\tau_0^3}{3} \tag{2.148}$$

and its numerator is computed utilizing Eq. (2.59) as

$$\left(\int_{-\infty}^{\infty} |X(f)|^2 df\right)^2 = |R_x(0)|^2 = \tau_0^2 \tag{2.149}$$

Note that this value represents the square of the signal total energy. Therefore, the effective bandwidth is

$$B_e = \frac{\left(\int_{-\infty}^{\infty} |X(f)|^2 df\right)^2}{\int_{-\infty}^{\infty} |X(f)|^4 df} = \frac{(\tau_0^2)}{\left(\frac{2\tau_0^3}{3}\right)} = \frac{3}{2\tau_0} \tag{2.150}$$

The effective duration for the signal $x_2(t)$ is

$$\tau_e = \frac{\left(\int_{-\infty}^{\infty} |x(t)|^2 dt\right)^2}{\int_{-\infty}^{\infty} |x(t)|^4 dt} \tag{2.151a}$$

$$\tau_e = \frac{\left(\int_{-\tau_0/2}^{\tau_0/2} (1)^2 dt\right)^2}{\int_{-\tau_0/2}^{\tau_0/2} (1)^4 dt} = \frac{\tau_0^2}{\tau_0} = \tau_0 \tag{2.151b}$$

Finally, the time bandwidth product for this signal is

$$B_e\tau_e = \frac{3}{2\tau_0}\tau_0 = \frac{3}{2} \tag{2.152}$$

Finite Duration Pulse Train Signal

The finite duration train signal was defined in the previous section; its complex envelope is given by

$$x(t) = Rect\left(\frac{t}{NT_t}\right) \sum_{n=-\infty}^{\infty} Rect\left(\frac{t-nT}{\tau_0}\right) \tag{2.153}$$

The corresponding FT is

$$X(f) = \frac{T_t\tau_0}{T} Sinc(fT_t) \otimes \sum_{n=-\infty}^{\infty} Sinc(nf_r\tau_0)\delta(f-nf_r) \tag{2.154}$$

The total energy for this signal is

$$\int_{-\infty}^{\infty} |X(f)|^2 df = \frac{T_t\tau_0}{T} \tag{2.155}$$

It can be shown (see Problem 2.17) that

$$\int_{-\infty}^{\infty} |R_x(t)|^2 dt = \int_{-\infty}^{\infty} |X(f)|^4 df \approx \left(\frac{4}{3}\right)\left(\frac{T_t}{T}\right)^3 \left(\frac{2}{3}\right)(\tau_0)^3 \tag{2.156}$$

It follows that the effective bandwidth is

$$B_e \approx \frac{\left(\frac{T_t \tau_0}{T}\right)^2}{\left(\frac{4}{3}\right)\left(\frac{T_t}{T}\right)^3 \left(\frac{2}{3}\right)(\tau_0)^3} = \left(\frac{3T}{4T_t}\right)\left(\frac{3}{2\tau_0}\right) \tag{2.157}$$

The result of Eq. (2.157) clearly indicates that the effective bandwidth of the pulse train decreases as the length of the train is increased. This should intuitively make a lot of sense, since the bandwidth is inversely proportional to signal duration. Of course, when $T_t = T$ (i.e., single pulse case) Eq. (2.157) becomes identical to Eq. (2.150); note that in this case the factor $3/4$ will disappear from Eq. (2.156).

The effective duration of this signal can be computed using Eq. (2.144). Again the numerator of Eq. (2.144) represents the square of the total signal energy given in Eq. (2.155). The denominator of Eq. (2.144) is equal to unity (see Problem 2.18). Thus, the effective duration is

$$\tau_e = \frac{T_t \tau_0}{T} \tag{2.158}$$

and the time bandwidth product of this waveform is

$$B_e \tau_e \approx \left(\frac{3T}{4T_t}\right)\left(\frac{3}{2\tau_0}\right)\left(\frac{T_t \tau_0}{T}\right) = \frac{9}{8} \tag{2.159}$$

LFM Signal

In this case, the LFM complex envelope can be written as

$$x(t) = Rect\left(\frac{t}{\tau_0}\right) e^{j\mu\pi t^2} \tag{2.160}$$

where $\mu = B/\tau_0$ and B is the LFM bandwidth. Make a change of variables $\mu' = \pi\mu$, then the modulus of the FT of this signal can be approximated from Eq. (2.142) as

$$|X(f)| \approx \sqrt{\frac{\pi}{\mu'}}\ Rect\left(\frac{\pi f}{\mu' \tau_0}\right) \tag{2.161}$$

The FT of the autocorrelation function is equal to the square of the modulus of the signal FT, i.e.,

$$FT\{R_x(\tau)\} = |X(f)|^2 = \frac{\pi}{\mu'} Rect\left(\frac{\pi f}{\mu' \tau_0}\right) \tag{2.162}$$

Therefore,

$$\left(\int_{-\infty}^{\infty} |X(f)|^2 df\right)^2 \approx \tau_0^2 \tag{2.163}$$

also

$$\int_{-\infty}^{\infty} |X(f)|^4 df \approx \frac{\pi \tau_0}{\mu'} \tag{2.164}$$

Then the effective bandwidth is

$$B_e \approx \frac{\tau_0^2}{\frac{\pi \tau_0}{\mu'}} = \frac{\mu' \tau_0}{\pi} \tag{2.165}$$

The effective duration is

$$\tau_e = \frac{\left(\int_{-\infty}^{\infty} |x(t)|^2 dt\right)^2}{\int_{-\infty}^{\infty} |x(t)|^4 dt} = \frac{\left(\int_{-\tau_0/2}^{\tau_0/2} (1)^2 dt\right)^2}{\int_{-\tau_0/2}^{\tau_0/2} (1)^4 dt} = \frac{\tau_0^2}{\tau_0} = \tau_0 \tag{2.166}$$

And the time bandwidth product for LFM waveforms is computed as

$$B_e \tau_e \approx \frac{\mu' \tau_0}{\pi} \tau_0 = \frac{\mu' \tau_0^2}{\pi} = \frac{\pi \mu \tau_0^2}{\pi} = \frac{B \tau_0^2}{\tau_0} = B \tau_0 \tag{2.167}$$

2.9. Discrete Time Systems and Signals

Advances in computer hardware and in digital technologies completely revolutionized radar systems signal and data processing techniques. Virtually all modern radar systems use some form of a digital representation (signal samples) of their received signals for the purposes of signal and data processing. These samples of a timelimited signal are nothing more than a finite set of

numbers (thought of as a vector) that represents discrete values of the continuous time domain signal. These samples are typically obtained by using Analog to Digital (A/D) conversion devices. Since in the digital world the radar receiver is now concerned with processing a set of finite numbers, its impulse response will also compose a set of finite numbers. Consequently, the radar receiver is now referred to as a discrete system. All input/output signal relationships are now carried out using discrete time samples. It must also be noted that just as in the case of continuous time domain systems, the discrete systems of interest to radar applications must also be causal, stable, and linear time invariant.

Consider a continuous lowpass signal that is essentially timelimited with duration τ and bandlimited with bandwidth B. This signal (as will be shown in the next section) can be completely represented by a set of $\{2\tau B\}$ samples. Since a finite set of discrete values (samples) is used to represent the signal, it is common to represent this signal by a finite dimensional vector of the same size. This vector is denoted by x, or simply by the sequence $x[n]$,

$$\mathsf{x} \equiv x[n] = [x(0) \;\; x(1) \;\; \ldots x(N-2) \;\; x(N-1)]^t \tag{2.168}$$

where the superscript t denotes transpose operation. The value N is at least $2\tau B$ for a real lowpass essentially limited signal $x(t)$ of duration τ and bandwidth B. If, however, the signal is complex, then N is at least τB and the components of the vector x are complex. The samples defined in Eq. (2.168) can be obtained from pulse to pulse samples at a fixed range (i.e., delay) of the radar echo signal. The PRF is denoted by f_r and the total observation interval is T_0; then N would be equal to $T_0 f_r$. Define the radar receiver transfer function as the discrete sequence $h[n]$ and the input signal sequence as $x[n]$; then the output sequence $y[n]$ is given by the convolution sum

$$y[n] = \sum_{m=0}^{M-1} h(m)x(n-m) \tag{2.169}$$

where $\{h[n] = [h(0) \;\; h(1) \;\; \ldots h(M-2) \;\; h(M-1)];\; M \le N\}$.

2.9.1. Sampling Theorem

Lowpass Sampling Theorem

In general, it is required to determine the necessary condition such that a signal can be fully reconstructed from its samples by filtering, or data processing in general. The answer to this question lies in the sampling theorem, which may be stated as follows: let the signal $x(t)$ be real-valued essentially bandlimited by the bandwidth B; this signal can be fully reconstructed from its

samples if the time interval between samples is no greater than $1/(2B)$. Figure 2.12 illustrates the sampling process concept. The sampling signal $p(t)$ is periodic with period T_s, which is called the sampling interval.

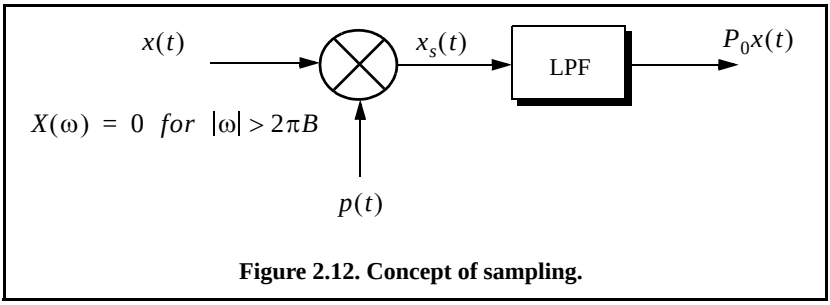

Figure 2.12. Concept of sampling.

The Fourier series expansion of $p(t)$ and the sampled signal $x_s(t)$ expressed using this Fourier series definition are, respectively, given by

$$p(t) = \sum_{n=-\infty}^{\infty} P_n e^{j\frac{2\pi nt}{T_s}} \tag{2.170a}$$

$$p(t) = \sum_{n=-\infty}^{\infty} x(t) P_n e^{j\frac{2\pi nt}{T_s}} \tag{2.170b}$$

$$p(t) = \sum_{n=-\infty}^{\infty} x(t) P_n e^{j\frac{2\pi nt}{T_s}} \tag{2.170b}$$

Taking the FT of Eq. (2.170b) yields

$$X_s(\omega) = \sum_{n=-\infty}^{\infty} P_n \; X\left(\omega - \frac{2\pi n}{T_s}\right) = P_0 X(\omega) + \sum_{\substack{n=-\infty \\ n \neq 0}}^{\infty} P_n \; X\left(\omega - \frac{2\pi n}{T_s}\right) \tag{2.171}$$

where $X(\omega)$ is the FT of $x(t)$. Therefore, we conclude that the spectral density, $X_s(\omega)$, consists of replicas of $X(\omega)$ spaced $(2\pi/T_s)$ apart and scaled by the Fourier series coefficients P_n. A lowpass filter (LPF) of bandwidth B can then be used to recover the original signal $x(t)$.

When the sampling rate is increased (i.e., T_s decreases), the replicas of $X(\omega)$ move farther apart from each other. Alternatively, when the sampling rate is decreased (i.e., T_s increases), the replicas get closer to one another. The

value of T_s such that the replicas are tangent to one another defines the minimum required sampling rate so that $x(t)$ can be recovered from its samples by using an LPF. It follows that

$$\frac{2\pi}{T_s} = 2\pi(2B) \Leftrightarrow T_s = \frac{1}{2B} \tag{2.172}$$

The sampling rate defined by Eq. (2.172) is known as the Nyquist sampling rate. When $T_s > (1/2B)$, the replicas of $X(\omega)$ overlap and, thus, $x(t)$ cannot be recovered cleanly from its samples. This is known as aliasing. In practice, ideal LPF cannot be implemented; hence, practical systems tend to over sample in order to avoid aliasing.

Example:

Assume that the sampling signal $p(t)$ *is given by* $p(t) = \sum_{n=-\infty}^{\infty} \delta(t - nT_s)$. *Compute an expression for* $X_s(\omega)$.

Solution:

The signal $p(t)$ *is called the Comb function, with exponential Fourier series*

$$p(t) = \sum_{n=-\infty}^{\infty} \frac{1}{T_s} e^{2\frac{\pi nt}{T_s}}$$

It follows that

$$x_s(t) = \sum_{n=-\infty}^{\infty} x(t) \frac{1}{T_s} e^{2\frac{\pi nt}{T_s}}$$

Taking the Fourier transform of this equation yields

$$X_s(\omega) = \frac{2\pi}{T_s} \sum_{n=-\infty}^{\infty} X\left(\omega - \frac{2\pi n}{T_s}\right)$$

It is desired to develop a general expression from which any lowpass signal can be recovered from its samples provided that Eq. (2.172) is satisfied. In order to do that, let $x(t)$ and $x_s(t)$ be the desired lowpass signal and its corresponding samples, respectively. Then an expression for $x(t)$ in terms of its samples can be derived as follows: First, obtain $X(\omega)$ by filtering the signal $X_s(\omega)$ using an ideal LPF whose transfer function is

$$H(\omega) = T_s Rect\left(\frac{\omega}{4\pi B}\right) \tag{2.173}$$

Thus,

$$X(\omega) = H(\omega)X_s(\omega) = T_s Rect\left(\frac{\omega}{4\pi B}\right)X_s(\omega) \quad \textbf{(2.174)}$$

The signal $x(t)$ is now obtained from the inverse FT of Eq. (2.174) as

$$x(t) = FT^{-1}\{X(\omega)\} = FT^{-1}\left\{T_s Rect\left(\frac{\omega}{4\pi B}\right)X_s(\omega)\right\} = \quad \textbf{(2.175)}$$

$$2BT_s Sinc(2\pi Bt) \otimes x_s(t)$$

The sampled signal $x_s(t)$ can be represented using an ideal sampling signal

$$p(t) = \sum_n \delta(t - nT_s) \quad \textbf{(2.176a)}$$

thus,

$$x_s(t) = \sum_n x(nT_s)\delta(t - nT_s) \quad \textbf{(2.176b)}$$

Substituting Eq. (2.176b) into Eq. (2.175) yields an expression for the signal $x(t)$ in terms of its samples

$$x(t) = 2BT_s \sum_n x(nT_s)\ \ Sinc(2\pi B(t - T_s))\ \ ; T_s \le \frac{1}{2B} \quad \textbf{(2.177)}$$

Bandpass Sampling Theorem

It was established in Section 2.6 that any bandpass signal can be expressed using the quadrature components as provided in Eq. (2.79) through Eq. (2.81). It follows that it is sufficient to construct the bandpass signal $x(t)$ from samples of the quadrature components $\{x_I(t), x_Q(t)\}$. Let the signal $x(t)$ be essentially bandlimited with bandwidth B, then each of the lowpass signals $x_I(t)$ and $x_Q(t)$ are also bandlimited each with bandwidth $B/2$. Hence, if either of these lowpass signal is sampled at a rate $f_s \le 1/B$ then the Nyquist criterion is not violated. Assume that both quadrature components are sampled synchronously, that is

$$x_I(t) = BT_s \sum_{n=-\infty}^{\infty} x_I(nT_s)\ \ Sinc(\pi B(t - nT_s)) \quad \textbf{(2.178)}$$

$$x_Q(t) = BT_s \sum_{n=-\infty}^{\infty} x_Q(nT_s)\ Sinc(\pi B(t-nT_s)) \tag{2.179}$$

where if the Nyquist rate is satisfied, then $BT_s = 1$ (unity time bandwidth product). Substituting Eq. (2.178) and Eq. (2.179) into Eq. (2.79) yields

$$x(t) = BT_s\left\{\sum_{n=-\infty}^{\infty}[x_I(nT_s)\cos 2\pi f_0 t - x_Q(nT_s)\sin 2\pi f_0 t]\right. \tag{2.180}$$
$$\left. Sinc(\pi B(t-nT_s))\right\}$$

$$x(t) = Re\left\{BT_s \sum_{n=-\infty}^{\infty}[x_I(nT_s) + jx_Q(nT_s)]e^{j2\pi f_0 t} Sinc(\pi B(t-nT_s))\right\} \tag{2.181}$$

where, of course, $T_s \le 1/B$ is assumed. This leads to the conclusion that if the total period over which the signal $x(t)$ is sampled is T_0, then $2BT_0$ samples are required, BT_0 samples for $x_I(t)$ and BT_0 samples for $x_Q(t)$.

2.9.2. The Z-Transform

The Z-transform is a transformation that maps samples of a discrete time-domain sequence into a new domain known as the z-domain. It is defined as

$$Z\{x(n)\} = X(z) = \sum_{n=-\infty}^{\infty} x(n)z^{-n} \tag{2.182}$$

where $z = re^{j\omega}$, and for most cases, $r = 1$. It follows that Eq. (2.182) can be rewritten as

$$X(e^{j\omega}) = \sum_{n=-\infty}^{\infty} x(n)e^{-jn\omega} \tag{2.183}$$

In the z-domain, the region over which $X(z)$ is finite is called the Region of Convergence (ROC).

Example:

Show that $Z\{nx(n)\} = -z\dfrac{d}{dz}X(z)$.

Solution:

Starting with the definition of the Z-transform,

$$X(z) = \sum_{n=-\infty}^{\infty} x(n)z^{-n}$$

Taking the derivative, with respect to z, of the above equation yields

$$\frac{d}{dz}X(z) = \sum_{n=-\infty}^{\infty} x(n)(-n)z^{-n-1}$$

$$= (-z^{-1}) \sum_{n=-\infty}^{\infty} nx(n)z^{-n}$$

It follows that

$$Z\{nx(n)\} = (-z)\frac{d}{dz}X(z)$$

A discrete LTI system has a transfer function $H(z)$ that describes how the system operates on its input sequence $x(n)$ in order to produce the output sequence $y(n)$. The output sequence $y(n)$ is computed from the discrete convolution between the sequences $x(n)$ and $h(n)$:

$$y(n) = \sum_{m=-\infty}^{\infty} x(m)h(n-m) \qquad \textbf{(2.184)}$$

However, since practical systems require the sequence $x(n)$ and $h(n)$ to be of finite length, we can rewrite Eq. (2.184) as

$$y(n) = \sum_{m=0}^{N} x(m)h(n-m) \qquad \textbf{(2.185)}$$

N denotes the input sequence length. The Z-transform of Eq. (2.185) is

$$Y(z) = X(z)H(z) \qquad \textbf{(2.186)}$$

and the discrete system transfer function is

$$H(z) = \frac{Y(z)}{X(z)} \tag{2.187}$$

Finally, the transfer function $H(z)$ can be written as

$$H(z)\Big|_{z = e^{j\omega}} = \left|H(e^{j\omega})\right| e^{\angle H(e^{j\omega})} \tag{2.188}$$

where $\left|H(e^{j\omega})\right|$ is the amplitude response, and $\angle H(e^{j\omega})$ is the phase response.

2.9.3. The Discrete Fourier Transform

The Discrete Fourier Transform (DFT) is a mathematical operation that transforms a discrete sequence, usually from the time domain into the frequency domain, in order to explicitly determine the spectral information for the sequence. The time-domain sequence can be real or complex. The DFT has finite length N and is periodic with period equal to N. The discrete Fourier transform pairs for the finite sequence $x(n)$ are defined by

$$X(k) = \sum_{n=0}^{N-1} x(n) e^{-j\frac{2\pi nk}{N}} \quad ; \; k = 0, \ldots, N-1 \tag{2.189}$$

$$x(n) = \frac{1}{N} \sum_{k=0}^{N-1} X(k) e^{j\frac{2\pi nk}{N}} \quad ; \; n = 0, \ldots, N-1 \tag{2.190}$$

The Fast Fourier Transform (FFT) is not a new kind of transform different from the DFT. Instead, it is an algorithm used to compute the DFT more efficiently. There are numerous FFT algorithms that can be found in the literature. In this book we will interchangeably use the DFT and the FFT to mean the same thing. Furthermore, we will assume radix-2 FFT algorithm, where the FFT size is equal to $N = 2^m$ for some integer m.

2.9.4. Discrete Power Spectrum

Practical discrete systems utilize DFTs of finite length as a means of numerical approximation for the Fourier transform. The input signals must be truncated to a finite duration (denoted by T) before they are sampled. This is necessary so that a finite length sequence is generated prior to signal processing. Unfortunately, this truncation process may cause some serious problems.

To demonstrate this difficulty, consider the time-domain signal $x(t) = \sin 2\pi f_0 t$. The spectrum of $x(t)$ consists of two spectral lines at $\pm f_0$. Now, when $x(t)$ is truncated to length T seconds and sampled at a rate $T_s = T/N$, where N is the number of desired samples, we produce the sequence $\{x(n);\ n = 0, 1, \ldots, N-1\}$.

The spectrum of $x(n)$ would still be composed of the same spectral lines if T is an integer multiple of T_s and if the DFT frequency resolution Δf is an integer multiple of f_0. Unfortunately, those two conditions are rarely met, and as a consequence, the spectrum of $x(n)$ spreads over several lines (normally the spread may extend up to three lines). This is known as spectral leakage. Since f_0 is normally unknown, this discontinuity caused by an arbitrary choice of T cannot be avoided. Windowing techniques can be used to mitigate the effect of this discontinuity by applying smaller weights to samples close to the edges.

A truncated sequence $x(n)$ can be viewed as one period of some periodic sequence with period N. The discrete Fourier series expansion of $x(n)$ is

$$x(n) = \sum_{k=0}^{N-1} X_k e^{j\frac{2\pi nk}{N}} \tag{2.191}$$

It can be shown that the coefficients X_k are given by

$$X_k = \frac{1}{N}\sum_{n=0}^{N-1} x(n) e^{-j\frac{2\pi nk}{N}} = \frac{1}{N}X(k) \tag{2.192}$$

where $X(k)$ is the DFT of $x(n)$. Therefore, the Discrete Power Spectrum (DPS) for the bandlimited sequence $x(n)$ is the plot of $|X_k|^2$ versus k, where the lines are Δf apart,

$$P_0 = \frac{1}{N^2}|X(0)|^2 \tag{2.193a}$$

$$P_k = \frac{1}{N^2}\{|X(k)|^2 + |X(N-k)|^2\} \quad ;\ k = 1, 2, \ldots, \frac{N}{2} - 1 \tag{2.193b}$$

$$P_{N/2} = \frac{1}{N^2}|X(N/2)|^2 \tag{2.193c}$$

Before proceeding to the next section, we will show how to select the FFT parameters. For this purpose, consider a bandlimited signal $x(t)$ with bandwidth B. If the signal is not bandlimited, an LPF can be used to eliminate fre-

quencies greater than B. In order to satisfy the sampling theorem, one must choose a sampling frequency $f_s = 1/T_s$, such that

$$f_s \geq 2B \tag{2.194}$$

The truncated sequence duration T and the total number of samples N are related by

$$T = NT_s \tag{2.195}$$

or equivalently,

$$f_s = N/T \tag{2.196}$$

It follows that

$$f_s = \frac{N}{T} \geq 2B \tag{2.197}$$

and the frequency resolution is

$$\Delta f = \frac{1}{NT_s} = \frac{f_s}{N} = \frac{1}{T} \geq \frac{2B}{N} \tag{2.198}$$

2.9.5. Windowing Techniques

Truncation of the sequence $x(n)$ can be accomplished by computing the product

$$x_w(n) = x(n)w(n) \tag{2.199}$$

where

$$w(n) = \left\{ \begin{array}{ll} f(n) & ;\ n = 0, 1, \ldots, N-1 \\ 0 & otherwise \end{array} \right\} \tag{2.200}$$

where $f(n) \leq 1$. The finite sequence $w(n)$ is called a windowing sequence, or simply a window. The windowing process should not impact the phase response of the truncated sequence. Consequently, the sequence $w(n)$ must retain linear phase. This can be accomplished by making the window symmetrical with respect to its central point.

If $f(n) = 1$ for all n, we have what is known as the rectangular window. It leads to the Gibbs phenomenon, which manifests itself as an overshoot and a ripple before and after a discontinuity. Figure 2.13 shows the amplitude spectrum of a rectangular window. Note that the first side-lobe is at $-13.46dB$ below the main lobe. Windows that place smaller weights on the samples near the edges will have less overshoot at the discontinuity points (lower side-

lobes); hence, they are more desirable than a rectangular window. However, reduction of the sidelobes is offset by a widening of the main lobe. Therefore, the proper choice of a windowing sequence is continuous trade-off between side-lobe reduction and main-lobe widening. Table 2.1 gives a summary of some commonly used windows with the corresponding impact on main beam widening and peak reduction.

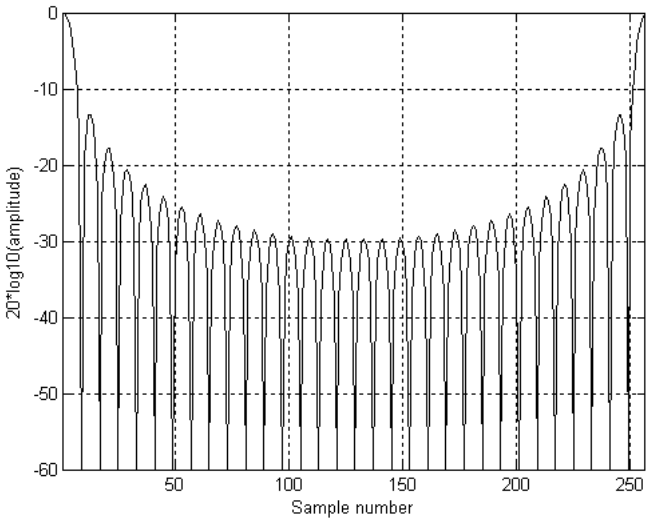

Figure 2.13. Normalized amplitude spectrum for rectangular window.

TABLE 2.1. Common windows

Window	Null-to-Null Beamwidth Rectangular Window is the Reference	Peak Reduction
Rectangular	*1*	*1*
Hamming	*2*	*0.73*
Hanning	*2*	*0.664*
Blackman	*6*	*0.577*
Kaiser ($\beta = 6$)	*2.76*	*0.683*
Kaiser ($\beta = 3$)	*1.75*	*0.882*

The multiplication process defined in Eq. (2.199) is equivalent to cyclic convolution in the frequency domain. It follows that $X_w(k)$ is a smeared (distorted) version of $X(k)$. To minimize this distortion, we would seek windows that have a narrow main lobe and small side-lobes. Additionally, using a window other than a rectangular window reduces the power by a factor P_w, where

$$P_w = \frac{1}{N}\sum_{n=0}^{N-1} w^2(n) = \sum_{k=0}^{N-1} |W(k)|^2 \qquad \textbf{(2.201)}$$

It follows that the DPS for the sequence $x_w(n)$ is now given by

$$P_0^w = \frac{1}{P_w N^2}|X(0)|^2 \qquad \textbf{(2.202)}$$

$$P_k^w = \frac{1}{P_w N^2}\{|X(k)|^2 + |X(N-k)|^2\} \qquad ;\ k = 1, 2, \ldots, \frac{N}{2} - 1 \qquad \textbf{(2.202b)}$$

$$P_{N/2}^w = \frac{1}{P_w N^2}|X(N/2)|^2 \qquad \textbf{(2.202c)}$$

where P_w is defined in Eq. (2.193). Table 2.2 lists some common windows. Figures 2.14 through 2.16 show the frequency domain characteristics for these windows. These plots can be reproduced using the following MATLAB code.

TABLE 2.2. Some common windows. $n = 0, N-1$

Window	Expression	First Side-lobe	Main Lobe Width
Rectangular	$w(n) = 1$	$-13.46dB$	1
Hamming	$w(n) = 0.54 - 0.46\cos\left(\frac{2\pi n}{N-1}\right)$	$-41dB$	2
Hanning	$w(n) = 0.5\left[1 - \cos\left(\frac{2\pi n}{N-1}\right)\right]$	$-32dB$	2
Kaiser	$w(n) = \frac{I_0[\beta\sqrt{1-(2n/N)^2}]}{I_0(\beta)}$ I_0 is the zero-order modified Bessel function of the first kind	$-46dB$ for $\beta = 2\pi$	$\sqrt{5}$ for $\beta = 2\pi$

```
%Use this program to reproduce figures 2.14 through 2.16.
clear all;
close all;
eps = 0.001;
N = 32;
win_rect (1:N) = 1;
win_ham = hamming(N);
win_han = hanning(N);
win_kaiser = kaiser(N, pi);
win_kaiser2 = kaiser(N, 5);
Yrect = abs(fft(win_rect, 256));
Yrectn = Yrect ./ max(Yrect);
Yham = abs(fft(win_ham, 256));
Yhamn = Yham ./ max(Yham);
Yhan = abs(fft(win_han, 256));
Yhann = Yhan ./ max(Yhan);
YK = abs(fft(win_kaiser, 256));
YKn = YK ./ max(YK);
YK2 = abs(fft(win_kaiser2, 256));
YKn2 = YK2 ./ max(YK2);
figure (1)
plot(20*log10(Yrectn+eps),'k')
xlabel('Sample number');
ylabel('20*log10(amplitude)')
axis tight;
grid
figure(2)
plot(20*log10(Yhamn + eps),'k')
xlabel('Sample number');
 ylabel('20*log10(amplitude)')
grid;
axis tight
figure (3)
plot(20*log10(Yhann+eps),'k')
xlabel('Sample number');
ylabel('20*log10(amplitude)'); grid
axis tight
figure(4)
plot(20*log10(YKn+eps),'k')
grid; hold on
plot(20*log10(YKn2+eps),'k--')
xlabel('Sample number');
ylabel('20*log10(amplitude)')
legend('Kaiser par. = \pi','Kaiser par. =5')
axis tight;
hold off
```

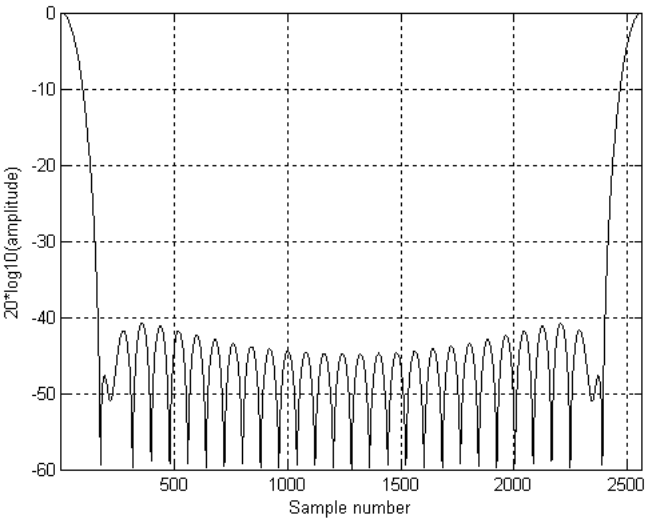

Figure 2.14. Normalized amplitude spectrum for Hamming window.

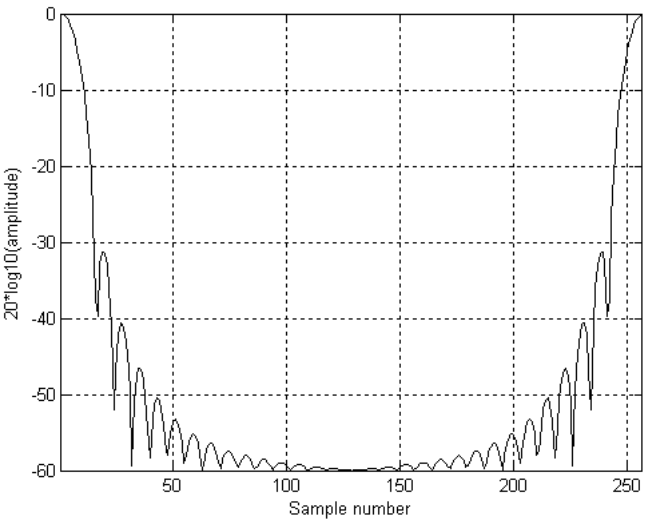

Figure 2.15. Normalized amplitude spectrum for Hanning window.

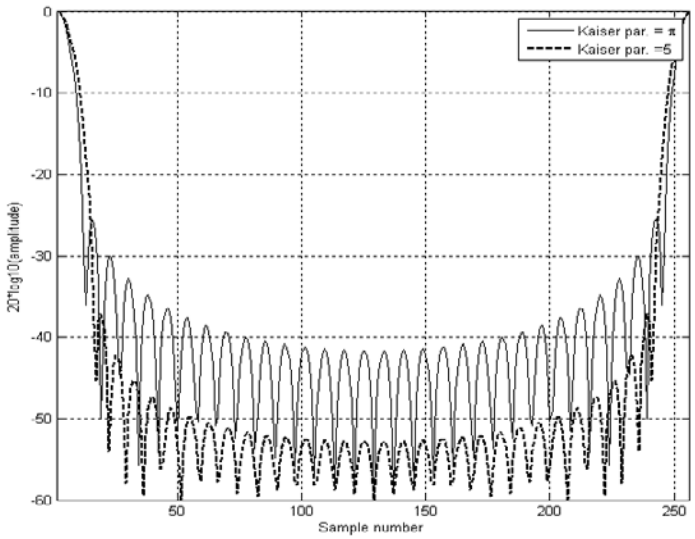

Figure 2.16. Normalized amplitude spectrum for Kaiser window.

2.9.6. Decimation and Interpolation

Decimation

Typically, radar systems use many signals for different functions, such as search, track, and discrimination to name a few. All signals are assumed to be essentially limited; however, since these signals have different functions, they do not have the same time and bandwidth durations (τ, B). Earlier in this chapter, it was established that the number of samples required to sufficiently recover any signal from its samples is $N \geq 2\tau B$. Therefore, it is important to use an A/D with high enough sampling rate to account for the largest possible number of samples required. As a result, it is often the case that some radar signals are sampled at a much higher rate than actually needed.

The process for decreasing the number of samples for a given sequence is called decimation. This is because the original data set has been reduced (decimated) in number. The process that increases the number of data samples is referred to as interpolation. The typical implementation for either operation is to alter the sampling rate, without violating the Nyquist sampling rate, of the input sequence. In decimation, the sampling rate is decreased by increasing the

time steps between successive samples. More precisely, if the t_1 is the original sampling interval and t_2 is the decimated sampling interval, then

$$t_2 = Dt_1 \tag{2.203}$$

D is the decimation ratio and it is greater than unity. If D is an integer, then decimation effectively decreases the original sequence by discarding $(D-1)$ samples of D samples. This is illustrated in Fig. 2.17 for $D = 3$.

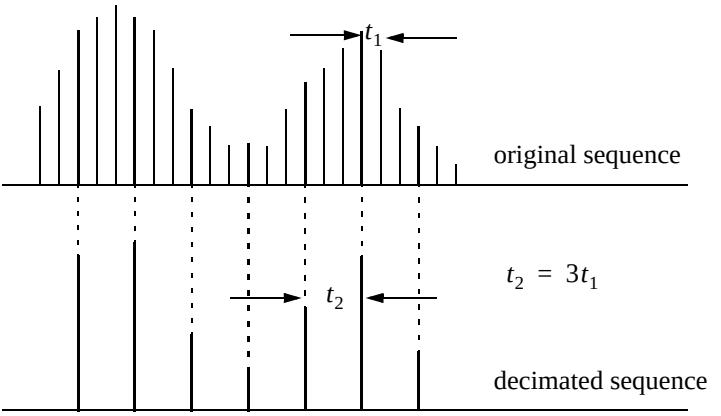

Figure 2.17. Decimation with $D = 3$. Every sample of the decimated sequence coincides with every third sample of the original sequence.

When D is not an integer, it is then necessary to first perform interpolation to determine new values for the new sequence. For example, if $D = 2.2$, then four out of every five samples in the decimated sequence are between samples in the original sequence and must be found by interpolation. This is illustrated in Fig. 2.18 for $D = 2.2$. In this example,

$$\left(t_2 = 2.2t_1 = \frac{11}{5}t_1\right) \Rightarrow 5t_2 = 11t_1 \tag{2.204}$$

which indicates that there are five samples in the decimated sequence for every eleven samples of the original sequence. Additionally, every fifth sample in the decimated sequence is equal to every eleventh sample of the original sequence.

Interpolation

Suppose that a signal $x(t)$ whose duration is T seconds has been sampled at a sampling rate t_1 to obtain a sequence

$$\mathrm{x} = x[n] = \{x(nt_1), n = 0, 1, \ldots, N_1 - 1\} \tag{2.205}$$

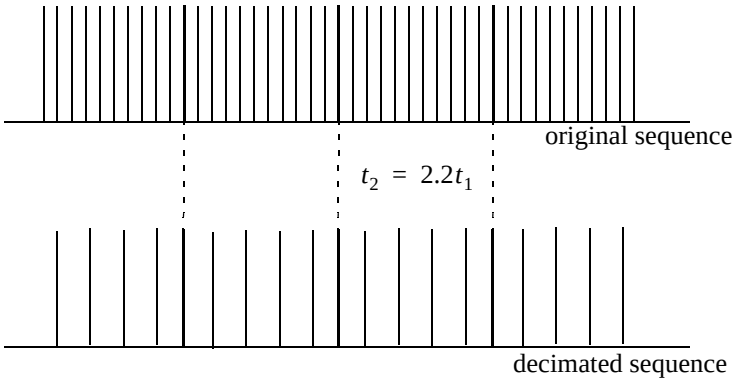

Figure 2.18. Decimation with $D = 2.2$. Every fifth sample of the decimated sequence coincides with a sample in the original sequence.

in this case, $N_1 = T/t_1$. Suppose you want to interpolate between the samples of $x[n]$ to generate a new sequence of size N_2 and sampling interval t_2, where $t_2 = t_1/k$. This effectively corresponds to a new sampling frequency $f_{s2} = kf_{s1}$ where $f_{s1} = 1/t_1$. This can be accomplished using Eq. (2.177) (see Problem 2.33); however, a more efficient interpolation can be performed using the FFT as will be described in the rest of this section.

Denote the FFT of the sequences $x_1[n]$ and $x_2[n]$ by $X_1[l]$ and $X_2[l]$. Assume that the signal $x(t)$ is essentially bandlimited with bandwidth $B = M\Delta f$ where M is an integer and $\Delta f = 1/T$. It follows that in order not to violate the sampling theorem

$$M\Delta f < f_{s1}/2 < f_{s2}/2 \tag{2.206}$$

It is clear that the coefficients of $X_1[l]$ and $X_2[l]$ are zero for all $|l| > M$. More precisely,

$$\begin{aligned} X_1[l] &= 0;\ l = M+1, M+2, \ldots, N_1 - 3 \\ X_2[l] &= 0;\ l = M+1, M+2, \ldots, N_2 - 3 \end{aligned} \tag{2.207}$$

Therefore, one can easily obtain the new sequence $X_2[l]$ from $X_1[l]$ by adding zeros in between the negative and positive frequencies from

$$N_1 - (2M+1) \ \ to \ \ N_2 - (2M+1) \tag{2.208}$$

and the sequence $x_2[n]$ is simply generated by computing the inverse DFT of the sequence $X_2[l]$. Interpolation can also be applied to the frequency domain

sequence. For this purpose, one can simply zero pad the time domain sequence to the desired size then take the DFT of the newly interpolated sequence.

Problems

2.1. Classify each of the following signals as an energy signal, a power signal, or neither.

(a) $\exp(0.5t)\ \ (t \geq 0)$,

(b) $\exp(-0.5t)\ \ (t \geq 0)$,

(c) $\cos t + \cos 2t\ \ (-\infty < t < \infty)$,

(d) $e^{-a|t|}\ \ (a > 0)$.

2.2. A definition for the instantaneous frequency was given in Eq. (2.58). A more general definition is

$$f_i(t) = \frac{1}{2\pi} Im\left\{ \frac{d}{dt} \ln \psi(t) \right\}$$

where *Im {.},* indicates imaginary part. Using this definition, calculate the instantaneous frequency for

(a) $x(t) = Rect\left(\frac{t}{\tau}\right) \cos(2\pi f_0 t)$

(b) $x(t) = Rect\left(\frac{t}{\tau}\right) \cos\left(2\pi f_0 t + \frac{B}{2\tau} t^2\right)$

2.3. Consider the two bandpass signals $x(t) = r_x(t)\cos(2\pi f_0 t + \phi_x(t))$ and $h(t) = r_h(t)\cos(2\pi f_0 t + \phi_h(t))$. Derive an expression for the complex envelope for the signal $s(t) = x(t) + h(t)$.

2.4. Consider the bandpass signal $x(t)$ whose complex envelope is equal to $\tilde{x}(t) = x_I(t) + jx_Q(t)$. Derive an expression for the autocorrelation function and the power spectrum density for $x(t)$ and $\tilde{x}(t)$.

2.5. Find the autocorrelation integral of the pulse train

$$y(t) = Rect(t/T) - Rect\left(\frac{t-T}{T}\right) + Rect\left(\frac{t-2T}{T}\right).$$

2.6. Compute the discrete convolution $y(n) = x(m) \bullet h(m)$ where

$$\{x(k), k = -1, 0, 1, 2\} = [-1.9, 0.5, 1.2, 1.5]$$
$$\{h(k), k = 0, 1, 2\} = [-2.1, 1.2, 0.8].$$

2.7. Define $\{x_I(n) = 1, -1, 1\}$ and $\{x_Q(n) = 1, 1, -1\}$. (a) Compute the discrete correlations: R_{x_I}, R_{x_Q}, $R_{x_I x_Q}$, and $R_{x_Q x_I}$. (b) A certain radar transmits the signal $s(t) = x_I(t)\cos 2\pi f_0 t - x_Q(t)\sin 2\pi f_0 t$. Assume that the autocorrelation $s(t)$ is equal to $y(t) = y_I(t)\cos 2\pi f_0 t - y_Q(t)\sin 2\pi f_0 t$. Compute and sketch $y_I(t)$ and $y_Q(t)$.

2.8. Compute the energy associated with the signal $x(t) = ARect(t/\tau)$.

2.9. (a) Prove that $\varphi_1(t)$ and $\varphi_2(t)$, shown in figure below, are orthogonal over the interval $(-2 \le t \le 2)$. (b) Express the signal $x(t) = t$ as a weighted sum of $\varphi_1(t)$ and $\varphi_2(t)$ over the same time interval

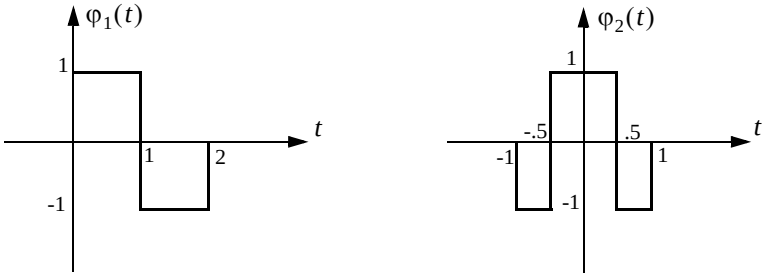

2.10. A periodic signal $x_p(t)$ is formed by repeating the pulse $x(t) = 2\Delta((t-3)/5)$ every 10 seconds. (a) What is the Fourier transform of $x(t)$? (b) Compute the complex Fourier series of $x_p(t)$. (c) Give an expression for the autocorrelation function $\bar{R}_{x_p}(t)$ and the power spectrum density $\bar{S}_{x_p}(\omega)$

2.11. If the Fourier series is

$$x(t) = \sum_{n=-\infty}^{\infty} X_n e^{j2\pi nt/T}$$

define $y(t) = x(t - t_0)$. Compute an expression for the complex Fourier series expansion of $y(t)$.

2.12. Show that (a) $\bar{R}_x(-t) = \bar{R}_x^*(t)$, (b) If $x(t) = f(t) + m_1$ and $y(t) = g(t) + m_2$, show that $\bar{R}_{xy}(t) = m_1 m_2$, where the average values for $f(t)$ and $g(t)$ are zeroes.

2.13. What is the power spectral density for the signal

$$x(t) = A\cos(2\pi f_0 t + \theta_0)\,?$$

2.14. Consider the signal

$$x(t) = Rect(t/\tau)\cos(\omega_0 t - Bt^2/2\tau)$$

and let $\tau = 15\mu s$ and $B = 10MHz$. What are the quadrature components?

2.15. Determine the quadrature components for the signal

$$h(t) = \delta(t) - \left(\frac{\omega_0}{\omega_d}\right)e^{-2t}\sin(\omega_0 t)u(t).$$

2.16. If $x(t) = x_1(t) - 2x_1(t-5) + x_1(t-10)$, determine the autocorrelation functions $R_{x_1}(t)$ and $R_x(t)$ when $x_1(t) = \exp(-t^2/2)$.

2.17. Derive Eq. (2.156).

2.18. Prove that the effective duration of a finite pulse train is equal to $(T_t\tau_0)/T$, where τ_0 is the pulsewidth, T is the PRI, and T_t is as defined in Fig. 2.8.

2.19. A certain bandlimited signal has bandwidth $B = 20KHz$. Find the FFT size required so that the frequency resolution is $\Delta f = 50Hz$. Assume radix 2 FFT and a record length of 1 second.

2.20. Write an expression for the autocorrelation function $R_y(t)$, where

$$y(t) = \sum_{n=1}^{5} Y_n Rect\left(\frac{t-n5}{2}\right) \text{ and } \{Y_n\} = \{0.8, 1, 1, 1, 0.8\}.$$

Give an expression for the density function $S_y(\omega)$.

2.21. An LTI system has impulse response

$$h(t) = \begin{cases} \exp(-2t) & t \geq 0 \\ 0 & t < 0 \end{cases}$$

(a) Find the autocorrelation function $R_h(\tau)$. (b) Assume the input of this system is $x(t) = 3\cos(100t)$. What is the output?

2.22. Let $\bar{S}_X(\omega)$ be the PSD function for the stationary random process $X(t)$. Compute an expression for the PSD function of

$$Y(t) = X(t) - 2X(t-T).$$

2.23. Assume that a certain sequence is determined by its FFT. If the record length is $2ms$ and the sampling frequency is $f_s = 10KHz$, find N.

2.24. Prove that

$$\sum_{n=-\infty}^{\infty} J_n(z) = 1.$$

2.25. Show that $J_{-n}(z) = (-1)^n J_n(z)$. Hint: You may utilize the relation

$$J_n(z) = \frac{1}{\pi}\int_0^{\pi} \cos(z\sin y - ny)dy.$$

2.26. Compute the Z-transform for

(a) $x_1(n) = \frac{1}{n!}u(n)$,

(b) $x_2(n) = \frac{1}{(-n)!}u(-n)$.

2.27. (a) Write an expression for the FT of $x(t) = Rect(t/3)$. (b) Assume that you want to compute the modulus of the FT using a DFT of size *512* with a sampling interval of *1* second. Evaluate the modulus at frequency $(80/512)Hz$. Compare your answer to the theoretical value and compute the error.

2.28. Generate *512* samples of the signal $x(t) = 2.0e^{-5t}\sin(4\pi t)$, using sampling interval equal to 0.002. Compute the resultant spectrum and then truncate the spectrum at *15* Hz. Generate the time-domain sequence for the truncated spectrum. Determine the sampling rate of the new sequence.

2.29. Assume that a time-domain sequence generated by using a sampling interval equal to *0.01* is given by $x(k) = \{0, 2, 5, 12, 5, 3, 3, -1, 1, 0\}$. Decimate this sequence so that the sampling interval is *0.02*.

2.30. Write a MATLAB program to decimate any sequence of finite length and demonstrate it using the previous problem.

2.31. You are given a sequence of samples $\{x(kT), k = -\infty, \ldots, \infty\}$ where the sampling interval T corresponds to twice the Nyquist rate. Give an expression to compute the samples of $x(t)$ at a new sampling rate corresponding to $T' = 0.7T$.

2.32. Write a short argument to explain why the matched filter used in radar application ought to be an LTI filter.

2.33. A certain bandlimited signal has bandwidth $B = 20KHz$. Find the FFT size required so that the frequency resolution is $\Delta f = 50Hz$. Assume radix 2 FFT and a record length of 1 second.

2.34. Assume that a certain sequence is determined by its FFT. If the record length is $2ms$ and the sampling frequency is $f_s = 10KHz$, find N.

Chapter 3 Random Variables and Processes

3.1. Random Variables

Consider an experiment with outcomes defined by a certain sample space. The rule or functional relationship that maps each point in this sample space into a real number is called a random variable. Random variables are designated by capital letters (e.g., X, Y, …), and a particular value of a random variable is denoted by a lowercase letter (e.g., x, y, …).

The Cumulative Distribution Function (*cdf*) associated with the random variable X is denoted as $F_X(x)$ and is interpreted as the total probability that the random variable X is less than or equal to the value x. More precisely,

$$F_X(x) = Pr\{X \le x\} \tag{3.1}$$

The probability that the random variable X is in the interval (x_1, x_2) is then given by

$$F_X(x_2) - F_X(x_1) = Pr\{x_1 \le X \le x_2\} \tag{3.2}$$

The probability that a random variable X has values in the interval (x_1, x_2) is

$$F_X(x_2) - F_X(x_1) = Pr\{x_1 \le X \le x_2\} = \int_{x_1}^{x_2} f_X(x)dx \tag{3.3}$$

It is often practical to describe a random variable by the derivative of its *cdf*, which is called the Probability Density Function *(pdf)*. The *pdf* of the random variable X is

$$f_X(x) = \frac{d}{dx}F_X(x) \tag{3.4}$$

or, equivalently,

$$F_X(x) = Pr\{X \le x\} = \int_{-\infty}^{x} f_X(\lambda)d\lambda \tag{3.5}$$

The *cdf* has the following properties:

$$\begin{aligned} 0 \le F_X(x) \le 1 \\ F_X(-\infty) = 0 \\ F_X(\infty) = 1 \\ F_X(x_1) \le F_X(x_2) \Leftrightarrow x_1 \le x_2 \end{aligned} \tag{3.6}$$

Define the nth moment for the random variable X as

$$E[X^n] = \overline{X^n} = \int_{-\infty}^{\infty} x^n f_X(x)dx \tag{3.7}$$

The first moment, $E[X]$, is called the mean value, while the second moment, $E[X^2]$, is called the mean squared value. When the random variable X represents an electrical signal across a 1Ω resistor, then $E[X]$ is the DC component, and $E[X^2]$ is the total average power.

The nth central moment is defined as

$$E[(X-\bar{X})^n] = \overline{(X-\bar{X})^n} = \int_{-\infty}^{\infty} (x-\bar{x})^n f_X(x)dx \tag{3.8}$$

and, thus, the first central moment is zero. The second central moment is called the variance and is denoted by the symbol σ_X^2,

$$\sigma_X^2 = \overline{(X-\bar{X})^2} \tag{3.9}$$

In practice, the random nature of an electrical signal may need to be described by more than one random variable. In this case, the joint *cdf* and *pdf* functions need to be considered. The joint *cdf* and *pdf* for the two random variables X and Y are, respectively, defined by

$$F_{XY}(x,y) = Pr\{X \le x; Y \le y\} \tag{3.10}$$

$$f_{XY}(x,y) = \frac{\partial^2}{\partial x \partial y} F_{XY}(x,y) \tag{3.11}$$

The marginal *cdf*s are obtained as follows:

$$F_X(x) = \int_{-\infty}^{x}\int_{-\infty}^{\infty} f_{UV}(u, v)dudv = F_{XY}(x, \infty)$$
$$F_Y(y) = \int_{-\infty}^{y}\int_{-\infty}^{\infty} f_{UV}(u, v)dvdu = F_{XY}(\infty, y) \quad \textbf{(3.12)}$$

If the two random variables are statistically independent, then the joint *cdf*s and *pdf*s are, respectively, given by

$$F_{XY}(x, y) = F_X(x)F_Y(y) \quad \textbf{(3.13)}$$

$$f_{XY}(x, y) = f_X(x)f_Y(y) \quad \textbf{(3.14)}$$

Let us now consider a case when the two random variables X and Y are mapped into two new variables U and V through some transformations T_1 and T_2 defined by

$$U = T_1(X, Y) \qquad ; \; V = T_2(X, Y) \quad \textbf{(3.15)}$$

The joint *pdf*, $f_{UV}(u, v)$, may be computed based on the invariance of probability under the transformation. One must first compute the matrix of derivatives; then the new joint *pdf* is computed as

$$f_{UV}(u, v) = f_{XY}(x, y)|J| \quad \textbf{(3.16)}$$

$$|J| = \begin{vmatrix} \dfrac{\partial x}{\partial u} & \dfrac{\partial x}{\partial v} \\ \dfrac{\partial y}{\partial u} & \dfrac{\partial y}{\partial v} \end{vmatrix} \quad \textbf{(3.17)}$$

where the determinant of the matrix of derivatives $|J|$ is called the Jacobian. The characteristic function for the random variable X is defined as

$$C_X(\omega) = E[e^{j\omega X}] = \int_{-\infty}^{\infty} f_X(x)e^{j\omega x}dx \quad \textbf{(3.18)}$$

The characteristic function can be used to compute the *pdf* for a sum of independent random variables. More precisely, let the random variable Y be

$$Y = X_1 + X_2 + \ldots + X_N \quad \textbf{(3.19)}$$

where $\{X_i \; ; \; i = 1, \ldots, N\}$ is a set of independent random variables. It can be shown that

$$C_Y(\omega) = C_{X_1}(\omega)C_{X_2}(\omega)\ldots C_{X_N}(\omega) \tag{3.20}$$

and the *pdf* $f_Y(y)$ is computed as the inverse Fourier transform of $C_Y(\omega)$ (with the sign of y reversed):

$$f_Y(y) = \frac{1}{2\pi}\int_{-\infty}^{\infty} C_Y(\omega)e^{-j\omega y}d\omega \tag{3.21}$$

The characteristic function may also be used to compute the nth moment for the random variable X as

$$E[X^n] = (-j)^n \frac{d^n}{d\omega^n}C_X(\omega)\bigg|_{\omega = 0} \tag{3.22}$$

3.2. Multivariate Gaussian Random Vector

Consider a joint probability for m random variables, $X_1, X_2, \ldots, X_m$. These variables can be represented as components of an $m \times 1$ random column vector, X. More precisely,

$$\mathsf{X} = \left[X_1\ X_2\ \ldots\ X_m\right]^t \tag{3.23}$$

where the superscript t indicates the transpose operation. The joint *pdf* for the vector X is

$$f_{\underline{X}}(\underline{x}) = f_{X_1, X_2, \ldots, X_m}(x_1, x_2, \ldots, x_m) \tag{3.24}$$

The mean vector is defined as

$$\mu_X = \left[E[X_1]\ E[X_2]\ \ldots\ E[X_m]\right]^t \tag{3.25}$$

and the covariance is an $m \times m$ matrix given by

$$C_X = E[\mathsf{X}\ \mathsf{X}^t] - \mu_X\ \mu_X^t \tag{3.26}$$

Note that if the elements of the vector X are independent, then the covariance matrix is a diagonal matrix.

A random vector X is multivariate Gaussian if its *pdf* is of the form

$$f_X(\underline{x}) = \frac{1}{\sqrt{(2\pi)^m |C_X|}}\exp\left(-\frac{1}{2}(x-\mu_X)^t C_X^{-1}(x-\mu_X)\right) \tag{3.27}$$

where μ_x is the mean vector, C_x is the covariance matrix, C_x^{-1} is inverse of the covariance matrix and $|C_x|$ is its determinant, and X is of dimension m. If A [1] is a $k \times m$ matrix of rank k, then the random vector $\mathsf{Y} = A\mathsf{X}$ is a k-variate Gaussian vector with

$$\mu_Y = A\mu_X \tag{3.28}$$

$$C_Y = A\Lambda_X A^t \tag{3.29}$$

The characteristic function for a multivariate Gaussian *pdf* is defined by

$$C_X = E[\exp\{j(\omega_1 X_1 + \omega_2 X_2 + \ldots + \omega_m X_m)\}] = \tag{3.30}$$

$$\exp\left\{j\mu_X^t\omega - \frac{1}{2}\omega^t C_X \omega\right\}$$

Then the moments for the joint distribution can be obtained by partial differentiation. For example,

$$E[X_1X_2X_3] = \frac{\partial^3}{\partial\omega_1\partial\omega_2\partial\omega_3}C_X(\omega_1, \omega_2, \omega_3) \qquad at \quad \omega = 0 \tag{3.31}$$

Example:

The vector X *is a 4-variate Gaussian with*

$$\mu_X = \begin{bmatrix}2 & 1 & 1 & 0\end{bmatrix}^t \text{ and } C_X = \begin{bmatrix}6 & 3 & 2 & 1\\ 3 & 4 & 3 & 2\\ 2 & 3 & 4 & 3\\ 1 & 2 & 3 & 3\end{bmatrix}$$

Define

$$\mathsf{X}_1 = \begin{bmatrix}X_1\\ X_2\end{bmatrix} \qquad \mathsf{X}_2 = \begin{bmatrix}X_3\\ X_4\end{bmatrix}$$

Find the distribution of X_1 *and the distribution of*

1. Note that matrices are denoted by italicized upper case bold face letters, while vectors are denoted by lower and upper regular (not italicized) letters.

$$\mathbf{Y} = \begin{bmatrix} 2X_1 \\ X_1 + 2X_2 \\ X_3 + X_4 \end{bmatrix}$$

Solution:

$\mathbf{X}_1$ *has a bivariate Gaussian distribution with*

$$\mu_{X_1} = \begin{bmatrix} 2 \\ 1 \end{bmatrix} \qquad C_{X_1} = \begin{bmatrix} 6 & 3 \\ 3 & 4 \end{bmatrix}$$

The vector $\mathbf{Y}$ *can be expressed as*

$$\mathbf{Y} = \begin{bmatrix} 2 & 0 & 0 & 0 \\ 1 & 2 & 0 & 0 \\ 0 & 0 & 1 & 1 \end{bmatrix} \begin{bmatrix} X_1 \\ X_2 \\ X_3 \\ X_4 \end{bmatrix} = \mathbf{A}\mathbf{X}$$

It follows that

$$\mu_Y = \mathbf{A}\mu_X = \begin{bmatrix} 4 & 4 & 1 \end{bmatrix}^t$$

$$C_Y = \mathbf{A} C_X \mathbf{A}^t = \begin{bmatrix} 24 & 24 & 6 \\ 24 & 34 & 13 \\ 6 & 13 & 13 \end{bmatrix}$$

A special case of Eq. (3.29) is when the matrix $\mathbf{A}$ is given by

$$\mathbf{A} = \begin{bmatrix} a_1 a_2 \ \ldots \ a_m \end{bmatrix} \tag{3.32}$$

It follows that $\mathbf{Y} = \mathbf{A}\mathbf{X}$ is a sum of random variables X_i, that is

$$Y = \sum_{i=1}^{m} a_i \ X_i \tag{3.33}$$

The finding in Eq. (3.33) leads to the conclusion that the linear sum of Gaussian variables is also a Gaussian variable with mean and variance given by

$$\bar{Y} = a_1 \bar{X}_1 + a_2 \bar{X}_2 + \ldots + a_m \bar{X}_m \tag{3.34}$$

$$\sigma_Y^2 = E[(X-\bar{X})^2] = \quad (3.35)$$
$$E[a_1(X_1-\bar{X}_1)+a_2(X_2-\bar{X}_2)+\ldots+a_m(X_m-\bar{X}_m)]$$

and if the variables X_i are independent then Eq.(3.35) reduces to

$$\sigma_Y^2 = a_1^2\sigma_{X_1}^2 + a_2^2\sigma_{X_2}^2 + \ldots + a_m^2\sigma_{X_m}^2 \quad (3.36)$$

finally, in this case, the probability density function $f_Y(y)$ is given by (which can also be derived from Eq. (3.20))

$$f_Y(y) = f_{X_1}(x_1) \otimes f_{X_2}(x_2) \otimes \ldots \otimes f_{X_m}(x_m) \quad (3.37)$$

where $\otimes$ indicates convolution.

3.2.1. Complex Multivariate Gaussian Random Vector

Consider the complex vector random variable

$$\tilde{\mathsf{X}} = \mathsf{X}_I + j\mathsf{X}_Q \quad (3.38)$$

where X_I and X_Q are real random multivariate Gaussian random vectors. The joint *pdf* for the complex random vector $\tilde{\mathsf{X}}$ is computed from the joint *pdf* of the two real vectors. The mean for the vector $\tilde{\mathsf{X}}$ is

$$E[\tilde{\mathsf{X}}] = E[\mathsf{X}_I] + jE[\mathsf{X}_Q] \quad (3.39)$$

The covariance matrix is also defined by

$$\tilde{C} = E[(\tilde{\mathsf{X}} - E[\tilde{\mathsf{X}}])(\tilde{\mathsf{X}} - E[\tilde{\mathsf{X}}])^\dagger] \quad (3.40)$$

where the operator † indicates complex conjugate transpose.

The *pdf* for the vector $\tilde{\mathsf{X}}$ is

$$f_{\tilde{X}}(\tilde{\mathsf{x}}) = \frac{\exp[-(\tilde{\mathsf{x}} - E[\mathsf{x}])^\dagger \tilde{C}^{-1}(\tilde{\mathsf{x}} - E[\mathsf{x}])]}{\pi^N |\tilde{C}|} \quad (3.41)$$

with the following three conditions holding true

$$E[(\mathsf{X}_{I_i} - E[\mathsf{X}_{I_i}])(\mathsf{X}_{Q_i} - E[\mathsf{X}_{Q_i}])^\dagger] = 0 \quad (3.42)$$

$$E[(\mathsf{X}_{I_i} - E[\mathsf{X}_{I_i}])(\mathsf{X}_{I_k} - E[\mathsf{X}_{I_k}])^\dagger] = \quad (3.43)$$
$$E[(\mathsf{X}_{Q_i} - E[\mathsf{X}_{Q_i}])(\mathsf{X}_{Q_k} - E[\mathsf{X}_{Q_k}])^\dagger] \quad ;all \;\; i,k$$

$$E[(\mathsf{X}_{I_i} - E[\mathsf{X}_{I_i}])(\mathsf{X}_{Q_k} - E[\mathsf{X}_{Q_k}])^{\dagger}] = -E[(\mathsf{X}_{Q_i} - E[\mathsf{X}_{Q_i}])(\mathsf{X}_{I_k} - E[\mathsf{X}_{I_k}])^{\dagger}] \quad ;all \quad i \neq k \tag{3.44}$$

3.3. Rayleigh Random Variables

Let X_I and X_Q be zero mean independent Gaussian random variables with zero mean and variance σ^2. Define two new random variables R and Φ as

$$\begin{aligned} X_I &= R\cos\Phi \\ X_Q &= R\sin\Phi \end{aligned} \tag{3.45}$$

The joint *pdf* of the two random variables $X_I;X_Q$ is

$$f_{X_I X_Q}(x_I, x_Q) = \frac{1}{2\pi\sigma^2}\exp\left(-\frac{x_I^2 + x_Q^2}{2\sigma^2}\right) = \frac{1}{2\pi\sigma^2}\exp\left(-\frac{(r\cos\varphi)^2 + (r\sin\varphi)^2}{2\sigma^2}\right) \tag{3.46}$$

The joint *pdf* for the two random variables $R;\Phi$ is given by

$$f_{R\Phi}(r, \varphi) = f_{X_I X_Q}(x_I, x_Q)|\mathcal{J}| \tag{3.47}$$

where $[\mathcal{J}]$ is a matrix of derivatives defined by

$$[\mathcal{J}] = \begin{bmatrix} \dfrac{\partial x_I}{\partial r} & \dfrac{\partial x_I}{\partial \varphi} \\ \dfrac{\partial x_Q}{\partial r} & \dfrac{\partial x_Q}{\partial \varphi} \end{bmatrix} = \begin{bmatrix} \cos\varphi & -r\sin\varphi \\ \sin\varphi & r\cos\varphi \end{bmatrix} \tag{3.48}$$

The determinant of the matrix of derivatives is called the Jacobian, and in this case it is equal to

$$|\mathcal{J}| = r \tag{3.49}$$

Substituting Eqs. (3.46) and (3.49) into Eq. (3.47) and collecting terms yield

$$f_{R\Phi}(r, \varphi) = \frac{r}{2\pi\sigma^2}\exp\left(-\frac{(r\cos\varphi)^2 + (r\sin\varphi)^2}{2\sigma^2}\right) = \frac{r}{2\pi\sigma^2}\exp\left(-\frac{r^2}{2\sigma^2}\right) \tag{3.50}$$

The *pdf* for R alone is obtained by integrating Eq. (3.50) over φ

$$f_R(r) = \int_0^{2\pi} f_{R\Phi}(r, \varphi)d\varphi = \frac{r}{\sigma^2}\exp\left(-\frac{r^2}{2\sigma^2}\right) \frac{1}{2\pi}\int_0^{2\pi} d\varphi \tag{3.51}$$

where the integral inside Eq. (3.51) is equal to 2π; thus,

$$f_R(r) = \frac{r}{\sigma^2}\exp\left(-\frac{r^2}{2\sigma^2}\right) \quad ;r \geq 0 \tag{3.52}$$

The *pdf* described in Eq. (3.52) is referred to as a Rayleigh probability density function.

The density function for the random variable Φ is obtained from

$$f_\Phi(\varphi) = \int_0^r f(r, \varphi)\ dr \tag{3.53}$$

substituting Eq. (3.50) into Eq. (3.53) and performing integration by parts yields

$$f_\Phi(\varphi) = \frac{1}{2\pi} \quad ;\ 0 < \varphi < 2\pi \tag{3.54}$$

which is a uniform probability density function.

3.4. The Chi-Square Random Variables

3.4.1. Central Chi-Square Random Variable with N Degrees of Freedom

Let the random variables $\{X_1, X_2, \ldots, X_N\}$ be zero mean, statistically independent Gaussian random variable with unity variance. The variable

$$\chi_N^2 = \sum_{i=1}^{N} X_i^2 \tag{3.55}$$

is called a central chi-square random variable with N degrees of freedom. The chi-square *pdf* is

$$f_{\chi_N^2}(x) = \begin{cases} \dfrac{x^{(N-2)/2}\ e^{(-x/2)}}{2^{N/2}\ \Gamma(N/2)} & x \geq 0 \\ 0 & x < 0 \end{cases} \tag{3.56}$$

where the Gamma function is define as

$$\Gamma(n) = \int_0^\infty \lambda^{n-1} e^{-\lambda}\, d\lambda \;;\; n > 0 \tag{3.57}$$

with the following recursion

$$\Gamma(n+1) = n\Gamma(n) \tag{3.58}$$

and

$$\Gamma(n+1) = n! \qquad ;\; n = 0, 1, 2, \ldots, and \;\; 0! = 1 \tag{3.59}$$

The mean and variance for the central chi-square are, respectively given by

$$E[\chi_N^2] = N \tag{3.60}$$

$$\sigma_{\chi_N^2} = 2N \tag{3.61}$$

Hence, the degrees of freedom N is the ratio of twice the squared mean to the variance

$$N = (2E^2[\chi_N^2])/\sigma_{\chi_N^2} \tag{3.62}$$

3.4.2. Noncentral Chi-Square Random Variable with N Degrees of Freedom

In the general case, the chi-square random variable requires that the Gaussian random variables $\{X_1, X_2, \ldots, X_N\}$ do not have zero means. Define a multivariate random variable Y such that

$$Y_i = X_i + \mu_{X_i} \;; i = 1, 2, \ldots, N \tag{3.63}$$

Consider the random variable

$$\chi'^2_N = \sum_{i=1}^{N} Y_i^2 = \sum_{i=1}^{N} (X_i + \mu_{X_i})^2 \tag{3.64}$$

the variable χ'^2_N is called the noncentral chi-square random variable with N degrees of freedom and with a noncentral parameter λ, where

$$\lambda = \sum_{i=1}^{N} \mu_{X_i}^2 = \sum_{i=1}^{N} E^2[Y_i] \tag{3.65}$$

The noncentral chi-square *pdf* is

$$f_{\chi_N'^2}(x) = \begin{cases} \left(\frac{1}{2}\right)\left(\frac{x}{\lambda}\right)^{(N-2)/4} e^{[-(x+\lambda)/2]} I_{(N-2)/2}(\sqrt{\lambda x}) & x \geq 0 \\ 0 & x < 0 \end{cases} \tag{3.66}$$

where I is the modified Bessel function (or occasionally called the hyperbolic Bessel function) of the first kind; and the subscripts is referred to as its order.

3.5. Random Processes

A random variable X is by definition a mapping of all possible outcomes of a random experiment to numbers. When the random variable becomes a function of both the outcomes of the experiment time, it is called a random process and is denoted by $X(t)$. Thus, one can view a random process as an ensemble of time-domain functions that are the outcome of a certain random experiment, as compared with single real numbers in the case of a random variable.

Since the *cdf* and *pdf* of a random process are time dependent, we will denote them as $F_X(x;t)$ and $f_X(x;t)$, respectively. The nth moment for the random process $X(t)$ is

$$E[X^n(t)] = \int_{-\infty}^{\infty} x^n f_X(x;t)dx \tag{3.67}$$

A random process $X(t)$ is referred to as stationary to order one if all its statistical properties do not change with time. Consequently, $E[X(t)] = \overline{X}$, where $\overline{X}$ is a constant. A random process $X(t)$ is called stationary to order two (or wide-sense stationary) if

$$f_X(x_1, x_2;t_1, t_2) = f_X(x_1, x_2;t_1 + \Delta t, t_2 + \Delta t) \tag{3.68}$$

for all t_1, t_2 and Δt.

Define the statistical autocorrelation function for the random process $X(t)$ as

$$\Re_X(t_1, t_2) = E[X(t_1)X(t_2)] \tag{3.69}$$

The correlation $E[X(t_1)X(t_2)]$ is, in general, a function of (t_1, t_2). As a consequence of the wide-sense stationary definition, the autocorrelation function depends on the time difference $\tau = t_2 - t_1$, rather than on absolute time; and thus, for a wide-sense stationary process we have

$$\begin{aligned} E[X(t)] &= \bar{X} \\ \Re_X(\tau) &= E[X(t)X(t+\tau)] \end{aligned} \tag{3.70}$$

If the time average and time correlation functions are equal to the statistical average and statistical correlation functions, the random process is referred to as an ergodic random process. The following is true for an ergodic process:

$$\lim_{T\to\infty} \frac{1}{T} \int_{-T/2}^{T/2} x(t)dt = E[X(t)] = \bar{X} \tag{3.71}$$

$$\lim_{T\to\infty} \frac{1}{T} \int_{-T/2}^{T/2} x^*(t)x(t+\tau)dt = \Re_X(\tau) \tag{3.72}$$

The covariance of two random processes $X(t)$ and $Y(t)$ is defined by

$$C_{XY}(t, t+\tau) = E[\{X(t) - E[X(t)]\}\{Y(t+\tau) - E[Y(t+\tau)]\}] \tag{3.73}$$

which can also be written as

$$C_{XY}(t, t+\tau) = \Re_{XY}(\tau) - \bar{X}\bar{Y} \tag{3.74}$$

3.6. Bandpass Gaussian Random Process

It is customary to define the bandpass Gaussian random process through its complex envelope as

$$\tilde{X}(t) = X_I(t) + jX_Q(t) \tag{3.75}$$

where both $X_I(t)$ and $X_Q(t)$ are lowpass Gaussian random processes with zero mean and variance σ^2. The *pdf* for a sample $\tilde{X}(t_0)$ of the complex envelope is the joint *pdf* for $X_I(t)$ and $X_Q(t)$. That is,

$$f_{\tilde{X}}(\tilde{x}(t_0)) = \frac{1}{2\pi\sigma^2}\exp\left[-\frac{x_I^2(t_0) + x_Q^2(t_0)}{2\sigma^2}\right] = \frac{1}{2\pi\sigma^2}\exp\left[-\frac{|\tilde{x}(t_0)|^2}{2\sigma^2}\right] \tag{3.76}$$

Now, if both lowpass processes do not have zero mean and instead have a mean defined by

$$\mu(t) = \mu_I(t)\cos(2\pi f_0 t) + j\mu_Q(t)\sin(2\pi f_0 t) \tag{3.77}$$

the mean complex envelope is

$$\tilde{\mu}(t) = \mu_I(t) + j\mu_Q(t) \tag{3.78}$$

It follows that Eq. (3.76) can be rewritten as

$$f_{\tilde{X}}(\tilde{x}(t_0)) = \frac{1}{2\pi\sigma^2}\exp\left[-\frac{[x_I(t_0)-\mu_I(t_0)]^2 + [x_Q(t_0)-\mu_Q(t_0)]^2}{2\sigma^2}\right] = \frac{1}{2\pi\sigma^2}\exp\left[\frac{\left|\tilde{x}(t_0)-\tilde{\mu}(t_0)\right|^2}{2\sigma^2}\right] \tag{3.79}$$

Consider a duration of the process than spans the interval $\{0, T_0\}$. Then this segment of the complex envelope of the random process can be represented using a complex random variable vector of at least $N = BT_0$ elements where B is the bandwidth of the process. Define

$$\tilde{X}_i = \tilde{X}\left(\frac{i}{B}\right) \quad ;i = 1, 2, \ldots, BT_0 \tag{3.80}$$

$$\tilde{\mathbf{X}}^{\dagger} = \left[\tilde{X}_1\ \tilde{X}_2\ \ldots \tilde{X}_{BT_0}\right] \tag{3.81}$$

By definition the covariance matrix $\tilde{C}$ is

$$\tilde{C} = E[(\tilde{\mathbf{X}} - \tilde{\mu})(\tilde{\mathbf{X}} - \tilde{\mu})^{\dagger}] = 2(\tilde{C}_I + j\tilde{C}_{IQ}) \tag{3.82}$$

where

$$\tilde{C}_I = E[(\tilde{\mathbf{X}}_I - \tilde{\mu}_I)(\tilde{\mathbf{X}}_I - \tilde{\mu}_I)^{\dagger}] \tag{3.83}$$

$$\tilde{C}_{IQ} = E[(\tilde{\mathbf{X}}_I - \tilde{\mu}_I)(\tilde{\mathbf{X}}_Q - \tilde{\mu}_Q)^{\dagger}] \tag{3.84}$$

Therefore, the *pdf* for the segment $\{\tilde{X}(t)\ ;0 < t < T_0\}$ is

$$f_{\tilde{X}}(\tilde{\mathbf{x}}) = \frac{\exp[-(\tilde{\mathbf{x}} - \tilde{\mu})^{\dagger}\tilde{C}^{-1}(\tilde{\mathbf{x}} - \tilde{\mu})]}{\pi^N|\tilde{C}|} \tag{3.85}$$

3.6.1. The Envelope of a Bandpass Gaussian Process

Consider the *pdf* of a segment of the envelope of a bandpass Gaussian random process. This process can expressed as

$$X(t) = X_I(t)\cos(2\pi f_0 t) - X_Q(t)\sin(2\pi f_0 t) \tag{3.86}$$

where $X_I(t)$ and $X_Q(t)$ are zero mean independent lowpass Gaussian processes. The envelope and phase are respectively denoted by $R(t)$ and $\Phi(t)$, where

$$R(t) = \sqrt{X_I(t)^2 + X_Q(t)^2} \tag{3.87}$$

and

$$\Phi(t) = \left[\tan\left(\frac{X_Q(t)}{X_I(t)}\right)\right]^{-1} \tag{3.88}$$

where

$$\begin{aligned} X_I(t) &= R(t)\cos(\Phi(t)) \\ X_Q(t) &= R(t)\sin(\Phi(t)) \end{aligned} \tag{3.89}$$

The two processes $R(t)$ and $\Phi(t)$ are also independent, and their respective *pdfs* were derived in Section 3.3 and were given in Eqs. (3.52) and (3.54), respectively.

Problems

3.1. Suppose you want to determine an unknown DC voltage v_{dc} in the presence of additive white Gaussian noise $n(t)$ of zero mean and variance σ_n^2. The measured signal is $x(t) = v_{dc} + n(t)$. An estimate of v_{dc} is computed by making three independent measurements of $x(t)$ and computing the arithmetic mean, $\underset{\sim}{v}_{dc} \approx (x_1 + x_2 + x_3)/3$. (a) Find the mean and variance of the random variable $\underset{\sim}{v}_{dc}$. (b) Does the estimate of v_{dc} get better by using ten measurements instead of three? Why?

3.2. Assume the X and Y miss distances of darts thrown at a bulls-eye dart board are Gaussian with zero mean and variance σ^2. (a) Determine the probability that a dart will fall between 0.8σ and 1.2σ. (b) Determine the radius of a circle about the bull's-eye that contains 80% of the darts thrown. (c) Consider a square with side s in the first quadrant of the board. Determine s so that the probability that a dart will fall within the square is 0.07.

3.3. (a) A random voltage $v(t)$ has an exponential distribution function $f_V(v) = a\exp(-av)$, where $(a > 0); (0 \le v < \infty)$. The expected value $E[V] = 0.5$. Determine $Pr\{V > 0.5\}$. Consider the network shown in figure below, where $x(t)$ is a random voltage with zero mean and autocorrelation function $\Re_x(\tau) = 1 + \exp(-a|t|)$. Find the power spectrum $S_x(\omega)$. What is the transfer function? Find the power spectrum $S_v(\omega)$.

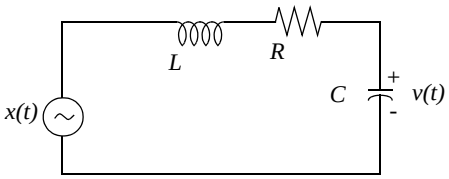

3.4. Let $\bar{S}_X(\omega)$ be the PSD function for the stationary random process $X(t)$. Compute an expression for the PSD function of

$$Y(t) = X(t) - 2X(t-T).$$

3.5. Let X be a random variable with

$$f_X(x) = \begin{cases} \frac{1}{\sigma} t^3 e^{-t} & t \geq 0 \\ 0 & elsewhere \end{cases}$$

(a) Determine the characteristic function $C_X(\omega)$. (b) Using $C_X(\omega)$, validate that $f_X(x)$ is a proper *pdf*. (c) Use $C_X(\omega)$ to determine the first two moments of X. (d) Calculate the variance of X.

3.6. Let the random variable Z be written in terms of two other random variables X and Y as follows: $Z = X + 3Y$. Find the mean and variance for the new random variable in terms of the other two.

3.7. Suppose you have the following sequences of statistically independent Gaussian random variables with zero means and variances σ^2. if

$$X_1, X_2, \ldots, X_N \;;\; X_i = A_i \cos\Theta_i \text{ and } Y_1, Y_2, \ldots, Y_N \;;\; Y_i = A_i \sin\Theta_i .$$

Define $Z = \sum_{i=1}^{N} A_i^2$. Find an expression that Z exceeds a threshold value v_T.

3.8. Repeat the previous problem when two single delay line cancellers are cascaded to produce a double delay line canceller.Let $X(t)$ be a stationary random process, $E[X(t)] = 1$ and the autocorrelation $\Re_x(\tau) = 3 + \exp(-|\tau|)$. Define a new random variola Y as

$$Y = \int_0^2 x(t)dt$$

Compute $E[Y(t)]$ and σ_Y^2.

3.9. Consider the single delay line canceller in the figure below. The input $x(t)$ is a wide sense stationary random process with variance σ_x^2 and mean μ_x and a covariance matrix Λ. Find the mean and variance and the autocorrelation function of the output $y(t)$.

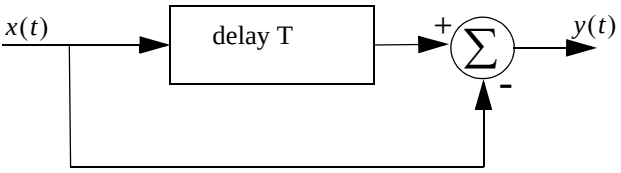

Chapter 4 The Matched Filter

4.1. The Matched Filter SNR

The topics of matched filtering and pulse compression (see Chapter 8) are central to almost all radar systems. In this chapter the focus is the matched filter. The unique characteristic of the matched filter is that it produces the maximum achievable instantaneous SNR at its output when a signal plus additive white noise is present at the input. Maximizing the SNR is key in all radar applications, as was described in Chapter 1 in the context of the radar equation and as will be discussed in Chapter 7 in the context of target detection.

Therefore, it is important to use a radar receiver which can be modeled as an LTI system that maximizes the signal's SNR at its output. For this purpose, the basic radar receiver of interest is often referred to as the matched filter receiver. The matched filter is an optimum filter in the sense of SNR because the SNR at its output is maximized at some delay t_0 that corresponds to the true target range R_0 (i.e., $t_0 = (2R_0)/c$). Figure 4.1 shows a simplified block diagram for the radar receiver of interest.

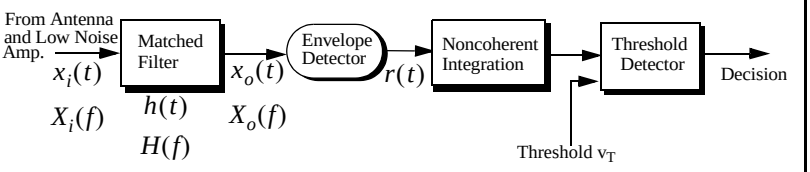

Figure 4.1. Simplified block diagram of the radar receiver

In order to derive the general expression for the transfer function and the impulse response of this optimum filter, adopt the following notation:

$h(t)$ is the optimum filter impulse response
$H(f)$ is the optimum filter transfer function
$x_i(t)$ is the input signal
$X_i(f)$ is the FT of the input signal
$x_o(t)$ is the output signal
$X_o(f)$ is the FT of the output signal
$n_i(t)$ is the input noise signal
$N_i(f)$ is the input noise PSD
$n_o(t)$ is the out noise signal
$N_o(f)$ is the output noise PSD

The optimum filter input signal can then be represented by

$$s_i(t) = x_i(t - t_0) + n_i(t) \tag{4.1}$$

where t_0 is an unknown time delay proportional to the target range. The optimum filter output signal is

$$s_o(t) = x_o(t - t_0) + n_o(t) \tag{4.2}$$

where

$$n_o(t) = n_i(t) \otimes h(t) \tag{4.3}$$

$$x_o(t) = x_i(t) \otimes h(t) \tag{4.4}$$

The operator ($\otimes$) indicates convolution. The FT of Eq. (4.4) is

$$X_o(f) = X_i(f)H(f) \tag{4.5}$$

Consequently the signal output at time t_0 can be calculated using the inverse FT, evaluated at t_0, as

$$x_o(t_0) = \int_{-\infty}^{\infty} X_i(f)H(f)e^{j2\pi f t_0}\, df \tag{4.6}$$

Additionally, the total noise power at the output of the filter is calculated using Parseval's theorem as

$$N_o = \int_{-\infty}^{\infty} N_i(f)|H(f)|^2\, df \tag{4.7}$$

Since the output signal power at time t_0 is equal to the modulus square of Eq. (4.6), then the instantaneous SNR at time t_0 is

$$SNR(t_0) = \frac{\left| \int_{-\infty}^{\infty} X_i(f)H(f)e^{j2\pi f t_0}\ df \right|^2}{\int_{-\infty}^{\infty} N_i(f)|H(f)|^2\ df} \tag{4.8}$$

Remember Schawrz's inequality which has the form

$$\frac{\left| \int_{-\infty}^{\infty} X_1(f)X_2(f)\ df \right|^2}{\int_{-\infty}^{\infty} |X_1(f)|^2\ df} \leq \int_{-\infty}^{\infty} |X_2(f)|^2\ df \tag{4.9}$$

The equal sign in Eq. (4.9) applies when $X_1(f) = KX_2{}^*(f)$ for some arbitrary constant K. Apply Schawrz's inequality to Eq. (4.8) with the following assumptions

$$X_1(f) = H(f)\sqrt{N_i(f)} \tag{4.10}$$

$$X_2(f) = \frac{X_i(f)e^{j2\pi f t_0}}{\sqrt{N_i(f)}} \tag{4.11}$$

It follows that the SNR is maximized when

$$H(f) = K\ \frac{X_i{}^*(f)e^{-j2\pi f t_0}}{N_i(f)} \tag{4.12}$$

An alternative way of writing Eq. (4.12) is

$$X_i(f)H(f)e^{j2\pi f t_0} = KN_i(f)|X_i(f)|^2 \tag{4.13}$$

The optimum filter impulse response is computed using inverse FT integral

$$h(t) = \int_{-\infty}^{\infty} K\ \frac{X_i{}^*(f)e^{-j2\pi f t_0}}{N_i(f)}\ e^{j2\pi f t}\ df \tag{4.14}$$

A special case of great interest to radar systems is when the input noise is bandlimited white noise with PSD given by

$$N_i(f) = \eta_0/2 \tag{4.15}$$

η_0 is a constant. The transfer function for this optimum filter is then given by

$$H(f) = X_i^*(f)e^{-j2\pi ft_0} \tag{4.16}$$

where the constant K was set equal to $\eta_0/2$. It follows that

$$h(t) = \int_{-\infty}^{\infty} [X_i^*(f)e^{-j2\pi ft_0}]\ e^{j2\pi ft}\ df \tag{4.17}$$

which can be written as

$$h(t) = x_i^*(t_0 - t) \tag{4.18}$$

Observation of Eq. (4.18) indicates that the impulse response of the optimum filter is matched to the input signal, and thus, the term *matched filter* is used for this special case. Under these conditions, the maximum instantaneous SNR at the output of the matched filter is

$$SNR(t_0) = \frac{\left| \int_{-\infty}^{\infty} X_i(f)H(f)e^{j2\pi ft_0}\ df \right|^2}{\eta_0/2} \tag{4.19}$$

and using Parseval's theorem the numerator in Eq. (4.19) is equal to the input signal energy, E_x; consequently one can write the output peak instantaneous SNR as

$$SNR(t_0) = \frac{2E_x}{\eta_0} \tag{4.20}$$

Note that Eq. (4.20) is unitless since the unit for η_0 are in Watts per Hertz (or Joules). Finally, one can draw the conclusion that the peak instantaneous SNR depends only on the signal energy and input noise power, and is independent of the waveform utilized by the radar.

As indicated by Eq. (4.18) the impulse response $h(t)$ may not be causal if the value for t_0 is less than the signal duration. Thus, an additional time delay term $\tau_0 \geq T$ is added to ensure causality, where T is the signal duration. Thus, a realizable matched filter response is given by

$$h(t) = \begin{cases} x_i^*(\tau_0 + t_0 - t) & ;t > 0,\ \tau_0 \geq T \\ 0 & ;t < 0 \end{cases} \tag{4.21}$$

The transfer function for this casual filter is

$$H(f) = \int_{-\infty}^{\infty} x_i^*(\tau_0 + t_0 - t)e^{-j2\pi ft}dt = \int_{\infty}^{-\infty} x_i^*(t + \tau_0 + t_0)e^{j2\pi ft}dt \tag{4.22}$$

$$= X_i^*(f)e^{-j2\pi f(\tau_0 + t_0)}$$

Substituting the right-hand side of Eq. (4.22) into Eq. (4.6) yields

$$x_o(\tau_0) = \int_{-\infty}^{\infty} X_i(f)X_i^*(f)e^{-j2\pi f(\tau_0 + t_0)}e^{j2\pi ft_0}\ df = \int_{-\infty}^{\infty} |X_i(f)|^2 e^{-j2\pi f\tau_0}\ df \tag{4.23}$$

which has a maximum value when τ_0. This result leads to the following conclusion: The peak value of the matched filter output is obtained by sampling its output at times equal to the filter delay after the start of the input signal, and the minimum value for τ_0 is equal to the signal duration T.

Example:

Compute the maximum instantaneous SNR at the output of a linear filter whose impulse response is matched to the signal $x(t) = \exp(-t^2/2T)$.

Solution:

The signal energy is

$$E_x = \int_{-\infty}^{\infty} |x(t)|^2 dt = \int_{-\infty}^{\infty} e^{(-t^2)/T}dt = \sqrt{\pi T}\ \ Joules$$

It follows that the maximum instantaneous SNR is

$$SNR = \frac{\sqrt{\pi T}}{\eta_0/2}$$

where $\eta_0/2$ *is the input noise power spectrum density.*

4.1.1. The Replica

Again, consider a radar system that uses a finite duration energy signal $x(t)$, and assume that a matched filter receiver is utilized. From Eq. (4.1) the input signal can be written as,

$$s(t) = x(t - t_0) + n(t) \tag{4.24}$$

The matched filter output $s_o(t)$ can be expressed by the convolution integral between the filter's impulse response and $s(t)$:

$$s_0(t) = \int_{-\infty}^{\infty} s(u)h(t-u)du \tag{4.25}$$

Substituting Eq. (4.21) into Eq. (4.25) yields

$$s_o(t) = \int_{-\infty}^{\infty} s(u)x^*(t - \tau_0 - t_0 + u)du = \bar{R}_{sx}(t - T_0) \tag{4.26}$$

where $T_0 = \tau_0 + t_0$ and $\bar{R}_{sx}(t - T_0)$ is a cross-correlation between $s(t)$ and $x(T_0 - t)$. Therefore, the matched filter output can be computed from the cross-correlation between the radar received signal and a delayed replica of the transmitted waveform. If the input signal is the same as the transmitted signal, the output of the matched filter would be the autocorrelation function of the received (or transmitted) signal. In practice, replicas of the transmitted waveforms are normally computed and stored in memory for use by the radar signal processor when needed.

4.2. Mean and Variance of the Matched Filter Output

Since the matched filter is an LTI filter, then when its input's statistics is Gaussian, its output statistics is also Gaussian, as discussed in Chapter 3. For this purpose, consider the following two hypotheses. Hypothesis H_0 is when the input to the matched filter consists of noise only. That is,

$$H_0 \Leftrightarrow s(t) = n_i(t) \tag{4.27}$$

where $n_i(t)$ is zero mean Gaussian bandlimited white noise with PSD $\eta_0/2$. Hypothesis H_1 is when the input consists of signal plus noise. That is,

$$H_1 \Leftrightarrow s(t) = x_i(t) + n_i(t) \tag{4.28}$$

Denote the conditional means and variances for both hypotheses by $E[s_o/H_0]$, the mean value of $s_0(\tau_0)$, when the signal is absent; $E[s_o/H_1]$ is

the mean value of $s_0(\tau_0)$ when the signal is present; $Var[s_o/H_0]$ is the variance of $s_0(\tau_0)$ when the signal is absent; and $Var[s_o/H_1]$ is the variance of $s_0(\tau_0)$ when the signal is present. It follows that

$$E[s_o/H_0] = 0 \tag{4.29}$$

$$E[s_o/H_1] = \int_{-\infty}^{\infty} |x_i(t)|^2 dt = E_x \tag{4.30}$$

where E_x is the signal energy. Finally,

$$Var[s_o/H_0] = Var[s_o/H_1] = E_x\eta_0/2 \tag{4.31}$$

4.3. General Formula for the Output of the Matched Filter

Two cases are analyzed; the first is when a stationary target is present. The second case is concerned with a moving target whose velocity is constant. Assume the range to the target is

$$R(t) = R_0 - v(t - t_0) \tag{4.32}$$

where v is the target radial velocity (i.e. the target velocity component on the radar line of sight.) The initial detection range R_0 is given by

$$t_0 = \frac{2R_0}{c} \tag{4.33}$$

where c is the speed of light and t_0 is the round trip delay it takes a certain radar pulse to travel from the radar to the target at range R_0 and back.

The general expression for the radar bandpass signal is

$$s(t) = s_I(t)\cos 2\pi f_0 t - s_Q(t)\sin 2\pi f_0 t \tag{4.34}$$

which can be written using its pre-envelope (analytic signal) as

$$s(t) = Re\{\psi(t)\} = Re\{\tilde{s}(t)e^{j2\pi f_0 t}\} \tag{4.35}$$

where $Re\{\ \}$ indicates "the real part of." Again $\tilde{s}(t)$ is the complex envelope.

4.3.1. Stationary Target Case

In this case, the received radar return is given by

$$s_r(t) = s\left(t - \frac{2R_0}{c}\right) = s(t - t_0) = Re\{\tilde{s}(t - t_0)e^{j2\pi f_0(t - t_0)}\} \tag{4.36}$$

It follows that the received analytic and complex envelope signals are, respectively, given by

$$\psi_r(t) = \tilde{s}(t - t_0)e^{-j2\pi f_0 t_0}e^{j2\pi f_0 t} \tag{4.37}$$

$$\tilde{s}_r(t) = \tilde{s}(t - t_0)e^{-j2\pi f_0 t_0} \tag{4.38}$$

Observation of Eq. (4.38) clearly indicates that the received complex envelope is more than just a delayed version of the transmitted complex envelope. It actually contains an additional phase shift φ_0 which represents the phase corresponding to the two-way optical length for the target range. That is,

$$\varphi_0 = -2\pi f_0 t_0 = -2\pi f_0 2\frac{R_0}{c} = -\frac{2\pi}{\lambda}2R_0 \tag{4.39}$$

where λ is the radar wavelength and is equal to c/f_0. Since a very small change in range can produce significant change in this phase term, this phase is often treated as a random variable with uniform probability density function over the interval $\{0, 2\pi\}$. Furthermore, the radar signal processor will first attempt to remove (correct for) this phase term through a process known as phase unwrapping.

Substituting Eq. (4.38) into Eq. (4.25) provides the output of the matched filter. It is given by

$$s_o(t) = \int_{-\infty}^{\infty} \tilde{s}_r(u)h(t - u)du \tag{4.40}$$

where the impulse response $h(t)$ is in Eq. (4.18). It follows that

$$s_o(t) = \int_{-\infty}^{\infty} \tilde{s}(u - t_0)e^{-j2\pi f_0 t_0}\tilde{s}^*(t - t_0 + u)du \tag{4.41}$$

Make the following change of variables:

$$z = u - t_0 \Rightarrow dz = du \tag{4.42}$$

Therefore, the output of the matched filter when a stationary target is present is computed from Eq (4.41) as

$$s_o(t) = e^{-j2\pi f_0 t_0} \int_{-\infty}^{\infty} \tilde{s}(z)\tilde{s}^*(t-z)dz = e^{-j2\pi f_0 t_0} \bar{R}_s(t) \tag{4.43}$$

where $\bar{R}_s(t)$ is the autocorrelation function for the signal $\tilde{s}(t)$.

4.3.2. Moving Target Case

In this case, the received signal only not is delayed in time by t_0 but also has a Doppler frequency shift f_d corresponding to the target velocity, where

$$f_d = 2vf_0/c = 2v/\lambda \tag{4.44}$$

The pre-envelope of the received signal can be written as

$$\psi_r(t) = \psi\left(t - \frac{2R(t)}{c}\right) = \tilde{s}\left(t - \frac{2R(t)}{c}\right) e^{j2\pi f_0\left(t - \frac{2R(t)}{c}\right)} \tag{4.45}$$

Substituting Eq. (4.32) into Eq. (4.45) yields

$$\psi_r(t) = \tilde{s}\left(t - \frac{2R_0}{c} + \frac{2vt}{c} - \frac{2vt_0}{c}\right) e^{j2\pi f_0\left(t - \frac{2R_0}{c} + \frac{2vt}{c} - \frac{2vt_0}{c}\right)} \tag{4.46}$$

Collecting terms yields

$$\psi_r(t) = \tilde{s}\left(t\left(1 + \frac{2v}{c}\right) - t_0\left(1 + \frac{2v}{c}\right)\right) e^{j2\pi f_0\left(t - \frac{2R_0}{c} + \frac{2vt}{c} - \frac{2vt_0}{c}\right)} \tag{4.47}$$

Define the scaling factor γ as

$$\gamma = 1 + \frac{2v}{c} \tag{4.48}$$

then Eq. (4.47) can be written as

$$\psi_r(t) = \tilde{s}(\gamma(t - t_0)) e^{j2\pi f_0\left(t - \frac{2R_0}{c} + \frac{2vt}{c} - \frac{2vt_0}{c}\right)} \tag{4.49}$$

Since $c \gg v$, the following approximation can be used

$$\tilde{s}(\gamma(t - t_0)) \approx \tilde{s}(t - t_0) \tag{4.50}$$

It follows that Eq. (4.49) can now be rewritten as

$$\psi_r(t) = \tilde{s}(t - t_0) e^{j2\pi f_0 t} e^{-j2\pi f_0 \frac{2R_0}{c}} e^{j2\pi f_0 \frac{2vt}{c}} e^{-j2\pi f_0 \frac{2vt_0}{c}} \tag{4.51}$$

Recognizing that $f_d = (2vf_0)/c$ and $t_0 = (2R_0)/c$, the received pre-envelope signal is

$$\psi_r(t) = \tilde{s}(t-t_0)e^{j2\pi f_0 t}e^{-j2\pi f_0 t_0}e^{j2\pi f_d t}e^{-j2\pi f_d t_0} = \tilde{s}(t-t_0)e^{j2\pi(f_0+f_d)(t-t_0)} \quad \textbf{(4.52)}$$

or

$$\psi_r(t) = \{\tilde{s}(t-t_0)e^{j2\pi f_d t}e^{-j2\pi(f_0+f_d)t_0}\}e^{j2\pi f_0 t} \quad \textbf{(4.53)}$$

Then by inspection the complex envelope of the received signal is

$$\tilde{s}_r(t) = \tilde{s}(t-t_0)e^{j2\pi f_d t}e^{-j2\pi(f_0+f_d)t_0} \quad \textbf{(4.54)}$$

Finally, it is concluded that the complex envelope of the received signal when the target is moving at a constant velocity v is a delayed (by t_0) version of the complex envelope signal of the stationary target case except that:

1. An additional phase shift term corresponding to the target's Doppler frequency is present, and
2. The phase shift term $(-2\pi f_d t_0)$ is present.

The output of the matched filter was derived in Eq. (4.25). Substituting Eq. (4.54) into Eq. (4.25) yields

$$s_o(t) = \int_{-\infty}^{\infty} \tilde{s}(u-t_0)e^{j2\pi f_d u}e^{-j2\pi(f_0+f_d)t_0}\tilde{s}^*(t-t_0+u)\,du \quad \textbf{(4.55)}$$

Applying the change of variables given in Eq. (4.42) and collecting terms provide

$$s_o(t) = e^{-j2\pi f_0 t_0}\int_{-\infty}^{\infty} \tilde{s}(z)\tilde{s}^*(t-z)e^{j2\pi f_d z}e^{j2\pi f_d t_0}e^{-j2\pi f_d t_0}\,dz \quad \textbf{(4.56)}$$

Observation of Eq. (4.56) shows that the output is a function of both t and f_d. Thus, it is more appropriate to rewrite the output of the matched filter as a two-dimensional function of both variables. That is,

$$s_o(t;f_d) = e^{-j2\pi f_0 t_0}\int_{-\infty}^{\infty} \tilde{s}(z)\tilde{s}^*(t-z)e^{j2\pi f_d z}\,dz \quad \textbf{(4.57)}$$

It is customary but not necessary to set $t_0 = 0$. Note that if the causal impulse response is used (i.e., Eq. (4.21)), the same analysis will hold true. However, in

this case, the phase term is equal to $\exp(-j2\pi f_0 T_0)$, instead of $\exp(-j2\pi f_0 t_0)$ where $T_0 = \tau_0 + t_0$.

4.4. Waveform Resolution and Ambiguity

As indicated by Eq. (4.20), the radar sensitivity (in the case of white additive noise) depends only on the total energy of the received signal and is independent of the shape of the specific waveform. This leads to the following question: If the radar sensitivity is independent of the waveform, what is the best choice for the transmitted waveform? The answer depends on many factors; however, the most important consideration lies in the waveform's range and Doppler resolution characteristics, which can be determined from the output of the matched fitter.

As discussed in Chapter 1, range resolution implies separation between distinct targets in range. Alternatively, Doppler resolution implies separation between distinct targets in frequency. Thus, ambiguity and accuracy of this separation are closely associated terms.

4.4.1. Range Resolution

Consider radar returns from two stationary targets (zero Doppler) separated in range by distance ΔR. What is the smallest value of ΔR so that the returned signal is interpreted by the radar as two distinct targets? In order to answer this question, assume that the radar transmitted bandpass pulse is denoted by $x(t)$,

$$x(t) = r(t)\cos(2\pi f_0 t + \phi(t)) \tag{4.58}$$

where f_0 is the carrier frequency, $r(t)$ is the amplitude modulation, and $\phi(t)$ is the phase modulation. The signal $x(t)$ can then be expressed as the real part of the pre-envelope signal $\psi(t)$, where

$$\psi(t) = r(t)e^{j(2\pi f_0 t - \phi(t))} = \tilde{x}(t)e^{2\pi f_0 t} \tag{4.59}$$

and the complex envelope is

$$\tilde{x}(t) = r(t)e^{-j\phi(t)} \tag{4.60}$$

It follows that

$$x(t) = Re\{\psi(t)\} \tag{4.61}$$

The returns from two close targets are, respectively, given by

$$x_1(t) = \psi(t - \tau_0) \tag{4.62}$$

$$x_2(t) = \psi(t - \tau_0 - \tau) \tag{4.63}$$

where τ is the difference in delay between the two target returns. One can assume that the reference time is τ_0, and thus without any loss of generality, one may set $\tau_0 = 0$. It follows that the two targets are distinguishable by how large or small the delay τ can be.

In order to measure the difference in range between the two targets, consider the integral square error between $\psi(t)$ and $\psi(t-\tau)$. Denoting this error as ε_R^2, it follows that

$$\varepsilon_R^2 = \int_{-\infty}^{\infty} |\psi(t) - \psi(t-\tau)|^2 \, dt \tag{4.64}$$

which can be written as

$$\varepsilon_R^2 = \int_{-\infty}^{\infty} |\psi(t)|^2 \, dt + \int_{-\infty}^{\infty} |\psi(t-\tau)|^2 \, dt - \tag{4.65}$$

$$\int_{-\infty}^{\infty} \{(\psi(t)\psi^*(t-\tau) + \psi^*(t)\psi(t-\tau)) \, dt\}$$

Using Eq. (4.59) into Eq. (4.65) yields

$$\varepsilon_R^2 = 2\int_{-\infty}^{\infty} |\tilde{x}(t)|^2 \, dt - 2Re\left\{\int_{-\infty}^{\infty} \psi^*(t)\psi(t-\tau) \, dt\right\} = \tag{4.66}$$

$$2\int_{-\infty}^{\infty} |\tilde{x}(t)|^2 \, dt - 2Re\left\{e^{-j\omega_0\tau}\int_{-\infty}^{\infty} \tilde{x}^*(t)\tilde{x}(t-\tau) \, dt\right\}$$

This squared error is minimum when the second portion of Eq. (4.66) is positive and maximum. Note that the first term in the right-hand side of Eq. (4.66) represents the total signal energy, and is assumed to be constant. The second term is a varying function of τ with its fluctuation tied to the carrier frequency. The integral inside the right most side of this equation is defined as the range ambiguity function,

$$\chi_R(\tau) = \int_{-\infty}^{\infty} \tilde{x}^*(t)\tilde{x}(t-\tau) \, dt \tag{4.67}$$

This range ambiguity function is equivalent to the integral given in Eq. (4.43) with $t_0 = 0$. Comparison between Eq. (4.67) and Eq. (4.43) indicates that the output of the matched filter and the range ambiguity function have the same envelope (in this case the Doppler shift f_d is set to zero). This indicates that the matched filter, in addition to providing the maximum instantaneous SNR at its output, also preserves the signal range resolution properties. The value of $\chi_R(\tau)$ that minimizes the squared error in Eq. (4.66) occurs when $\tau = 0$.

Target resolvability in range is measured by the squared magnitude $|\chi_R(\tau)|^2$. It follows that if $|\chi_R(\tau)| = \chi_R(0)$ for some nonzero value of τ, then the two targets are indistinguishable. Alternatively, if $|\chi_R(\tau)| \neq \chi_R(0)$ for some nonzero value of τ, then the two targets may be distinguishable (resolvable). As a consequence, the most desirable shape for $\chi_R(\tau)$ is a very sharp peak (thumb tack shape) centered at $\tau = 0$ and falling very quickly away from the peak. The minimum range resolution corresponding to a time duration τ_e or effective bandwidth B_e is

$$\Delta R = \frac{c\tau_e}{2} = \frac{c}{2B_e} \tag{4.68}$$

The effective time duration and the effective bandwidth for any waveform were defined in Chapter 2 and are repeated here as Eq. (4.69) and Eq. (4.70), respectively

$$\tau_e = \left[\int_{-\infty}^{\infty} |\tilde{x}(t)|^2 dt\right]^2 \Big/ \int_{-\infty}^{\infty} |\tilde{x}(t)|^4 dt \tag{4.69}$$

$$B_e = \left[\int_{-\infty}^{\infty} |\tilde{X}(f)|^2 \, df\right]^2 \Big/ \left(\int_{-\infty}^{\infty} |\tilde{X}(f)|^4 \, df\right) \tag{4.70}$$

4.4.2. Doppler Resolution

The Doppler shift corresponding to the target radial velocity is

$$f_d = \frac{2v}{\lambda} = \frac{2vf_0}{c} \tag{4.71}$$

where v is the target radial velocity, λ is the wavelength, f_0 is the frequency, and c is the speed of light.

The FT of the pre-envelope is

$$\Psi(f) = \int_{-\infty}^{\infty} \psi(t) e^{-j2\pi ft} \, dt \tag{4.72}$$

Due to the Doppler shift associated with the target, the received signal spectrum will be shifted by f_d. In other words, the received spectrum can be represented by $\Psi(f - f_d)$. In order to distinguish between the two targets located at the same range but having different velocities, one may use the integral square error. More precisely,

$$\varepsilon_f^2 = \int_{-\infty}^{\infty} \left| \Psi(f) - \Psi(f - f_d) \right|^2 \, df \tag{4.73}$$

Using similar analysis as that which led to Eq. (4.66), one should maximize

$$Re\left\{ \int_{-\infty}^{\infty} \Psi^*(f) \Psi(f - f_d) \, df \right\} \tag{4.74}$$

Taking the FT of the pre-envelope (analytic signal) defined in Eq. (4.59) yields

$$\Psi(f) = \tilde{X}(2\pi f - 2\pi f_0) \tag{4.75}$$

Thus,

$$\int_{-\infty}^{\infty} \tilde{X}^*(2\pi f) \tilde{X}(2\pi f - 2\pi f_d) \, df = \tag{4.76}$$

$$\int_{-\infty}^{\infty} \tilde{X}^*(2\pi f - 2\pi f_0) \tilde{X}(2\pi f - 2\pi f_0 - 2\pi f_d) \, df$$

The complex frequency correlation function is then defined as

$$\chi_f(f_d) = \int_{-\infty}^{\infty} \tilde{X}^*(2\pi f) \tilde{X}(2\pi f - 2\pi f_d) \, df = \int_{-\infty}^{\infty} |\tilde{x}(t)|^2 \, ^{j2\pi f_d t} \, dt \tag{4.77}$$

The velocity resolution (Doppler resolution) is by definition

$$\Delta v = (c \Delta f_d) / (2 f_0) \tag{4.78}$$

where Δf_d is the minimum resolvable Doppler difference between the Doppler frequencies corresponding to two moving targets, i.e., $\Delta f_d = f_{d1} - f_{d2}$, where

f_{d1} and f_{d2} are the two individual Doppler frequencies for targets 1 and 2, respectively. The Doppler resolution Δf_d is equal to the inverse of the total effective duration of the waveform. Thus,

$$\Delta f_d = \left(\int_{-\infty}^{\infty} |\chi_f(f_d)|^2 df_d \right) / (\chi_f^2(0)) = \left(\int_{-\infty}^{\infty} |\tilde{x}(t)|^4 dt \right) / \left[\int_{-\infty}^{\infty} |\tilde{x}(t)|^2 dt \right]^2 = \frac{1}{\tau_e} \quad \textbf{(4.79)}$$

4.4.3. Combined Range and Doppler Resolution

In this general case, one needs to use a two-dimensional function in the pair of variables (τ, f_d). For this purpose, assume that the pre-envelope of the transmitted waveform is

$$\psi(t) = \tilde{x}(t) e^{j2\pi f_0 t} \quad \textbf{(4.80)}$$

Then the delayed and Doppler-shifted signal is (see Eq. (4.53))

$$\psi(t-\tau) = \tilde{x}(t-\tau) e^{j2\pi(f_0 - f_d)(t-\tau)} \quad \textbf{(4.81)}$$

Computing the integral square error between Eq. (4.80) and Eq. (4.81) yields

$$\varepsilon^2 = \int_{-\infty}^{\infty} |\psi(t) - \psi(t-\tau)|^2 dt \quad \textbf{(4.82a)}$$

$$\varepsilon^2 = 2\int_{-\infty}^{\infty} |\psi(t)|^2 dt - 2Re\left\{ \int_{-\infty}^{\infty} \psi^*(t) - \psi(t-\tau) dt \right\} \quad \textbf{(4.82b)}$$

which can be written as

$$\varepsilon^2 = 2\int_{-\infty}^{\infty} |\tilde{x}(t)|^2 \, dt - 2Re\left\{ e^{j2\pi(f_0 - f_d)\tau} \int_{-\infty}^{\infty} \tilde{x}(t)\tilde{x}^*(t-\tau) e^{j2\pi f_d t} dt \right\} \quad \textbf{(4.83)}$$

Again, in order to maximize this squared error for $\tau \neq 0$, one must minimize the last term of Eq. (4.83). Define the combined range and Doppler correlation function as

$$\chi(\tau, f_d) = \int_{-\infty}^{\infty} \tilde{x}(t)\tilde{x}^*(t-\tau) e^{j2\pi f_d t} dt \quad \textbf{(4.84)}$$

In order to achieve the most range and Doppler resolution, the modulus square of this function must be minimized at $\tau \neq 0$ and $f_d \neq 0$. Note that the output of the matched filter, except for a phase term, is identical to that given in Eq. (4.84). This means that the output of the filter exhibits maximum instantaneous SNR as well as the most achievable range and Doppler resolutions. The modulus square of Eq. (4.84) is often referred to as the ambiguity function:

$$\left|\chi(\tau, f_d)\right|^2 = \left|\int_{-\infty}^{\infty} \tilde{x}(t)\tilde{x}^*(t-\tau)e^{j2\pi f_d t}dt\right|^2 \tag{4.85}$$

The ambiguity function is often used by radar designers and analysts to determine the *goodness* of a given radar waveform, where this *goodness* is measured by its range and Doppler resolutions. Remember that since the matched filter is used, maximum SNR is guaranteed.

4.5. Range and Doppler Uncertainty

The formula derived in Eq. (4.84) represents the output of the matched filter when the signal at its input comprises target returns only and has no noise components, an assumption that cannot be true in practical situations. In general, the input at the matched filter contains both target and noise returns. The noise signal is assumed to be an additive random process that is uncorrelated with the target and has bandlimited white spectrum. Referring to Eq. (4.84), a peak at the output of the matched filter at (τ_1, f_{d1}) represents a target whose delay (range) corresponds to τ_1 and Doppler frequency equal to f_{d1}. Therefore, measuring targets' exact range and Doppler frequency is determined from measuring peak locations occurring in the two-dimensional space (τ, f_d). This last statement, however, is correct only if noise is not present at the input of the matched filter. When noise is present and because noise is random, it will generate ambiguity (uncertainty) about the exact location of the ambiguity function peaks in the (τ, f_d) space.

4.5.1. Range Uncertainty

Consider the case when the return signal complex envelope is (assuming stationary target)

$$\tilde{s}_r(t) = \tilde{x}_r(t) + \tilde{n}(t) \tag{4.86}$$

where $\tilde{x}_r(t)$ is the target return signal complex envelope and $\tilde{n}(t)$ is the noise signal complex envelope. The integral squared error between the total received signal (target plus noise) and the shifted (delayed) transmitted waveform is

$$\varepsilon^2 = \int_0^{T_{max}} \left|\tilde{x}(t-\tau) - \tilde{s}_r(t)\right|^2 \, dt \tag{4.87}$$

where T_{max} corresponds to maximum range under consideration. Expanding this squared error yields

$$\varepsilon^2 = 2\int_0^{T_{max}} |\tilde{x}(t)|^2 \, dt + 2\int_0^{T_{max}} |\tilde{n}(t)|^2 \, dt - 2Re\left\{\int_0^{T_{max}} \tilde{x}^*(t-\tau)\tilde{s}_r(t)dt\right\} \tag{4.88}$$

which can be written as

$$\varepsilon^2 = E_x + E_n - 2Re\left\{\int_0^{T_{max}} \tilde{x}^*(t-\tau)\tilde{x}_r(t)dt + \int_0^{T_{max}} \tilde{x}^*(t-\tau)\tilde{n}(t)dt\right\} \tag{4.89}$$

This expression is minimum at some value τ that makes the integral term inside Eq. (4.88) maximum and positive. More precisely, the following correlation functions must be maximized

$$R_{x_r x}(\tau) = \int_0^{T_{max}} \tilde{x}^*(t-\tau)\tilde{x}_r(t)dt \tag{4.90}$$

$$R_{nx}(\tau) = \int_0^{T_{max}} \tilde{x}^*(t-\tau)\tilde{n}(t)dt \tag{4.91}$$

Therefore, Eq. (4.89) can be written as

$$\varepsilon^2 = E - 2Re\{R_{x_r x}(\tau) + R_{nx}(\tau)\} \tag{4.92}$$

Expanding the quantity $\{R_{x_r x}(\tau)\}$ using Taylor series expansion about the point $\tau = t_0$, where $t_0 = 2R/c$, and R is the exact target range leads to

$$R_{x_r x}(\tau) = R_{x_r x}(t_0) + R'_{x_r x}(t_0)(\tau - t_0) + \frac{R''_{x_r x}(t_0)(\tau - t_0)^2}{2!} + \ldots \tag{4.93}$$

where R' and R'', respectively, indicate the first and second derivatives with respect to delay. Remember that since the real part of the correlation function is an even function, all its odd number derivatives are equal to zero. Now,

approximate Eq. (4.93) by using the first three terms (terms 1 and 3 are, of course, equal to zero) to get

$$Re\{R_{x_r x}(\tau)\} \approx R_{x_r x}(t_0) + \frac{R''_{x_r x}(t_0)(\tau - t_0)^2}{2} \tag{4.94}$$

There is some value τ_1 close to the exact target range, t_0, that will minimize the expression in Eq. (4.92). In order to find this minimum value, differentiate the quantity $Re\{R_{x_r x}(\tau) + R_{nx}(\tau)\}$ with respect to τ and set the result equal to zero to find τ_1. More specifically,

$$Re\left\{\frac{d}{d\tau}R_{x_r x}(\tau) + \frac{d}{d\tau}R_{nx}(\tau)\right\} = Re\{R'_{x_r x}(\tau) + R'_{nx}(\tau)\} = 0 \tag{4.95}$$

The derivative of the $Re\{R_{x_r x}(\tau)\}$ can be found from Eq. (4.94) as

$$Re\left\{\frac{d}{d\tau}R_{x_r x}(\tau)\right\} = \frac{d}{d\tau}\left(R_{x_r x}(t_0) + \frac{R''_{x_r x}(t_0)(\tau - t_0)^2}{2!}\right) = R''_{x_r x}(t_0)(\tau - t_0) \tag{4.96}$$

Substituting the result of Eq. (4.96) into Eq. (4.95) and collecting terms yield

$$(\tau_1 - t_0) = -\frac{Re\{R'_{nx}(\tau_1)\}}{R''_{x_r x}(t_0)} \tag{4.97}$$

The value $(\tau_1 - t_0)$ represent the amount of target range error measurement. It is more meaningful, since noise is random, to compute this error in terms of the standard deviation of its rms value. Hence, the standard deviation for range measurement error is

$$\sigma_\tau = (\tau_1 - t_0)_{rms} = -\frac{Re\{R'_{nx}(\tau_1)\}_{rms}}{R''_{x_r x}(t_0)} \tag{4.98}$$

By using the differentiation property of the Fourier transform and Parseval's theorem the denominator of Eq. (4.89) can be determined by

$$R''_{x_r x}(t_0) = (2\pi)^2 \int_{-\infty}^{\infty} f^2 \, |X(f)|^2 df \tag{4.99}$$

Next, from relations developed in Chapter 2, one can write the FT of $R_{nx}(\tau)$ as

$$FT\{R_{nx}(\tau)\} = X^*(f)\frac{\eta_0}{2} \tag{4.100}$$

where $\eta_0/2$ is the noise power spectrum density value (white noise). From the Fourier transform properties, the FT of the derivative of $R_{nx}(\tau)$ is

$$FT\{R'_{nx}(\tau)\} = (j2\pi f)\left(X^*(f)\frac{\eta_0}{2}\right) = (j2\pi f)S_{nx}(f) \tag{4.101}$$

The rms value for $R'_{nx}(\tau)$ is by definition

$$\{R'_{nx}(\tau)\}_{rms} = \sqrt{\lim_{T_{max}} \frac{1}{T_{max}} \int_0^{T_{max}} R'_{nx}(\tau)\ d\tau} \tag{4.102}$$

which can be rewritten using Parseval's theorem as

$$\{R'_{nx}(\tau)\}_{rms} = \sqrt{\int_0^{T_{max}} \left|FT\{R'_{nx}(\tau)\}\right|^2\ df} \tag{4.103}$$

substituting Eq. (4.101) into Eq. (4.103) yields

$$\{R'_{nx}(\tau)\}_{rms} = \sqrt{\frac{\eta_0}{2}(2\pi)^2 \int_0^{T_{max}} f^2\ |X(f)|^2\ df} \tag{4.104}$$

Finally, the standard deviation for range measurement error can be written as

$$\sigma_\tau = \frac{\sqrt{\eta_0/2}}{\sqrt{(2\pi)^2 \int_{-\infty}^{\infty} f^2\ |X(f)|^2 df}} \tag{4.105}$$

Define the bandwidth rms value, B_{rms}^2, as

$$B_{rms}^2 = \frac{(2\pi)^2 \int_{-\infty}^{\infty} f^2\ |X(f)|^2 df}{\int_{-\infty}^{\infty} |X(f)|^2 df} \tag{4.106}$$

It follows that Eq. (4.105) can now be written as

$$\sigma_\tau = \frac{\sqrt{\eta_0/2}}{B_{rms}\sqrt{\int_{-\infty}^{\infty}|X(f)|^2 df}} = \frac{\sqrt{\eta_0/2}}{B_{rms}\sqrt{E_x}} = \frac{1}{B_{rms}\sqrt{2E_x/\eta_0}} \quad \textbf{(4.107)}$$

which leads to the conclusion that the uncertainty in range measurement is inversely proportional to the rms bandwidth and the square root of the ratio of signal energy to the noise power density (square root of the SNR).

4.5.2. Doppler (Velocity) Uncertainty

For this purpose, assume that the target range is completely known. In the next section the case where both target range and target Doppler are not known will be analyzed. Denote the signal transmitted by the radar as $x(t)$ and the received signal (target plus noise) as $x_r(t)$. The integral square difference between the two returns can be written as

$$\varepsilon^2 = \int_0^{f_{max}} |X(f-f_c) - X_r(f)|^2 \, df \quad \textbf{(4.108)}$$

where $X(f)$ is the FT of $x(t)$, $X_r(f)$ is the FT of $x_r(t)$, and f_{max} is the maximum anticipated target Doppler. Again expand Eq. (4.108) to get

$$\varepsilon^2 = \int_0^{f_{max}} |X(f)|^2 \, df + \int_0^{f_{max}} |X_r(f)|^2 \, df - 2Re\left\{\int_0^{f_{max}} |X^*(f-f_c)X_r(f)|^2 \, df\right\} \quad \textbf{(4.109)}$$

Minimizing the error squared in Eq. (4.109) requires maximizing the value

$$Re\left\{\int_0^{f_{max}} |X^*(f-f_c)X_r(f)|^2 \, df\right\}$$

Conducting similar analysis as that performed in the previous section, the duration rms, τ_{rms}^2, value can be defined as

$$\tau_{rms}^2 = \left((2\pi)^2 \int_{-\infty}^{\infty} t^2 \, |x(t)|^2 dt\right) \Big/ \left(\int_{-\infty}^{\infty} |x(t)|^2 dt\right) \quad \textbf{(4.110)}$$

The standard deviation in the Doppler measurement can be derived as

$$\sigma_{f_d} = \frac{1}{\tau_{rms}\sqrt{2E_x/\eta_0}} \tag{4.111}$$

Comparison of Eq. (4.111) and Eq. (4.107) indicates that the error in estimating Doppler is inversely proportional to the signal duration, while the error in estimating range is inversely proportional to the signal bandwidth. Therefore, and as expected, larger bandwidths minimize the range measurement errors and longer integration periods minimize the Doppler measurement errors.

4.5.3. Range-Doppler Coupling

In the previous two sections, range estimate error and Doppler estimate error were derived by assuming that they are uncoupled estimates. In other words, range error was derived assuming stationary target, while Doppler error was derived assuming completely known target range. In this section a more general formula for the combined range and Doppler errors is derived.

The analytic signal for this case was derived in Section 4.3 and was given in Eq. (4.52) which is repeated here as Eq. (4.112) for easy reference:

$$\psi_r(t) = \tilde{s}(t-t_0)e^{j2\pi f_0 t}e^{-j2\pi f_0 t_0}e^{j2\pi f_d t}e^{-j2\pi f_d t_0} = \tilde{s}(t-t_0)e^{j2\pi(f_0+f_d)(t-t_0)} \tag{4.112}$$

One can assume with any loss of generality that $t_0 = 0$, thus, Eq. (4.112) can be expressed as

$$\psi_r(t) = \tilde{s}(t)e^{j2\pi(f_0+f_d)t} = r(t)e^{j\varphi(t)}e^{j2\pi(f_0+f_d)t} \tag{4.113}$$

where the complex envelope signal, $\tilde{s}(t)$, can be expressed as

$$\tilde{s}(t) = r(t)e^{j\varphi(t)} \tag{4.114}$$

Range Error Estimate

From the analysis performed in Section 4.5.1, the estimate for the range error is determined by maximizing the function

$$Re\{R_{ss}(\tau, f_d) + R_{ns}(\tau)\} \tag{4.115}$$

It follows that for some fixed value f_{d1} there is a value τ_1 close to $t_0 = 0$ that will maximize Eq. (4.115); that is,

$$Re\{R'_{ss}(\tau_1, f_{d1}) + R'_{ns}(\tau_1)\} = 0 \tag{4.116}$$

Again the Taylor series expansion of R_{ss} about $\tau = 0$ is

$$R_{ss}(\tau, f_d) = Re\left\{ R_{ss}(0, f_{d1}) + R'_{ss}(0, f_{d1})(\tau) + \frac{R''_{ss}(0, f_{d1})\tau^2}{2!} + \ldots \right\} \quad \textbf{(4.117)}$$

Thus,

$$Re\left\{ \frac{d}{d\tau} R_{ss}(\tau, f_d) \right\} \approx Re\{ R'_{ss}(0, f_{d1}) + R''_{ss}(0, f_{d1})\tau \} \quad \textbf{(4.118)}$$

Substituting Eq. (4.118) into Eq. (4.116) and solving for τ_1 yields

$$\tau_1 = -\frac{Re\{ R'_{ns}(\tau_1) + R'_{ss}(0, f_{d1}) \}}{Re\{ R''_{ss}(0, f_{d1}) \}} \quad \textbf{(4.119)}$$

The value of $R''_{ss}(0, f_{d1})$ is not much different from $R''_{ss}(0, 0)$; thus,

$$\tau_1 \approx -\frac{Re\{ R'_{ns}(\tau_1) + R'_{ss}(0, f_{d1}) \}}{R''_{ss}(0, 0)} \quad \textbf{(4.120)}$$

To evaluate the term $R'_{ss}(0, f_{d1})$, start with the definition of $R_{ss}(\tau, f_d)$,

$$R_{ss}(\tau, f_d) = \int_{-\infty}^{\infty} r(t-\tau) e^{-j\varphi(t-\tau)} r(t) e^{j(\varphi(t) + 2\pi f_d t)} dt \quad \textbf{(4.121)}$$

Compute the derivative of Eq. (4.121) with respect to τ

$$R'_{ss}(\tau, f_d) = -\int_{-\infty}^{\infty} \{ r'(t-\tau) r(t) - j\varphi'(t-\tau) r(t-\tau) r(t) \} \times e^{j[\varphi(t) - \varphi(t-\tau) + 2\pi f_d t]} dt \quad \textbf{(4.122)}$$

Evaluating Eq. (4.122) at $\tau = 0$ and $f_d = f_{d1}$ gives

$$R'_{ss}(0, f_{d1}) = -\int_{-\infty}^{\infty} \{ r'(t) r(t) - j\varphi'(t) r^2(t) \} \times e^{j[2\pi f_{d1} t]} dt \quad \textbf{(4.123)}$$

The complex exponential term in Eq. (4.123) can be approximated using small angle approximation as

$$e^{j[2\pi f_{d1} t]} = \cos(2\pi f_{d1} t) + j \sin(2\pi f_{d1} t) \approx 1 + 2\pi f_{d1} t \quad \textbf{(4.124)}$$

Next substitute Eq. (4.124) into Eq. (4.123), collect terms, and compute its real part to get

$$Re\{R'_{ss}(0, f_{d1})\} = -\int_{-\infty}^{\infty} r'(t)r(t)dt - 2\pi f_{d1}\int_{-\infty}^{\infty} t\varphi'(t)r^2(t)dt \qquad \textbf{(4.125)}$$

The first integral is evaluated (using FT properties and Parseval's theorem) as

$$\int_{-\infty}^{\infty} r'(t)r(t)dt = (j2\pi)\int_{-\infty}^{\infty} f_d|R(f)|^2 df \qquad \textbf{(4.126)}$$

Remember that since the envelope function $r(t)$ is a real lowpass signal, its Fourier transform is an even function; thus, Eq. (4.126) is equal to zero. Using this result, Eq. (4.125) becomes

$$Re\{R'_{ss}(0, f_{d1})\} = -2\pi f_{d1}\int_{-\infty}^{\infty} t\varphi'(t)r^2(t)dt \qquad \textbf{(4.127)}$$

Substitute Eq. (4.127) into Eq. (4.120) to get

$$\tau_1 = -\frac{Re\{R'_{ns}(\tau_1)\} - 2\pi f_{d1}\int_{-\infty}^{\infty} t\varphi'(t)r^2(t)dt}{R''_{ss}(0, 0)} \qquad \textbf{(4.128)}$$

Equation (4.128) provides a measure for the degree of coupling between range and Doppler estimates. Clearly, if $\varphi(t) = 0 \Rightarrow \varphi'(t) = 0$, then there is zero coupling between the two estimates. Define the range-Doppler coupling constant as

$$\rho_{\tau RDC} = \left(2\pi\int_{-\infty}^{\infty} t\varphi'(t)|\tilde{s}(t)|^2 dt\right) \Big/ \left(\int_{-\infty}^{\infty} |\tilde{s}(t)|^2 dt\right) \qquad \textbf{(4.129)}$$

Doppler Error Estimate

Applying similar analysis as that performed in the preceding section to the spectral cross correlation function yields an expression for the range-Doppler coupling term. It is given by

$$\rho_{f_d RDC} = \frac{2\pi \int_{-\infty}^{\infty} f \ \Phi'(f)|\tilde{S}(f)|^2 df}{\int_{-\infty}^{\infty} |\tilde{S}(f)|^2 df} \tag{4.130}$$

where $\Phi(f)$ is the FT of $\varphi(t)$.

It can be shown that Eq. (4.129) and Eq. (4.130) are equal (see Problem 4.15). Given this result, the subscripts τ and f_d in Eq. (4.129) and Eq. (4.130) are dropped and the range-Doppler term is simply referred to as ρ_{RDC}.

4.5.4. Range-Doppler Coupling in LFM Signals

Referring to Eq. (4.113) and Eq. (4.114), the phase for an LFM signal can be expressed as

$$\varphi(t) = \mu' t^2 \tag{4.131}$$

where $\mu' = (\pi B)/\tau_0$, B is the LFM bandwidth, and τ_0 is the pulsewidth. Substituting Eq. (4.131) into Eq. (4.129) yields

$$\rho_{RDC} = \frac{4\pi\mu' \int_{-\infty}^{\infty} t^2 |\tilde{s}(t)|^2 dt}{\int_{-\infty}^{\infty} |\tilde{s}(t)|^2 dt} = \frac{\mu'}{\pi}\tau_e^2 \tag{4.132}$$

where τ_e is the effective duration. Thus,

$$\sigma_\tau^2 = \frac{(\eta_0/2)}{B_e^2 2E_x} + \frac{f_{d1}^2 \rho_{RDC}^2}{B_e^4} \tag{4.133}$$

Similarly,

$$\sigma_{f_d}^2 = \frac{(\eta_0/2)}{\tau_e^2 2E_x} + \frac{t_1^2 \rho_{RDC}^2}{\tau_e^4} \tag{4.134}$$

where f_{d1} and t_1 are constants. Since estimates of range or Doppler when noise is present cannot be 100% exact, it is better to replace these constants with their equivalent mean-squared errors. That is, let

$$f_{d1}^2 = \sigma_{fd}^2 \quad , \quad t_1^2 = \sigma_\tau^2 \tag{4.135}$$

where σ_τ is as in Eq. (4.133) and σ_{fd} is in Eq. (4.134). Thus, Eq. (4.133) can be written as

$$\sigma_{\tau_{RDC}}^2 = \frac{(\eta_0/2)}{B_e^2 2E_x} + \frac{\rho_{RDC}^2}{B_e^4}\left(\frac{(\eta_0/2)}{\tau_e^2 2E_x} + \frac{\rho_{RDC}^2 \sigma_\tau^2}{\tau_e^4}\right) \tag{4.136}$$

which can be algebraically manipulated to get

$$\sigma_{\tau_{RDC}}^2 = \frac{(\eta_0/2)}{B_e^2 2E_x} \frac{1}{(1-(\rho_{RDC}^2/B_e^2\tau_e^2))} \tag{4.137}$$

Using similar analysis,

$$\sigma_{f_{dRDC}}^2 = \frac{(\eta_0/2)}{\tau_e^2 2E_x} \frac{1}{(1-(\rho_{RDC}^2/B_e^2\tau_e^2))} \tag{4.138}$$

These results lead to the conclusion that one can estimate target range and Doppler simultaneously only when the product of the rms bandwidth and rms duration is very large (i.e., very large time bandwidth products). This is the reason radars using LFM waveforms cannot estimate target Doppler accurately unless very large time bandwidth products are utilized. Often, the LFM waveforms are referred to as "Doppler insensitive" waveforms.

4.6. Target Parameter Estimation

Target parameters of interest to radar applications include, but are not limited to, target range (delay), amplitude, phase, Doppler, and angular location (azimuth and elevation). Target information (parameters) is typically embedded in the return signals amplitude and phase. Different classes waveforms are used by the radar signal and data processors to extract different target parameters more efficiently than others. Since radar echoes typically comprise signal plus additive noise, most if not all the target information is governed by the statistics of the input noise, whose statistical parameters most likely are not known but can be estimated. Thus, statistical estimates of the target parameters (amplitude, phase, delay, Doppler, etc.) are utilized instead of the actual corresponding measurements. The general form of the radar signal can be expressed in the following form

$$x(t) = Ar(t-t_0)\cos[2\pi(f_0+f_d)(t-t_0) + \phi(t-t_0) + \phi_0] \tag{4.139}$$

where A is the signal amplitude, $r(t)$ is the envelope lowpass signal, ϕ_0 is some constant phase, f_0 is the carrier frequency, t_0 and f_d are the target delay

and Doppler, respectively. The analysis in this section closely follows Melsa and Cohen[1].

4.6.1. What Is an Estimator?

In the case of radar systems it always safe to assume, due to the central limit theorem, that the input noise is always Gaussian with mainly unknown parameters. Furthermore, one can assume that this noise is bandlimited white noise. Consequently, the primary question that needs to be answered is as follows: Given that the probability density function of the observation is known (Gaussian in this case) and given a finite number of independent measurements, can one determine an estimate of a given parameter (such as range, Doppler, amplitude, or phase)?

Let $f_X(x;\theta)$ be the *pdf* of a random variable X with an unknown parameter θ. Define the values $\{x_1, x_2, \ldots, x_N\}$ as N observed independent values of the variable X. Define the function or estimator $\hat{\theta}(x_1, x_2, \ldots, x_N)$ as an estimate of the unknown parameter θ. The bias of estimation is defined as

$$E[\hat{\theta} - \theta] = b \tag{4.140}$$

where $E[\ ]$ represents the "expected value of." The estimator $\hat{\theta}$ is referred to as an unbiased estimator if and only if

$$E[\hat{\theta}] = \theta \tag{4.141}$$

One of the most popular and common measures of the quality or effectiveness of an estimator is the Mean Square Deviation (MSD) referred to symbolically as $\Delta^2(\hat{\theta})$. For an unbiased estimator

$$\Delta^2(\hat{\theta}) = \sigma^2_{\hat{\theta}} \tag{4.142}$$

where $\sigma^2_{\hat{\theta}}$ is the estimator variance. It can be shown that the Cramer-Rao bound for this MSD is given by

$$\sigma^2(\hat{\theta}) \geq \sigma^2_{min}(\theta) = \frac{1}{N\int_{-\infty}^{\infty}\left(\frac{\partial}{\partial\theta}\log\{f_X(x;\theta)\}\right)^2 f_X(x;\theta)\ dx} \tag{4.143}$$

The efficiency of this unbiased estimator is defined by

1. Melsa, J. L. Cohen, D. L., *Decision and Estimation Theory*, McGraw-Hill, New York, 1978.

$$\varepsilon(\hat{\theta}) = \frac{\sigma^2_{min}(\theta)}{\sigma^2(\hat{\theta})} \tag{4.144}$$

when $\varepsilon(\hat{\theta}) = 1$ the unbiased estimator is called an efficient estimate.

Consider an essentially timelimited signal $x(t)$ with effective duration τ_e and assume a bandlimited white noise with PSD $\eta_0/2$. In this case, Eq. (4.144) is equivalent to

$$\sigma^2(\hat{\theta}_i) \geq 1 \Big/ \left(\frac{2}{\eta_0} \int_0^{NT_r} \left(\frac{\partial}{\partial \theta_i} x(t) \right)^2 dt \right) \tag{4.145}$$

where $\hat{\theta}_i$ is the estimate for the i^{th} parameter of interest and T_r is the pulse repetition interval for the pulsed sequence. In the next two sections, estimates of the target amplitude and phase are derived. It must be noted that since these estimates represent independent random variables, they are referred to as uncoupled estimates; that is, the computation of one estimate does not depend on apriori knowledge of the other estimates.

4.6.2. Amplitude Estimation

The signal amplitude A in Eq. (4.139) is the parameter of interest, in this case. Taking the partial derivative of Eq. (4.139) with respect to A and squaring the result yields

$$\left(\frac{\partial}{\partial t_0} x(t) \right)^2 = (r(t-t_0)\cos[2\pi(f_0 + f_d)(t-t_0) + \phi(t-t_0) + \phi_0])^2 \tag{4.146}$$

Thus,

$$\int_0^{NT_r} \left(\frac{\partial}{\partial A} x(t) \right)^2 dt = \int_0^{NT_r} (x(t))^2 \, dt = NE_x \tag{4.147}$$

where E_x is the signal energy (from Parseval's theorem). Substituting Eq. (4.147) into Eq. (4.145) and collecting terms yield the variance for the amplitude estimate as

$$\sigma_A^2 \geq \frac{1}{\frac{2}{\eta_0} NE_x} = \frac{1}{N \; SNR} \tag{4.148}$$

In this case Eq. (4.20) used in Eq. (4.148) and SNR is the signal to noise ratio of the signal at the output of the matched filter. This clearly indicates that the signal amplitude estimate is improved as the SNR is increased.

4.6.3. Phase Estimation

In this case, it is desired to compute the best estimate for the signal phase ϕ_0. Again taking the partial derivative of the signal in Eq. (4.139) with respect to ϕ_0 and squaring the result yield

$$\left(\frac{\partial}{\partial\phi_0}x(t)\right)^2 = (-r(t-t_0)\sin[2\pi(f_0+f_d)(t-t_0)+\phi(t-t_0)+\phi_0])^2 \quad \textbf{(4.149)}$$

It follows that

$$\int_0^{NT_r}\left(\frac{\partial}{\partial\phi_0}x(t)\right)^2 dt = \int_0^{NT_r}(x(t))^2\,dt = NE_x \quad \textbf{(4.150)}$$

Thus, the variance of the phase estimate is

$$\sigma_{\phi_0}^2 \geq \frac{1}{\frac{2}{\eta_0}NE_x} = \frac{1}{N\ SNR} \quad \textbf{(4.151)}$$

Problems

4.1. Show that the SNR at the output of the matched filter can be written as

$$SNR = \frac{2}{\alpha\pi}(S_i(\alpha))^2$$

where $\alpha = (\pi BT)/2$, B is the bandwidth, T is the pulsewidth. Assume that the radar is using unmodulated rectangular pulse of width T and that there is a target detected at range R. The value S_i is the signal power at the input of the matched filter.

4.2. Compute the frequency response for the filter matched to the signal

(a) $x(t) = \exp\left(\frac{-t^2}{2T}\right)$;

(b) $x(t) = u(t)\exp(-\alpha t)$ where α is a positive constant.

4.3. Repeat the example in Section 4.1 using $x(t) = u(t)\exp(-\alpha t)$.

4.4. Prove the properties of the radar ambiguity function.

4.5. A radar system uses LFM waveforms. The received signal is of the form $s_r(t) = As(t-\tau)+n(t)$, where τ is a time delay that depends on range, $s(t) = Rect(t/\tau')\cos(2\pi f_0 t-\phi(t))$, and $\phi(t) = -\pi Bt^2/\tau'$. Assume that the radar bandwidth is $B = 5MHz$, and the pulse width is $\tau' = 5\mu s$. (a) Give

the quadrature components of the matched filter response that is matched to $s(t)$. (b) Write an expression for the output of the matched filter. (c) Compute the increase in SNR produced by the matched filter.

4.6. (a) Write an expression for the ambiguity function of an LFM waveform, where $\tau' = 6.4\mu s$ and the compression ratio is 32. (b) Give an expression for the matched filter impulse response.

4.7. (a) Write an expression for the ambiguity function of a LFM signal with bandwidth $B = 10MHz$, pulse width $\tau' = 1\mu s$, and wavelength $\lambda = 1cm$. (b) Plot the zero Doppler cut of the ambiguity function. (c) Assume a target moving toward the radar with radial velocity $v_r = 100m/s$. What is the Doppler shift associated with this target? (d) Plot the ambiguity function for the Doppler cut in part (c). (e) Assume that three pulses are transmitted with PRF $f_r = 2000Hz$. Repeat part (b).

4.8. (a) Give an expression for the ambiguity function for a pulse train consisting of 4 pulses, where the pulse width is $\tau' = 1\mu s$ and the pulse repetition interval is $T = 10\mu s$. Assume a wavelength of $\lambda = 1cm$. (b) Sketch the ambiguity function contour.

4.9. Hyperbolic frequency modulation (HFM) is better than LFM for high radial velocities. The HFM phase is

$$\phi_h(t) = \frac{\omega_0^2}{\mu_h}\ln\left(1 + \frac{\mu_h \alpha t}{\omega_0}\right)$$

where μ_h is an HFM coefficient and α is a constant. (a) Give an expression for the instantaneous frequency of an HFM pulse of duration τ'_h. (b) Show that HFM can be approximated by LFM. Express the LFM coefficient μ_l in terms of μ_h and in terms of B and τ'.

4.10. Consider a sonar system with range resolution $\Delta R = 4cm$. (a) A sinusoidal pulse at frequency $f_0 = 100KHz$ is transmitted. What is the pulse width, and what is the bandwidth? (b) By using an up-chirp LFM, centered at f_0, one can increase the pulse width for the same range resolution. If you want to increase the transmitted energy by a factor of 20, give an expression for the transmitted pulse. (c) Give an expression for the causal filter matched to the LFM pulse in part b.

4.11. A pulse train $y(t)$ is given by

$$y(t) = \sum_{n=0}^{2} w(n)x(t - n\tau')$$

where $x(t) = \exp(-t^2/2)$ is a single pulse of duration τ' and the weighting sequence is $\{w(n)\} = \{0.5, 1, 0.7\}$. Find and sketch the correlations R_x, R_w, and R_y.

4.12. Repeat the previous problem for $x(t) = \exp(-t^2/2)\cos 2\pi f_0 t$.

4.13. Derive Eq. (4.29) and Eq. (4.30) when the input noise is not white.

4.14. Show that the zero Doppler cut for the ambiguity function of an arbitrary phase coded pulse with a pulse width τ_p is given by $Y(f) = \left|\sin c(f\tau_p)\right|^2$.

4.15. Show that

$$\int_{-\infty}^{\infty} tx^*(t)x'(t)\ dt = -\int_{-\infty}^{\infty} fX^*(f)X'(f)\ df$$

where $X(f)$, is the FT of $x(t)$ and $x'(t)$ is its derivative with respect to time. The function $X'(f)$ is the derivative of $X(f)$ with respect to frequency.

Chapter 5 The Ambiguity Function - Analog Waveforms

5.1. Introduction

The radar ambiguity function represents the output of the matched filter, and it describes the interference caused by the range and/or Doppler shift of a target when compared to a reference target of equal RCS. The ambiguity function evaluated at $(\tau, f_d) = (0, 0)$ is equal to the matched filter output that is perfectly matched to the signal reflected from the target of interest. In other words, returns from the nominal target are located at the origin of the ambiguity function. Thus, the ambiguity function at nonzero τ and f_d represents returns from some range and Doppler different from those for the nominal target.

The formula for the output of the matched filter was derived in Chapter 4, it is, assuming a moving target with Doppler frequency f_d,

$$\chi(\tau, f_d) = \int_{-\infty}^{\infty} \tilde{x}(t)\tilde{x}^*(t-\tau)e^{j2\pi f_d t}dt \tag{5.1}$$

The modulus square of Eq. (5.1) is referred to as the ambiguity function. That is,

$$\left|\chi(\tau, f_d)\right|^2 = \left|\int_{-\infty}^{\infty} \tilde{x}(t)\tilde{x}^*(t-\tau)e^{j2\pi f_d t}dt\right|^2 \tag{5.2}$$

The radar ambiguity function is normally used by radar designers as a means of studying different waveforms. It can provide insight about how different radar waveforms may be suitable for the various radar applications. It is also used to determine the range and Doppler resolutions for a specific radar waveform. The three-dimensional (3-D) plot of the ambiguity function versus frequency and time delay is called the radar ambiguity diagram.

Denote E_x as the energy of the signal $\tilde{x}(t)$,

$$E_x = \int_{-\infty}^{\infty} |\tilde{x}(t)|^2 dt \tag{5.3}$$

The following list includes the properties for the radar ambiguity function:

1) The maximum value for the ambiguity function occurs at $(\tau, f_d) = (0, 0)$ and is equal to $4E_x^2$,

$$max\{|\chi(\tau;f_d)|^2\} = |\chi(0;0)|^2 = (2E_x)^2 \tag{5.4}$$

$$|\chi(\tau;f_d)|^2 \le |\chi(0;0)|^2 \tag{5.5}$$

2) The ambiguity function is symmetric,

$$|\chi(\tau;f_d)|^2 = |\chi(-\tau;-f_d)|^2 \tag{5.6}$$

3) The total volume under the ambiguity function is constant,

$$\int\int |\chi(\tau;f_d)|^2 \, d\tau \, df_d = (2E_x)^2 \tag{5.7}$$

4) If the function $X(f)$ is the Fourier transform of the signal $x(t)$, then by using Parseval's theorem we get

$$|\chi(\tau;f_d)|^2 = \left| \int X^*(f) X(f-f_d) e^{-j2\pi f\tau} df \right|^2 \tag{5.8}$$

5) Suppose that $|\chi(\tau;f_d)|^2$ is the ambiguity function for the signal $\tilde{x}(t)$. Adding a quadratic phase modulation term to $\tilde{x}(t)$ yields

$$\tilde{x}_1(t) = \tilde{x}(t) e^{j\pi\mu t^2} \tag{5.9}$$

where μ is a constant. It follows that the ambiguity function for the signal $\tilde{x}_1(t)$ is given by

$$|\chi_1(\tau;f_d)|^2 = |\chi(\tau;(f_d + \mu\tau))|^2 \tag{5.10}$$

5.2. Examples of the Ambiguity Function

The ideal radar ambiguity function is represented by a spike of infinitesimally small width that peaks at the origin and is zero everywhere else, as illustrated in Fig. 5.1. An ideal ambiguity function provides perfect resolution between neighboring targets regardless of how close they may be to each other. Unfortunately, an ideal ambiguity function cannot physically exist because the

ambiguity function must have finite peak value equal to $(2E_x)^2$ and a finite volume also equal to $(2E_x)^2$. Clearly, the ideal ambiguity function cannot meet those two requirements.

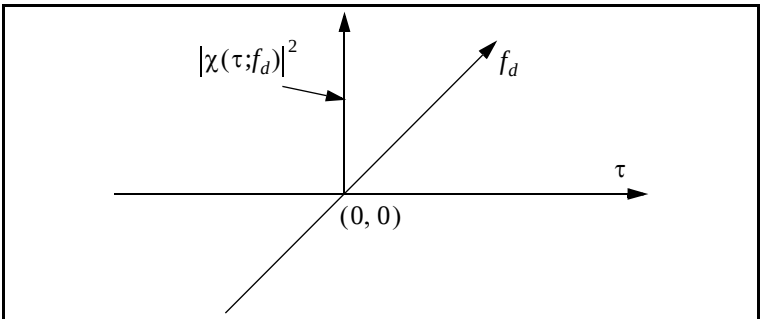

Figure 5.1. Ideal ambiguity function.

5.2.1. Single Pulse Ambiguity Function

The complex envelope of a single pulse is $\tilde{x}(t)$ defined by

$$\tilde{x}(t) = \frac{1}{\sqrt{\tau_0}} Rect\left(\frac{t}{\tau_0}\right) \tag{5.11}$$

From Eq. (5.1) we have

$$\chi(\tau;f_d) = \int_{-\infty}^{\infty} \tilde{x}(t)\tilde{x}^*(t-\tau)e^{j2\pi f_d t}dt \tag{5.12}$$

Substituting Eq. (5.11) into Eq. (5.12) and performing the integration yield

$$|\chi(\tau;f_d)|^2 = \left|\left(1-\frac{|\tau|}{\tau_0}\right)\frac{\sin(\pi f_d(\tau_0-|\tau|))}{\pi f_d(\tau_0-|\tau|)}\right|^2 \qquad |\tau| \le \tau_0 \tag{5.13}$$

Figures 5.2 a and b show 3-D and contour plots of single pulse ambiguity functions. This figure can be reproduced using the following MATLAB code

```
close all; clear all;
eps = 0.000001;
taup = 3;
[x] = single_pulse_ambg (taup);
taux = linspace(-taup,taup, size(x,1));
fdy = linspace(-5/taup+eps,5/taup-eps, size(x,1));
mesh(taux,fdy,x);
```

```
xlabel ('Delay in seconds');
ylabel ('Doppler in Hz');
zlabel ('Ambiguity function')
figure(2)
contour(taux,fdy,x);
xlabel ('Delay in seconds');
ylabel ('Doppler in Hz'); grid
```

The ambiguity function cut along the time-delay axis τ is obtained by setting $f_d = 0$. More precisely,

$$|\chi(\tau;0)| = \left(1 - \frac{|\tau|}{\tau_0}\right)^2 \qquad |\tau| \le \tau_0 \tag{5.14}$$

Note that the time autocorrelation function of the signal $\tilde{x}(t)$ is equal to $\chi(\tau;0)$. Similarly, the cut along the Doppler axis is

$$|\chi(0;f_d)|^2 = \left|\frac{\sin \pi \tau_0 f_d}{\pi \tau_0 f_d}\right|^2 \tag{5.15}$$

Figures 5.3 and 5.4, respectively, show the plots of the uncertainty function cuts defined by Eq. (5.14) and Eq. (5.15). Since the zero Doppler cut along the time-delay axis extends between $-\tau_0$ and τ_0, close targets will be unambiguous if they are at least τ_0 seconds apart.

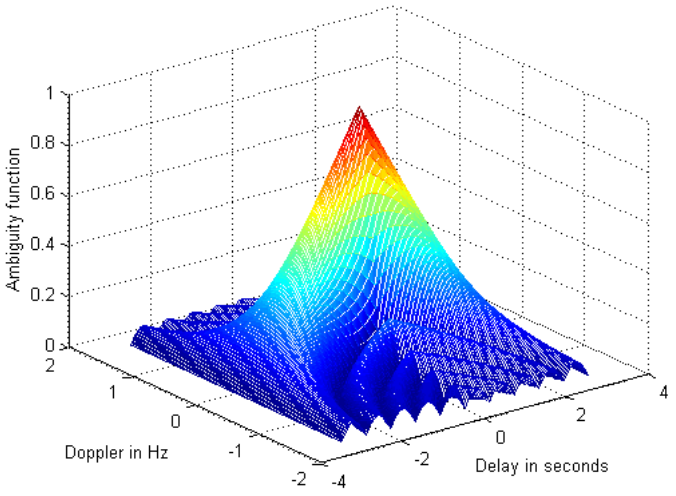

Figure 5.2a. Single pulse 3-D ambiguity plot. Pulse width is 3 seconds.

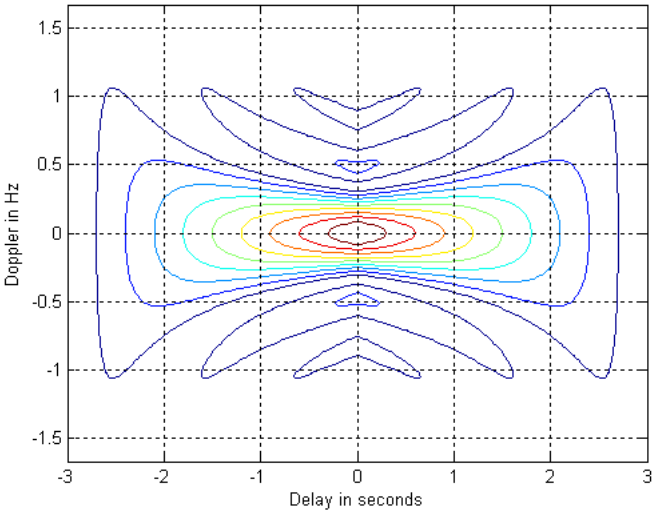

Figure 5.2b. Contour plot corresponding to Fig. 5.2a.

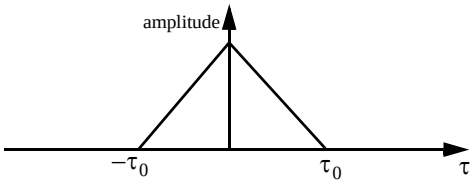

Figure 5.3. Zero Doppler ambiguity function cut along the time-delay axis.

The zero time cut along the Doppler frequency axis has a $(\sin x/x)^2$ shape. It extends from $-\infty$ to ∞. The first null occurs at $f_d = \pm 1/\tau_0$. Hence, it is possible to detect two targets that are shifted by $1/\tau_0$, without any ambiguity. Thus, a single pulse range and Doppler resolutions are limited by the pulse width τ_0. Fine range resolution requires that a very short pulse be used. Unfortunately, using very short pulses requires very large operating bandwidths and may limit the radar average transmitted power to impractical values.

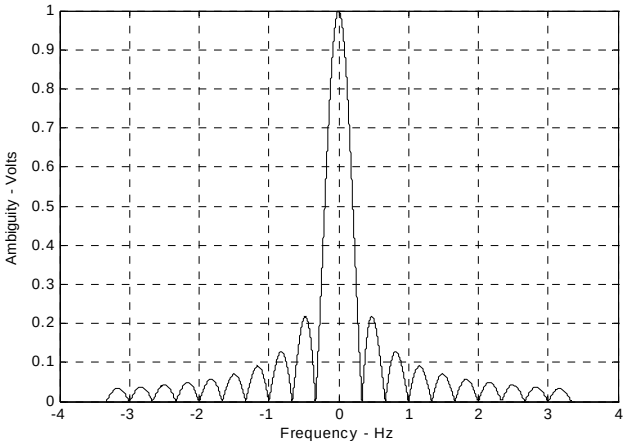

Figure 5.4. Ambiguity function of a single frequency pulse (zero delay). The pulse width is 3 seconds.

5.2.2. LFM Ambiguity Function

Consider the LFM complex envelope signal defined by

$$\tilde{x}(t) = \frac{1}{\sqrt{\tau_0}} Rect\left(\frac{t}{\tau_0}\right) e^{j\pi\mu t^2} \tag{5.16}$$

In order to compute the ambiguity function for the LFM complex envelope, we will first consider the case when $0 \le \tau \le \tau_0$. In this case the integration limits are from $-\tau_0/2$ to $(\tau_0/2) - \tau$. Substituting Eq. (5.16) into Eq. (5.1) yields

$$\chi(\tau; f_d) = \frac{1}{\tau_0} \int_{-\infty}^{\infty} Rect\left(\frac{t}{\tau_0}\right) Rect\left(\frac{t-\tau}{\tau_0}\right) e^{j\pi\mu t^2} e^{-j\pi\mu(t-\tau)^2} e^{j2\pi f_d t} dt \tag{5.17}$$

It follows that

$$\chi(\tau; f_d) = \frac{e^{-j\pi\mu\tau^2}}{\tau_0} \int_{\frac{-\tau_0}{2}}^{\frac{\tau_0}{2}-\tau} e^{j2\pi(\mu\tau + f_d)t} dt \tag{5.18}$$

Finishing the integration process in Eq. (5.18) yields

$$\chi(\tau;f_d) = e^{j\pi\tau f_d\left(1-\frac{\tau}{\tau_0}\right)}\frac{\sin\left(\pi\tau_0(\mu\tau+f_d)\left(1-\frac{\tau}{\tau_0}\right)\right)}{\pi\tau_0(\mu\tau+f_d)\left(1-\frac{\tau}{\tau_0}\right)} \qquad 0\le\tau\le\tau_0 \qquad \textbf{(5.19)}$$

Similar analysis for the case when $-\tau_0 \le \tau \le 0$ can be carried out, where, in this case, the integration limits are from $(-\tau_0/2)-\tau$ to $\tau_0/2$. The same result can be obtained by using the symmetry property of the ambiguity function ($|\chi(-\tau,-f_d)| = |\chi(\tau,f_d)|$). It follows that an expression for $\chi(\tau;f_d)$ that is valid for any τ is given by

$$\chi(\tau;f_d) = e^{j\pi\tau f_d\left(1-\frac{|\tau|}{\tau_0}\right)}\frac{\sin\left(\pi\tau_0(\mu\tau+f_d)\left(1-\frac{|\tau|}{\tau_0}\right)\right)}{\pi\tau_0(\mu\tau+f_d)\left(1-\frac{|\tau|}{\tau_0}\right)} \qquad |\tau|\le\tau_0 \qquad \textbf{(5.20)}$$

and the LFM ambiguity function is

$$|\chi(\tau;f_d)|^2 = \left|\left(1-\frac{|\tau|}{\tau_0}\right)\frac{\sin\left(\pi\tau_0(\mu\tau+f_d)\left(1-\frac{|\tau|}{\tau_0}\right)\right)}{\pi\tau_0(\mu\tau+f_d)\left(1-\frac{|\tau|}{\tau_0}\right)}\right|^2 \qquad |\tau|\le\tau_0 \qquad \textbf{(5.21)}$$

Again the time autocorrelation function is equal to $\chi(\tau,0)$. The reader can verify that the ambiguity function for a down-chirp LFM waveform is given by

$$|\chi(\tau;f_d)|^2 = \left|\left(1-\frac{|\tau|}{\tau_0}\right)\frac{\sin\left(\pi\tau_0(\mu\tau-f_d)\left(1-\frac{|\tau|}{\tau_0}\right)\right)}{\pi\tau_0(\mu\tau-f_d)\left(1-\frac{|\tau|}{\tau_0}\right)}\right|^2 \qquad |\tau|\le\tau_0 \qquad \textbf{(5.22)}$$

Incidentally, either Eq. (5.21) or (5.22) can be obtained from Eq. (5.13) by applying property 5 from Section 5.1. Figures 5.5 a and b show 3-D and contour plots for the LFM uncertainty and ambiguity functions for $\tau_0 = 1$ second and $B = 5Hz$ for a down-chirp pulse. This figure can be reproduced using the following MATLAB code.

```
% Use this program to reproduce Fig. 5.5 of text
close all;
clear all;
eps = 0.0001;
taup = 1.;
b = 5.;
up_down = -1.;
x = lfm_ambg(taup, b, up_down);
```

```
taux = linspace(-1.*taup,taup,size(x,1));
fdy = linspace(-1.5*b,1.5*b,size(x,1));
figure(1)
mesh(taux,fdy,sqrt(x))
xlabel ('Delay in seconds')
ylabel ('Doppler in Hz')
zlabel ('Ambiguity function')
axis tight
figure(2)
contour(taux,fdy,sqrt(x))
xlabel ('Delay in seconds')
ylabel ('Doppler in Hz')
grid
```

The up-chirp ambiguity function cut along the time delay axis τ is

$$|\chi(\tau;0)|^2 = \left| \left(1 - \frac{|\tau|}{\tau_0}\right) \frac{\sin\left(\pi\mu\tau\tau_0\left(1 - \frac{|\tau|}{\tau_0}\right)\right)}{\pi\mu\tau\tau_0\left(1 - \frac{|\tau|}{\tau_0}\right)} \right|^2 \qquad |\tau| \le \tau_0 \qquad \textbf{(5.23)}$$

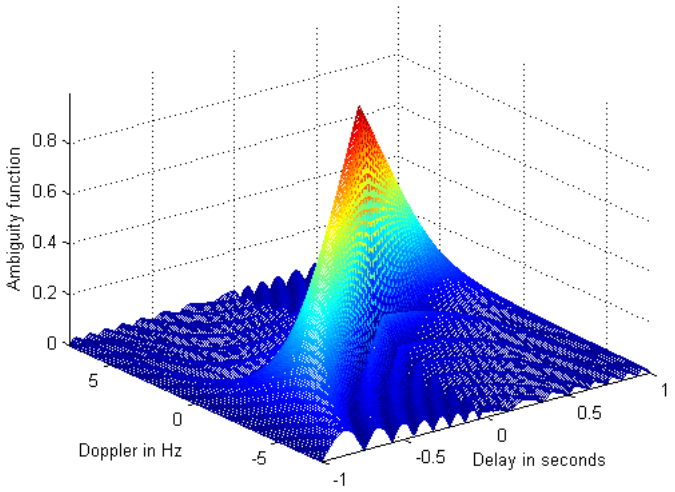

Figure 5.5a. Down-chirp LFM 3-D ambiguity plot. Pulse width is 1 second; and bandwidth is 5 Hz.

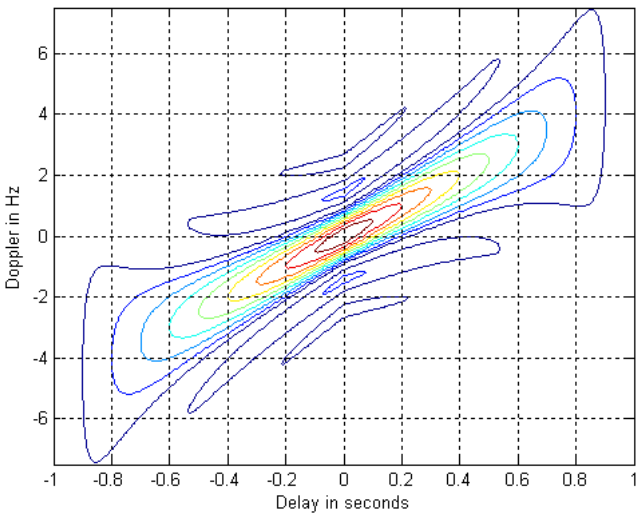

Figure 5.5b. Contour plot corresponding to Fig. 5.5a.

Note that the LFM ambiguity function cut along the Doppler frequency axis is similar to that of the single pulse. This should not be surprising since the pulse shape has not changed (only frequency modulation was added). However, the cut along the time-delay axis changes significantly. It is now much narrower compared to the unmodulated pulse cut. In this case, the first null occurs at

$$\tau_{n1} \approx 1/B \tag{5.24}$$

Figure 5.6 shows a plot for a cut in the uncertainty function corresponding to Eq. (5.23). This figure can be reproduced using the following MATLAB code

```
close all; clear all;
taup = 1;
b =20.;
up_down = 1.;
taux = -1.5*taup:.01:1.5*taup;
mu = up_down * b / 2. / taup;
ii = 0.;
for tau = -1.5*taup:.01:1.5*taup
  ii = ii + 1;
  val1 = 1. - abs(tau) / taup;
  val2 = pi * taup * (1.0 - abs(tau) / taup);
```

```
  val3 = (0 + mu * tau);
  val = val2 * val3;
  x(ii) = abs( val1 * (sin(val+eps)/(val+eps)));
end
figure(1)
plot(taux,10*log10(x+0.001))
grid
xlabel ('Delay in seconds')
ylabel ('Ambiguity in dB')
axis tight
```

Equation (5.24) indicates that the effective pulse width (compressed pulse width) of the matched filter output is completely determined by the radar bandwidth. It follows that the LFM ambiguity function cut along the time-delay axis is narrower than that of the unmodulated pulse by a factor

$$\xi = \frac{\tau_0}{(1/B)} = \tau_0 B \qquad \textbf{(5.25)}$$

ξ is referred to as the compression ratio (also called time-bandwidth product and compression gain). All three names can be used interchangeably to mean the same thing. As indicated by Eq. (5.25) the compression ratio also increases as the radar bandwidth is increased.

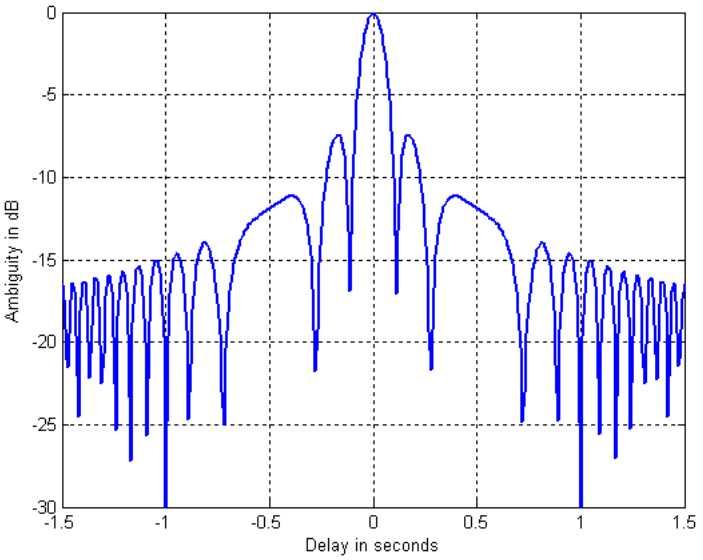

Figure 5.6. Zero Doppler ambiguity of an LFM pulse ($\tau_0 = 1$, $b = 20$).

Example:

Compute the range resolution before and after pulse compression corresponding to an LFM waveform with the following specifications: Bandwidth $B = 1GHz$ *and pulse width* $\tau_0 = 10ms$.

Solution:

The range resolution before pulse compression is

$$\Delta R_{uncomp} = \frac{c\tau_0}{2} = \frac{3\times 10^8 \times 10\times 10^{-3}}{2} = 1.5\times 10^6 \ \ meters$$

Using Eq. (5.23) yields

$$\tau_{n1} = \frac{1}{1\times 10^9} = 1 \ \ ns$$

$$\Delta R_{comp} = \frac{c\tau_{n1}}{2} = \frac{3\times 10^8 \times 1\times 10^{-9}}{2} = 15 \ \ cm$$

5.2.3. Coherent Pulse Train Ambiguity Function

Figure 5.7 shows a plot of a coherent pulse train. The pulse width is denoted as τ_0 and the PRI is T. The number of pulses in the train is N; hence, the train's length is $(N-1)T$ seconds. A normalized individual pulse $\tilde{x}(t)$ is defined by

$$\tilde{x}_1(t) = \frac{1}{\sqrt{\tau_0}} Rect\left(\frac{t}{\tau_0}\right) \qquad \textbf{(5.26)}$$

When coherency is maintained between the consecutive pulses, then an expression for the normalized train is

$$\tilde{x}(t) = \frac{1}{\sqrt{N}} \sum_{i=0}^{N-1} \tilde{x}_1(t - iT) \qquad \textbf{(5.27)}$$

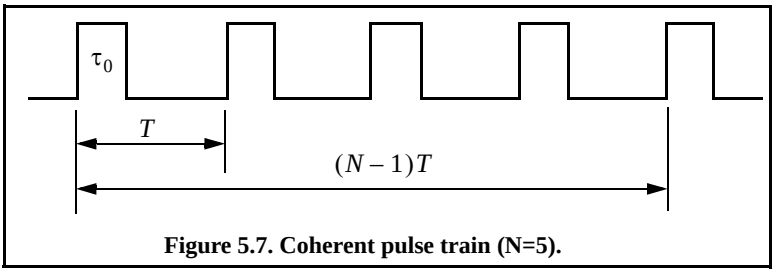

Figure 5.7. Coherent pulse train (N=5).

The output of the matched filter is

$$\chi(\tau;f_d) = \int_{-\infty}^{\infty} \tilde{x}(t)\tilde{x}^*(t-\tau)e^{j2\pi f_d t}dt \tag{5.28}$$

Substituting Eq. (5.27) into Eq. (5.28) and interchanging the summations and integration yield

$$\chi(\tau;f_d) = \frac{1}{N}\sum_{i=0}^{N-1}\sum_{j=0}^{N-1}\int_{-\infty}^{\infty} \tilde{x}_1(t-iT)\ \tilde{x}_1{}^*(t-jT-\tau)e^{j2\pi f_d t}dt \tag{5.29}$$

Making the change of variable $t_1 = t - iT$ yields

$$\chi(\tau;f_d) = \frac{1}{N}\sum_{i=0}^{N-1} e^{j2\pi f_d iT}\sum_{j=0}^{N-1}\int_{-\infty}^{\infty} \tilde{x}_1(t_1)\ \tilde{x}_1{}^*(t_1-[\tau-(i-j)T])e^{j2\pi f_d t_1}dt_1 \tag{5.30}$$

The integral inside Eq. (5.30) represents the output of the matched filter for a single pulse, and is denoted by χ_1. It follows that

$$\chi(\tau;f_d) = \frac{1}{N}\sum_{i=0}^{N-1} e^{j2\pi f_d iT}\sum_{j=0}^{N-1}\chi_1[\tau-(i-j)T;f_d] \tag{5.31}$$

When the relation $q = i - j$ is used, then the following relation is true:

$$\sum_{i=0}^{N}\sum_{m=0}^{N} = \sum_{q=-(N-1)}^{0}\sum_{i=0}^{N-1-|q|}\Bigg|_{for\ j=i-q} + \sum_{q=1}^{N-1}\sum_{j=0}^{N-1-|q|}\Bigg|_{for\ i=j+q} \tag{5.32}$$

Substituting Eq. (5.32) into Eq. (5.31) gives

$$\chi(\tau;f_d) = \frac{1}{N}\sum_{q=-(N-1)}^{0}\left\{\chi_1(\tau-qT;f_d)\sum_{i=0}^{N-1-|q|} e^{j2\pi f_d iT}\right\} \tag{5.33}$$

$$+\frac{1}{N}\sum_{q=1}^{N-1}\left\{e^{j2\pi f_d qT}\chi_1(\tau-qT;f_d)\sum_{j=0}^{N-1-|q|} e^{j2\pi f_d jT}\right\}$$

Setting $z = \exp(j2\pi f_d T)$, and using the relation

$$\sum_{j=0}^{N-1-|q|} z^j = \frac{1-z^{N-|q|}}{1-z} \tag{5.34}$$

yield

$$\sum_{i=0}^{N-1-|q|} e^{j2\pi f_d iT} = e^{[j\pi f_d(N-1-|q|T)]} \frac{\sin[\pi f_d(N-1-|q|)T]}{\sin(\pi f_d T)} \tag{5.35}$$

Using Eq. (5.35) in Eq. (5.31) yields two complementary sums for positive and negative q. Both sums can be combined as

$$\chi(\tau;f_d) = \frac{1}{N} \sum_{q=-(N-1)}^{N-1} \chi_1(\tau - qT;f_d) e^{[j\pi f_d(N-1+q)T]} \frac{\sin[\pi f_d(N-|q|)T]}{\sin(\pi f_d T)} \tag{5.36}$$

The second part of the right-hand side of Eq. (5.36) is the impact of the train on the ambiguity function; while the first part is primarily responsible for its shape details (according to the pulse type being used).

Finally, the ambiguity function associated with the coherent pulse train is computed as the modulus square of Eq. (5.36). For $\tau_0 < T/2$, the ambiguity function reduces to

$$|\chi(\tau;f_d)| = \frac{1}{N} \sum_{q=-(N-1)}^{N-1} |\chi_1(\tau - qT;f_d)| \left|\frac{\sin[\pi f_d(N-|q|)T]}{\sin(\pi f_d T)}\right| \quad ;|\tau| \le NT \tag{5.37}$$

Within the region $|\tau| \le \tau_0 \Rightarrow q = 0$, Eq. (5.37) can be written as

$$|\chi(\tau;f_d)| = |\chi_1(\tau;f_d)| \left|\frac{\sin[\pi f_d NT]}{N\sin(\pi f_d T)}\right| \quad ;|\tau| \le \tau_0 \tag{5.38}$$

Thus, the ambiguity function for a coherent pulse train is the superposition of the individual pulse's ambiguity functions. The ambiguity function cuts along the time delay and Doppler axes are, respectively, given by

$$|\chi(\tau;0)|^2 = \left| \sum_{q=-(N-1)}^{N-1} \left(1 - \frac{|q|}{N}\right)\left(1 - \frac{|\tau - q|T}{\tau_0}\right) \right|^2 ; \ |\tau - qT| < \tau_0 \tag{5.39}$$

$$|\chi(0;f_d)|^2 = \left|\frac{1}{N}\frac{\sin(\pi f_d \tau_0)}{\pi f_d \tau_0} \frac{\sin(\pi f_d NT)}{\sin(\pi f_d T)}\right|^2 \tag{5.40}$$

Figures 5.8a and 5.8b show the 3-D ambiguity plot and the corresponding contour plot for $N = 5$, $\tau_0 = 0.4$, and $T = 1$. This plot can be reproduced using the following MATLAB code.

```
clear all; close all;
taup = 0.4; pri = 1; n = 5;
x = train_ambg(taup, n, pri);
figure(1)
time = linspace(-(n-1)*pri-taup, n*pri-taup, size(x,2));
doppler = linspace(-1/taup, 1/taup, size(x,1));
surf(time, doppler, x); %mesh(time, doppler, x);
xlabel('Delay in seconds');  ylabel('Doppler in Hz');
zlabel('Ambiguity function'); axis tight;
figure(2)
contour(time, doppler, (x)); % surf(time, doppler, x);
xlabel('Delay in seconds');  ylabel('Doppler in Hz'); grid; axis tight;
```

Figures 5.8c and 5.8d, respectively shows sketches of the zero Doppler and zero delay cuts in the ambiguity function. The ambiguity function peaks along the frequency axis are located at multiple integers of the frequency $f = 1/T$. Alternatively, the peaks are at multiple integers of T along the delay axis. Width of the ambiguity function peaks along the delay axis is $2\tau_0$. The peak width along the Doppler axis is $1/(N-1)T$.

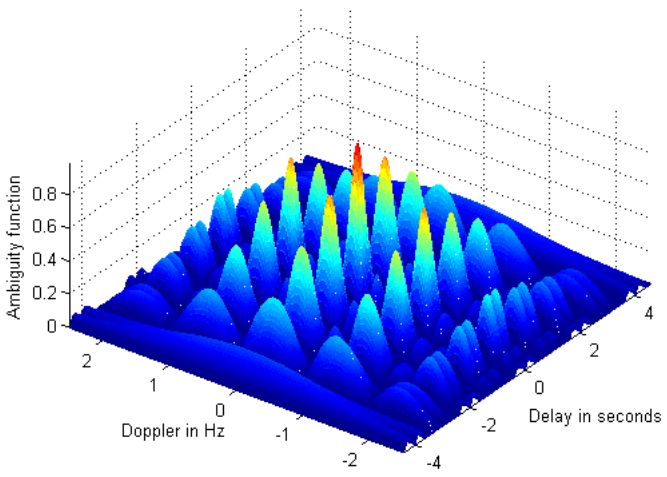

Figure 5.8a. Three-dimensional ambiguity plot for a five-pulse equal amplitude coherent train. Pulse width is 0.4 seconds; and PRI is 1 second, N=5.

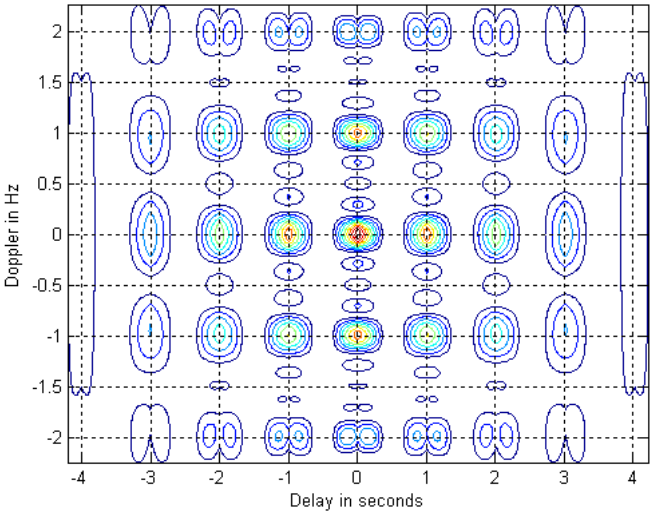

Figure 5.8b. Contour plot corresponding to Fig. 5.8a.

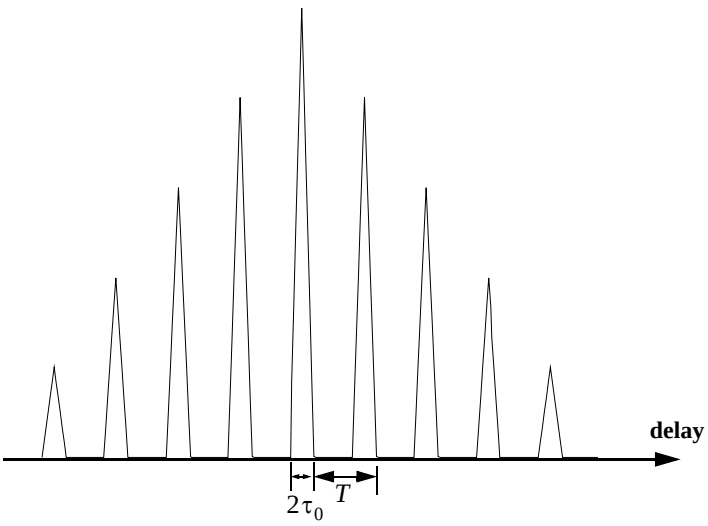

Figure 5.8c. Zero Doppler cut corresponding to Fig. 5.8a.

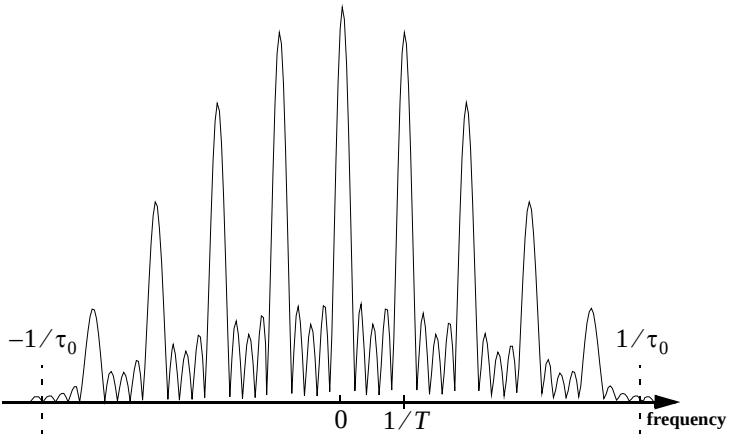

Figure 5.8d. Zero delay cut corresponding to Fig. 5.8a.

5.2.4. Pulse Train Ambiguity Function with LFM

In this case, the signal is as given in the previous section except for the LFM modulation within each pulse. This is illustrated in Fig. 5.9. Again let the pulse width be denoted by τ_0 and the PRI by T. The number of pulses in the train is N; hence, the train's length is $(N-1)T$ seconds. A normalized individual pulse $\tilde{x}_1(t)$ is defined by

$$\tilde{x}_1(t) = \frac{1}{\sqrt{\tau_0}} Rect\left(\frac{t}{\tau_0}\right) e^{j\pi\frac{B}{\tau_0}t^2} \qquad \textbf{(5.41)}$$

where B is the LFM bandwidth.

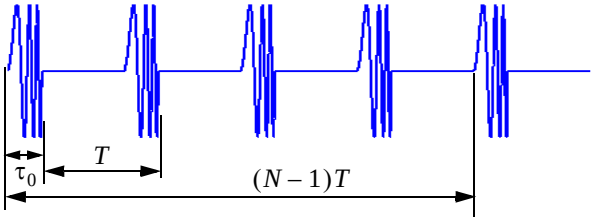

Figure 5.9. LFM pulse train (N=5).

The signal is now given by

$$\tilde{x}(t) = \frac{1}{\sqrt{N}} \sum_{i=0}^{N-1} \tilde{x}_1(t - iT) \tag{5.42}$$

Utilizing property 5 of Section 5.1 and Eq. (5.37) yields the following ambiguity function

$$\left|\chi(\tau; f_d)\right| = \sum_{q=-(N-1)}^{N-1} \left|\chi_1\left(\tau - qT; f_d + \frac{B}{\tau_0}\tau\right)\right| \left|\frac{\sin[\pi f_d (N - |q|)T]}{N \sin(\pi f_d T)}\right| \quad ; |\tau| \le NT \tag{5.43}$$

where χ_1 is the ambiguity function of the single pulse. Note that the shape of the ambiguity function is unchanged from the case of unmodulated train along the delay axis. This should be expected since only a phase modulation has been added which will impact the shape only along the frequency axis.

Figures 5.10 a and b show the ambiguity plot and its associated contour plot for the same example listed in the previous section except, in this case, LFM modulation is added and $N = 3$ pulses. This figure can be reproduced using the following MATLAB code.

```
% figure 5.10
clear all; close all;
taup = 0.4;
pri = 1;
n = 3;
bw = 10;
x = train_ambg_lfm(taup, n, pri, bw);
figure(1)
time = linspace(-(n-1)*pri-taup, n*pri-taup, size(x,2));
doppler = linspace(-bw,bw, size(x,1));
%mesh(time, doppler, x);
surf(time, doppler, x); shading interp;
xlabel('Delay in seconds');
ylabel('Doppler in Hz');
zlabel('Ambiguity function');
axis tight;
title('LFM pulse train, B\tau = 40, N = 3 pulses')
figure(2)
contour(time, doppler, (x));
%surf(time, doppler, x); shading interp; view(0,90);
xlabel('Delay in seconds');
ylabel('Doppler in Hz');
grid; axis tight;
title('LFM pulse train, B\tau = 40, N = 3 pulses')
```

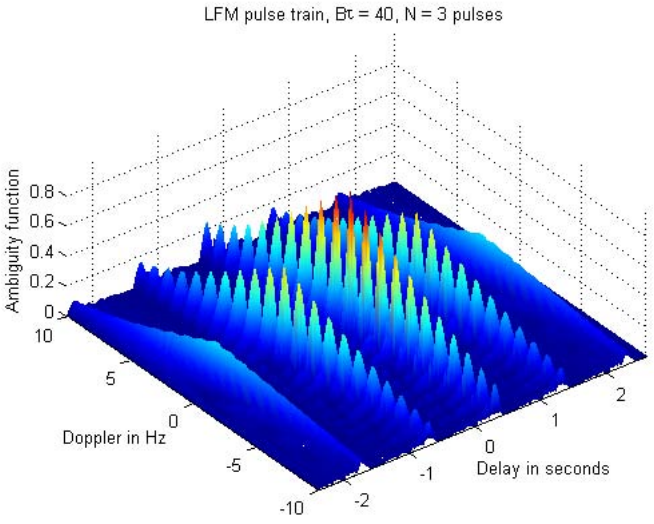

Figure 5.10a. Three-dimensional ambiguity plot for an LFM pulse train.

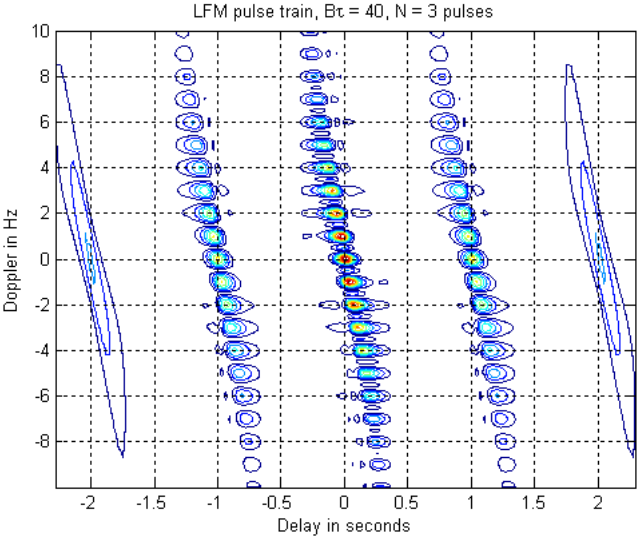

Figure 5.10b. Contour plot corresponding to Fig. 5.10a.

Understanding the difference between the ambiguity diagrams for a coherent pulse train and an LFM pulse train can be done with the help of Fig. 5.11a and Fig. 5.11b. In both figures a train of three pulses is used; in both cases the pulse width is $\tau_0 = 0.4\,sec$ and the period is $T = 1\,sec$. In the case, of LFM pulse train each pulse has LFM modulation with $B\tau_0 = 20$. Locations of the ambiguity peaks along the delay and Doppler axes are the same in both cases. This is true because peaks along the delay axis are T seconds apart and peaks along the Doppler axis are $1/T$ apart; in both cases T is unchanged. Additionally, the width of the ambiguity peaks along the Doppler axis are also the same in both cases, because this value depends only on the pulse train length which is the same in both cases (i.e., $(N-1)T$).

Width of the ambiguity peaks along the delay axis are significantly different, however. In the case of coherent pulse train, this width is approximately equal to twice the pulse width. Alternatively, this value is much smaller in the case of the LFM pulse train. The ratio between the two values is as given in Eq. (5.25). This clearly leads to the expected conclusion that the addition of LFM modulation significantly enhances the range resolution. Finally, the presence of the LFM modulation introduces a slope change in the ambiguity diagram; again a result that is also expected.

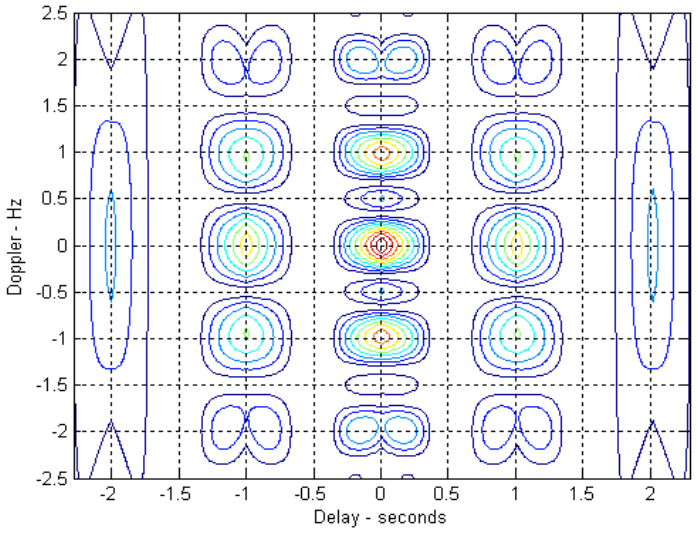

Figure 5.11a. Contour plot for the ambiguity function of a coherent pulse train. $N = 3; \tau_0 = 0.4;\ T = 1$

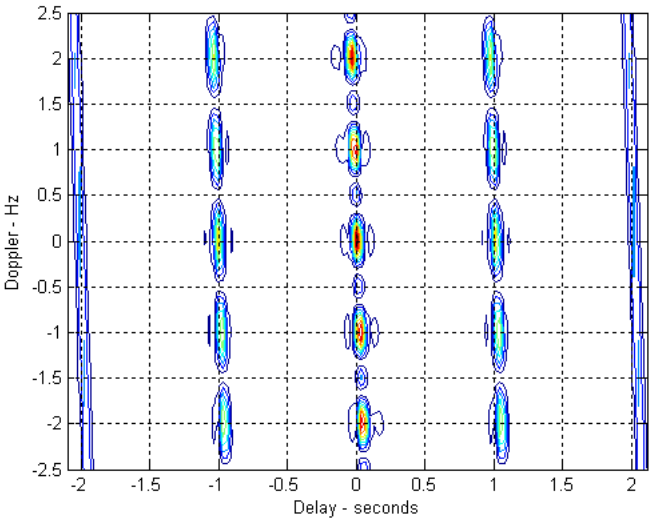

Figure 5.11b. Contour plot for the ambiguity function of a coherent pulse train. $N = 3;\ B\tau_0 = 20;\ T = 1$

5.3. Stepped Frequency Waveforms

Stepped Frequency Waveforms (SFW) is a class of radar waveforms that are used in extremely wide bandwidth applications where very large time bandwidth product (or compression ratio as defined in Eq. (5.25)) is required. One may think of SFW as a special case of an extremely wide bandwidth LFM waveform. For this purpose, consider an LFM signal whose bandwidth is B_i and whose pulsewidth is T_i and refer to it as the primary LFM. Divide this long pulse into N subpulses each of width τ_0 to generate a sequence of pulses whose PRI is denoted by T. It follows that $T_i = (n-1)T$. One reason SFW is favored over an extremely wideband LFM is that it may be very difficult to maintain the LFM slope when the time bandwidth product is large. By using SFW, the same equivalent bandwidth can be achieved; however, phase errors are minimized since the LFM is chirped over a much shorter duration.

Define the beginning frequency for each subpulse as that value measured from the primary LFM at the leading edge of each subpulse, as illustrated in Fig. 5.12. That is

$$f_i = f_0 + i\Delta f;\ \ i = 0, N-1 \qquad \textbf{(5.44)}$$

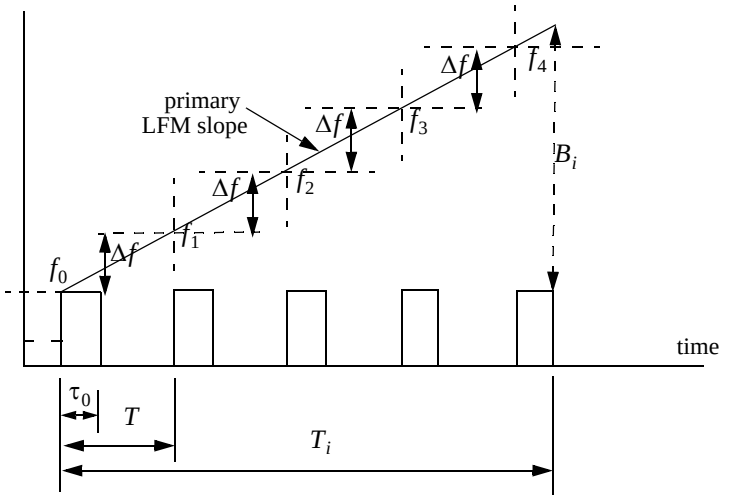

Figure 5.12. Example of stepped frequency waveform burst; $N = 5$.

where Δf is the frequency step from one subpulse to another. The set of n subpulses is often referred to as a burst. Each subpulse can have its own LFM modulation. To this end, assume that the subpulse LFM modulation corresponds to an LFM slope of $\mu = B/\tau_0$.

The complex envelope of a single subpluse with LFM modulation is

$$\tilde{x}_1 = \frac{1}{\sqrt{\tau_0}} Rect\left(\frac{t}{\tau_0}\right) e^{j\pi\mu t^2} \tag{5.45}$$

Of course if the subpulses do not have any LFM modulation, then the same equation holds true by setting $\mu = 0$. The overall complex envelope of the whole burst is

$$\tilde{x}(t) = \frac{1}{\sqrt{N}} \sum_{i=0}^{N-1} \tilde{x}_1(t - iT) \tag{5.46}$$

The ambiguity function of the matched filter corresponding to Eq. (5.46) can be obtained from that of the coherent pulse train developed in Section 5.2.3 along with property 5 of the ambiguity function. The details are fairly straightforward and are left to the reader as an exercise. The result is (see Problem 5.2)

$$|\chi(\tau;f_d)| = \sum_{q=-(N-1)}^{N-1} \left|\chi_1\left(\tau - qT;\left(f_d + \frac{B}{\tau_0}\tau\right)\right)\right| \times \left|\frac{\sin\left[\pi\left(f_d + \frac{\Delta f}{T}\tau\right)(N-|q|)T\right]}{N\sin\left(\pi\left(f_d + \frac{\Delta f}{T}\tau\right)T\right)}\right| \quad ;|\tau| \le NT \tag{5.47}$$

where χ_1 is the ambiguity function of the single pulse. Unlike the case in Eq. (5.43), the second part of the right-hand side of Eq. (5.47) is now modified according to property 5 of Section 5.1. This is true since each subpulse has its own beginning frequency derived from the primary LFM slope.

5.4. Nonlinear FM

As clearly shown by Fig. 5.6 the output of the matched filter corresponding to an LFM pulse has sidelobe levels similar to those of the $\sin(x)/x$ signal, that is, 13.4 dB below the main beam peak. In many radar applications, these sidelobe levels are considered too high and may present serious problems for detection particularly in the presence of nearby interfering targets or other noise sources. Therefore, in most radar applications, sidelobe reduction of the output of the matched filter is always required. This sidelobe reduction can be accomplished using windowing techniques as described in Chapter 2. However, windowing techniques reduce the sidelobe levels at the expense of reducing of the SNR and widening the main beam (i.e., loss of resolution) which are considered to be undesirable features in many radar applications.

These effects can be mitigated by using non-linear FM (NLFM) instead of LFM waveforms. In this case, the LFM waveform spectrum is shaped according to a specific predetermined frequency function. Effectively, in NLFM, the rate of change of the LFM waveform phase is varied so that less time is spent on the edges of the bandwidth, as illustrated in Fig. 5.13. The concept of NLFM can be better analyzed and understood in the context of the stationary phase.

5.4.1. The Concept of Stationary Phase

Consider the following bandpass signal

$$x(t) = x_I(t)\cos(2\pi f_0 t + \phi(t)) - x_Q(t)\sin(2\pi f_0 t + \phi(t)) \tag{5.48}$$

where $\phi(t)$ is the frequency modulation. The corresponding analytic signal (pre-envelope) is

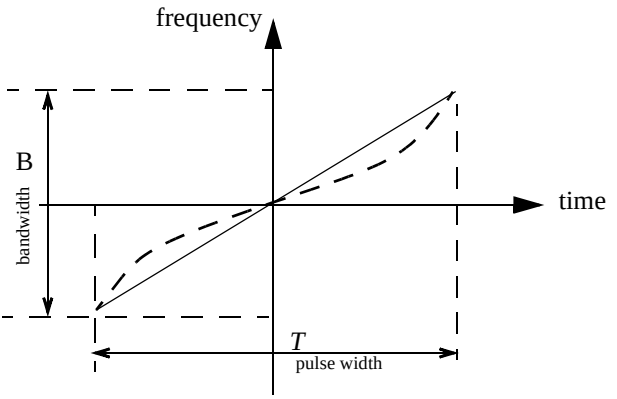

Figure 5.13. A cartoon showing frequency versus time for an LFM waveform (solid line) and a NLFM (dashed line).

$$\psi(t) = \tilde{x}(t)e^{j2\pi f_0 t} = r(t)e^{j\phi(t)}e^{j2\pi f_0 t} \tag{5.49}$$

where $\tilde{x}(t)$ is the complex envelope and is given by

$$\tilde{x}(t) = r(t)e^{j\phi(t)} \tag{5.50}$$

The lowpass signal $r(t)$ represents the envelope of the transmitted signal; it is given by

$$r(t) = \sqrt{x_I^2(t) + x_Q^2(t)} \tag{5.51}$$

It follows that the FT of the signal $\tilde{x}(t)$ can then be written as

$$X(\omega) = \int_{-\infty}^{\infty} r(t)e^{j(-\omega t + \phi(t))}\, dt \tag{5.52}$$

$$X(\omega) = |X(\omega)|e^{j\Phi(\omega)} \tag{5.53}$$

where $|X(\omega)|$ is the modulus of the FT and $\Phi(\omega)$ is the corresponding phase frequency response. It is clear that the integrand is an oscillating function of time varying at a rate

$$\frac{d}{dt}[\omega t - \phi(t)] \tag{5.54}$$

Most contribution to the FT spectrum occurs when this rate of change is minimal. More specifically, it occurs when

$$\frac{d}{dt}[\omega t - \phi(t)] = 0 \Rightarrow \omega - \phi'(t) = 0 \tag{5.55}$$

The expression in Eq. (5.55) is parametric since it relates two independent variables. Thus, for each value ω_n there is only one specific $\phi'(t_n)$ that satisfies Eq. (5.55). Thus, the time when this phase term is stationary will be different for different values of ω_n. Expanding the phase term in Eq. (5.55) about an incremental value t_n using Taylor series expansion yields

$$\omega_n t - \phi(t) = \omega_n t_n - \phi(t_n) + (\omega_n - \phi'(t_n))(t - t_n) - \frac{\phi''(t_n)}{2!}(t - t_n)^2 + \ldots \tag{5.56}$$

An acceptable approximation of Eq. (5.56) is obtained by using the first three terms, provided that the difference $(t - t_n)$ is very small. Now, using the right-hand side of Eq. (5.55) into Eq. (5.56) and terminating the expansion to the first three terms yield

$$\omega_n t - \phi(t) = \omega_n t_n - \phi(t_n) - \frac{\phi''(t_n)}{2!}(t - t_n)^2 \tag{5.57}$$

By substituting Eq. (5.57) into Eq. (5.52) and using the fact that $r(t)$ is relatively constant (slow varying) when compared to the rate at which the carrier signal is varying, gives

$$X(\omega_n) = r(t_n) \int_{t_n^-}^{t_n^+} e^{-j\left(\omega_n t_n - \phi(t_n) - \frac{\phi''(t_n)}{2}(t - t_n)^2\right)} \, dt \tag{5.58}$$

where t_n^+ and t_n^- represent infinitesimal changes about t_n. Equation (5.58) can be written as

$$X(\omega_n) = r(t_n) e^{j(-\omega_n t_n - \phi(t_n))} \int_{t_n^-}^{t_n^+} e^{j\left(\frac{\phi''(t_n)}{2}(t - t_n)^2\right)} \, dt \tag{5.59}$$

Consider the changes of variables

$$t - t_n = \lambda \Rightarrow dt = d\lambda \tag{5.60}$$

$$\sqrt{\phi''(t_n)}\lambda = \sqrt{\pi}\, y \Rightarrow d\lambda = \frac{\sqrt{\pi}}{\sqrt{\phi''(t_n)}} dy \tag{5.61}$$

Using these changes of variables leads to

$$X(\omega_n) = \frac{2\sqrt{\pi}\ r(t_n)}{\sqrt{\phi''(t_n)}} e^{j(-\omega_n t_n - \phi(t_n))} \int_0^{y_0} e^{j\left(\frac{\pi y^2}{2}\right)}\ dy \tag{5.62}$$

where

$$y_0 = \sqrt{\frac{|\phi''(t_n)|}{\pi}} \tag{5.63}$$

The integral in Eq. (5.62) is that of the form of a Fresnel integral, which has an upper limit approximated by

$$\frac{\exp\left(j\frac{\pi}{4}\right)}{\sqrt{2}} \tag{5.64}$$

Substituting Eq. (5.64) into Eq. (5.62) yields

$$X(\omega_n) = \frac{\sqrt{2\pi}\ r(t_n)}{\sqrt{\phi''(t_n)}} e^{j\left(-\omega_n t_n - \phi(t_n) + \frac{\pi}{4}\right)} \tag{5.65}$$

Thus, for all possible values of ω

$$|X(\omega_t)|^2 \approx 2\pi \frac{r^2(t)}{|\phi''(t)|} \Rightarrow |X(\omega)| = \frac{\sqrt{2\pi}}{\sqrt{|\phi''(t)|}}\ r(t) \tag{5.66}$$

The subscript t was used to indicate the dependency of ω on time.

Using a similar approach that led to Eq. (5.66), an expression for $\tilde{x}(t_n)$ can be obtained. From Eq. (5.53), the signal $\tilde{x}(t)$

$$\tilde{x}(t) = \frac{1}{2\pi} \int_{-\infty}^{\infty} |X(\omega)|\ e^{j(\Phi(\omega) + \omega t)}\ d\omega \tag{5.67}$$

The phase term $\Phi(\omega)$ is (using Eq. (5.65))

$$\Phi(\omega) = -\omega t - \phi(t) + \frac{\pi}{4} \tag{5.68}$$

Differentiating with respect to ω yields

$$\frac{d}{d\omega}\Phi(\omega) = -t - \left(\frac{dt}{d\omega}\right)\left[\omega - \frac{d}{dt}\phi(t)\right] = \Phi'(\omega) \tag{5.69}$$

Using the stationary phase relation in Eq. (5.55) (i.e., $\omega - \phi'(t) = 0$) yields

$$\Phi'(\omega) = -t \tag{5.70}$$

and

$$\Phi''(\omega) = -\frac{dt}{d\omega} \tag{5.71}$$

Define the signal group time delay function as

$$T_g(\omega) = -\Phi'(\omega) \tag{5.72}$$

then the signal instantaneous frequency is the inverse of the $T_g(\omega)$. Figure 5.14 shows a drawing illustrating this inverse relationship between the NLFM frequency modulation and the corresponding group time delay function.

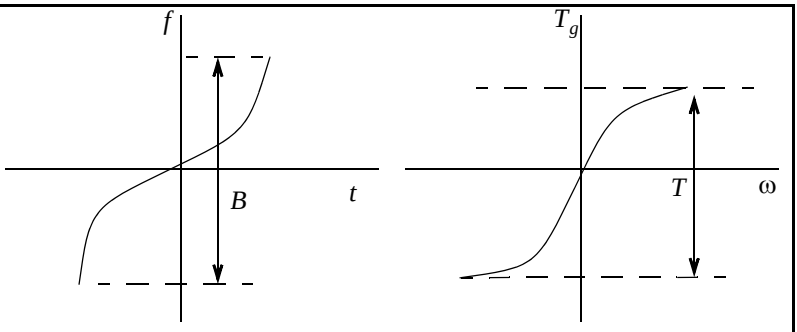

Figure 5.14. Matched filter time delay and frequency modulation for a NLFM waveform.

Comparison of Eq. (5.67) and Eq. (5.52) indicates that both equation have similar form. Thus, if one substitutes $X(\omega)/2\pi$ for $r(t)$, $\Phi(\omega)$ for $\phi(t)$, ω for t, and $-t$ for ω in Eq. (5.52), a similar expression to that in Eq. (5.65) can be derived. That is,

$$\left|\tilde{x}(t_\omega)\right|^2 \approx \frac{1}{2\pi}\frac{\left|X(\omega)\right|^2}{\left|\Phi''(\omega)\right|} \tag{5.73}$$

the subscript ω was used to indicate the dependency of t on frequency. However, from Eq. (5.60)

$$\left|\tilde{x}(t)\right|^2 = \left|r(t)e^{j\phi(t)}\right|^2 = r^2(t) \tag{5.74}$$

It follows that Eq. (5.73) can be rewritten as

$$r^2(t_\omega) \approx \frac{1}{2\pi}\frac{|X(\omega)|^2}{|\Phi''(\omega)|} \Rightarrow r(t) = \frac{|X(\omega)|}{\sqrt{2\pi|\Phi''(\omega)|}} \tag{5.75}$$

substituting Eq. (5.71) into Eq. (5.75) yields a general relationship for any t

$$r^2(t)\ dt = \frac{1}{2\pi}|X(\omega)|^2 d\omega \tag{5.76}$$

Clearly, the functions $r(t)$, $\phi(t)$, $X(\omega)$, and $\Phi(\omega)$ are related to each other as Fourier transform pairs, as given by

$$r(t)e^{j\phi(t)} = \frac{1}{2\pi}\int_{-\infty}^{\infty} |X(\omega)|\ e^{j(\Phi(\omega)+\omega t)}\ d\omega \tag{5.77}$$

$$|X(\omega)|\ e^{j\Phi(\omega)} = \int_{-\infty}^{\infty} r(t)\ e^{-j(\omega t-\phi(t))}\ d\omega \tag{5.78}$$

They are also related using the Parseval's theorem by

$$\int_{-\infty}^{t} r^2(\zeta)\ d\zeta = \frac{1}{2\pi}\int_{\omega}^{\infty}|X(\lambda)|^2\ d\lambda \tag{5.79}$$

or

$$\int_{-\infty}^{t} r^2(\zeta)\ d\zeta = \frac{1}{2\pi}\int_{-\infty}^{\omega}|X(\lambda)|^2\ d\lambda \tag{5.80}$$

The formula for the output of the matched filter was derived earlier and is repeated here as Eq. (5.81)

$$\chi(\tau, f_d) = \int_{-\infty}^{\infty} \tilde{x}(t)\tilde{x}^*(t-\tau)e^{j2\pi f_d t}dt \tag{5.81}$$

Substituting the right-hand side of Eq. (5.50) into Eq. (5.89) yields

$$\chi(\tau, f_d) = \int_{-\infty}^{\infty} r(t)r^*(t-\tau)e^{j2\pi f_d t}dt \tag{5.82}$$

It follows that the zero Doppler and zero delay cuts of the ambiguity function can be written as

$$\chi(\tau, 0) = \frac{1}{2\pi}\int_{-\infty}^{\infty} |X(\omega)|^2 \; e^{j\omega\tau} d\omega \tag{5.83}$$

$$\chi(0, f_d) = \int_{-\infty}^{\infty} |r(t)|^2 \; e^{j2\pi f_d t} dt \tag{5.84}$$

These two equations, imply that the shape of the ambiguity function cuts are controlled by selecting different functions X and r (related as defined in Eq. (5.76)). In other words, the ambiguity function main beam and its delay axis sidelobes can be controlled (shaped) by the specific choices of these two functions; and hence, the term *spectrum shaping* is used. Using this concept of spectrum shaping, one can control the frequency modulation of an LFM (see Fig. 5.13) to produce an ambiguity function with the desired sidelobe levels.

5.4.2. Frequency Modulated Waveform Spectrum Shaping

One class of FM waveforms which takes advantage of the stationary phase principles to control (shape) the spectrum is

$$|X(\omega;n)|^2 = \left(\cos\pi\left(\frac{\pi\omega}{B_n}\right)\right)^n \quad ; \; |\omega| \le \frac{B_n}{2} \tag{5.85}$$

where the value n is an integer greater than zero. It can be easily shown using direct integration and by utilizing Eq. (5.85) that

$$n = 1 \Rightarrow T_{g1}(\omega) = \frac{T}{2}\sin\left(\frac{\pi\omega}{B_1}\right) \tag{5.86}$$

$$n = 2 \Rightarrow T_{g2}(\omega) = T\left[\frac{\omega}{B_2} + \frac{1}{2\pi}\sin\left(\frac{2\pi\omega}{B_2}\right)\right] \tag{5.87}$$

$$n = 3 \Rightarrow T_{g3}(\omega) = \frac{T}{4}\left\{\sin\left(\frac{\pi\omega}{B_3}\right)\left[\left(\cos\frac{\pi\omega}{B_3}\right)^2 + 2\right]\right\} \tag{5.88}$$

$$n = 4 \Rightarrow T_{g4}(\omega) = T\left\{\frac{\omega}{B_4} + \frac{1}{2\pi}\sin\frac{2\pi\omega}{B_4} + \frac{2}{3\pi}\left(\cos\frac{\pi\omega}{B_4}\right)^3 \sin\frac{\pi\omega}{B_4}\right\} \tag{5.89}$$

Figure 5.15 shows a plot for Eq. (5.86) through Eq. (5.89). These plots assume $T = 1$ and the x-axis is normalized, with respect to B. This figure can be reproduced using the following MATLAB code:

```
% Figure 5.15
clear all; close all;
delw = linspace(-.5,.5,75);
T1 = .5 .* sin(pi.*delw);
T2 = delw + (1/2/pi) .* sin(2*pi.*delw);
T3 = .25 .* (sin(pi.*delw)) .* ((cos(pi.*delw)).^2 + 2);
T4 = delw + (1/2/pi) .* sin(2*pi.*delw) + (2/3/pi) .* (cos(pi.*delw)).^3 .* sin(delw);
figure (1)
plot(delw,T1,'k*',delw,T2,'k:',delw,T3,'k.',delw,T4,'k');
grid
ylabel('Group delay function'); xlabel('\omega/B')
legend('n=1','n=2','n=3','n=4')
```

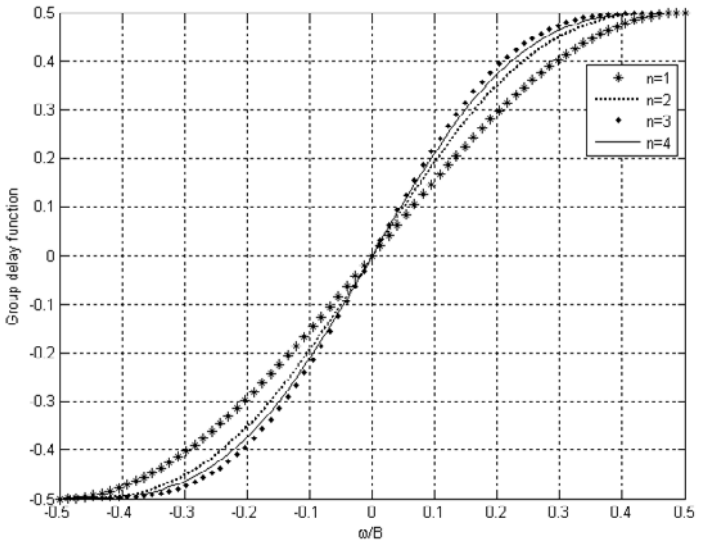

Figure 5.15. Group time delay of Eq. (5.85).

The Doppler mismatch (i.e, a peak of the ambiguity function at a delay value other than zero) is proportional to the amount of Doppler frequency f_d. Hence, an error in measuring target range is always expected when LFM waveforms are used. To achieve sidelobe levels for the output of the matched filter that do not exceed a predetermined level use this class of NLFM waveforms

$$|X(\omega;n;k)|^2 = k + (1-k)\left(\cos\pi\left(\frac{\pi\omega}{B_n}\right)\right)^n \qquad ;|\omega| \le \frac{B_n}{2} \tag{5.90}$$

For example, using the combination $n = 2$, $k = 0.08$ yields sidelobe levels less than $-40dB$.

5.5. Ambiguity Diagram Contours

Plots of the ambiguity function are called ambiguity diagrams. For a given waveform, the corresponding ambiguity diagram is normally used to determine the waveform properties such as the target resolution capability, measurements (time and frequency) accuracy, and its response to clutter. The ambiguity diagram contours are cuts in the 3-D ambiguity plot at some value, Q, such that $Q < |\chi(0, 0)|^2$. The resulting plots are ellipses (see Problem 5.11). The width of a given ellipse along the delay axis is proportional to the signal effective duration, τ_e, defined in Chapter 2. Alternatively, the width of an ellipse along the Doppler axis is proportional to the signal effective bandwidth, B_e.

Figure 5.16 shows a sketch of typical ambiguity contour plots associated with a single unmodulated pulse. As illustrated in Fig. 5.16, narrow pulses provide better range accuracy than long pulses. Alternatively, the Doppler accuracy is better for a wider pulse than it is for a short one. This trade-off between range and Doppler measurements comes from the uncertainty associated with the time-bandwidth product of a single sinusoidal pulse, where the product of uncertainty in time (range) and uncertainty in frequency (Doppler) cannot be much smaller than unity (see Problem 5.12). Figure 5.17 shows the ambiguity contour plot associated with an LFM waveform. The slope is an indication of the LFM modulation. The values σ_τ, σ_{f_d}, $\sigma_{\tau RDC}$, and $\sigma_{f_d RDC}$ were derived in Chapter 4 and were, respectively given in Eq. (4.107), Eq. (4.111), Eq. (4.136), and Eq. (4.137).

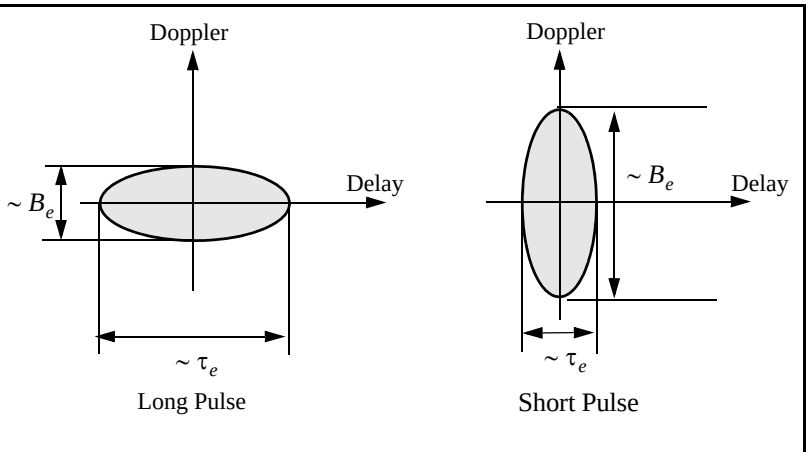

Figure 5.16. Ambiguity contour plot associated with a sinusoid modulated gated CW pulse.

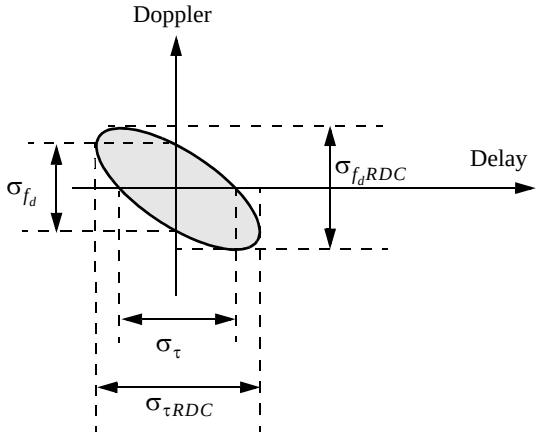

Figure 5.17. Ambiguity contour plot for an up-chirp LFM waveform.

5.6. Interpretation of Range-Doppler Coupling in LFM Signals

An expression of the range-Doppler for LFM signals was derived in Chapter 4. Range-Doppler coupling affects the radar's ability to compute target range and Doppler estimates. An interpretation of this term in the context of the ambiguity function can be explained further with the help of Eq. (5.20). Observation of this equation indicates that ambiguity function for the LFM pulse has a peak value not at $\tau = 0$ but rather at

$$(B/\tau_0)\tau - f_d = 0 \Rightarrow \tau = f_d - \tau_0/B \qquad \textbf{(5.91)}$$

This Doppler mismatch (i.e, a peak of the ambiguity function at a delay value other than zero) is proportional to the amount of Doppler frequency f_d. Hence, an error in measuring target range is always expected when LFM waveforms are used.

Most radar systems using LFM waveforms will correct for the effect of range-Doppler coupling by repeating the measurement with an LFM waveform of the opposite slope and averaging the two measurements. This way, the range measurement error is negated and the true target range is extracted from the averaged value. However, some radar systems, particularly those used for long range surveillance applications, may actually take advantage of range-Doppler coupling effect; and here is how it works: Typically radars during the search mode utilize very wide range bins which may contain many targets with differ-

ent distinct Doppler frequencies. It follows that the output of the matched filter has several targets that have equal delay but different Doppler mismatches.

All targets with Doppler mismatches greater than $1/\tau_0$ are significantly attenuated by the ambiguity function (because of the sharp decaying slope of the ambiguity function along the Doppler axis) and thus will most likely go undetected along the Doppler axis. The combined target complex within that range bin is then detected by the LFM as if all targets had Doppler mismatch corresponding to the target whose Doppler mismatch is less or equal to $1/\tau_0$. Thus, all targets within that wide range bin are detected as one narrowband target. Because of this range-Doppler coupling LFM waveforms are often referred to as Doppler intolerant (insensitive) waveforms.

5.7. MATLAB Programs and Functions

This section presents listings for all the MATLAB programs used to produce all of the MATLAB-generated figures in this chapter. They are listed in the same order in which they appear in the text.

5.7.1. Single Pulse Ambiguity Function

The MATLAB function *"single_pulse_ambg.m"* implements Eq. (5.11). The syntax is as follows:

single_pulse_ambg [taup]

taup is the pulse width.

MATLAB Function** "single_pulse_ambg.m" **Listing

```
function [x] = single_pulse_ambg (taup)
eps = 0.000001;
i = 0;
del = 2*taup/150;
for tau = -taup:del:taup
  i = i + 1;
  j = 0;
  fd = linspace(-5/taup,5/taup,151);
  val1 = 1. - abs(tau) / taup;
  val2 = pi * taup .* (1.0 - abs(tau) / taup) .* fd;
  x(:,i) = abs( val1 .* sin(val2+eps)./(val2+eps));
end
```

5.7.2. LFM Ambiguity Function

The function *"lfm_ambg.m"* implements Eq. (5.20). The syntax is as follows:

lfm_ambg [taup, b, up_down]

where

Symbol	Description	Units	Status
taup	*pulse width*	*seconds*	*input*
b	*bandwidth*	*Hz*	*input*
up_down	*up_down = 1 for up-chirp* *up_down = -1 for down-chirp*	*none*	*input*

MATLAB Function** "lfm_ambg.m" **Listing

```
function [x] = single_pulse_ambg (taup)
% Single umodulated pulse
eps = 0.000001;
i = 0;
del = 2*taup/150;
for tau = -taup:del:taup
  i = i + 1;
  j = 0;
  fd = linspace(-5/taup,5/taup,151);
  val1 = 1. - abs(tau) / taup;
  val2 = pi * taup .* (1.0 - abs(tau) / taup) .* fd;
  x(:,i) = abs( val1 .* sin(val2+eps)./(val2+eps));
end
```

5.7.3. Pulse Train Ambiguity Function

The function "*train_ambg.m*" implements Eq. (5.35). The syntax is as follows:

train_ambg [taup, n, pri]

where

Symbol	Description	Units	Status
taup	*pulse width*	*seconds*	*input*
n	*number of pulses in train*	*none*	*input*
pri	*pulse repetition interval*	*seconds*	*input*

MATLAB Function** "train_ambg.m" **Listing

```
function x = train_ambg(taup, n, pri)
% This code was developed by Stephen Robinson, a senior radar engineer at
% deciBel Research in Hunstville AL
if (taup >= pri/2)
  'ERROR. Pulse width must be less than the PRI/2.'
```

```
   return
end
eps = 1.0e-6;
bw = 1/taup;
q = -(n-1):1:n-1;
offset = 0:0.0533:pri;
[Q, S] = meshgrid(q, offset);
Q = reshape(Q, 1, length(q)*length(offset));
S = reshape(S, 1, length(q)*length(offset));
tau = (-taup * ones(1,length(S))) + S;
fd = -bw:0.033:bw;
[T, F] = meshgrid(tau, fd);
Q = repmat(Q, length(fd), 1);
S = repmat(S, length(fd), 1);
N = n * ones(size(T));
val1 = 1.0-(abs(T))/taup;
val2 = pi*taup*F.*val1;
val3 = abs(val1.*sin(val2+eps)./(val2+eps));
val4 = abs(sin(pi*F.*(N-abs(Q))*pri+eps)./sin(pi*F*pri+eps));
x = val3.*val4./N;
[rows, cols] = size(x);
x = reshape(x, 1, rows*cols);
T = reshape(T, 1, rows*cols);
indx = find(abs(T) > taup);
x(indx) = 0.0;
x = reshape(x, rows, cols);
return
```

5.7.4. Pulse Train Ambiguity Function with LFM

The function "*train_ambg_lfm.m*" implements Eq. (5.43). The syntax is as follows:

x = train_ambg_lfm(taup, n, pri, bw)

where

Symbol	Description	Units	Status
taup	*pulse width*	*seconds*	*input*
n	*number of pulses in train*	*none*	*input*
pri	*pulse repetition interval*	*seconds*	*input*
bw	*the LFM bandwidth*	*Hz*	*input*
x	*array of bimodality function*	*none*	*output*

Note this function will generate identical results to the function *"train_ambg.m"* when the value of *bw* is set to zero. In this case, Eq. (4.43) and (4.35) are identical.

MATLAB Function** "train_ambg_lfm.m" **Listing

```
function x = train_ambg_lfm(taup, n, pri, bw)
% This code was developed by Stephen Robinson, a senior radar engineer at
% deciBel Research in Hunstville AL
if (taup >= pri/2)
   'ERROR. Pulse width must be less than the PRI/2.'
   return
end
eps = 1.0e-6;
q = -(n-1):1:n-1;
offset = 0:0.0533:pri;
[Q, S] = meshgrid(q, offset);
Q = reshape(Q, 1, length(q)*length(offset));
S = reshape(S, 1, length(q)*length(offset));
tau = (-taup * ones(1,length(S))) + S;
fd = -bw:0.033:bw;
[T, F] = meshgrid(tau, fd);
Q = repmat(Q, length(fd), 1);
S = repmat(S, length(fd), 1);
N = n * ones(size(T));
val1 = 1.0-(abs(T))/taup;
val2 = pi*taup*(F+T*(bw/taup)).*val1;
val3 = abs(val1.*sin(val2+eps)./(val2+eps));
val4 = abs(sin(pi*F.*(N-abs(Q))*pri+eps)./sin(pi*F*pri+eps));
x = val3.*val4./N;
[rows, cols] = size(x);
x = reshape(x, 1, rows*cols);
T = reshape(T, 1, rows*cols);
indx = find(abs(T) > taup);
x(indx) = 0.0;
x = reshape(x, rows, cols);
return
```

Problems

5.1. Derive Eq. (5.47).

5.2. Show that Eq. (5.79) and Eq. (5.80) are equivalent.

5.3. Derive an expression for the ambiguity function of a Gaussian pulse defined by

$$x(t) = \frac{1}{\sqrt{\sigma}\ \sqrt[1/4]{\pi}} \exp\left[\frac{-t^2}{2\sigma^2}\right] \qquad ;0 < t < T$$

where T is the pulsewidth and σ is a constant.

5.4. Write a MATLAB code to plot the 3-D and the contour plots for the results in Problem 5.3.

5.5. Derive an expression for the ambiguity function of a V-LFM waveform, illustrated in figure below. In this case, the overall complex envelope is

$$\tilde{x}(t) = \tilde{x}_1(t) + \tilde{x}_2(t) \qquad ;-(T < t < T)$$

where

$$\tilde{x}_1(t) = \frac{1}{\sqrt{2T}} \exp[-\mu t^2] \qquad ;-T < t < 0$$

and

$$\tilde{x}_2(t) = \frac{1}{\sqrt{2T}} \exp[\mu t^2] \qquad ;0 < t < T$$

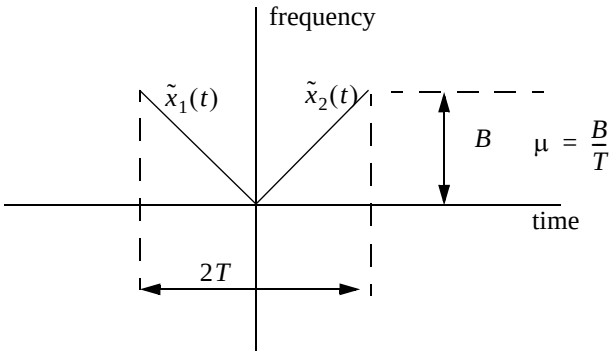

5.6. Using the stationary phase concept, find the instantaneous frequency for the waveform whose envelope and complex spectrum are, respectively, given by

$$r(t) = \frac{1}{\sqrt{T}} \exp\left[-\left(\frac{2t}{T}\right)^2\right] \qquad ;0 < t < T$$

and

$$|X(f)| = \frac{1}{\sqrt{B}} \exp\left[-\left(\frac{2f}{B}\right)^2\right]$$

5.7. Using the stationary phase concept find the instantaneous frequency for the waveform whose envelope and complex spectrum are respectively given by

$$r(t) = \frac{1}{\sqrt{\tau_0}} Rect\left(\frac{t}{\tau_0}\right) \qquad ; \ 0 < t < \tau_0$$

and

$$|X(\omega)| = \frac{2}{\sqrt{B}} \frac{1}{\sqrt{1 + (2\omega / B)^2}}$$

5.8. Write detailed MATLAB code to compute the ambiguity function for an NLFM waveform. Your code must be able to produce 3-D and contour plots of the resulting ambiguity function. Hint: Use Eq. (5.90).

5.9. Revisit the analyses performed in Chapter 2 for the effective bandwidth and effective duration of the LFM waveform. Write a short discussion to outline how do the range and Doppler resolution are different from the theoretical limits used in this chapter.

5.10. Write a detailed MATLAB code to compute the ambiguity function for an SFW waveform. Your code must be able to produce 3-D and contour plots of the resulting ambiguity function. Hint: use Eq. (5.43).

5.11. Prove that cuts in the ambiguity function are always defined by an ellipse. Hint: Approximate the ambiguity function using a Taylor series expansion about the values $(\tau, f_d) = (0, 0)$; use only the first three terms in the Taylor series expansion.

5.12. The radar uncertainty principle establishes a lower bound for the time bandwidth product. More specifically, if the radar effective duration is τ_e and its effective bandwidth is B_e; show that $B_e^2 \tau_e^2 - \rho_{RDC}^2 \geq \pi^2$, where ρ_{RDC} is the range-Doppler coupling coefficient defined in Chapter 4. Hint: Assume a signal $x(t)$, write down the definition of ρ_{RDC}, and use Shwarz inequality on the integral

$$(-j2\pi) \int_{-\infty}^{\infty} t x^*(t) x'(t) dt .$$

Chapter 6 The Ambiguity Function - Discrete Coded Waveforms

The concepts of resolution and ambiguity were introduced in Chapter 4. The relationship between the waveform resolution (range and Doppler) and its corresponding ambiguity function was discussed and analyzed. It was determined that the *goodness* of a given waveform is based on its range and Doppler resolutions, which can be analyzed in the context of the ambiguity function. For this purpose, a few common analog radar waveforms were analyzed in Chapter 5. In this chapter, another type of radar waveform based on discrete codes is introduced. This topic has been and continues to be a major research thrust area for many radar scientist, designers, and engineers. Discrete coded waveforms are more effective in improving range characteristics than Doppler (velocity) characteristics. Furthermore, in some radar applications, discrete coded waveforms are heavily favored because of their inherent anti-jamming capabilities. In this chapter, a quick overview of discrete coded waveforms is presented. Three classes of discrete codes are analyzed. They are unmodulated pulse-train codes (uniform and staggered), phase-modulated (binary or polyphase) codes, and frequency modulated codes.

6.1. Discrete Code Signal Representation

The general form for a discrete coded signal can be written as

$$x(t) = e^{j\omega_0 t}\sum_{n=1}^{N} u_n(t) = e^{j\omega_0 t}\sum_{n=1}^{N} P_n(t)e^{j(\omega_n t + \theta_n)} \qquad \textbf{(6.1)}$$

where ω_0 is the carrier frequency in radians, (ω_n, θ_n) are constants, N is the code length (number of bits in the code), and the signal $P_n(t)$ is given by

$$P_n(t) = a_n Rect\left(\frac{t}{\tau_0}\right) \qquad \textbf{(6.2)}$$

the constant a_n is either (1) or (0), and

$$Rect\left(\frac{t}{\tau_0}\right) = \begin{cases} 1 & ; \quad 0 < t < \tau_0 \\ 0 & ; \ elsewhere \end{cases} \tag{6.3}$$

Using this notation the discrete code can be described through the sequence

$$U[n] = \{u_n \ , n = 1, 2, \ldots, N\} \tag{6.4}$$

which, in general, is a complex sequence depending on the values of ω_n and θ_n. The sequence $U[n]$ is called the code and for convenience it will be denoted by U.

In general, the output of the matched filter is

$$\chi(\tau, f_d) = \int_{-\infty}^{\infty} x^*(t)x(t+\tau)e^{-j2\pi f_d t}dt \tag{6.5}$$

Substituting Eq. (6.1) into Eq. (6.5) yields

$$\chi(\tau, f_d) = \sum_{n=1}^{N}\sum_{k=1}^{N}\int_{-\infty}^{\infty} u_n^*(t)u_k(t+\tau)e^{-j2\pi f_d t}dt \tag{6.6}$$

Depending on the choice of combination for a_n, ω_n, and θ_n, different class of codes can be generated. More precisely, pulse-train codes are generated when

$$\theta_n = \omega_n = 0 \quad ; \ and \ \ a_n = 1, or \ \ 0 \tag{6.7}$$

Binary phase codes and polyphase codes are generated when

$$\omega_n = 0 \quad ; \ and \ \ a_n = 1 \tag{6.8}$$

Finally, frequency codes are generated when

$$\theta_n = 0 \quad ; \ and \ \ a_n = 1, or \ \ 0 \tag{6.9}$$

6.2. Pulse-Train Codes

The idea behind this class of code is to divide a relatively long pulse of length T_P into N subpulses, each being a rectangular pulse with pulsewidth τ_0 and amplitude of 1 or 0. It follows that the code U is the sequence of 1's and 0's. More precisely, the signal representing this class of code can written as

$$x(t) = e^{j\omega_0 t}\sum_{n=1}^{N} P_n(t) = e^{j\omega_0 t}\sum_{n=1}^{N} a_n Rect\left(\frac{t}{\tau_0}\right) \tag{6.10}$$

One way to generate a train-pulse class code can be by setting

$$a_n = \begin{cases} 1 & n-1 = 0 \ \ modulu \ \ q \\ 0 & n-1 \neq 0 \ \ modulu \ \ q \end{cases} \tag{6.11}$$

where q is a positive integer that divides evenly into $N-1$. That is,

$$M-1 = (N-1)/q \tag{6.12}$$

where M is the number of 1's in the code. For example, when $N = 21$ and $q = 5$, then $M = 5$, and the resulting code is

$$\{U\} = \{10000 \ \ 10000 \ \ 10000 \ \ 10000 \ \ 1\} \tag{6.13}$$

This is illustrated in Fig. 6.1. In previous chapters this code would have been represented by the following continuous time domain signal

$$x_1(t) = e^{j\omega_0 t} \sum_{m=0}^{4} Rect\left(\frac{t-mT}{\tau_0}\right) \tag{6.14}$$

where the period is $T = 5\tau_0$. Using this analogy yields

$$\frac{T_p}{M-1} \equiv T \tag{6.15}$$

and Eq. (6.10) can now be written as

$$x(t) = e^{j\omega_0 t} \sum_{m=1}^{M-1} Rect\left(\frac{t-m\left(\frac{T_p}{M-1}\right)}{\tau_0}\right) \tag{6.16}$$

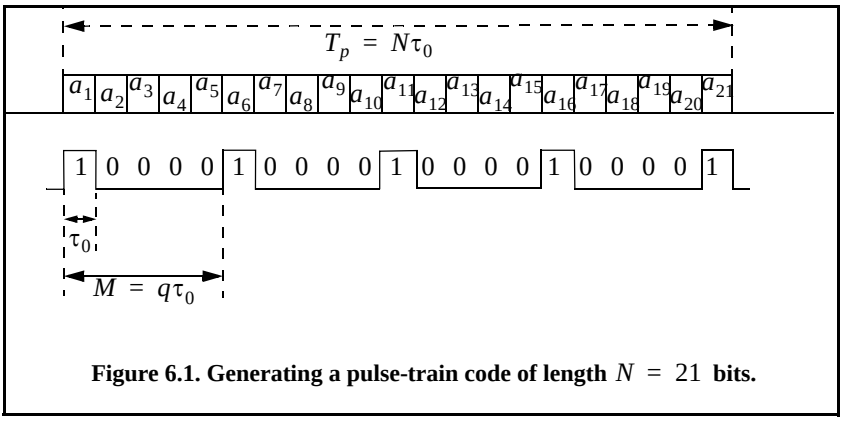

Figure 6.1. Generating a pulse-train code of length $N = 21$ bits.

In Chapter 5 (Section 5.2.3) an expression for the ambiguity function for a coherent train of pulses was derived. Comparison of Eq. (6.16) and Eq. (5.37) show that the two equations are equivalent when the condition in Eq. (6.15) is true except for the ratio $(1/\sqrt{N})$. It follows that the ambiguity function for the signal defined in Eq. (6.16) is

$$|\chi(\tau;f_d)| = \sum_{k=-M}^{M} \left| \frac{\sin\left[\pi f_d\left([M-|k|]\frac{T_p}{M-1}\right)\right]}{\sin\left(\pi f_d \frac{T_p}{M-1}\right)} \right| \left| \frac{\sin\left[\pi f_d\left(\tau_0 - \left|\tau - \frac{kT_p}{M-1}\right|\right)\right]}{\pi f_d} \right| \quad \textbf{(6.17)}$$

The zero Doppler and zero delay cuts of the ambiguity function are derived from Eq. (6.17). They are given by

$$|\chi(\tau;0)| = M\tau_0 \sum_{k=-M}^{M} \left[1 - \frac{|k|}{M}\right]\left(1 - \frac{\left|\tau - \frac{kT_p}{M-1}\right|}{\tau_0}\right) \quad \textbf{(6.18)}$$

$$|\chi(0;f_d)| = \sum_{k=-M}^{M} \left| \frac{\sin\left[\pi M f_d\left(\frac{T_p}{M-1}\right)\right]}{\sin\left(\pi f_d \frac{T_p}{M-1}\right)} \right| \left| \frac{\sin(\pi f_d \tau_0)}{\pi f_d \tau_0} \right| \quad \textbf{(6.19)}$$

Figure 6.2a shows the three-dimensional ambiguity plot for the code shown in Fig. 6.1, while Fig. 6.2b shows the corresponding contour plot. This figure can be reproduced using the following MATLAB code.

```
close all; clear all;
U = [1 0 0 0 0 1 0 0 0 0 1 0 0 0 0 1];
ambiguity = ambiguity_code(U);
```

A cartoon showing contour cuts of the ambiguity function for a pulse-train code is shown in Fig. 6.2c. Clearly, the width of the ambiguity function main lobe (i.e., resolution) is directly tied to the code length. As one would expect, longer codes will produce narrower main lobe and thus have better resolution than shorter ones. Further observation of Fig. 6.2 shows that this ambiguity function has strong grating lobe structure along with high sidelobe levels. The presence of such strong lobing structure limits the effectiveness of the code and will cause detection ambiguities. These lobes are a direct result from the uniform equal spacing between the 1's within a code (i.e., periodicity of the code). These lobes can be significantly reduced by getting rid of the periodic structure of the code, i.e., placing the pulses at nonuniform spacing. This is called code staggering (PRF staggering).

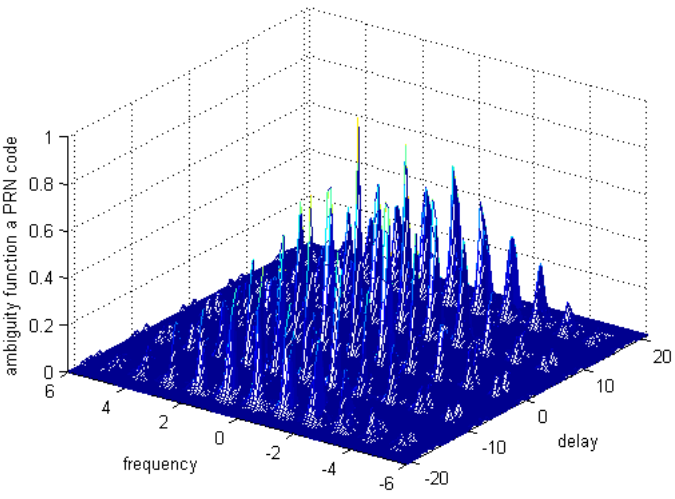

Figure 6.2a. Ambiguity function for the pulse-train code shown in Fig. 6.1.

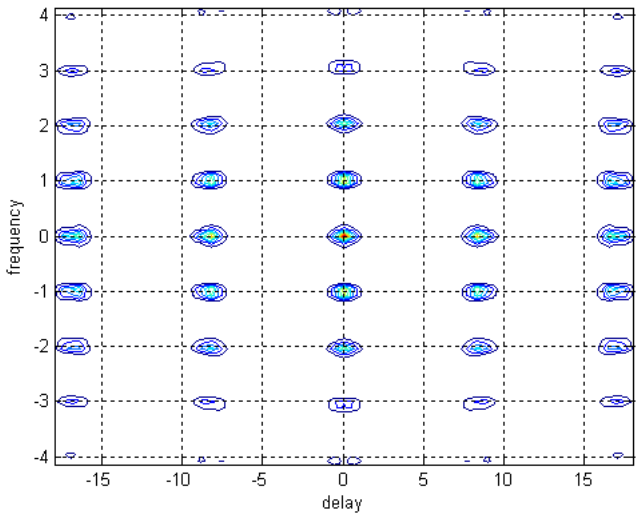

Figure 6.2b. Contour plot corresponding to Fig. 6.2a.

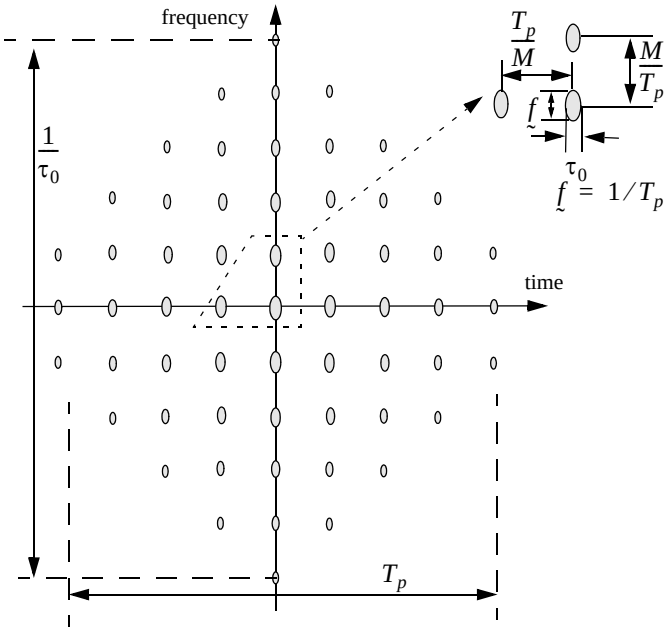

Figure 6.2c. Cartoon of the ambiguity contour plot for a pulse-train code.

For example, consider a pulse-train code of length $N = 21$. A staggered train-pulse code can then be obtained by using the following sequence a_n

$$\{a_n\} = 1 \qquad n = 1, 4, 6, 12, 15, 21 \tag{6.20}$$

Thus, the resulting code is

$$\{U\} = \{100101000001001000001\} \tag{6.21}$$

Figure 6.3 shows the ambiguity plot corresponding to this code. As indicated by Fig. 6.3 the ambiguity function corresponding to a staggered pulse-train code approaches a thumb-tack shape. The choice of the optimum staggered code has been researched extensively by numerous people. Resnick[1] defined the optimum staggered pulse-train code as that whose ambiguity function has absolutely uniform sidelobe levels that are equal to unity. Other researchers, have introduced different definitions for optimum staggering, none of which is necessarily better than the others, except when considered for the particular application being analyzed by the respective researcher.

1. Resnick, J. B., *High Resolution Waveforms Suitable for a Multiple Target Environment*, MS Thesis, MIT, Cambridge, MA, June 1962.

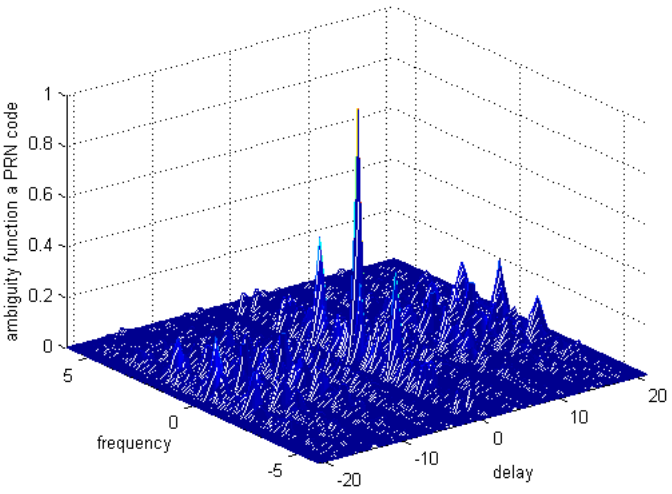

Figure 6.3a. Ambiguity function for the pulse-train code in Eq. (6.21).

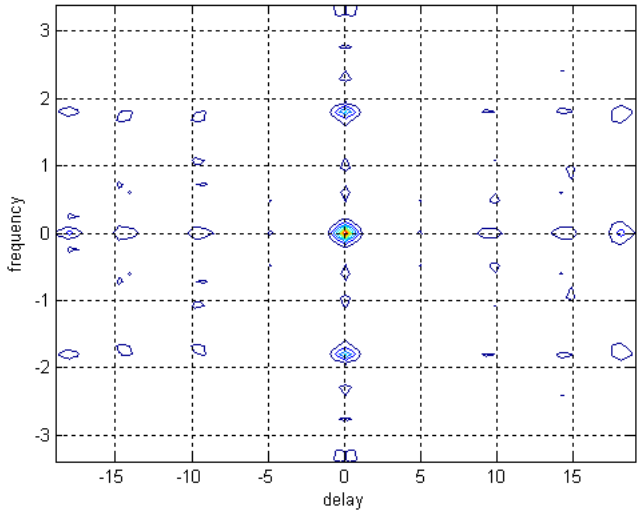

Figure 6.3b. Contour plot corresponding to Fig. 6.3a.

6.3. Phase Coding

The signal corresponding to this class of code is obtained from Eq. (6.1) by letting $\omega_n = 0$. It follows that

$$x(t) = e^{j\omega_0 t}\sum_{n=1}^{N} u_n(t) = e^{j\omega_0 t}\sum_{n=1}^{N} P_n(t)e^{j\theta_n} \tag{6.22}$$

Two subclasses of phase codes are analyzed. They are binary phase codes and polyphase codes.

6.3.1. Binary Phase Codes

In this case, the phase θ_n is set equal to either (0) or (π), and hence, the term *binary* is used. For this purpose, define the coefficient D_n as

$$D_n = e^{j\theta_n} = \pm 1 \tag{6.23}$$

The ambiguity function for this class of code is derived by substituting Eq. (6.22) into Eq. (6.5). The resulting ambiguity function is given by

$$\chi(\tau;f_d) = \begin{cases} \chi_0(\tau', f_d)\displaystyle\sum_{n=1}^{N-k} D_n D_{n+k} e^{-j2\pi f_d(n-1)\tau_0} + \\ \chi_0(\tau_0 - \tau', f_d)\displaystyle\sum_{n=1}^{N-(k+1)} D_n D_{n+k+1} e^{-j2\pi f_d n\tau_0} \end{cases} \qquad 0 < \tau < N\tau_0 \tag{6.24}$$

where

$$\tau = k\tau_0 + \tau' \qquad \begin{cases} 0 < \tau' < \tau_0 \\ k = 0, 1, 2, \ldots, N \end{cases} \tag{6.25}$$

$$\chi_0(\tau', f_d) = \int_0^{\tau_0 - \tau'} \exp(-j2\pi f_d t)dt \qquad 0 < \tau' < \tau_0 \tag{6.26}$$

The corresponding zero Doppler cut is then given by

$$\chi(\tau;0) = \tau_0\left(1 - \frac{|\tau'|}{\tau_0}\right)\sum_{n=1}^{N-|k|} D_n D_{n+k} + |\tau'|\sum_{n=1}^{N-|k+1|} D_n D_{n+k+1} \tag{6.27}$$

and when $\tau' = 0$ then

$$\chi(k;0) = \tau_0 \sum_{n=1}^{N-|k|} D_n D_{n+k} \qquad \textbf{(6.28)}$$

Barker Codes

In this case, a long pulse of width T_p is divided into N smaller pulses; each is of width $\tau_0 = T_p/N$. Then, the phase of each subpulse is chosen as either 0 or π radians relative to some code. It is customary to characterize a subpulse that has 0 phase (amplitude of +1 Volt) as either "1" or "+." Alternatively, a subpulse with phase equal to π (amplitude of -1 Volt) is characterized by either "0" or "-." Barker code is optimum in accordance with the definition set by Resnick. Figure 6.4 illustrates this concept for a Barker code of length seven. A Barker code of length N is denoted as B_N. There are only seven known Barker codes that share this unique property; they are listed in Table 6.1. Note that B_2 and B_4 have complementary forms that have the same characteristics.

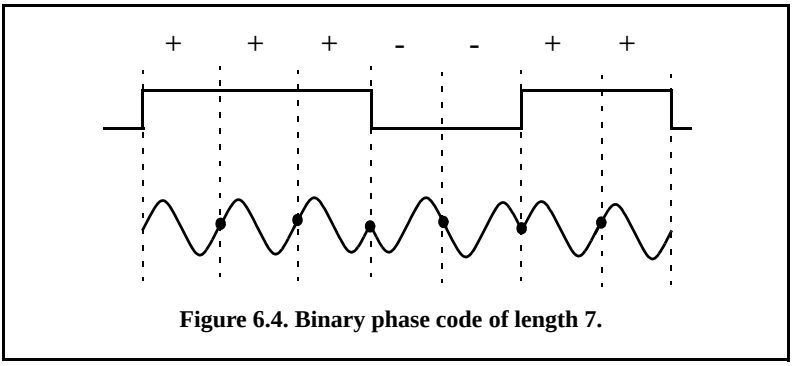

Figure 6.4. Binary phase code of length 7.

In general, the autocorrelation function (which is an approximation for the matched filter output) for a B_N Barker code will be $2N\tau_0$ wide. The main lobe is $2\tau_0$ wide; the peak value is equal to N. There are $(N-1)/2$ side-lobes on either side of the main lobe; this is illustrated in Fig. 6.5 for a B_{13}. Notice that the main lobe is equal to 13, while all side-lobes are unity.

The most side-lobe reduction offered by a Barker code is $-22.3dB$, which may not be sufficient for the desired radar application. However, Barker codes can be combined to generate much longer codes. In this case, a B_M code can be used within a B_N code (M within N) to generate a code of length MN. The compression ratio for the combined B_{MN} code is equal to MN. As an example, a combined B_{54} is given by

$$B_{54} = \{11101, 11101, 00010, 11101\} \qquad \textbf{(6.29)}$$

and is illustrated in Fig. 6.6. Unfortunately, the side-lobes of a combined Barker code autocorrelation function are no longer equal to unity. Some side-lobes of a combined Barker code autocorrelation function can be reduced to zero if the matched filter is followed by a linear transversal filter with impulse response given by

$$h(t) = \sum_{k=-N}^{N} \beta_k \delta(t - 2k\tau_0) \tag{6.30}$$

where N is the filter's order, the coefficients β_k ($\beta_k = \beta_{-k}$) are to be determined, $\delta(\cdot)$ is the delta function, and τ_0 is the Barker code subpulse width. A filter of order N produces N zero side-lobes on either side of the main lobe. The main lobe amplitude and width do not change, as illustrated in Fig. 6.7.

TABLE 6.1. Barker codes

Code Symbol	Code Length	Code Elements	Side Lode Reduction (dB)
B_2	2	+-	6.0
		++	
B_3	3	++-	9.5
B_4	4	++-+	12.0
		+++-	
B_5	5	+++-+	14.0
B_7	7	+++--+-	16.9
B_{11}	11	+++---+--+-	20.8
B_{13}	13	+++++--++-+-+	22.3

In order to illustrate this approach, consider the case where the input to the matched filter is B_{11}, and assume $N = 4$. The autocorrelation for a B_{11} is

$$\phi_{11} = \{-1, 0, -1, 0, -1, 0, -1, 0, -1, 0, 11, 0, -1, 0, -1, 0, -1, 0, -1, 0, -1\} \tag{6.31}$$

The output of the transversal filter is the discrete convolution between its impulse response and the sequence ϕ_{11}. At this point we need to compute the coefficients β_k that guarantee the desired filter output (i.e., unchanged main lobe and four zero side-lobe levels).

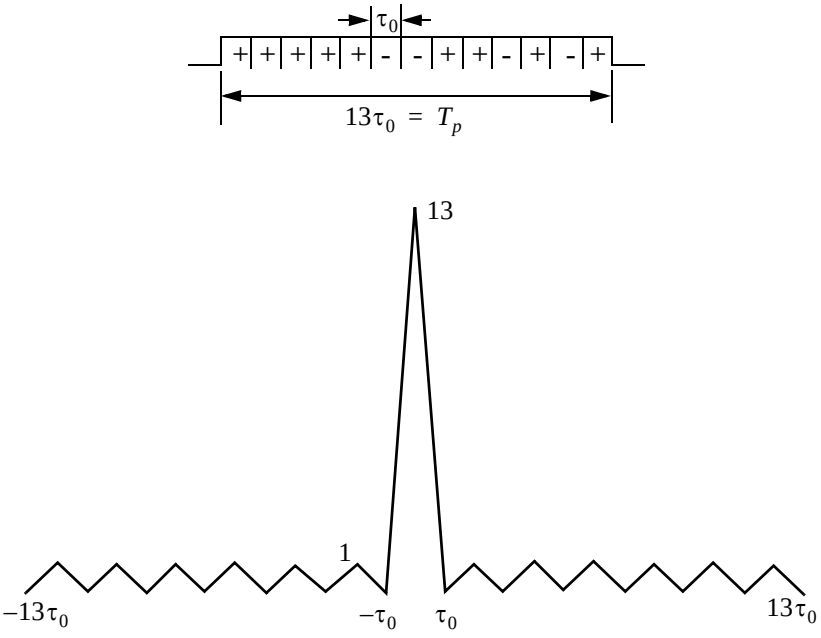

Figure 6.5. Barker code of length 13, and its corresponding auto-correlation function.

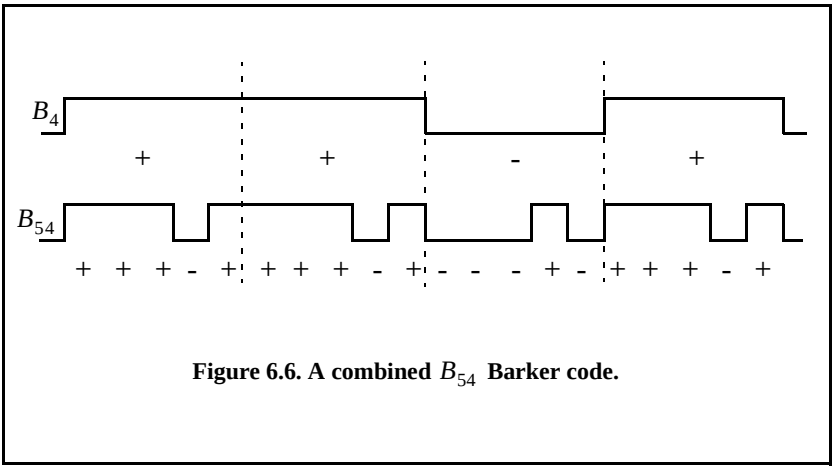

Figure 6.6. A combined B_{54} Barker code.

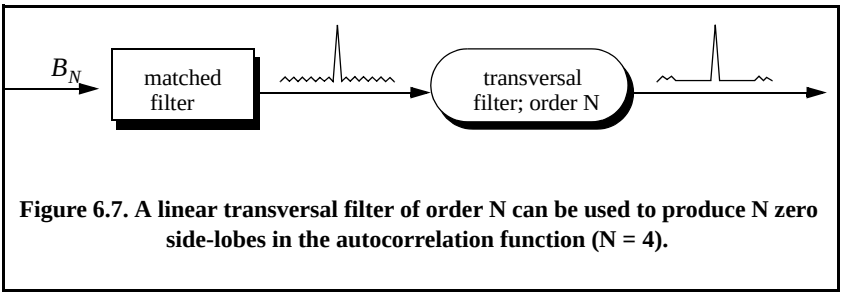

Figure 6.7. A linear transversal filter of order N can be used to produce N zero side-lobes in the autocorrelation function (N = 4).

Performing the discrete convolution as defined in Eq. (6.30) and collecting equal terms ($\beta_k = \beta_{-k}$) yield the following set of five linearly independent equations:

$$\begin{bmatrix} 11 & -2 & -2 & -2 & -2 \\ -1 & 10 & -2 & -2 & -1 \\ -1 & -2 & 10 & -2 & -1 \\ -1 & -2 & -1 & 11 & -1 \\ -1 & -1 & -1 & -1 & 11 \end{bmatrix} \begin{bmatrix} \beta_0 \\ \beta_1 \\ \beta_2 \\ \beta_3 \\ \beta_4 \end{bmatrix} = \begin{bmatrix} 11 \\ 0 \\ 0 \\ 0 \\ 0 \end{bmatrix} \tag{6.32}$$

Solving Eq. (6.32) yields

$$\begin{bmatrix} \beta_0 \\ \beta_1 \\ \beta_2 \\ \beta_3 \\ \beta_4 \end{bmatrix} = \begin{bmatrix} 1.1342 \\ 0.2046 \\ 0.2046 \\ 0.1731 \\ 0.1560 \end{bmatrix} \tag{6.33}$$

Note that setting the first equation equal to 11 and all other equations to 0 and then solving for β_k guarantees that the main peak remains unchanged, and that the next four side-lobes are zeros. So far we have assumed that coded pulses have rectangular shapes. Using other pulses of other shapes, such as Gaussian, may produce better side-lobe reduction and a larger compression ratio.

Figure 6.8 shows the output of this function when B_{13} is used as an input. Figure 6.9 is similar to Fig. 6.8, except in this case B_7 is used as an input. Figure 6.10 shows the ambiguity function, the zero Doppler cut, and the contour plot for the combined Barker code defined in Fig. 6.6.

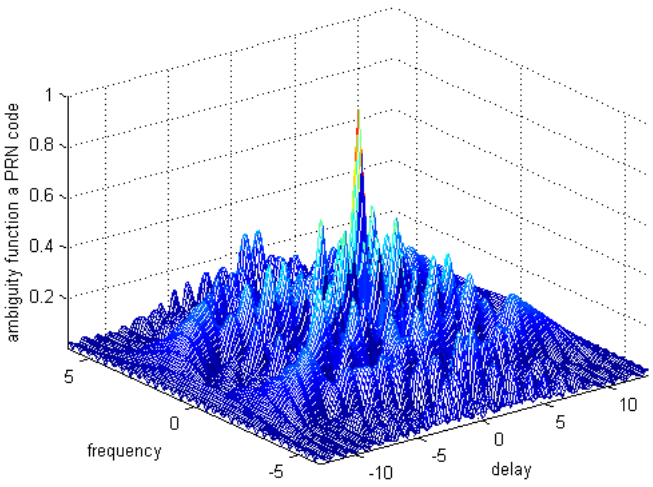

Figure 6.8a. Ambiguity function for B_{13} Barker code.

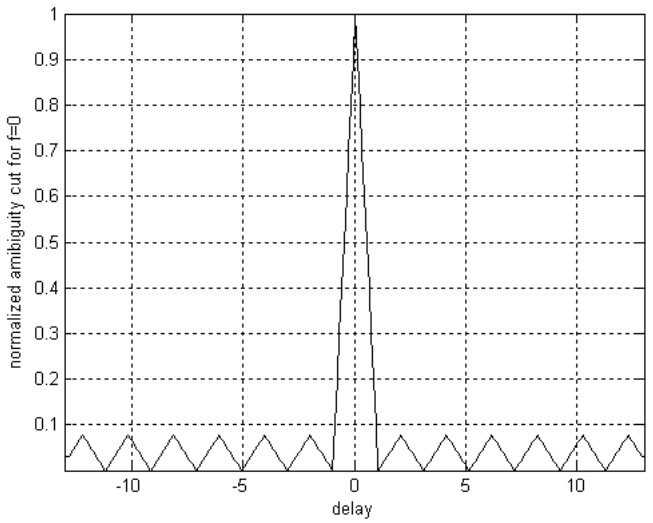

Figure 6.8b. Zero Doppler cut for the B_{13} ambiguity function.

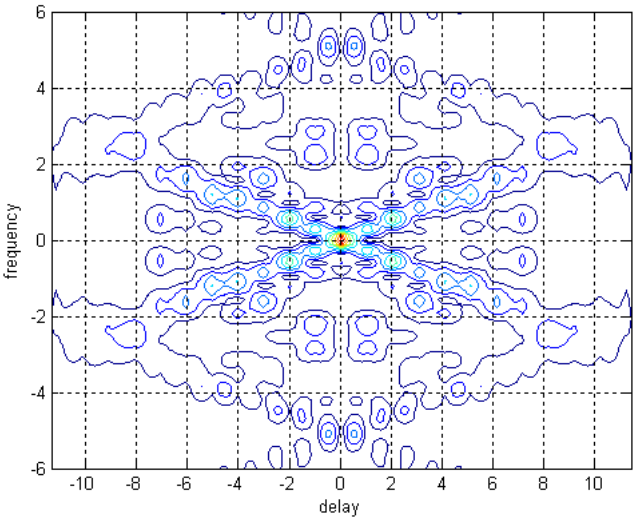

Figure 6.8c. Contour plot corresponding to Fig. 6.8a.

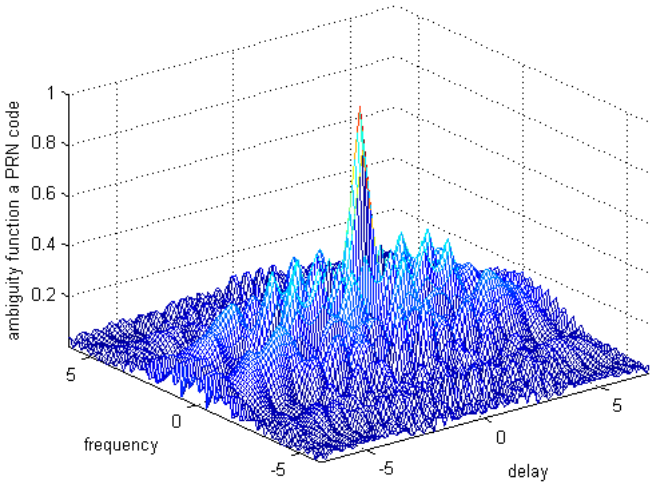

Figure 6.9a. Ambiguity function for B_7 Barker code.

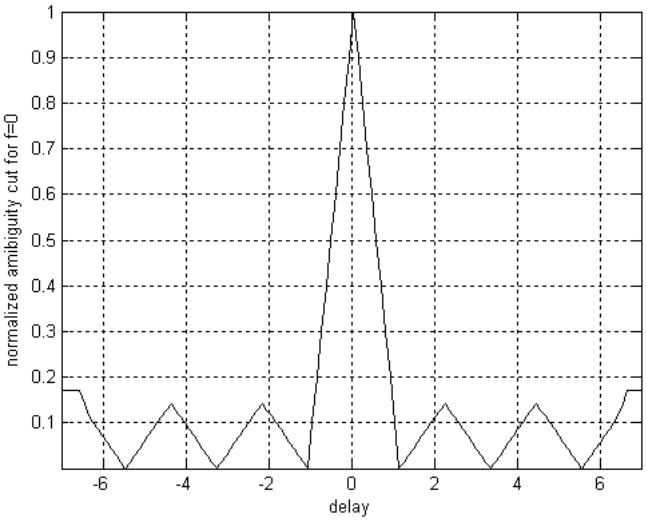

Figure 6.9b. Zero Doppler cut for the B_7 ambiguity function.

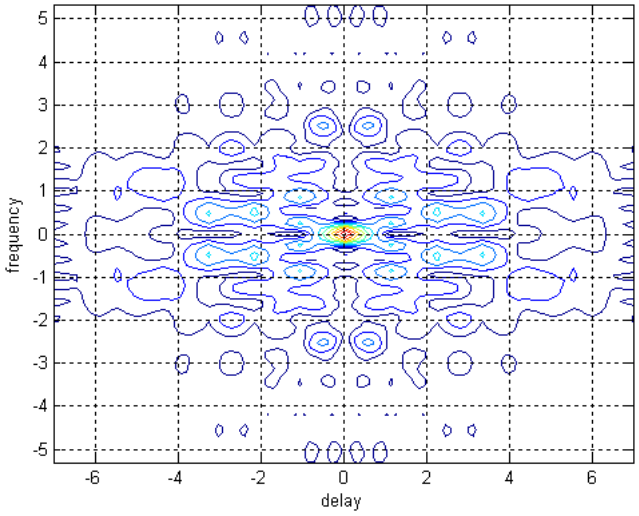

Figure 6.9c. Contour plot corresponding to Fig. 6.9a.